Search for quarks in cosmic rays

D. A. Simpson

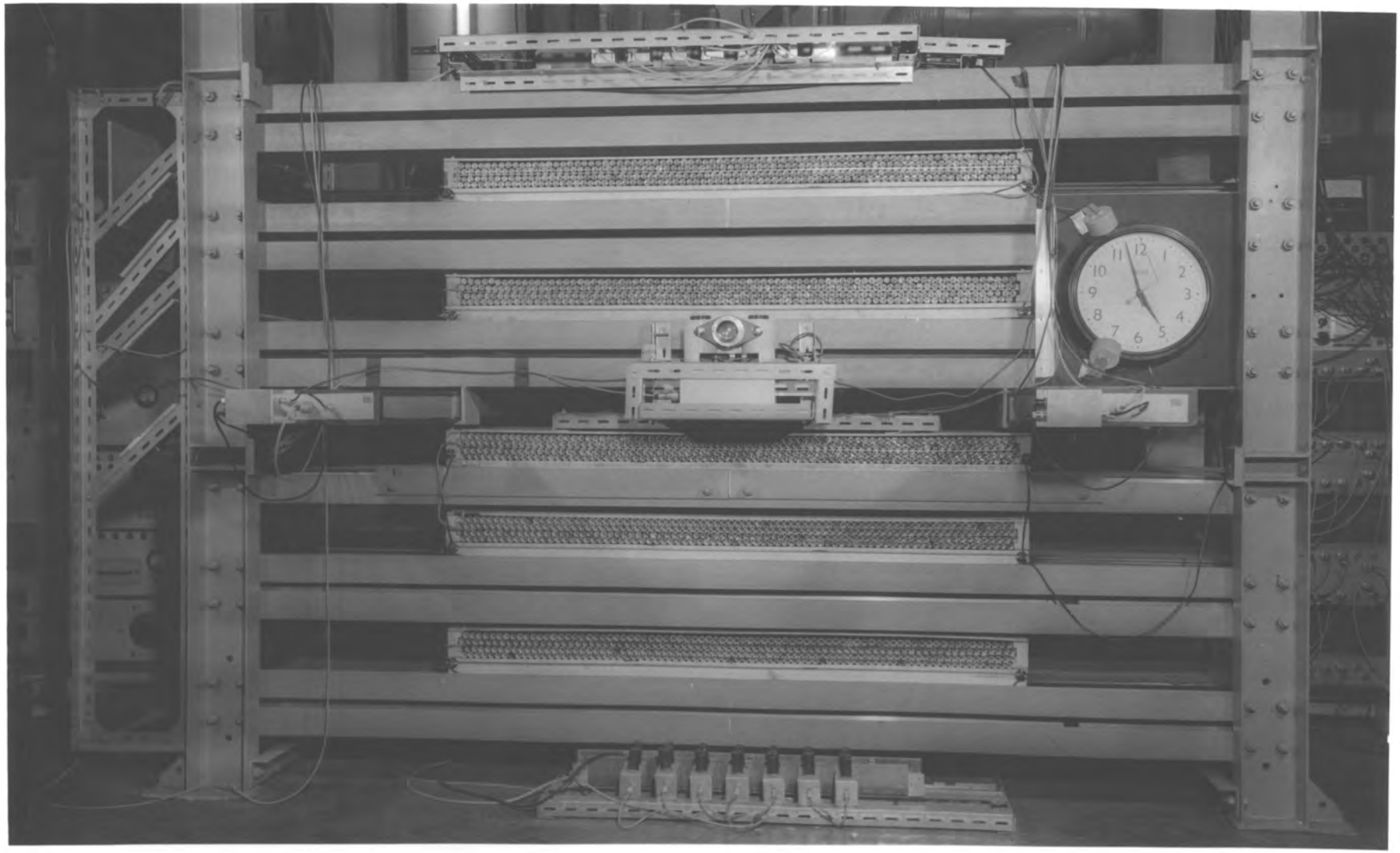

Plate 1

The Front View of the Telescope

Used in the Present Experiment

SEARCH FOR QUARKS IN COSMIC RAYS

by

D.A. Simpson, B.Sc., M.Sc.

A Thesis submitted to the

University of Durham

for the Degree of Doctor of Philosophy.

December, 1967.

CONTENTS

ABSTRACT

The characteristics of a scintillation counter - neon flash tube telescope have been investigated. The response of the scintillation counter and the efficiency of the neon flash tube trays for relativistic muons was measured. The equivalent characteristics for relativistic $\frac{1}{3}e$ and $\frac{2}{3}e$ quarks were evaluated from the above data. The efficiency of the telescope for detecting relativistic $\frac{1}{3}e$ and $\frac{2}{3}e$ quarks was thus obtained.

The telescope was operated in a search for $\frac{1}{3}e$ and $\frac{2}{3}e$ quarks in cosmic rays at sea-level. The telescope was sensitive to $\frac{1}{3}e$ quarks in the β range 0.4 to 1.0 and to $\frac{2}{3}e$ quarks in the β range 0.8 to 1.0. In the running time obtained no quarks were detected. The rate of relativistic quarks is given with 90% confidence as:

$$< 1.2 \times 10^{-10} \text{ cm}^{-2} \text{ sterad}^{-1} \text{ sec}^{-1} \text{ for } \tfrac{1}{3}e \text{ quarks}$$

$$\text{and } < 8.0 \times 10^{-11} \text{ cm}^{-2} \text{ sterad}^{-1} \text{ sec}^{-1} \text{ for } \tfrac{2}{3}e \text{ quarks.}$$

From these rates the upper limit of the production cross-section for quarks as a function of quark mass was evaluated and compared with theoretical predictions.

The characteristics of a glass plate spark chamber and a stack of neon flash tubes operated in the localised discharge regime were investigated.

PREFACE

This thesis describes the work performed by the author in the Physics Department of the University of Durham while he was a Research Student under the supervision of Dr. F. Ashton.

An experiment to investigate the existance of quarks in cosmic rays at sea-level has been performed. The development, building and day-to-day running was the author's responsibility with assistance from Mr. G.N. Kelly.

CHAPTER 1

INTRODUCTION

1.1 Symmetry in elementary particles

Fundamental physics has been based in the past on the analytical notion that a system is best understood by reducing it to its component parts. Prior to 1930, most physical phenomena could be explained by the classical concept of three elementary particles, the proton, the electron, and the photon, interacting through two basic types of force, electromagnetic and gravitational. In the realm of the nucleus, however, with a large repulsive coulomb force between protons, a strong nuclear force was postulated by Yukawa (1935) to account for the stability of nuclei. The forces between particles can best be expressed as an exchange of intermediate 'virtual' particles between the colliding particles. Based on the range of the nuclear force Yukawa predicted the π meson as the intermediary. This particle was subsequently found by Lattes etal. (1947) in nuclear emulsions exposed to cosmic rays at mountain altitudes. With the development of accelerators and the advent of bubble chambers a whole range of new particles, both sub-nuclear and heavier than the proton (baryons) have been discovered in bewildering profusion. The understanding and classification of this wide spectrum of particles is

one of the major problems of fundamental physics today.

Progress in classification has been made by studying the conservation laws which govern particle interactions and it is found that particles can be divided into groups; spin 0 mesons, spin $\frac{1}{2}$ and $\frac{3}{2}$ baryons for instance. In the strong interactions of the baryon group three conservation laws are obeyed; the conservation of electric charge (this is thought to be absolute), the conservation of baryonic charge (to account for the stability and abundance of the proton), and the conservation of hypercharge (to account for the association of positive and neutral kaons with Λ and Σ baryons produced in π-N collisions).

The most successful model to explain these observed regularities is based on the theories of unitary symmetry and the existence of three (because of the three types of charge) sub-nuclear particles as proposed by Gell-Mann (1964) and independantly by Zweig (1964). The name 'quark' for these particles was given by Gell-Mann and is now in general use. The quantum numbers (charges) and general characteristics are given in Table 1.1 for the three quarks p, n, and λ. The mass of λ is 146 MeV heavier than p and n to account for the regular increases in mass of the heavier baryons.

Unitary symmetry requires the quark content of any system to be conserved (excepting the production and annihilation of quark-antiquark pairs) but given any dynamical situation involving p, n,

Table 1.1 Characteristics of quarks p, n and λ

Symbol	Q	S	B	spin	mass	decay schemes and lifetime
p	$+\frac{2}{3}e$	0	$\frac{1}{3}$	$\frac{1}{2}$	several GeV	stable
n	$-\frac{1}{3}e$	0	$\frac{1}{3}$	$\frac{1}{2}$	ditto	$\rightarrow q(+\frac{2}{3}e) + e^- + \bar{\nu}_e$ ~mins
λ	$-\frac{1}{3}e$	-1	$\frac{1}{3}$	$\frac{1}{2}$	ditto +146 MeV	$\rightarrow q(+\frac{2}{3}e) + \pi^-$ $\sim 10^{-10}$ sec

Q = electric charge

S = strangeness

B = baryon charge

S +B = hypercharge

and λ, a new dynamically possible situation is obtained by re-arranging the initial combinations. Thus quarks can be regarded as the 'building blocks' for baryons and thus define their properties and conservation laws. The octet and decuplet groups of baryons with spin $\frac{1}{2}$ and $\frac{3}{2}$ respectively are shown with their constituent quarks in Figure 1.1. Strangeness and mass increase from one line to the one above. From this model it was possible to predict the existence of the Ω^- particle, its electric charge, hypercharge, and mass. Another success of the model, based on the sub-integral charge of constituent quarks, was the prediction of the magnetic moment ratio of neutron to proton. The predicted value is -0.667 compared

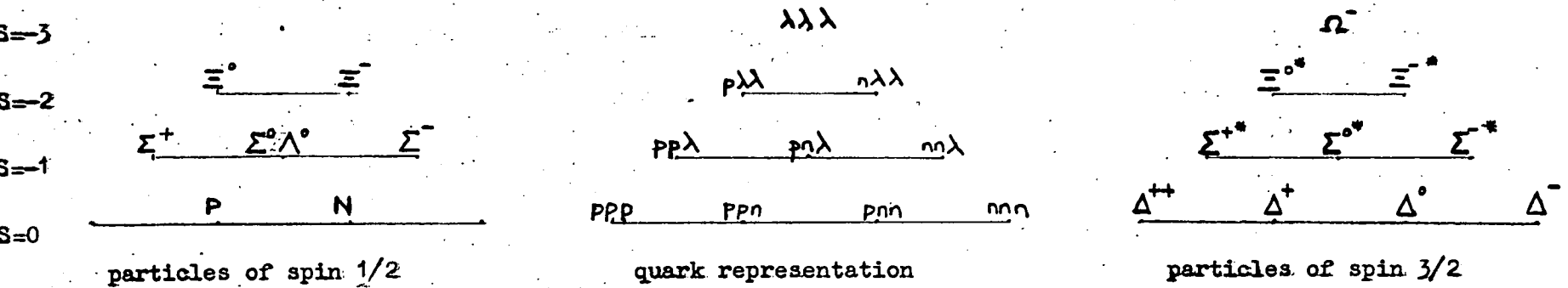

particles of spin 1/2 | quark representation | particles of spin 3/2

Figure 1.1 Schemes for baryons of spin 1/2 & 3/2 showing their quark representations. The lightest particles are at the bottom, the heavier ones are above. The same quark combination can represent different particles because of the different possible alignments of spin.

with the experimental value of -0.685.

Thus unitary symmetry and the quark model have brought an order to the previous chaos of elementary particles and is proving a very useful tool in the theory of elementary particles and their interactions. However, the question remains whether the quark actually exists as a sub-nuclear element which could be detected as such, or whether it is just a convenient mathematical device.

1.2 Searching for quarks

Since the theory of quarks was first produced many experiments have been performed to look for fractionally charged and heavy mass particles. Accelerator experiments carried out at CERN and Brookhaven failed to substantiate the theoretical prediction for the production of quarks. Recently Schiff (1966) has suggested that a selection rule on the interaction of quarks such as requiring the charge (electric or baryonic) of a cluster of quarks to be an integral number would restrict quarks to the nucleus such that they would not be detected. However the negative results of accelerator experiments could be due to the heavy mass of the quark. With present machines giving protons of energy 30 GeV, the energy in the C.M. system of colliding nucleons is ~ 4 GeV. This figure gives, therefore, the lower limit of the quark mass.

For proton energies in excess of 30 GeV workers have turned to cosmic rays. The primary cosmic rays consist of 85-88% protons and

the differential energy spectrum is shown in Figure 1.2, although there is a wide range of energy the rate decreases as $E^{-2.5}$ where E is the kinetic energy in GeV and thus if quarks are produced in proton-air nuclei collisions the majority will be produced close to the threshold energy. The protons diffuse through the atmosphere reaching sea-level after ~5 interactions with ~.05 times their primary energy with a sea-level spectrum shown in Figure 1.2. The majority of secondary particles in the proton-air nuclei interactions are pions and these decay such that the intensity of particles at sea-level contains 70% muons with the spectrum shown in Figure 1.2, the median energy for muons is ~2 GeV. In a manner similar to protons, quarks if produced will also diffuse through the atmosphere losing energy and eventually being absorbed in an air or earth nucleus. The production and propagation of quarks in the atmosphere is considered in Chapter 4.

The cosmic ray experiments have been performed at sea-level, at mountain altitudes, and deep underground. They have all with one exception been scintillation counter telescopes, with minor differences, used in the search for fractionally charged particles. However, up to the start of the present experiment no results had been published for a telescope employing a visual detector for identifying the track of the incident particle. As well as experiments designed to detect incident quarks, experiments have been

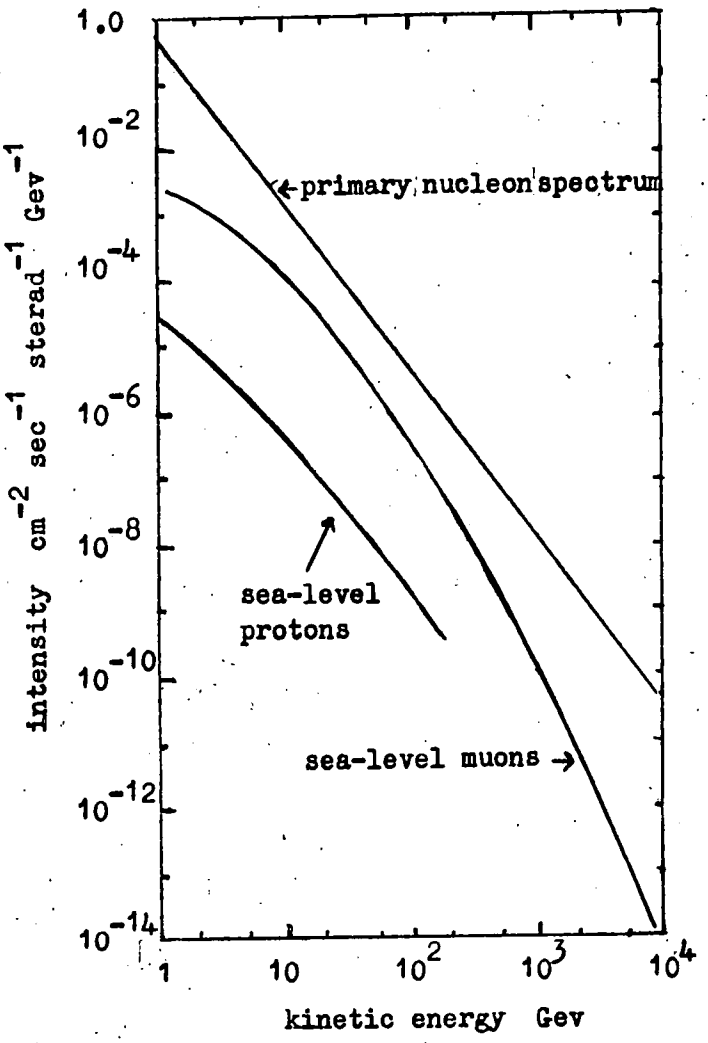

Figure 1.2 Differential spectra of sea-level protons and muons and the primary nucleon spectrum given by:-

$N(E)dE = 0.45E^{-2.5}dE$ per cm^2 sec. sterad. Gev.

performed to search for quarks absorbed in the nuclei of material on the earth's surface including the atmosphere and also in the sun's periphery. The effect of quark production by primary protons on the production of other secondaries has also been studied. A fuller analysis of other experiments is given in Chapter 5.

1.3 The scintillation counter - neon flash tube telescope

The telescope is designed to detect $\pm \frac{1}{3}e$ and $\pm \frac{2}{3}e$ quarks on their equivalent energy loss in a scintillation counter (i.e. $\frac{1}{9}E$ and $\frac{4}{9}E$, where E is the most probable energy loss of a relativistic charge e particle, measured by selecting relativistic muons). Six plastic scintillation counters (140 x 75 x 5 cm^3) are arranged in a vertical stack of aperture 0.47 m^2 sterad. . Pulses from each counter are displayed on a cathode ray oscilloscope which is photographed. Nine trays of neon flash tubes are arranged orthogonally in the stack to give a three dimensional picture of the track of the incident particle and for each selected event both views are photographed separately. The telescope is described in more detail in Chapter 2. The expected pulse height distributions for quarks in a scintillation counter and hence the efficiency of detection is considered in Chapter 3. The results are analysed in Chapter 6 and a summary is given in Chapter 7.

Work performed on a glass plate spark chamber and the localised discharge in neon flash tubes is discussed in Appendices A and B respectively.

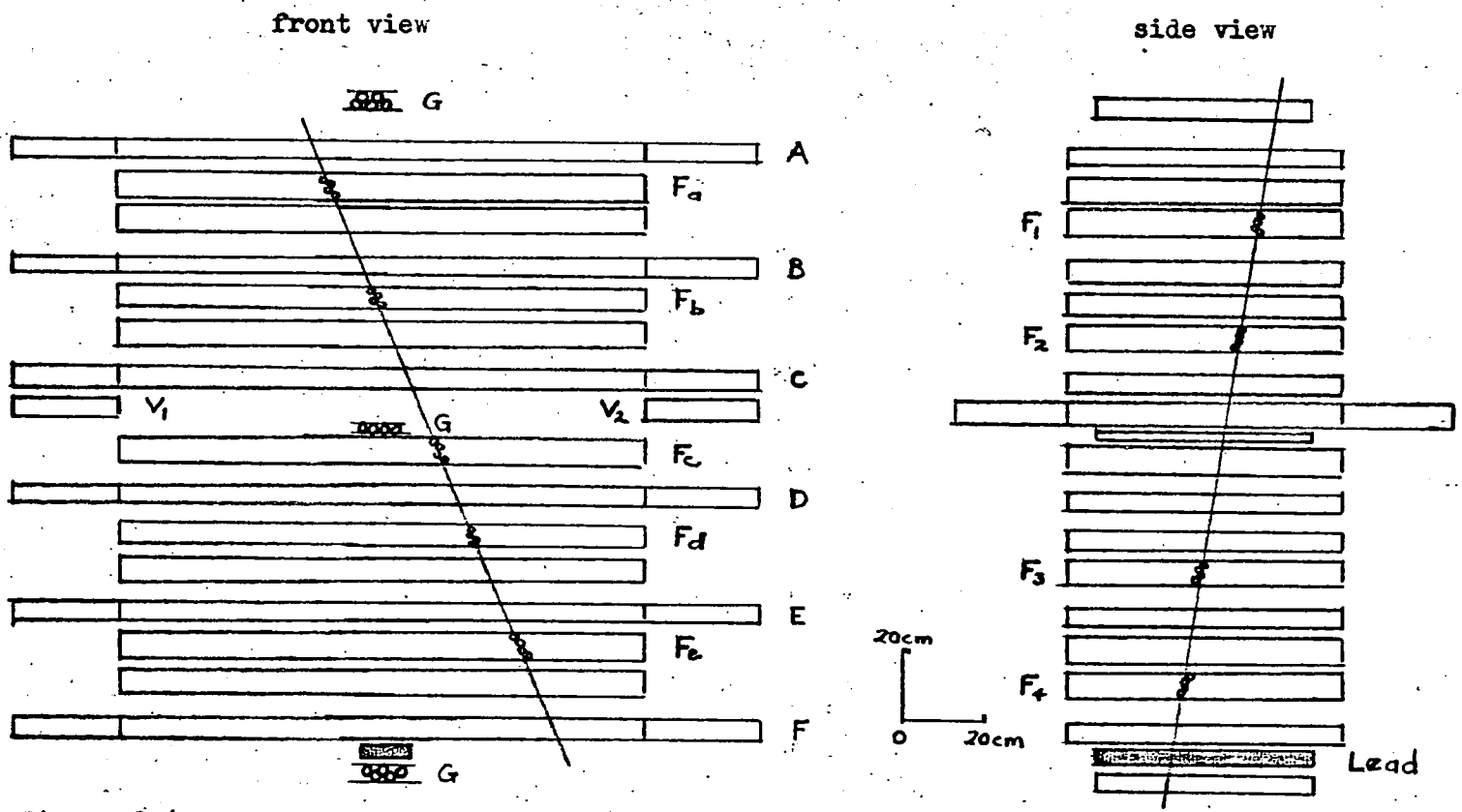

Figure 2.1 Quark telescope apparatus.
6 scintillation counters A-F 2 anticoincidence counters V_1 & V_2
5 flash tube trays in the front view $F_a - F_e$
4 flash tube trays in the side view $F_1 - F_4$
3 geiger trays G.

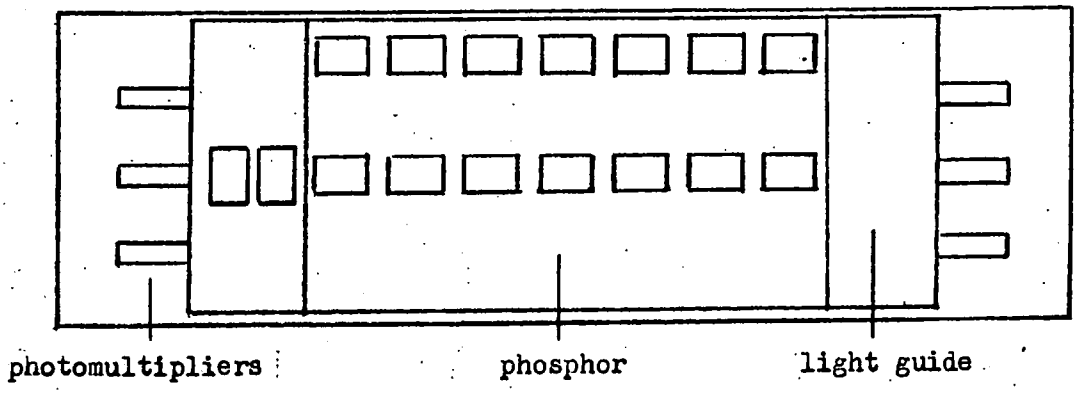

(a) The large counter. The rectangles mark the positions of the small telescope in the measurement of the response of the counter as a function of position.

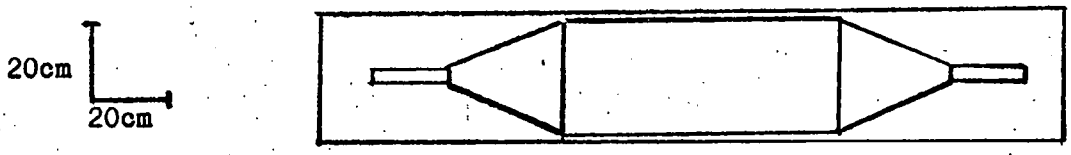

(b) The anticoincidence counter.

Figure 2.2 Scale diagram of the scintillation counters.

area is in contact with the support to facilitate a more efficient transmission of light by total interal reflection.

The six photomultipliers are five Mullard 53 AVP and one 56 AVP, the resistance chains for the dynode voltage supply were chosen for a high gain and are shown in Figure 2.3. A positive supply voltage is applied to the photomultipliers and the output is taken from the anode. This is a negative pulse with a decay time of 100 n sec. The three outputs from one side are fed together into an emitter follower which in turn feeds a 50 Ω system of electronic units designed by the Rutherford High Energy Physics Laboratory (RL 2000 series).

Because of the possibility of Cerenkov radiation in the light guides, two anticoincidence counters (70 x 30 x 5 cm) were placed in line with the light guides as shown in Figure 2.1, labelled V_1 and V_2. The design of these counters is also shown in Figure 2.2. They have trapezoid light guides at the 30 cm edge and each is viewed by two 53 AVP photomultipliers with the same resistance chain as those in the large counter. Each output is fed into an emitter follower which in turn feeds the selection system.

2.1.3 The neon flash tube trays

The flash tubes are of glass painted black except for the viewing end, with an internal diameter of 1.5 cm and are filled with commercial grade neon to 60 cm of mercury pressure. Each tray consists of four layers of flash tubes

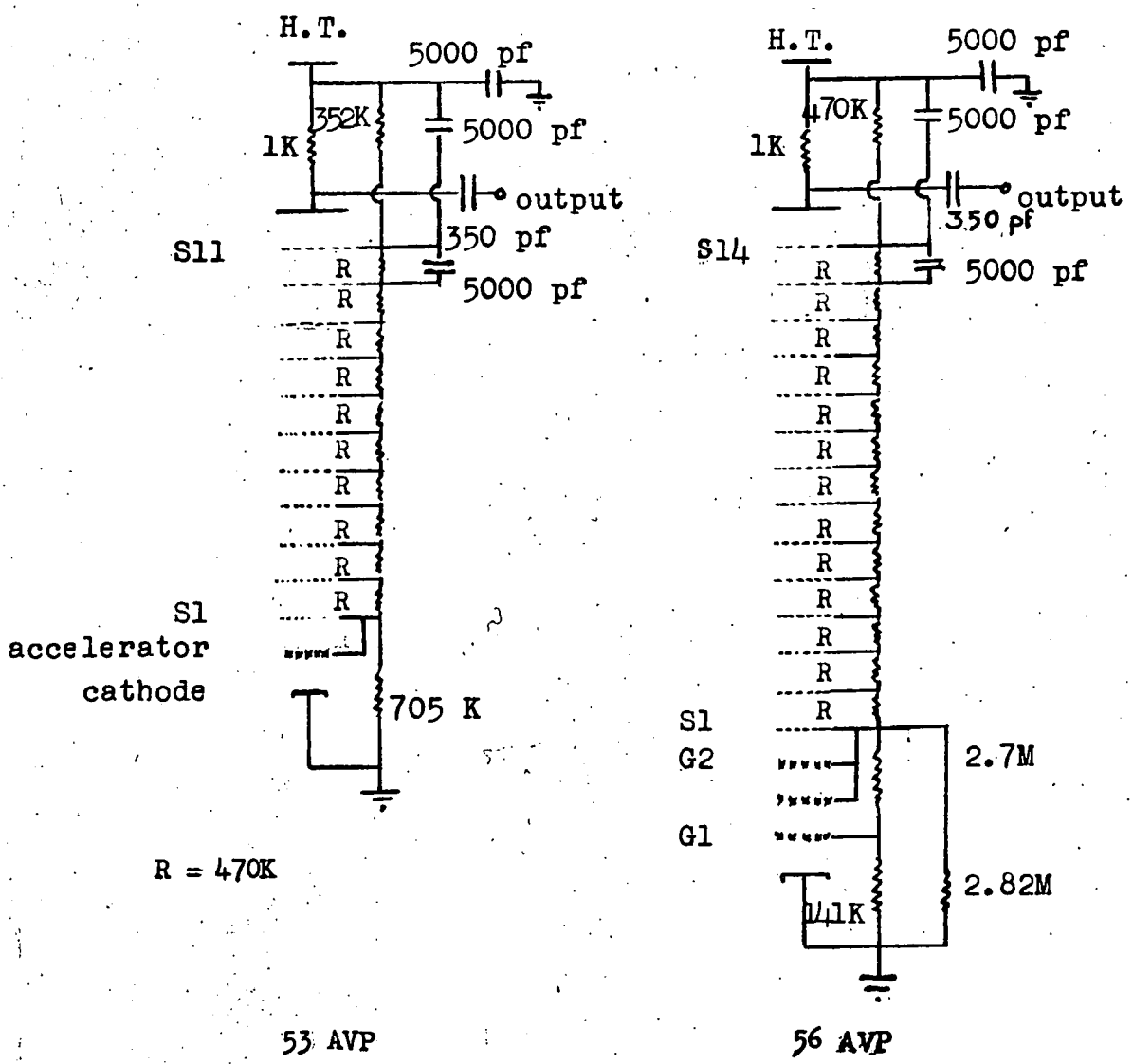

Figure 2.3 Resistance chains for photomultipliers.

which are staggered to ensure maximum track efficiency. The operational area of the trays is the same as that of the phosphor (140×75 cm^2). The flash tubes are supported in a blockboard frame, the top and bottom areas being covered with aluminium foil, these acted as earth plates. The pulsed electrode is an aluminium sheet between the second and third layers of flash tubes.

The 140 cm length of the phosphor is referred to as the front and five trays (F_a - F_e in Figure 2.1) with 77 to 78 tubes per layer are in this view. The 75 cm length of the phosphor is referred to as the side and four trays (F_1 - F_4) with 43 to 44 tubes per layer are in this view. For each event a separate photograph is taken of each view, to aid correlation in scanning a clock is incorporated in each.

The pulsing unit for the flash tubes consists of an 8 kV hydrogen thyratron, a pulse transformer and then an enclosed spark gap (Trigatron CV85) which discharges a bank of condensers through a pulse transformer. The resulting high voltage pulse of magnitude 12 kV, rise time 2 μsec and duration 5 μsec is applied to the central electrode of the nine flash tube trays. A delay of 5 μsec was incorporated before the flash tubes were triggered to avoid pick up on the trace of the cathode ray oscilloscope (C.R.O.) displaying the scintillation counter pulses.

2.2 The selection, display and recording system

To select particles on their energy loss in the scintillation counter, pulses from a counter are accepted if they lie within a certain pulse height region, the system then demands a coincidence from a given number of counters of such pulse heights. Thus basically the system is comprised of discriminators set at given levels followed by a coincidence unit.

The quark search was divided into two parts. The first was a search for $\frac{2}{3}e$ quarks only and this was called the T series. The second was a search for the $\frac{1}{3}e$ and $\frac{2}{3}e$ quarks and this was called the Q series. The logic diagrams for the electronic selection system are shown in Figures 2.4 and 2.5 for the T and Q series respectively. In the T series the selection demanded a five-fold coincidence of counters A B D E F with pulse heights in the range 0.20E to 0.85E. The resolving time of the coincidence circuit was 20 n sec. In the Q series the $\frac{1}{3}e$ quark selection was a six-fold coincidence of pulse heights in the range 0.05E to 0.30E and the $\frac{2}{3}e$ quark selection was a five-fold coincidence of counters A B D E F in the range 0.30E to 0.85E in coincidence with a pulse in counter C $>$ 0.30E. The resolving time of the coincidence in the Q series was 10 n sec. Counter C was independant of the selection in the $\frac{2}{3}e$ quark acceptance so that the distribution of the pulse heights obtained could be compared with those of other counters for a check on possible bias in the selection system.

As well as the output pulse feeding the selection system the pulse was also fed into the display circuit. In the case of the T

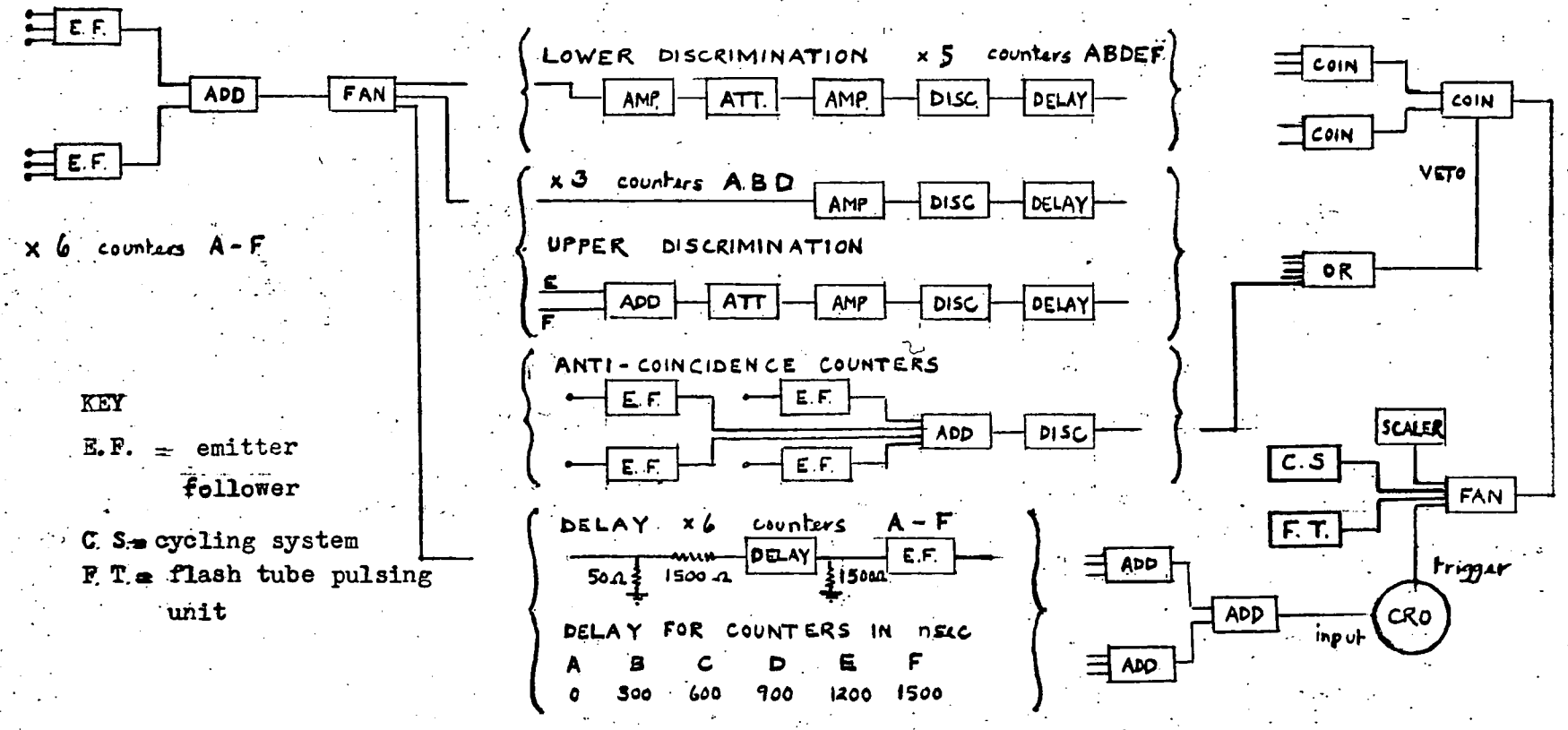

Figure 2.4 Logic diagram for selection in the T series
The circuit diagram for the emitter followers is shown in Appendix C.

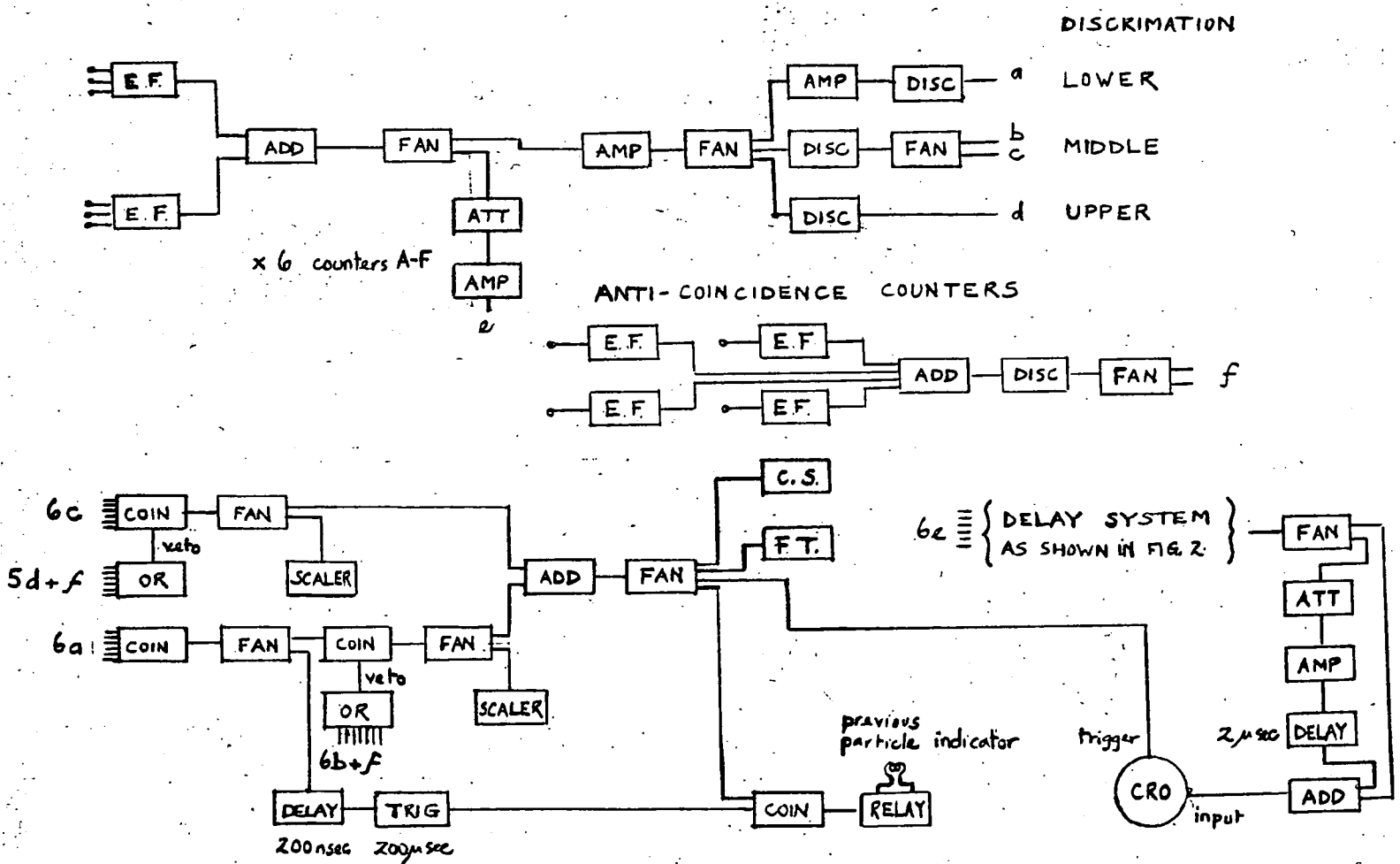

Figure 2.5 Logic diagram for selection in Q series

series the pulses from each counter, A - F, were delayed in increasing steps of 300 n sec and then mixed together. The pulses could thus be displayed on a single trace of a C.R.O. which had been triggered by the coincidence pulse from the selection system. In the Q series, because of a larger range in possible pulse heights, the six pulses were observed directly as in the T series and then were amplified and delayed and displayed again. Typical traces for events in the T and Q series are shown in Figure 2.6, the values $\bar{v}$ and $\alpha/\bar{v}$ %are defined in paragraph 2.3.5. The C.R.O. also incorporated a watch so that the film could be easily correlated to the two flash tube films.

As well as triggering the C.R.O. the coincidence pulse is delayed 5μ sec and triggers the flash tube pulsing unit. The pulse also triggers a cycling system which illuminates the fiducial bulbs and clocks in the front and side flash tube views and the watch in the C.R.O. and finally winds on the cameras in preparation for the next event.

For the acceptance of muons in a C run, described in detail in paragraph 2.3.5, the 0.85E veto is removed from the $\frac{2}{3}$e quark selection. As the rate of muons passing through the telescope is ~ 30 sec^{-1} the cycling system operates a veto on the C.R.O. trigger and the flash tube pulsing circuit so that only one event per frame is obtained.

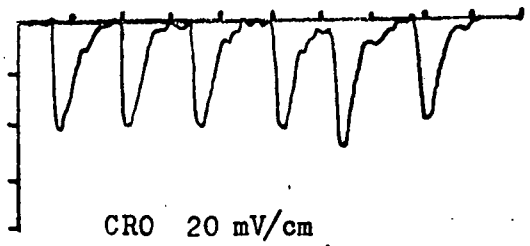

CRO 20 mV/cm
200 n sec/cm

Muon in T7
$\bar{v}$ = 0.85E $\frac{\alpha}{\bar{v}}$ = 4.2%

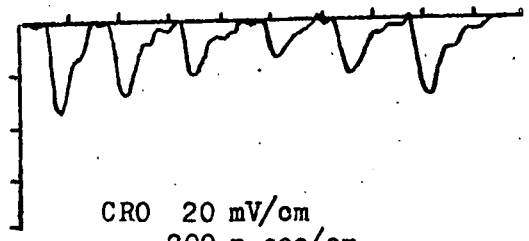

CRO 20 mV/cm
200 n sec/cm

Quark candidate iii in T61
$\bar{v}$ = 0.52E $\frac{\alpha}{\bar{v}}$ = 10.3%

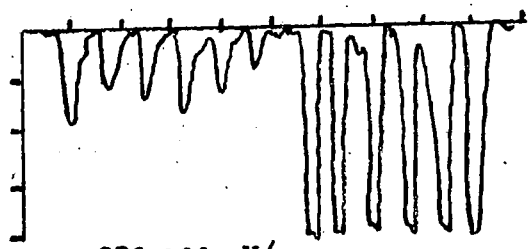

CRO 200 mV/cm
400 n sec/cm

Muon in QU18
$\bar{v}$ = 0.85E $\frac{\alpha}{\bar{v}}$ = 3.2%

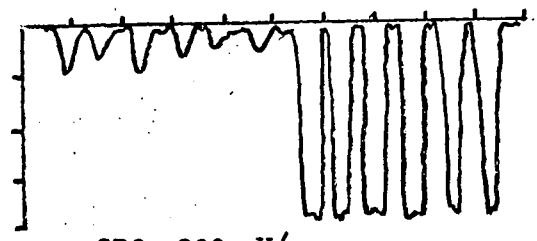

CRO 200 mV/cm
400 n sec /cm

Quark candidate in QU18
$\bar{v}$ = 0.46E $\frac{\alpha}{\bar{v}}$ = 12.5%

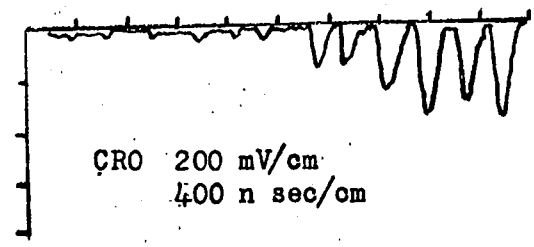

CRO 200 mV/cm
400 n sec/cm

Quark candidate in QL26
$\bar{v}$ = 0.16E $\frac{\alpha}{\bar{v}}$ = 11.7%

Figure 2.6 C.R.O. display pulse forms for T and Q series

Because of the long sensitive time of the flash tubes it is an advantage to have a knowledge of previous particle within that time. This is discussed in detail in paragraph 2.4.2. For the latter half of the μ series a coincidence between a 200μsec pulse triggered by a six-fold event ($>$ 0.05E) delayed by $\sim$ 200 n sec and an accepted event illuminated a bulb in the front flash tube view. This indicated that a particle had traversed the telescope in the 200μsec before the accepted event. The previous particle indicator is shown in relation to the selection system in Figure 2.5. The circuit was designed by Mr. T. Takahashi and is shown in Appendix C.

2.3 The scintillation counter

2.3.1 Introduction

In an experiment of this type where the selection depends on the output pulse height from a scintillation counter the most important parameter is the resolution of the counter. For relativistic muons traversing a counter the output pulse heights will form a distribution. The resolution of the counter is defined as the full width at half height of the distribution expressed as a percentage of its most probable pulse height. The resolution depends on four variables:-

1) the fluctuations in the energy loss of the incident particle in the counter,

2) the response of the counter as a function of the position of the incident particle,

3) the fluctuations in the number of photoelectrons produced in a photomultiplier as the result of a given number of photons collected,

4) the fluctuations in gain of the photomultiplier due to the statistical nature of the electron multiplication process.

This is analysed in Chapter 3 to give the expected distributions for $\frac{1}{3}e$ and $\frac{2}{3}e$ quarks. In this chapter the experimental data obtained in the study of the scintillation counter and the photomultipliers is presented.

2.3.2 Matching the photomultipliers

Before proceeding to measure the response of the scintillation counter it is necessary to match the six photomultipliers of each counter so that the average gain of each photomultiplier is equal. Mismatching would, of course, lead to an increase in the width of the distribution from the counter. This was achieved by placing each photomultiplier in turn (prior to fixing in the scintillation counter) in a light tight box and measuring the output pulse height at different supply voltages due to a fixed source of light. The source of light was a spark generated in the arc discharge of a mercury-wetted relay (Kerns et al. (1959)). The light pulse has a decay time of 3 n sec, the same as that for the phosphor.

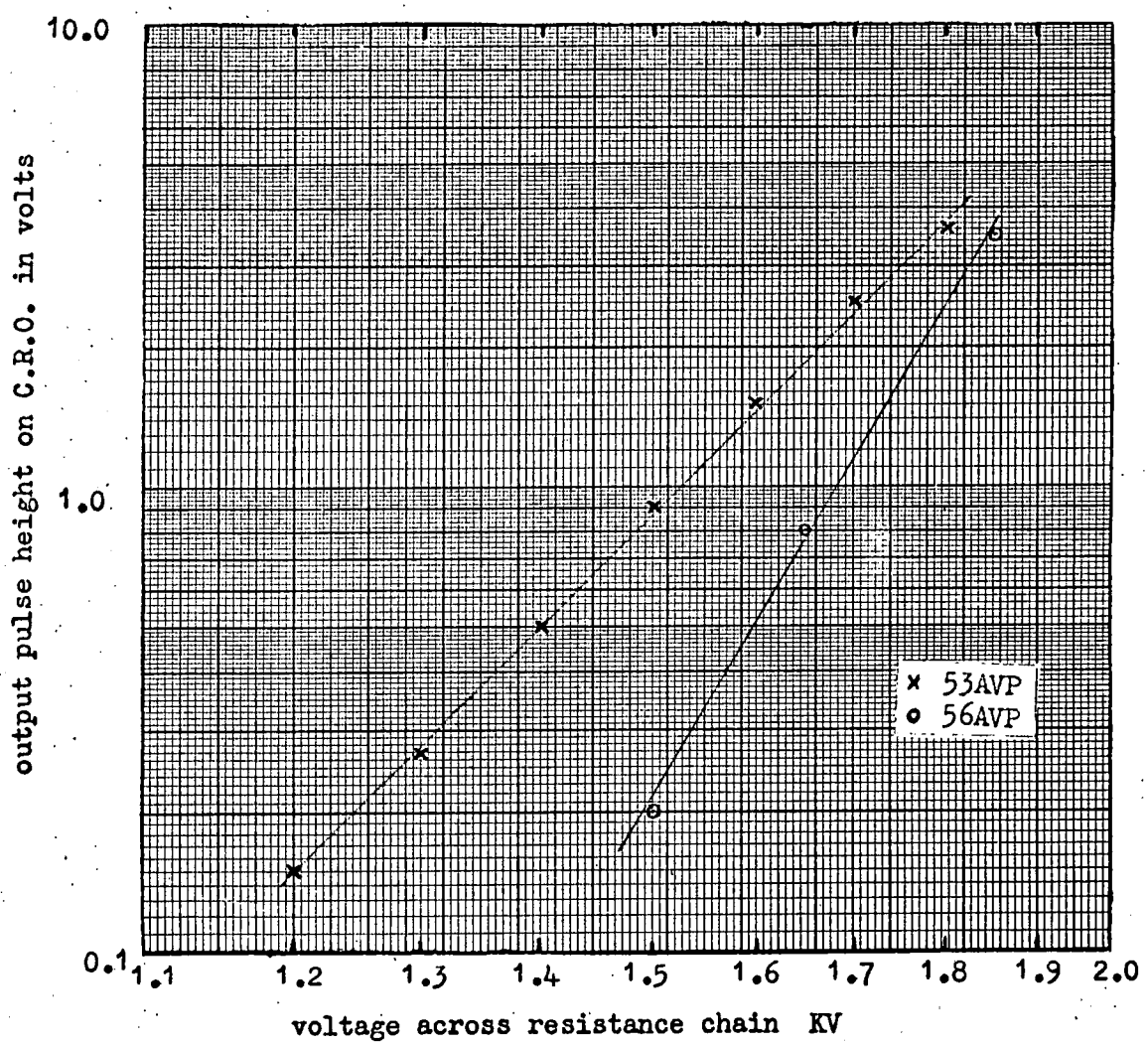

Figure 2.7 Variation of output pulse height with voltage on the photomultiplier.

It was found that although the tubes had differing gains, the variation of gain as a function of supply voltage was the same for the same type of photomultiplier such that the output pulse height in volts H, fits the relation:

$$H = A V^{n}$$

where A is a constant, V is the supply voltage in kilovolts and n is 8 and 14 for a 53 AVP and 56 AVP respectively. Typical curves for a 53 AVP and 56 AVP photomultiplier are shown in Figure 2.7. Thus from these response curves the supply voltage necessary such that all photomultipliers had the same gain could be found.

An important point to note is that over the output pulse height range measured (0.1 to 5.0 volts) the curve shows no saturation effect. From the calibration of the electronics the most probable pulse height from the scintillation counter of a muons distribution would come on this plot at 650 mV and thus over the range of possible pulse heights in a muon distribution, the photomultiplier gives a linear response.

After the photomultipliers were cemented to the light guides and the supply voltages adjusted for equal gain a further check on gain was achieved by selecting particles incident through the telescope by means of a geiger coincidence telescope positioned as shown in Figure 2.1. The coincidence pulse triggered a C.R.O. on which the pulses from each photomultiplier were displayed and their heights recorded. The distributions obtained in this way verified that the

photomultipliers had equal gain.

2.3.3 The number of photo electrons collected in each counter for the passage of a single relativistic muon

As mentioned earlier the response of a counter depends on the total number of photoelectrons collected. The number collected by a counter for the traversal of a single relativistic muon can be estimated in two ways.

The first method depends on the efficiency of the phosphor and the geometrical response of the scintillation counter. From the analysis discussed in 2.3.4 the average fraction of light collected by the six photomultipliers in a counter is 0.05. For a relativistic muon with energy loss in the counter of 9 MeV and an efficiency of the phosphor of 200 eV/photon (Currie et al. (1961)) the number of photons reaching the six photocathodes is 2250. For a conversion efficiency of photons to photoelectrons of 10% (Barnaby et al. (1960)) the number of photoelectrons produced is 225.

The second method depends on the output pulse height of a photomultiplier for a single electron emitted from the photocathode. This pulse height can then be compared with the output pulse height of a counter for the traversal of a relativistic muon and thus give the number of photoelectrons collected. The noise distribution of a photomultiplier in the dark is due to the emission of thermal electrons from the photocathode and to a lesser extent the emission of electrons from the dynodes. The average output pulse height of

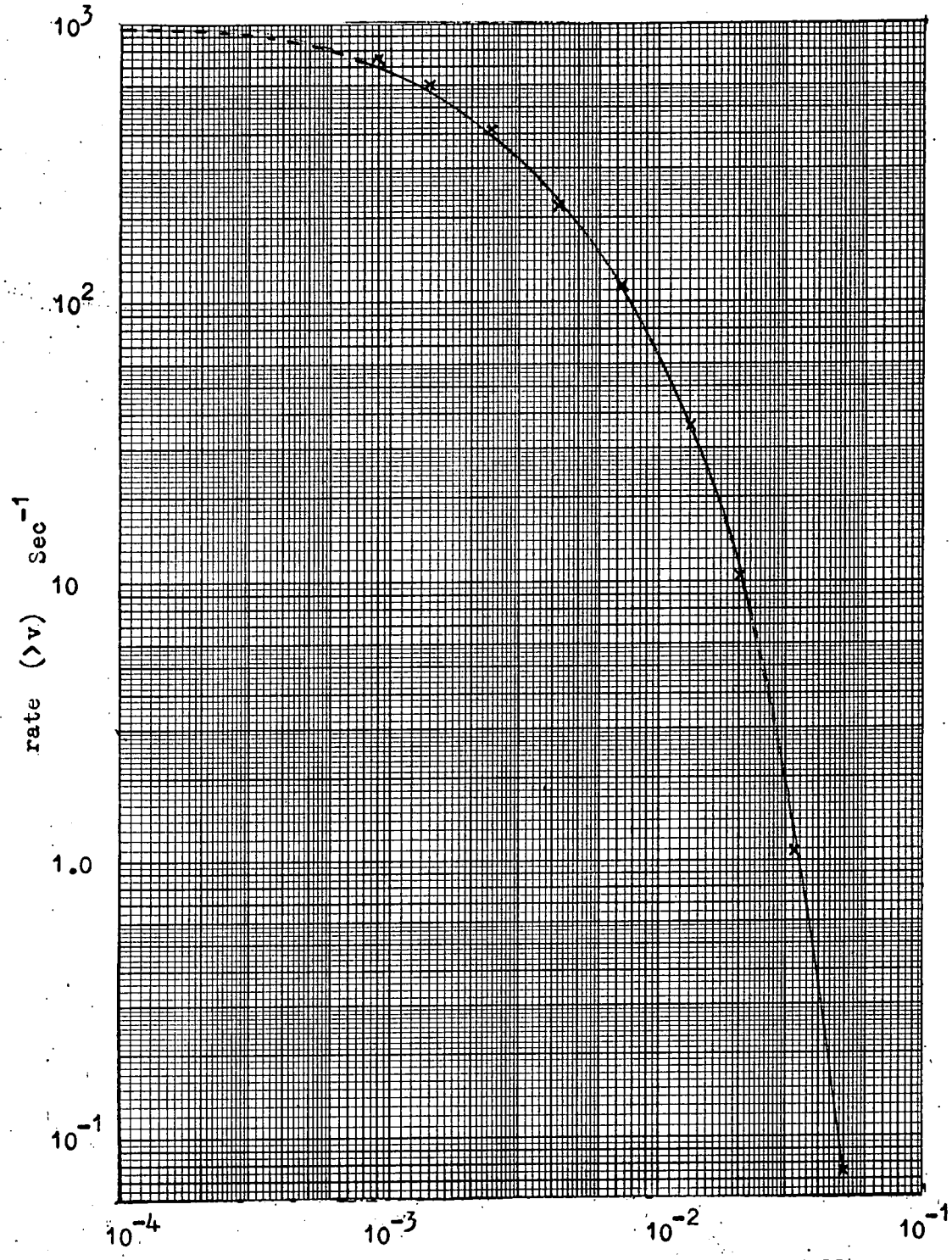

Figure 2.8 Integral noise distribution from photomultiplier 53AVP.

the noise distribution should, therefore, give the pulse height due to a single electron emitted from the photocathode.

This was measured in the following way. A 53 AVP photomultiplier was placed in a light tight box. The output was fed into an emitter follower of one of the telescope counters. The outputs of two of the counters photomultipliers remained connected although their voltage supply was disconnected. The output system of the photomultiplier under investigation was thus the same as any photomultiplier in the telescope. The photomultiplier was operated at 1.75 kV and the output pulses from the emitter follower were fed through a discriminator to a scaler. An integral pulse height distribution was obtained and is shown in Figure 2.5 plotted as a function of pulse height at the input to the emitter follower.

To obtain the differential of this distribution the rate was assumed to tend to a value of 10^{3} sec^{-1} for pulse heights below 10^{-4} volts. The mean of the differential distribution was calculated to be 4.25 mV. The value for the photomultipliers at the gain operated in the scintillation counters is 3.0 mV. Since the electronic system is unchanged the output pulse from the counter for the collection of one photoelectron will also be 3.0 mV. The average output pulse height from the six counters is 650 mV and hence the number of photoelectrons collected is 217. The errors on the value of 4.25 mV are difficult to estimate but the number of photoelectrons

is in good agreement with the previous value. In Chapter 3 a value of 220 is used to evaluate the expected distributions of $\frac{1}{3}e$ and $\frac{2}{3}e$ relativistic quarks.

2.3.4 Linearity of the scintillation counter

An important factor in the acceptance of particles is the linearity of the counter. This was studied for one counter, the response of the three photomultipliers at one end being measured as a function of the position of particles traversing the counter. This was achieved by selecting muons with a scintillation counter telescope comprising of two plastic scintillation counters of area 15 x 10 cm^2. The coincidence pulse was used to trigger a C.R.O. and the pulse from the counter was observed and the height measured. Pulse height distributions were obtained for muons incident along the centre line and a line 25 cm from the centre for the positions shown in Figure 2.2. The telescope was also positioned above the light guide nearest to the detecting end and the response due to Cerenkov light in the perspex was obtained.

The results for the centre line are shown in Figure 2.9 compared with the result published by Ashton et al. (1965). The response for the line 25 cm from the centre line was found to be within 10% of that for the centre. The total response of the counter is the sum of the curve shown in Figure 2.9 and its mirror image about the centre point. The maximum non-uniformity for a counter is defined as:

$$\frac{R_o - R_M}{R_M} \times 100\%$$

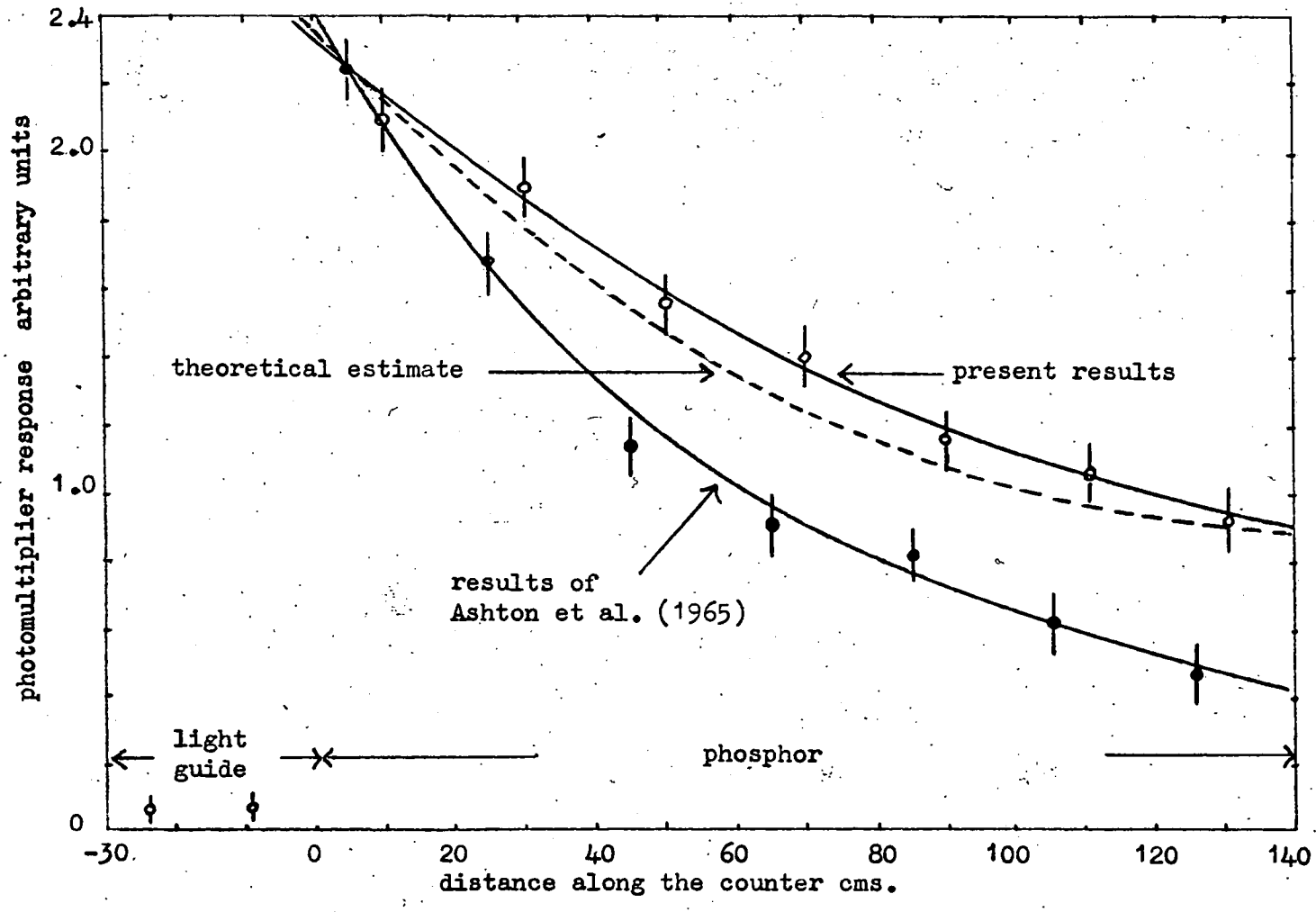

Figure 2.9 Response from one end of the scintillation counter as a function of position of incident particles along the centre line. The theoretical estimate and the results of Ashton et al. (1965) are normalised to the best line at 5cms. The response due to Cerenkov light in the light guide is also shown.

where R_o is the total response at the nearest point in the phosphor to the photomultipliers and R_M is the total response in the middle of the counter. From the above result the maximum non-uniformity for the counter is 20% compared with 30% for the counter of Ashton et al. Two possible explanations for this are that the quality of the phosphor is improved and the geometry of the light guides is different.

The Cerenkov light is seen to be down by a factor ~ 36 on the average response of the counter. Hence Cerenkov light should not effect the selection in the quark runs. However, the anticoincidence counters still serve a useful function in reducing the number of events due to photoelectron showers.

A theoretical analysis of the response of a counter is possible by considering the amount of light collected by one photomultiplier as a function of position along the counter. The light collected is direct and that total internally reflected off the four sides (other than the photomultiplier edges) of the counter. Hence the cone of possible light for collection is limited by the refractive index of the perspex and phosphor (1.58) to an angle of 48° to the line between the point and the photomultiplier. The photomultipliers cover the whole depth (5 cm) of the counter and hence the greater proportion of light collected will be due to reflections on the large area (140×75 cm^2) surfaces.

If the area of the photomultipliers is A cm^2 and the depth of the counter d cm, the solid angle subtended at a distance x cm due

to direct light is:

$$\Omega_o = \frac{A}{x^2}$$

for the first reflected image:

$$\Omega_1 = \frac{A}{x^2 + d^2} \times \frac{x}{(x^2 + d^2)^{1/2}}$$

and for the n^{th} reflected image:

$$\Omega_n = \frac{A}{x^2 + (nd)^2} \times \frac{x}{(x^2 + (nd)^2)^{1/2}}$$

The absorption of light by the phosphor and perspex will effectively reduce this solid angle by a factor:

$$e^{-(30^2 + (nd)^2)^{\frac{1}{2}}/\lambda_{LG}}$$

in the light guide, where λ_{LG} is the absorption length of the light guide,

and $e^{-((x-30)^2 + (nd)^2)^{\frac{1}{2}}/\lambda_p}$

in the phosphor, where λ_p is the absorption length of the phosphor.

The response from a given point will be the sum of the solid angles over all possible reflections. This was done for λ_{LG} = 100 cm (Brini et al. 1955) and λ_p = 200 cm and the result is shown in Figure 2.9 normalised to the best fit of the experimental points at 5 cm (2.0 arbitrary units ≡ 0.15 steradians). The average amount of light collected by six photomultipliers is 0.6 steradians and hence the fraction of light collected in the counter is $0.6/4\pi = 0.05$.

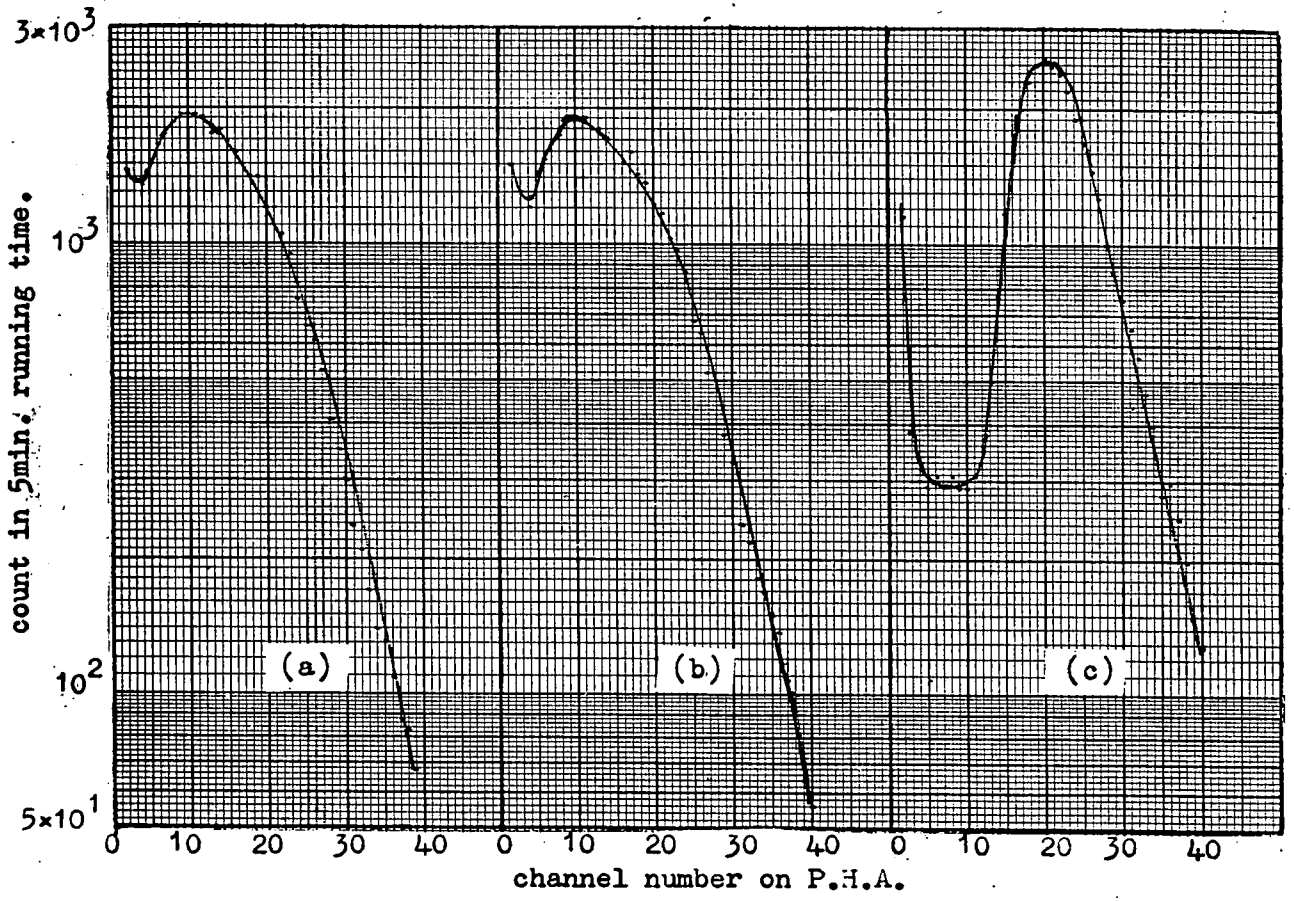

Figure 2.10 P.H.A. distributions of a scintillation counter. (a) & (b) are distributions from each emitter follower (c) is the distribution obtained after both outputs had been added. Channel 20 correspohds to a pulse height at the input to the emitter follower of 750mv.

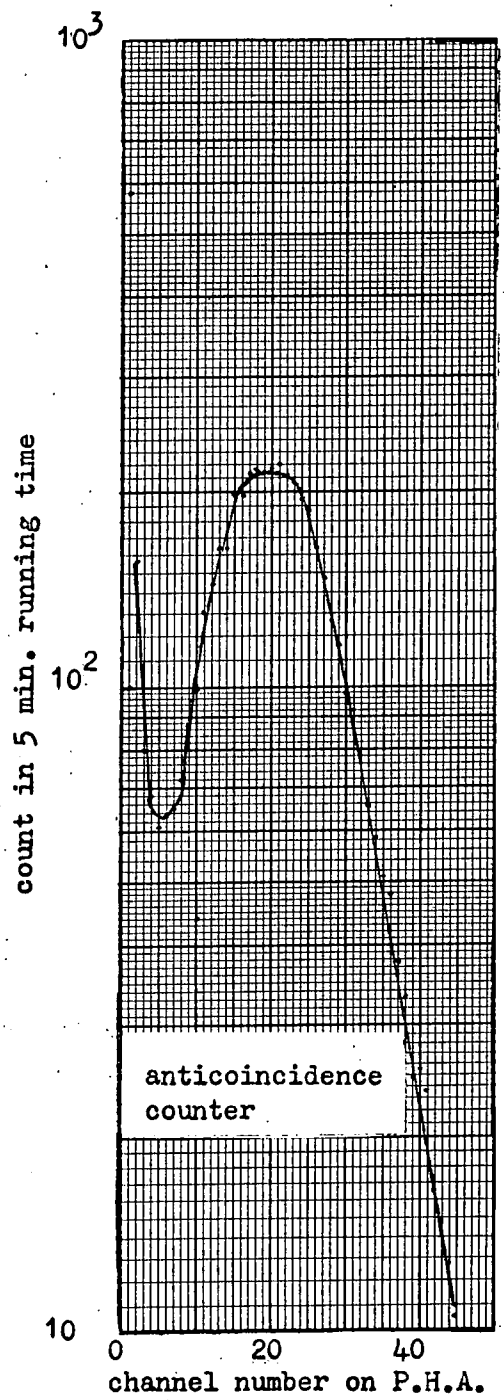

Figure 2.11 P.H.A. distribution of the anticoincidence counter with both emitter follower outputs added. Channel 20 corresponds to a pulse height at the input to the emitter follower of 500mv.

2.3.5 Muon distributions in the scintillation counter

Three types of muon distributions were obtained. The first was with the use of a pulse height analyser, (P.H.A.). In this case the distributions were obtained by feeding the output from the emitter follower directly into the P.H.A. without any gating selection so that a distribution of incident particles of all possible energies, angles and position in the counter was obtained. The distribution from the two emitter followers of a counter was obtained separately and also the distribution after the outputs of the emitter followers had been added. This was done for all six counters and the result for one counter is shown in Figure 2.10. It is seen that the distributions from each emitter follower have the same shape with a width at half height $\sim$ 180%. The distribution of the sum of both shows an expected increase in the most probable pulse height of a factor two and a width at half height of 55%. The distributions from the anticoincidence counters were obtained with the emitter follower outputs at each end added and the result for one counter is shown in Figure 2.11.

The second type of distribution was obtained by selecting muons incident through the stack by removing the veto on the $\frac{2}{3}$e quark selection, i.e. demanding a six-fold coincidence of pulse heights $>$ 0.30E in the case of the Q selection. This is called a C run and was used throughout the T and Q series as a calibration of the

counters to obtain the value of E, that is the most probable pulse height at the input of the emitter follower due to a relativistic muon traversing the counter.

As in the T and Q series the pulses from the six counters were displayed on a C.R.O. and photographed. After processing the film was scanned and the heights of the pulses measured in volts. Distributions of the pulse heights obtained were plotted for each counter and the medians found. Using the pulse generator calibration from the input of the emitter follower to the output on the C.R.O. for each counter these pulse heights and the median values are converted to pulse heights in volts at the input of the emitter follower. The median values obtained are used to normalise the response of counters B to F to that of counter A. Thus distributions are obtained of the output pulse height in volts for each counter. These distributions can be added (because of the normalisation) to give a distribution for all six counters, this has the advantage of having better statistics.

The pulse height distributions from the counters are skew because of the nature of the energy loss processes in the counter. The most probable pulse height E is less than the median value E_M, from the distribution for all six counters the following relation is obtained:

$$E_M = (1.12 \pm .02)E$$

This is used to find the most probable pulse height for the single

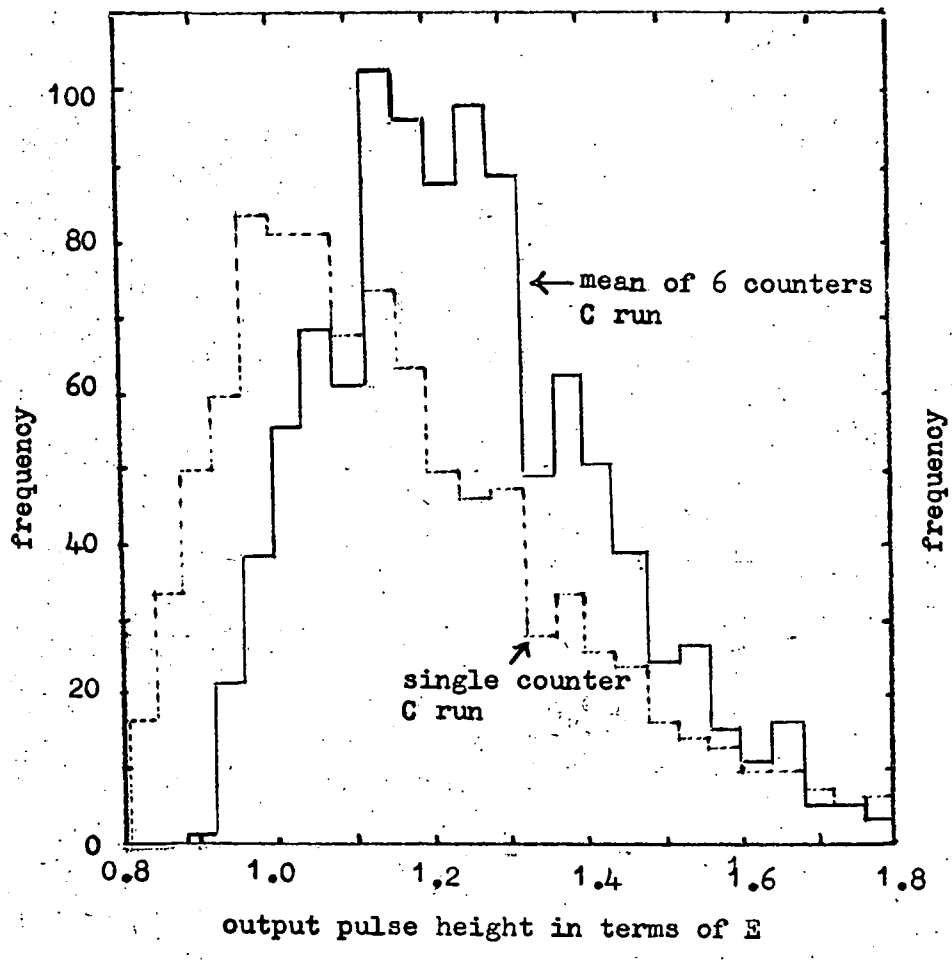

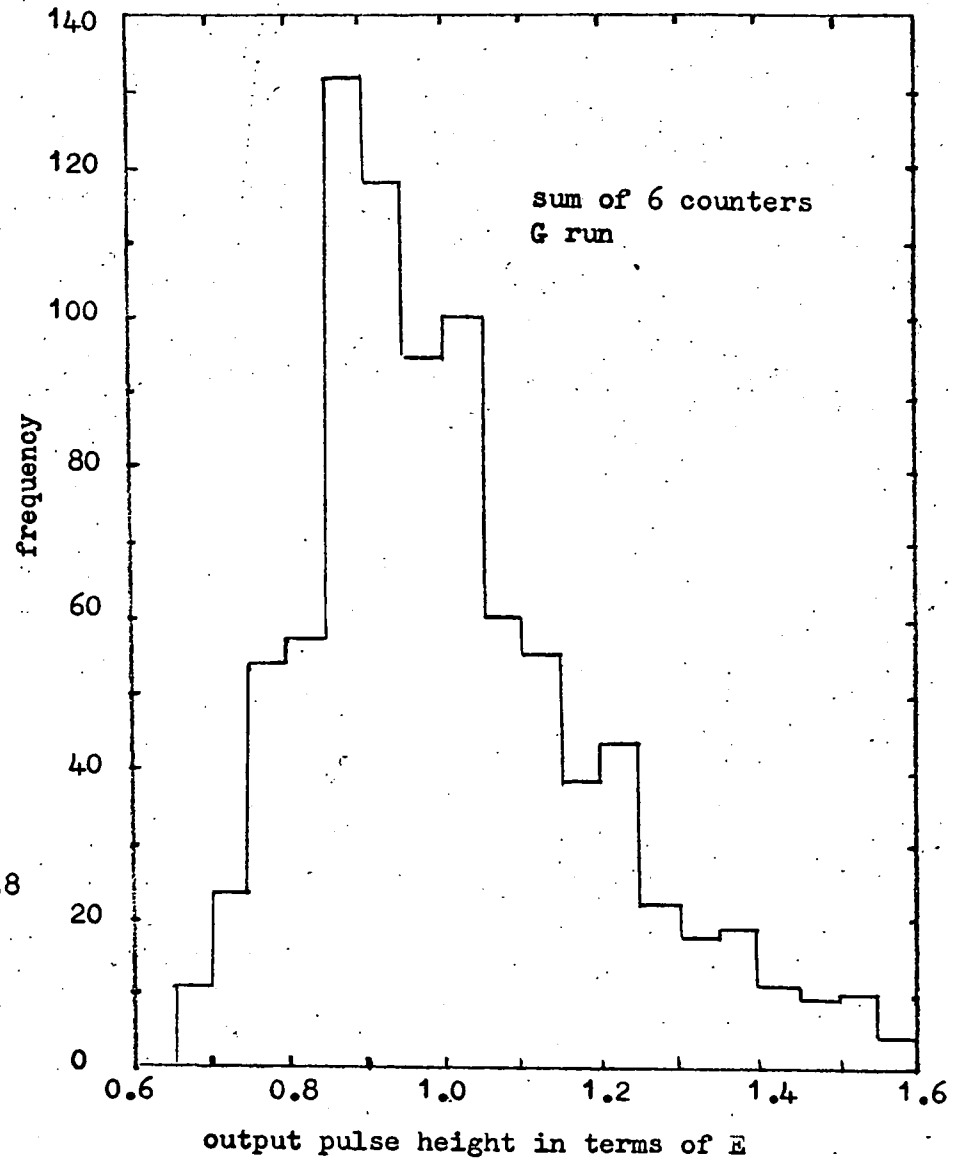

Figure 2.12 Muon pulse height distributions obtained in C & G runs.

counter distributions and the pulse height distributions at the input to the emitter follower are finally given in terms of E. Such a distribution for one counter is shown in Figure 2.12, the other counters have the same shape with resolution within 40 $\pm$ 3%.

Besides computing the pulse heights, x_n for counters n = A-F, the mean of the six pulse heights $\bar{v}$, the standard error on the mean $\propto$ and the value $\propto/\bar{v}$ %were calculated where:

$$\propto^2 = \frac{1}{30} \sum_{n=A-F} (x_n - \bar{v})^2$$

Because the single counter distribution is skew, the mean of the six counter distributions will show an increase in the most probable pulse height. The distribution of the mean is compared with that for a single counter in Figure 2.12, the most probable height of the mean distribution is 1.2E compared with E for a single counter. In Chapter 3 the expected distributions for $\frac{1}{3}$e and $\frac{2}{3}$e quarks for a single counter are derived. These are more Gaussian in shape because of the photomultiplier fluctuations and the mean of these distributions shows no such increase in the most probable pulse height. Hence the expected most probable value of $\bar{v}$ for $\frac{1}{3}$e and $\frac{2}{3}$e relativistic quarks is 0.11E and 0.44E. The value $\propto/\bar{v}$ %is a measure of the width of a particle distribution and is used in the analysis of the quark candidates as a measure of the singularity of the six counter pulse heights. A distribution of $\propto/\bar{v}$ % for muons obtained in a C run is shown in Figure 2.13, the most probable value is ~7% and only 3%

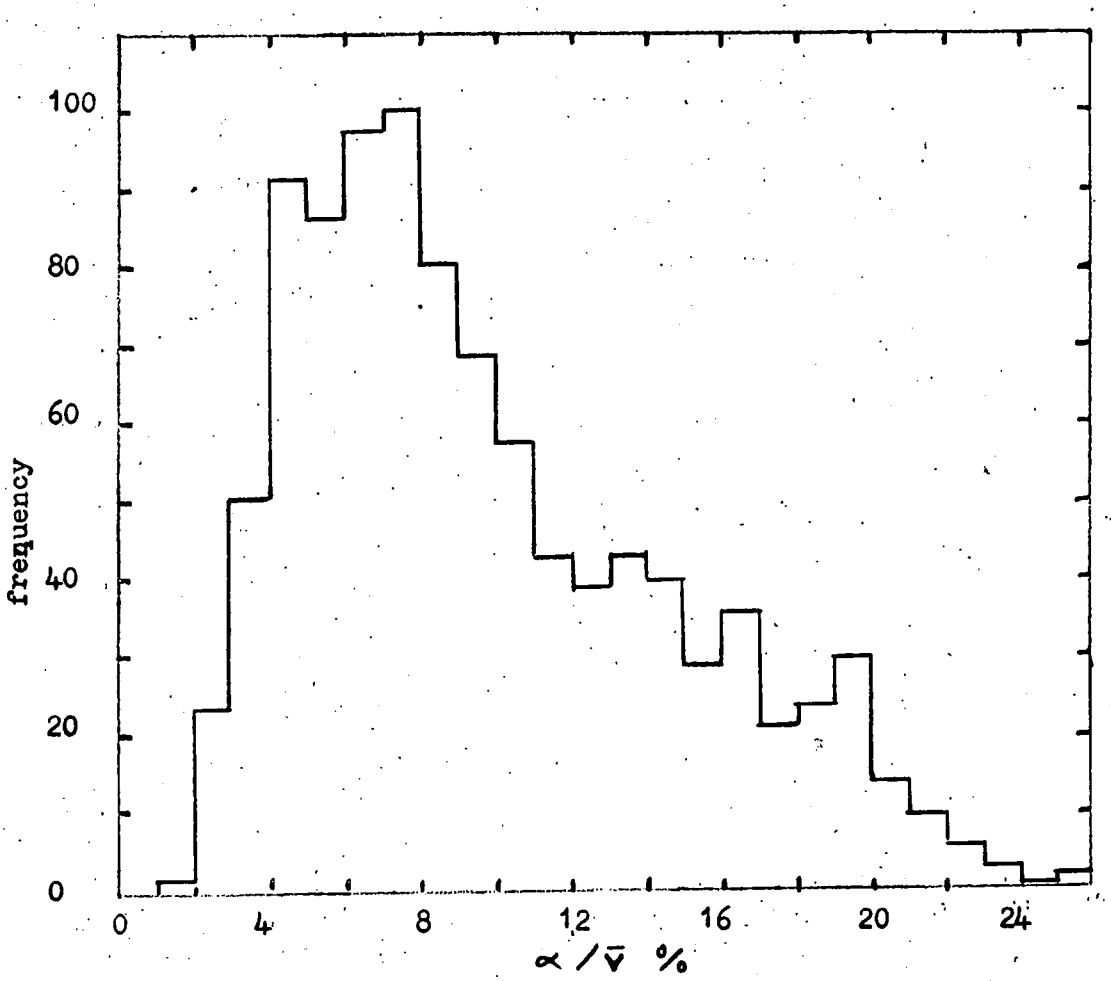

Figure 2.13 Frequency distribution of $\alpha/\bar{v}$ % for muons accepted in C run.

of muons have $\alpha/\bar{v} > 20\%$.

As the C run muons are used to define E for relativistic particles a check on any possible effect due to lower energy particles was investigated. This was done by using the third type of muon distribution. Muons were selected by a geiger coincidence positioned as shown in Figure 2.1. Above the bottom geiger tray was placed 5 cm of lead. Together with the material in the stack, this would cut out muons with $\beta < 0.96$ and so all muons would have minimum ionisation to within 3%. This type of acceptance was called a G run. Pulse heights in volts were measured at the C.R.O. for all counters and figure 2.12 shows the distribution obtained from all six counters with the pulse heights given in terms of E. The width of the G distribution for all six counters is 25% compared with the width of the C distribution for all six counters of 40%. The most probable pulse height for the C distribution is up by a factor 1.1 on that for the G distribution. This could be due to the effect of non-relativistic particles, however two other factors also have an effect. These are due to selection of the runs, in the G run muons are selected in the centre of the counter where the response is a minimum and they are also restricted in angle. In the C distribution, muons are incident over the whole area of a counter leading to a higher response and they are also incident over larger angles. Comparing the response at the centre of the counter with the average response gives a factor $1.08 \pm .01$. For a C and G run the distribution of angle in the front

view was measured and the ratio of the medians was 1.05 ± .01. If these are subtracted in quadrature from the difference between the C and G runs the effect of non-relativistic muons is $3.5^{6.0}_{0}$% and so the C distribution can be taken to present relativistic muons.

2.4 The neon-flash tubes

2.4.1 Efficiency of the neon flash tubes

The two important factors in the use of the visual technique are the efficiency of the flash tubes for $\frac{2}{3}e$ and $\frac{1}{3}e$ quarks and the efficiency for charge e particles as a function of time delay between the passage of the incident particle and the application of the field, i.e. the sensitive time of the flash tube, This latter parameter leads to tracks due to previous particles appearing in accepted events, this is studied in greater detail in the next section.

The efficiency as a function of time delay can be measured and with a knowledge of the diffusion and absorption of the electrons produced by the ionising particle the probability of producing a flash can be found and thus the efficiency for $\frac{1}{3}e$ and $\frac{2}{3}e$ quarks predicted.

Lloyd (1960) has applied a theoretical treatment to the production and recombination of the discharge electrons and gives the expected efficiency as a function of time delay for an adjustable parameter, afq, where a is the internal radius of the flash tube,

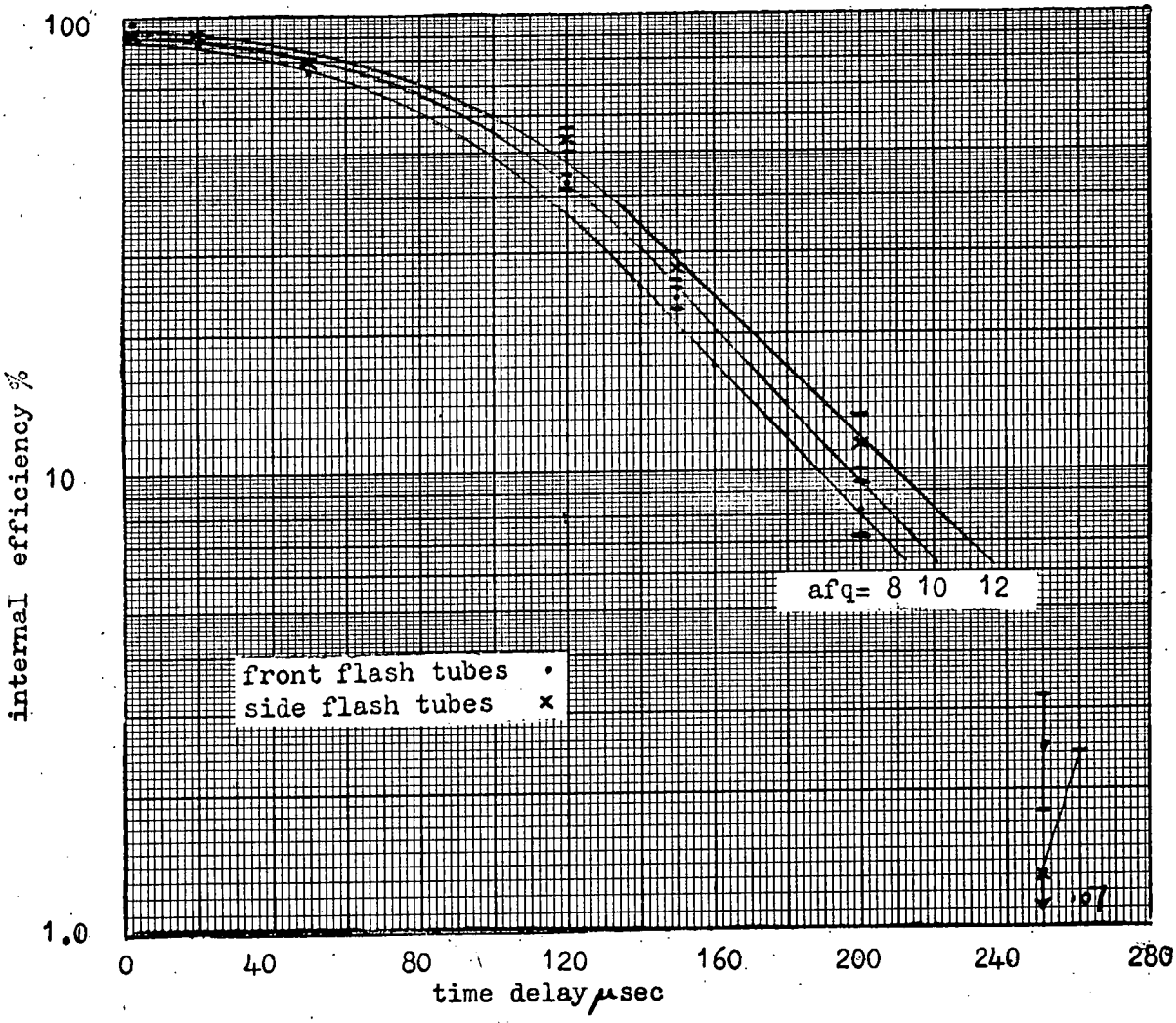

Figure 2.14 Comparison of experimental data and theoretical curves due to Lloyd for the efficiency of flash tubes for charge e particles as a function of time delay.

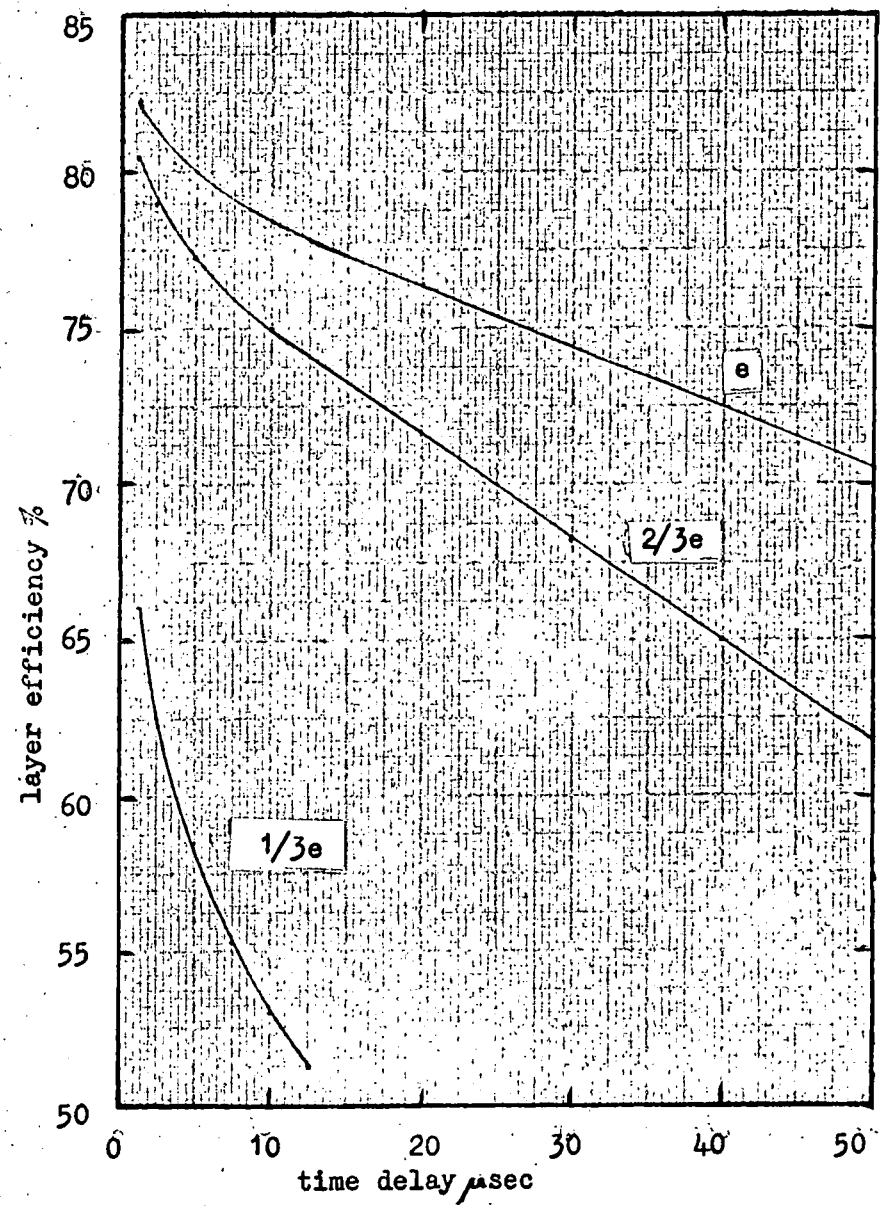

Figure 2.15 Theoretical layer efficiency for charge e, 2/3e, and 1/3e particles in the flash tubes.

f is the probability of one electron in the tube initiating a discharge,

and q is the probability of producing a free electron per cm.

Muons were selected as in a C run and photographs of the front and side flash tube views obtained for delay times between the incident particle and application of the field in the range 5 to 250 μsec. The layer efficiency of the tracks was obtained and this was converted to the internal efficiency of the flash tube and the results plotted as a function of time delay compared with the theoretical curves of Lloyd for afq values of 8, 10 and 12 in Figure 2.14.

The value of afq = 12 was assumed to represent the characteristics of the flash tubes used in the stack. Since, for a given set of flash tubes, the only variable parameter is q and $q \propto (ze)^2$, the values for $\frac{2}{3}e$ and $\frac{1}{3}e$ quarks are 5.3 and 1.3 respectively. The theoretical curves for these values are shown in Figure 2.15 in terms of layer efficiency. At the delay time of 5 μsec used in the T and Q series the layer efficiency for muons and $\frac{2}{3}e$ quarks is $\sim$80% and for $\frac{1}{3}e$ quarks is $\sim$60%. Thus in the detection of quarks the flash tubes should indicate a well defined track.

2.4.2 Previous particle tracks in the flash tubes

From the efficiency-time delay curve shown in Figure 2.14 the time for the efficiency to fall to the minimum definition of a track (i.e. 3 flashes in a straight line in different layers) is

$\sim 170\,\mu$sec. For the rate of muons through the telescope of 30 sec^{-1}, the number of triggered events for a previous particle track will be ~ 200. For an experimental verification of this value the field was applied to the flash tube trays at random and the front and side flash tube views were photographed. The film was scanned for a track (as defined above) in geometry in both the front and side views. From the 1148 frames obtained the number of tracks was 8. The flash tube diagrams for these tracks are shown in Figure 2.19 to 2.22 at the end of the chapter. From this data the number of frames per previous particle track is 144 ± 51.

As previously mentioned, a previous particle indicator was incorporated in the selection system for the latter half of the Q series. In the Q lower selection 8 previous particles were indicated in 1391 events, i.e. the number of frames per previous particle track is 174 ± 62. The flash tube diagrams for these track events are shown in Figures 2.23 to 2.26.

An important parameter used later in the analysis of the quark candidates is the merit factor N/M for a track, where N is the total number of flashes in the track and M is the number of background flashes. For a layer efficiency of 80%, $N = 16$ in the front view and $N = 13$ in the side view. For any trigger of the flash tube stack there will be a number of background events due to the remaining ionisation of previous ionising particles. The mean value of the

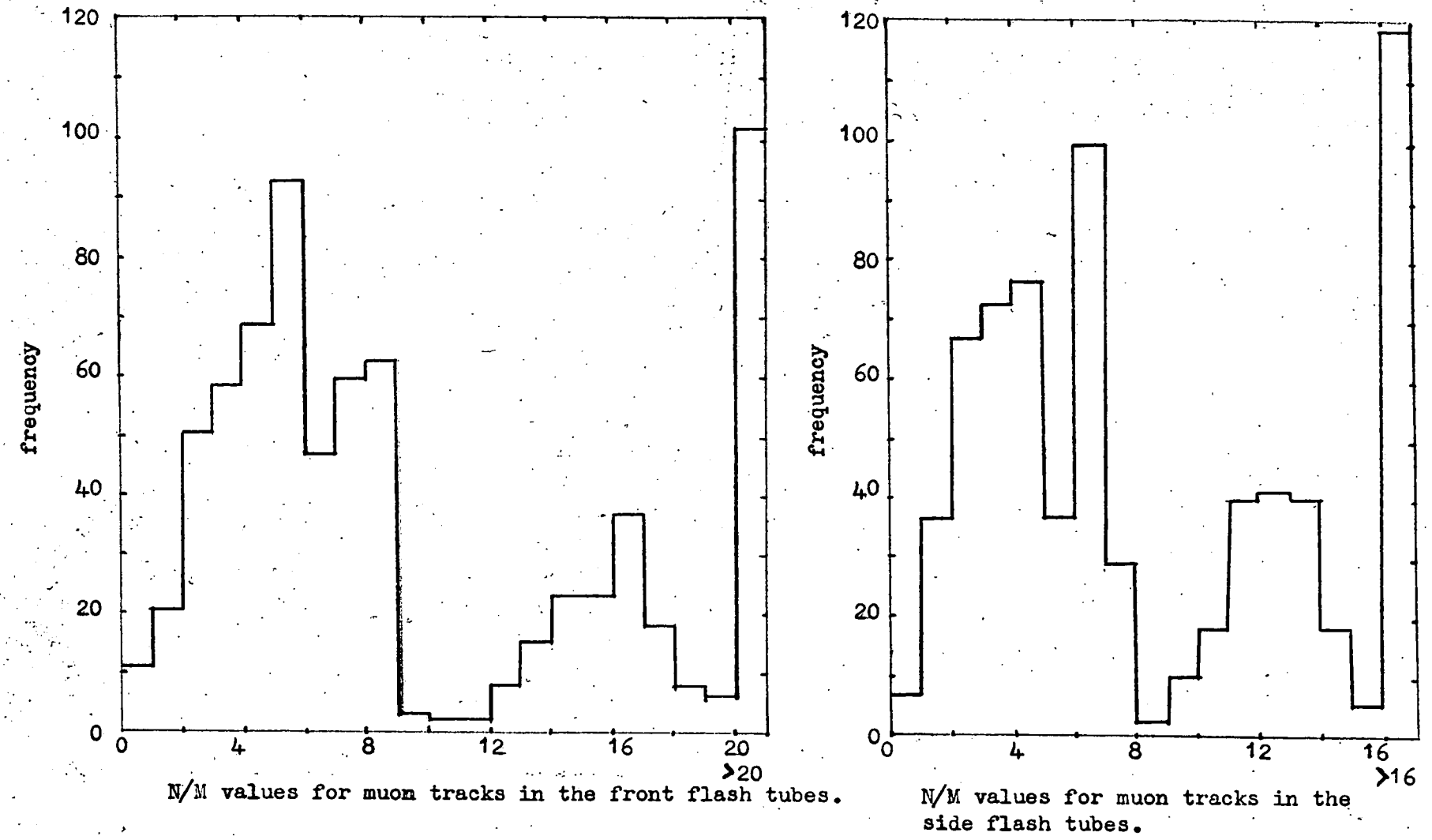

Figure 2.16 Frequency distributions of the merit factor N/M for muon tracks in the front and side flash tube views.

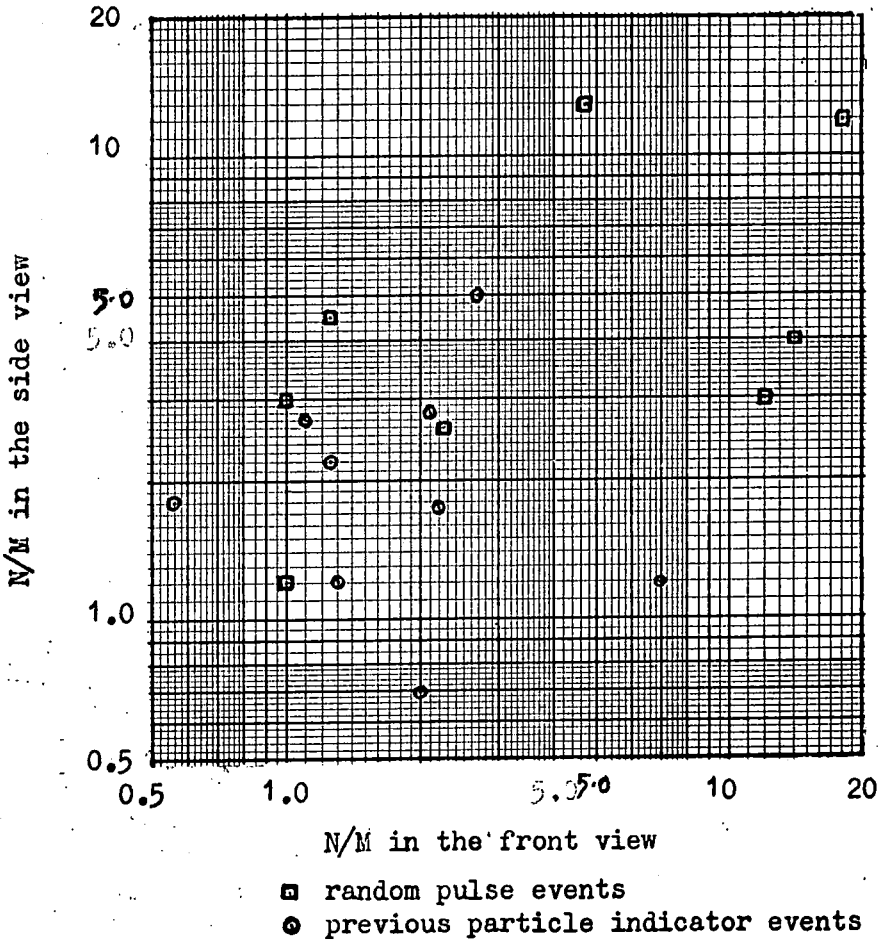

Figure 2.17 Scatter plot of N/M values for tracks obtained in the random pulse run and in the Q lower series where a previous particle was indicated.

background flashes in the front and side views is 3.4 and 2.6 respectively and therefore the mean values of N/M should be 4.7 and 5.0 respectively. However since the variation in the number of background flashes is large, this will be shown in the values of N/M. For muons accepted in the Q series the values of N/M were measured for the front and side views and the result is shown in Figure 2.16 as a frequency distribution of N/M. In the front view 4.5% of events have N/M $\leqslant$ 2.0 and in the side view 6.1% of the events have N/M $\leqslant$ 2.0 and hence 90% of muons have tracks with N/M $>$ 2.0. Since the efficiency of the flash tubes for $\frac{2}{3}$e and $\frac{1}{3}$e quarks relative to that for muons is 1.0 and 0.75 respectively, the 90% limit of N/M will be 2.0 and 1.5 respectively.

The N/M values for the 16previous particle tracks shown in Figures 2.19 to 2.26 are calculated and are shown on a scatter plot in Figure 2.17. This plot is used in Chapter 6 to distinguish previous particle tracks in the quark candidates.

2.5 Running checks during the T and Q series

As mentioned previously the pulse heights measured in scanning are converted to pulse heights at the input of the emitter follower in terms of E and thus a calibration for E and the electronic system is needed. The electronics were calibrated by feeding a pulse generator pulse of 100 n sec width into the emitter follower of each counter and measuring the output on the C.R.O. This calibration was

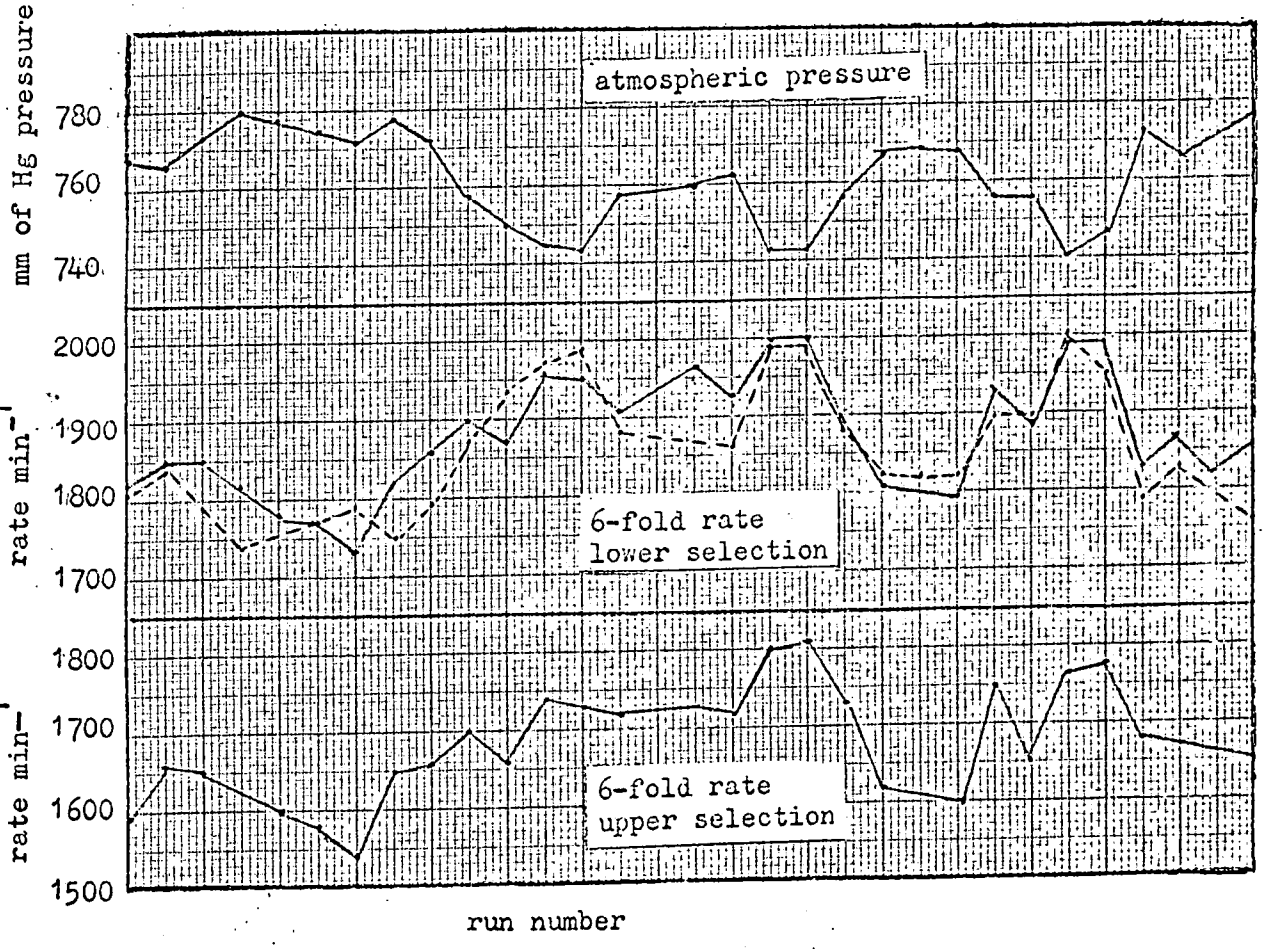

Figure 2.18 Comparision of lower and upper selection 6-fold rates in the Q series with atmospheric pressure.
The dotted line represents a variation of 3.5% about 1870 min^{-1} for 1cm variation from 76 cm of Hg pressure.

checked before every run. The value of E for each counter was obtained with a C run as described previously, this was done every fortnight.

As a further check on the response of the counters and discrimination levels, the counting rates of all the counters above all the levels were measured before every run together with the six-fold, six-fold with anticoincidence, and anticoincident rates. The six-fold rates showed fluctuations but these are seen to be due to the barometric effect. A sample of the six-fold variation is shown in Figure 2.18 for the lower and upper levels in the Q series together with the variation in atmospheric pressure. The barometric coefficient is a decrease of 3.5% in rate for an increase of 1 cm of mercury in atmospheric pressure. The average rate in the lower selection is 1870 min^{-1} and the average atmospheric pressure 76 cm of mercury. The barometric coefficient variations are calculated for these values and the result plotted in Figure 2.18 and gives good agreement with the measured rate. The rates are a sensitive check on the stability of the response of the scintillation counters and the calibration and setting of the electronics.

The actual values of the discrimination levels are found from the results obtained during a run. The pulse height of all the events selected in a particular selection were plotted and the limits of the distribution taken as the discrimination levels. These were

then used with the expected distributions to calculate the efficiency of selection (effective running time) for $\frac{2}{3}e$ quarks and $\frac{1}{3}e$ quarks as a function of β. In the $\frac{2}{3}e$ selection a number of 'leak through' muons will be accepted. These not only give a good value of the upper discrimination level but also are a good check on the value of E and the electronic calibration. By the nature of their tracks a running check is available on the efficiency of the neon flash tubes.

Figures 2.19 to 2.22

Flash tube diagrams for the 8 events with a track obtained in the random pulsing run with the merit factor for each track, N/M (where N is the number of flashes in the track and M is the number of background). The 8 events were observed in 1148 random triggers of the apparatus.

Figures 2.23 to 2.26

Flash tube diagrams for the 8 events in the Q lower series (QL 50-97) where a previous particle was indicated. Pulse height information and values of N/M for each track are given. The 8 events were observed in a sample of 1391 triggers of the apparatus.

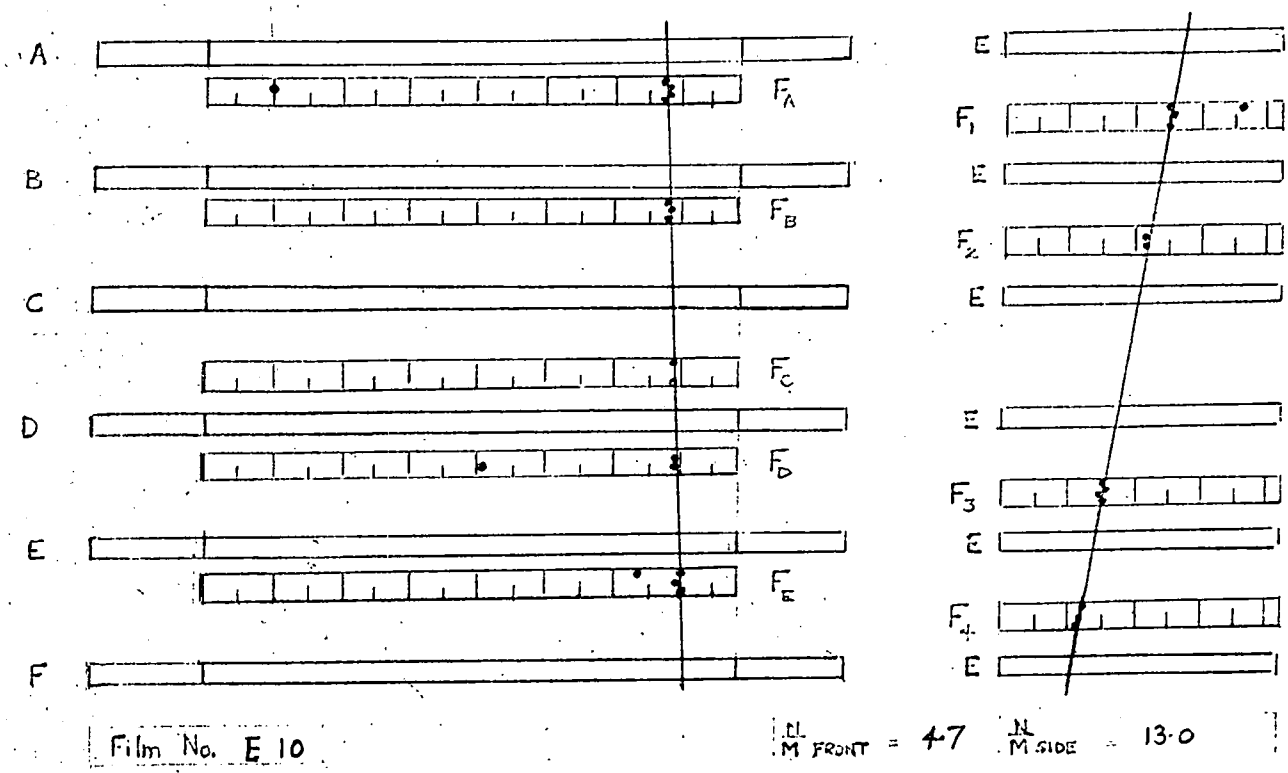

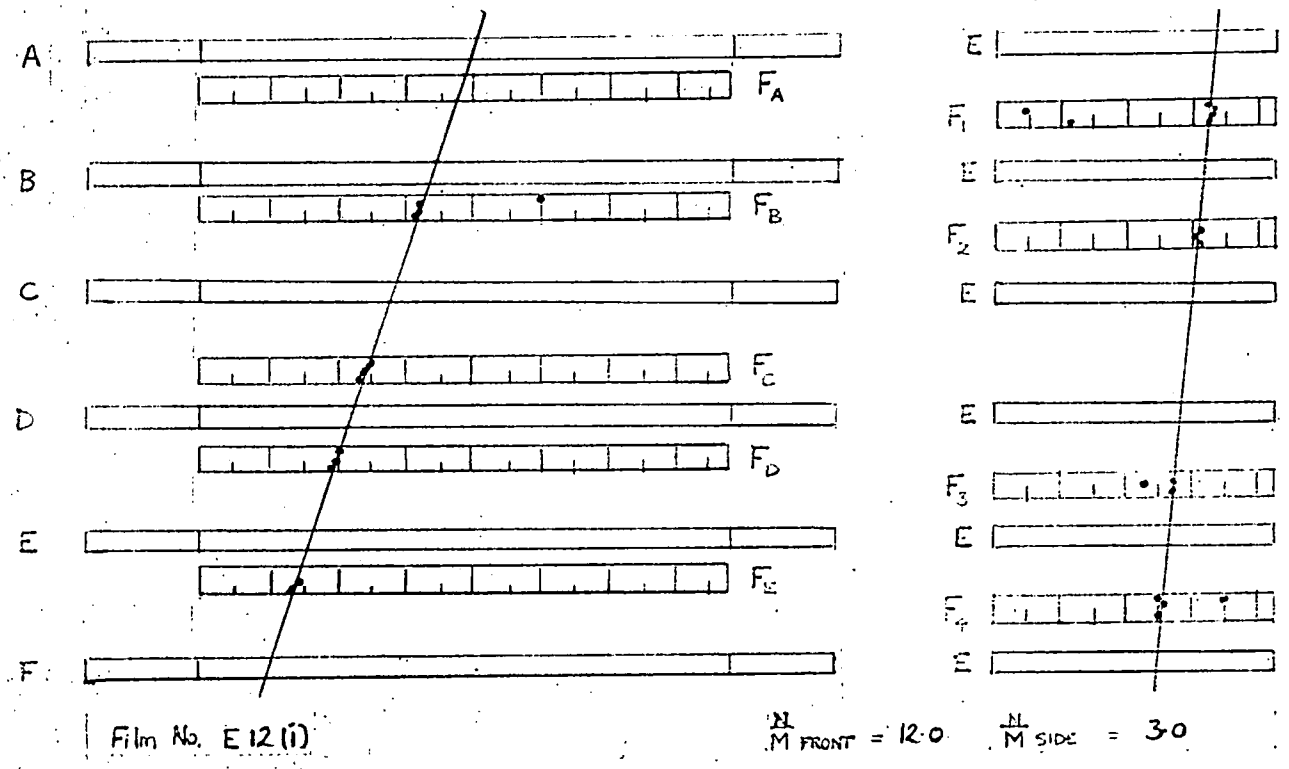

Figure 2.19 Flash tube diagram of track events obtained in random pulsing run.

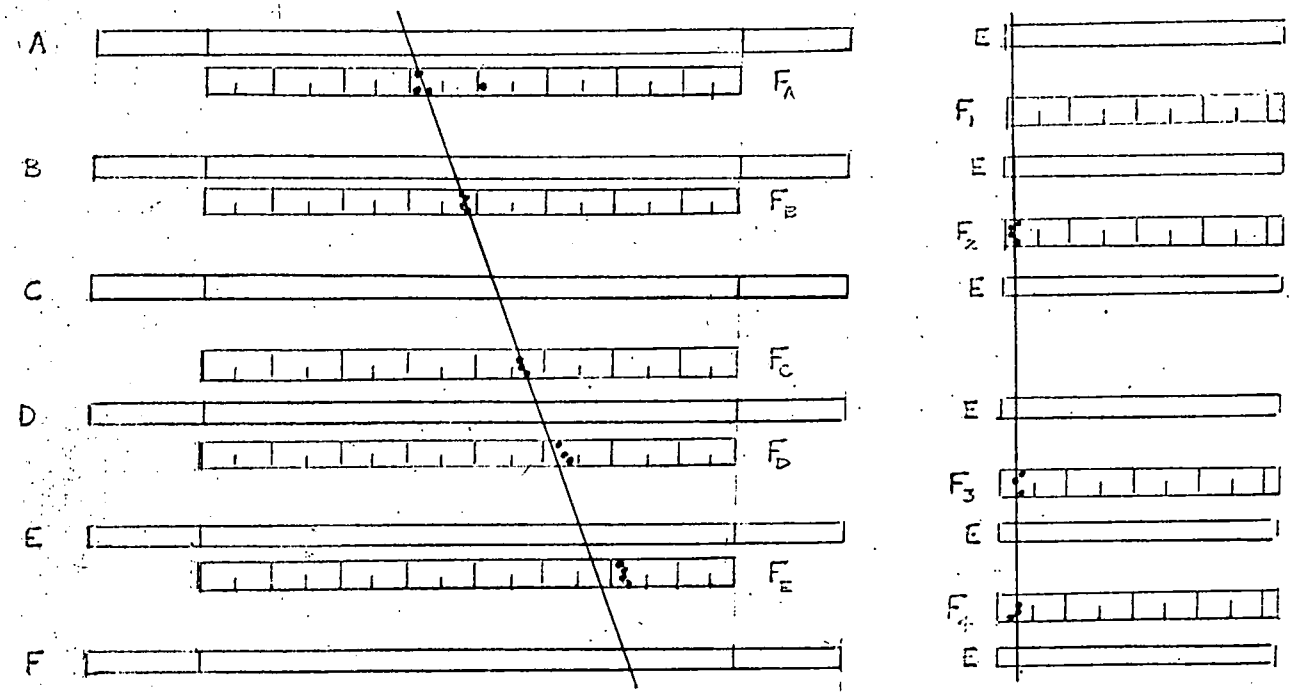

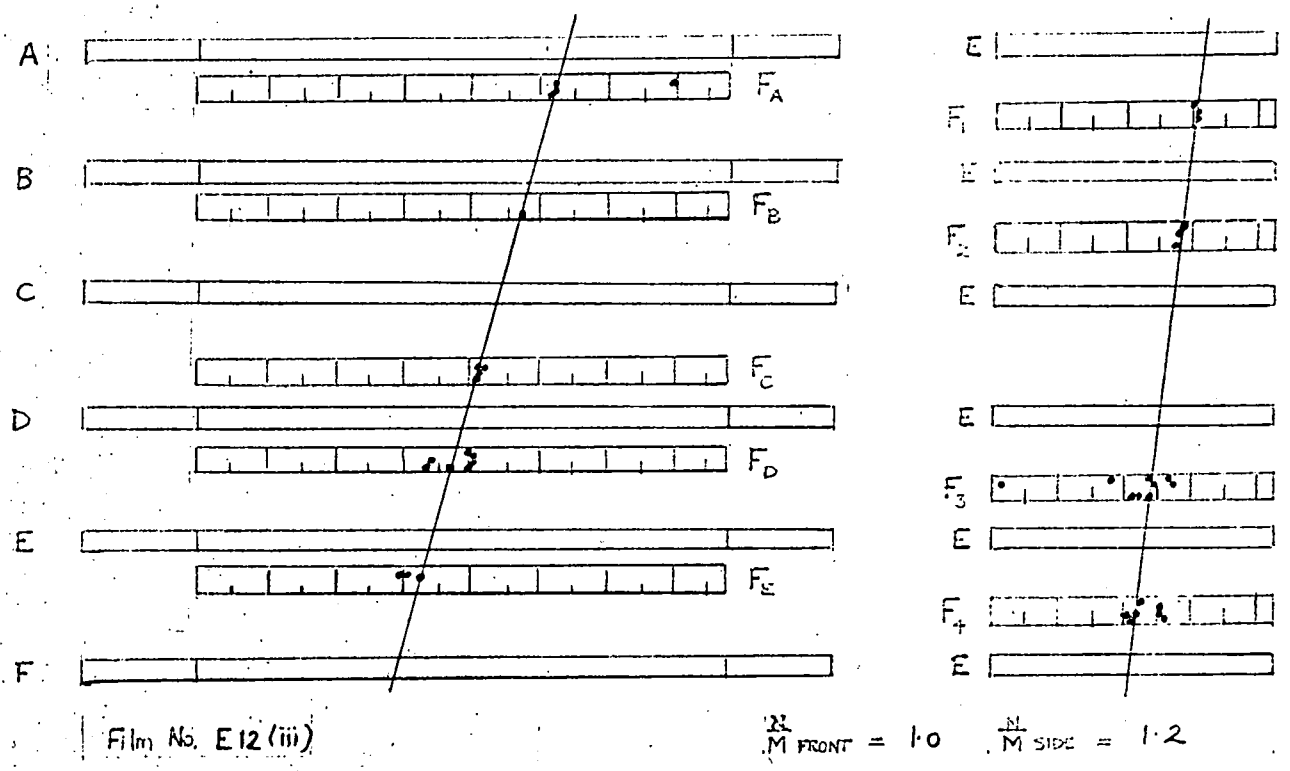

Figure 2.20 Flash tube diagram of track events obtained in random pulsing run.

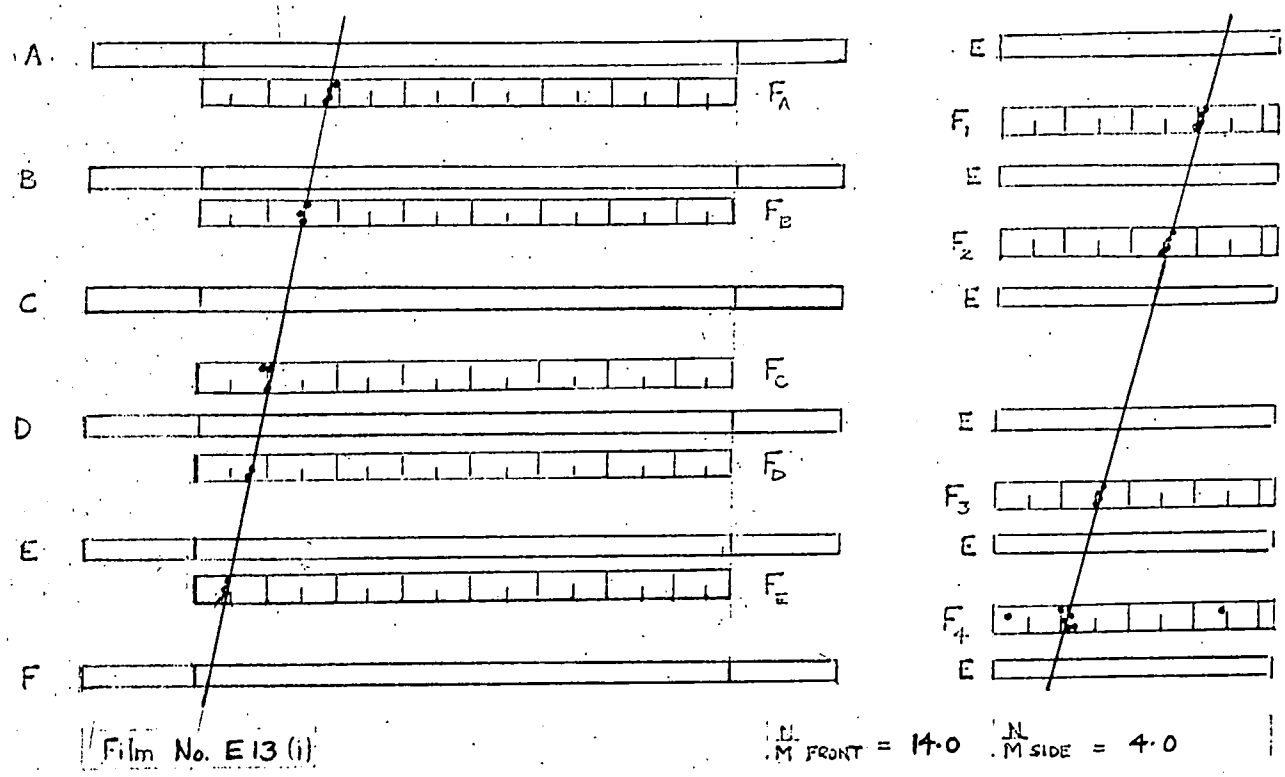

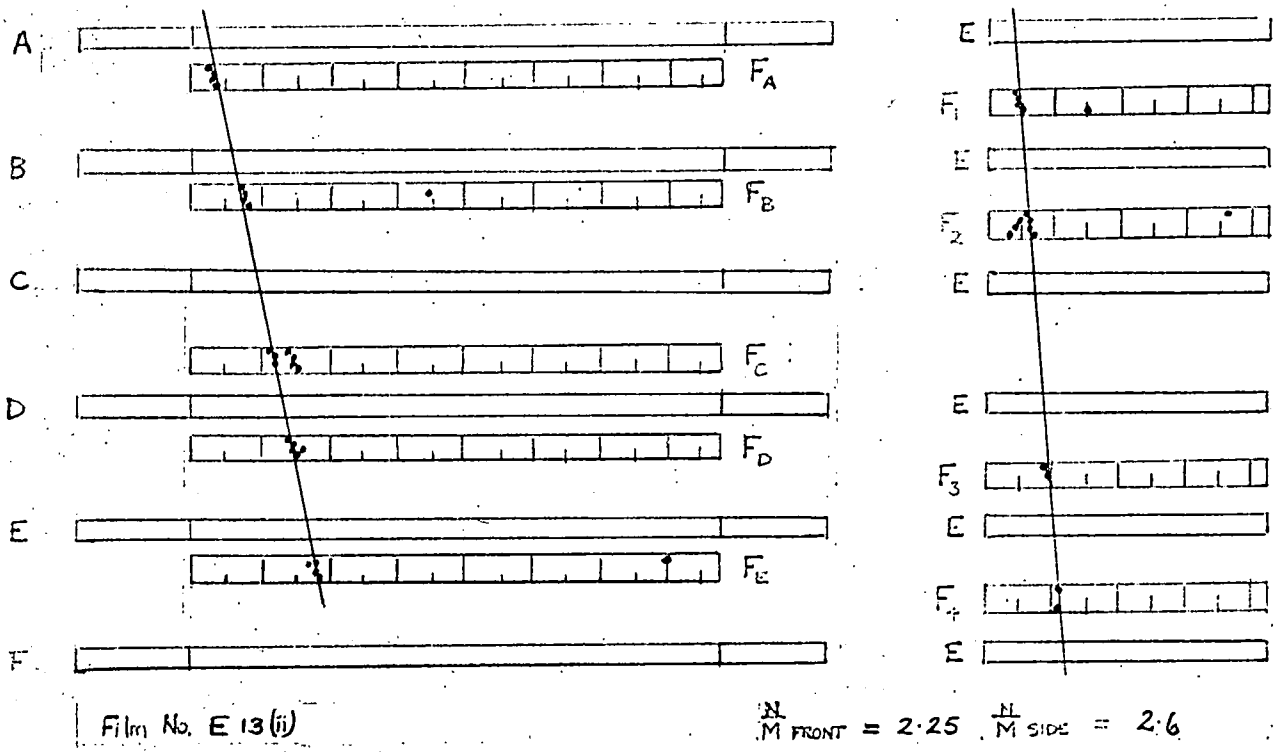

Figure 2.21 Flash tube diagram of track events obtained in random pulsing run.

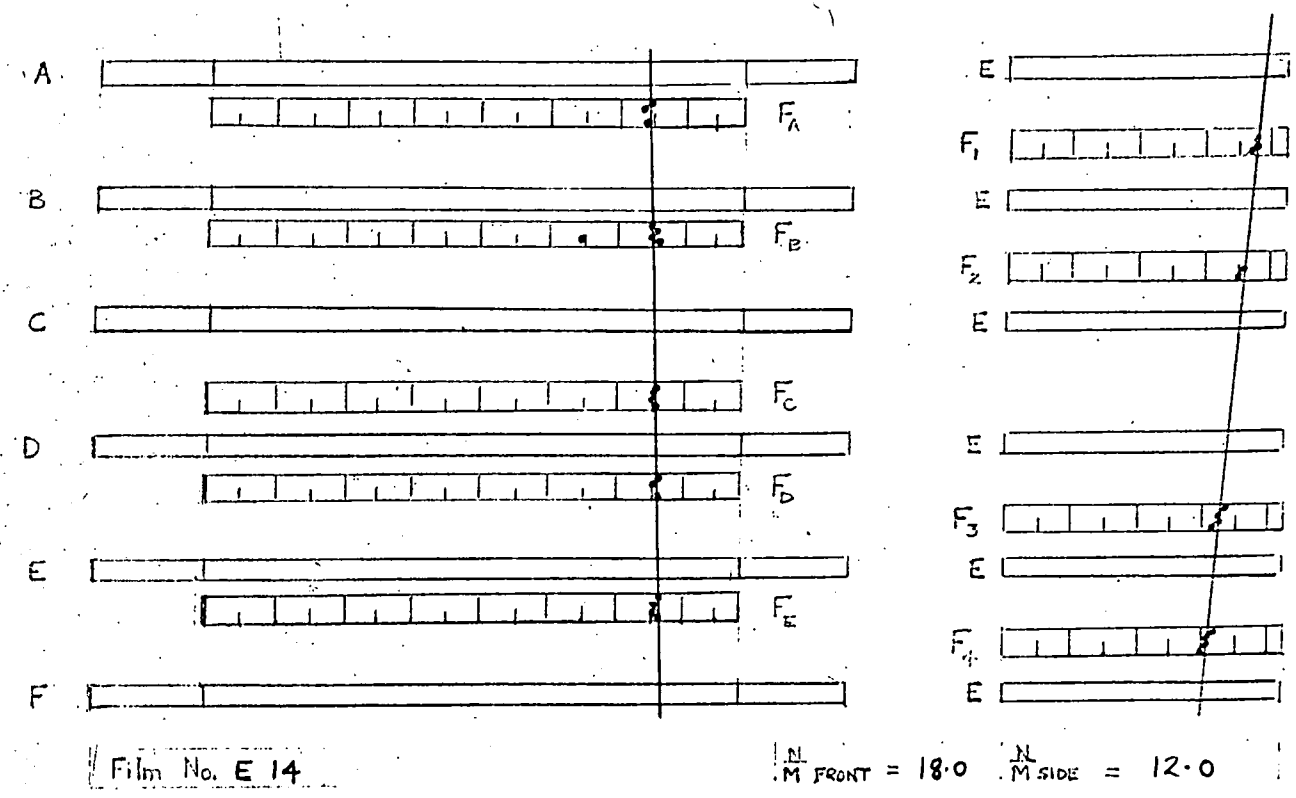

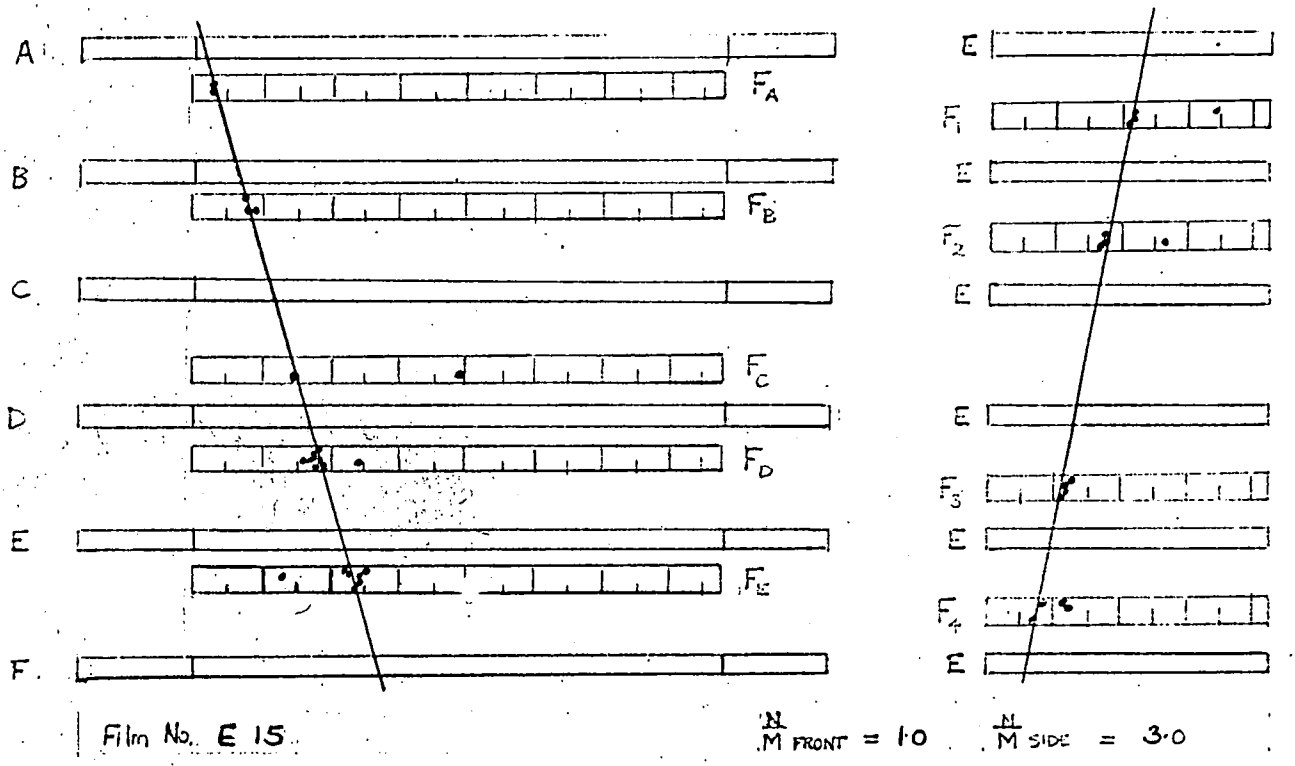

Figure 2.22 Flash tube diagram of track events obtained in random pulsing run.

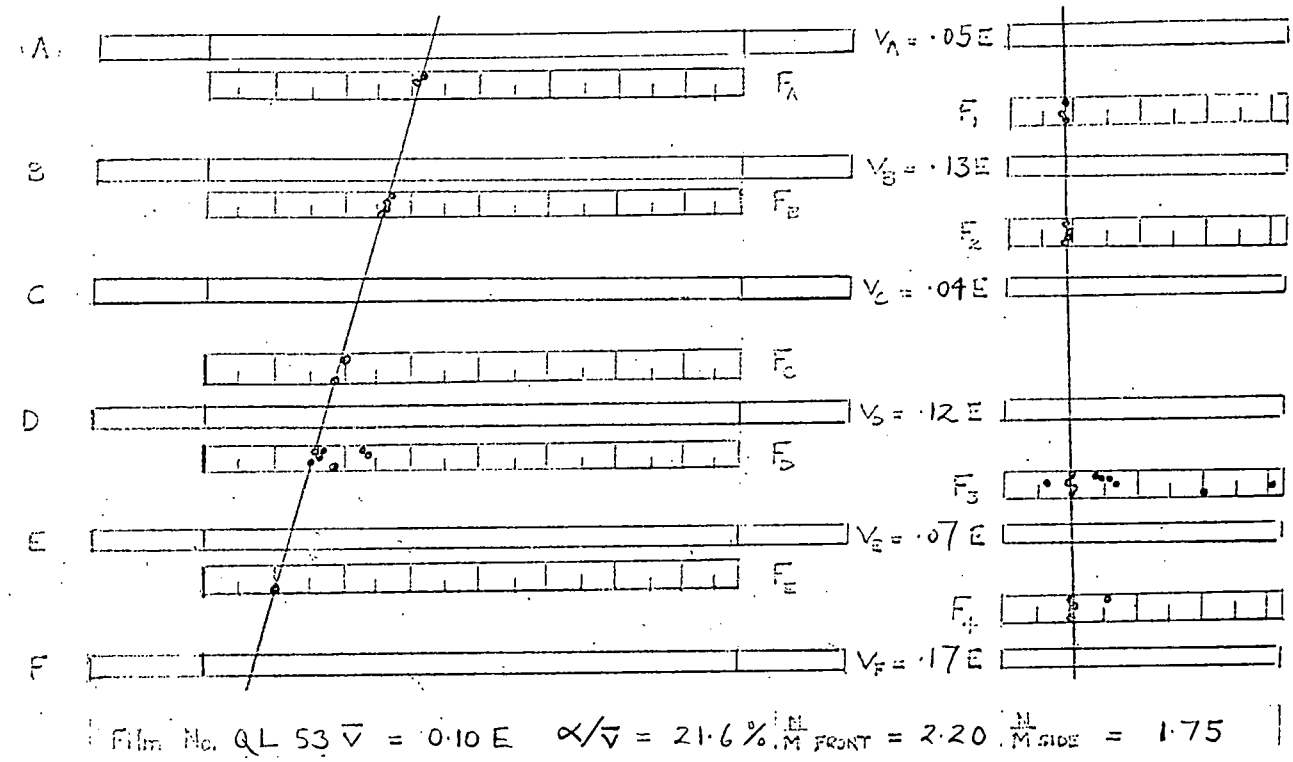

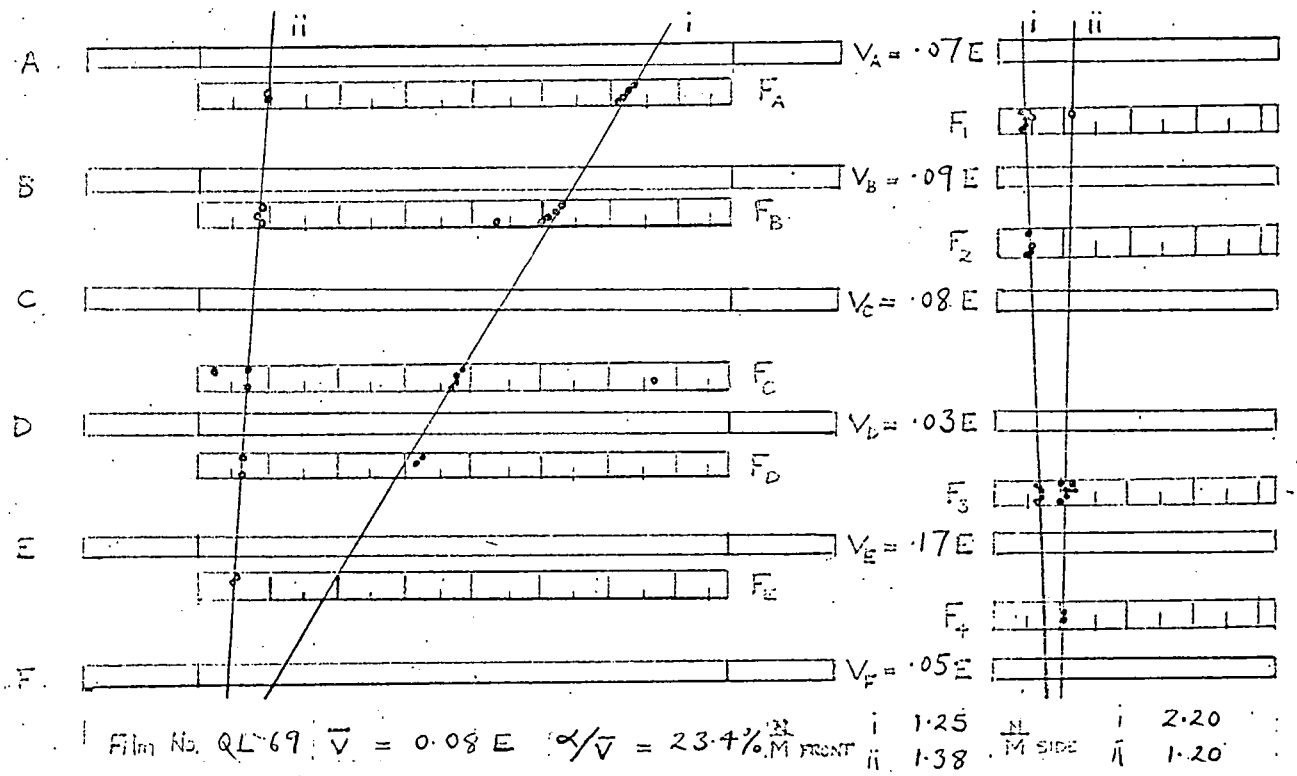

Figure 2.23 Flash tube diagram of events in the ψ lower series where a previous particle was indicated.

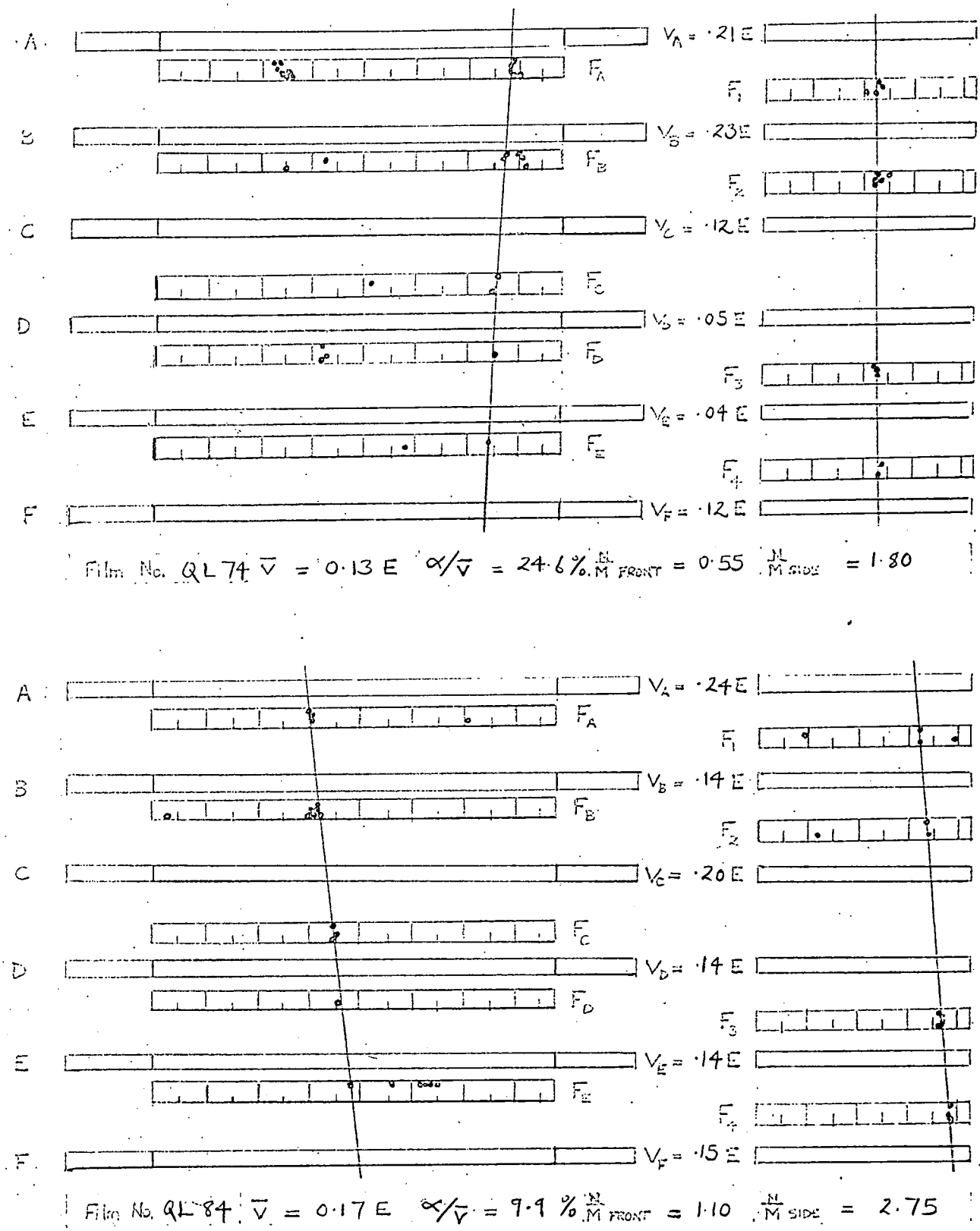

Figure 2.24 Flash tube diagram of events in the ψ lower series where a previous particle was indicated.

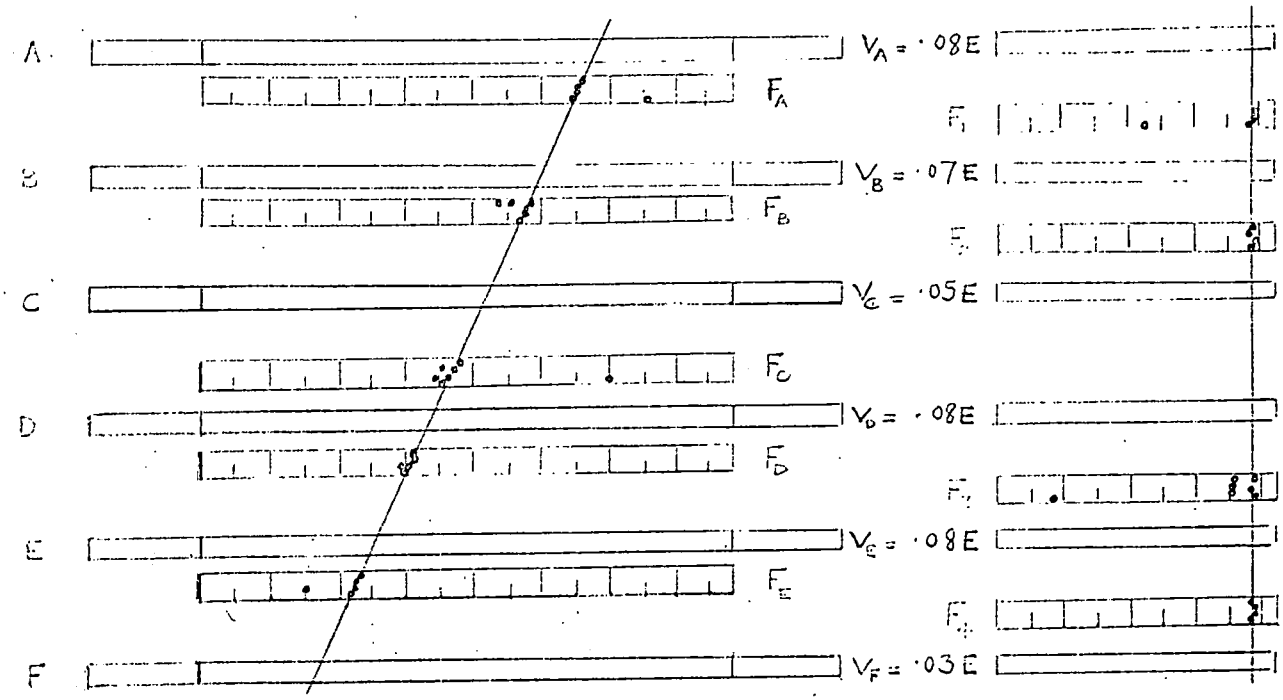

Film No. QL 90i $\bar{V}$ = 0·07 E $\alpha/\bar{V}$ = 11·9 % $\frac{N}{M}_{FRONT}$ = 2·11 $\frac{N}{M}_{SIDE}$ = 2·80

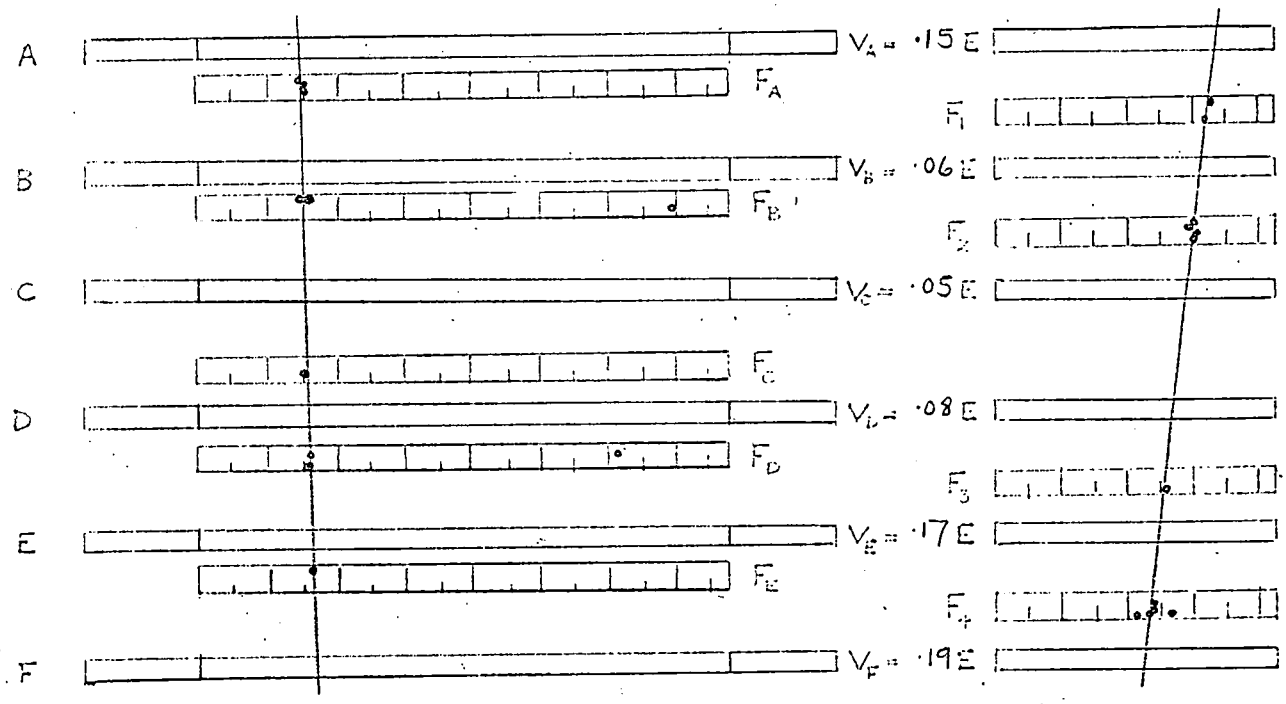

Film No. QL 90ii $\bar{V}$ = 0·12 E $\alpha/\bar{V}$ = 21·3 % $\frac{N}{M}_{FRONT}$ = 2·67 $\frac{N}{M}_{SIDE}$ = 5·00

Figure 2.25 Flash tube diagram of events in the Q lower series where a previous particle was indicated.

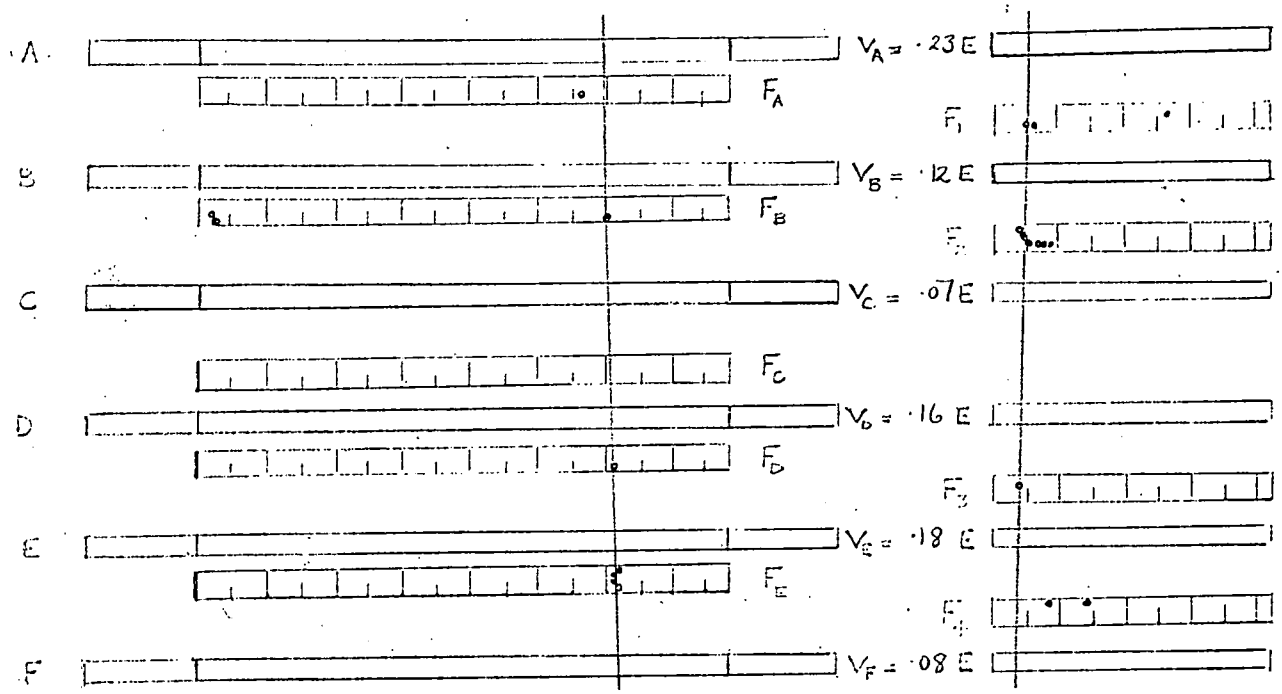

Film No. QL 93 i $\bar{V}$ = 0·14 E $\alpha/\bar{v}$ = 17·6 % $\frac{N}{M}_{FRONT}$ = 2·00 $\frac{N}{M}_{SIDE}$ = 0·71

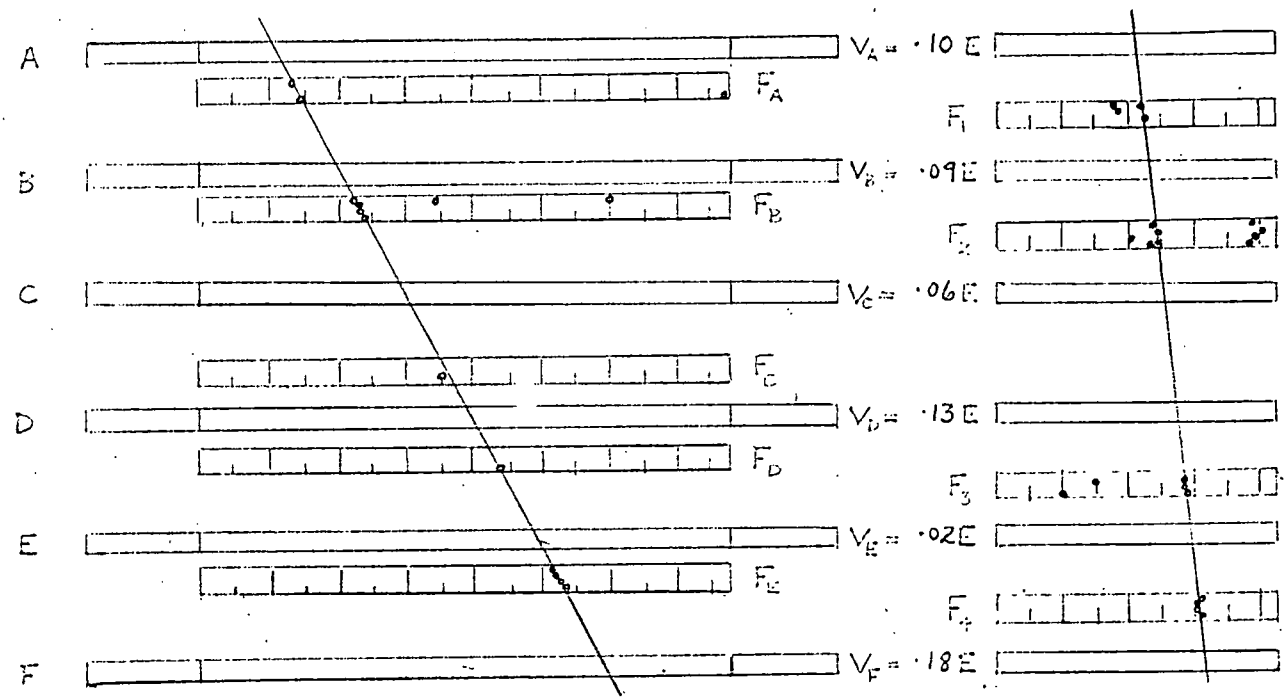

Film No. QL 93 ii $\bar{V}$ = 0·10 $\alpha/\bar{v}$ = 23·6 % $\frac{N}{M}_{FRONT}$ = 7·00 $\frac{N}{M}_{SIDE}$ = 1·20

Figure 2.26 Flash tube diagram of events in the Q lower series where a previous particle was indicated.

CHAPTER 3

ENERGY LOSS DISTRIBUTIONS IN THE TELESCOPE

3.1 Energy loss in the scintillation counter

A charged particle moving through matter loses energy by several mechanisms; collisions with the atomic electrons of the medium, direct pair production, bremsstrahlung, Cerenkov radiation and nuclear interactions.

In the telescope the energy loss is measured in a relatively thin scintillation counter which sets limitations on what can be measured. High energy losses, for example, direct pair production and fast knock-on electrons, cannot be measured because the electrons may have a range greater than the thickness of the counter. This means that the average energy loss cannot be measured by a thin counter. What is measured is the most probable energy loss which is due to the more frequent low energy transfer collisions of the charged particle with the atomic electrons of the medium, i.e. the excitation and ionisation of the electrons of the medium. It is the excitation energy which is converted into scintillation light and Birks (1951) shows that the light output per unit length, $\frac{dL}{dx}$ is related to the energy loss per unit length, $\frac{dE}{dx}$ by:

$$\frac{dL}{dx} = \frac{P \frac{dE}{dx}}{1 + Q \frac{dE}{dx}}$$

For the energy loss of a single particle in the present counter

$$\frac{dL}{dx} \propto \frac{dE}{dx} .$$

The most probable energy loss E_p for a charge ze particle of momentum p and mass μ is given by Sternheimer (1952, 1953, 1956), as:

$$E = \frac{At}{\beta^2} \left\{ B + 1.06 + 2\ln\left(\frac{p}{\mu c}\right) + \ln\left(\frac{At}{\beta^2}\right) - \beta^2 - \delta \right\}$$

where the constants have the following values for NE 102 phosphor:

$$A = 2\,Nf\left(\frac{ze^2}{mc^2}\right)^2 m_e c^2 = 0.0833 \text{ MeV gm}^{-1} \text{ cm}^2 \text{ for } z = 1.0,$$

f is the ratio of the atomic number to atomic weight,

$B = 18.69$,

and $t = 5.16$ gm cm^{-2} for the present counter.

δ is the density correction which effectively cancels out the relativistic increase in energy loss

$$\delta = 2\ln\left(\frac{p}{\mu c}\right) + C \quad , \qquad C = -3.13$$

this is applicable for $p/\mu c > 100$,

for $0.1 < p/\mu c < 100$ an extra term

$0.514 \left\{ 2 - \log_{10}\left(\frac{p}{\mu c}\right) \right\}^{2.595}$ is included.

A plot of most probable energy loss of a muon in the scintillation counter as a function of momentum and β is given in Figure 3.1

Particles of a given kind and incident energy do not lose the same amount of energy in traversing a given thickness of material because the collisions which are responsible for the energy loss are independant. Landau (1944) obtained a distribution of energy

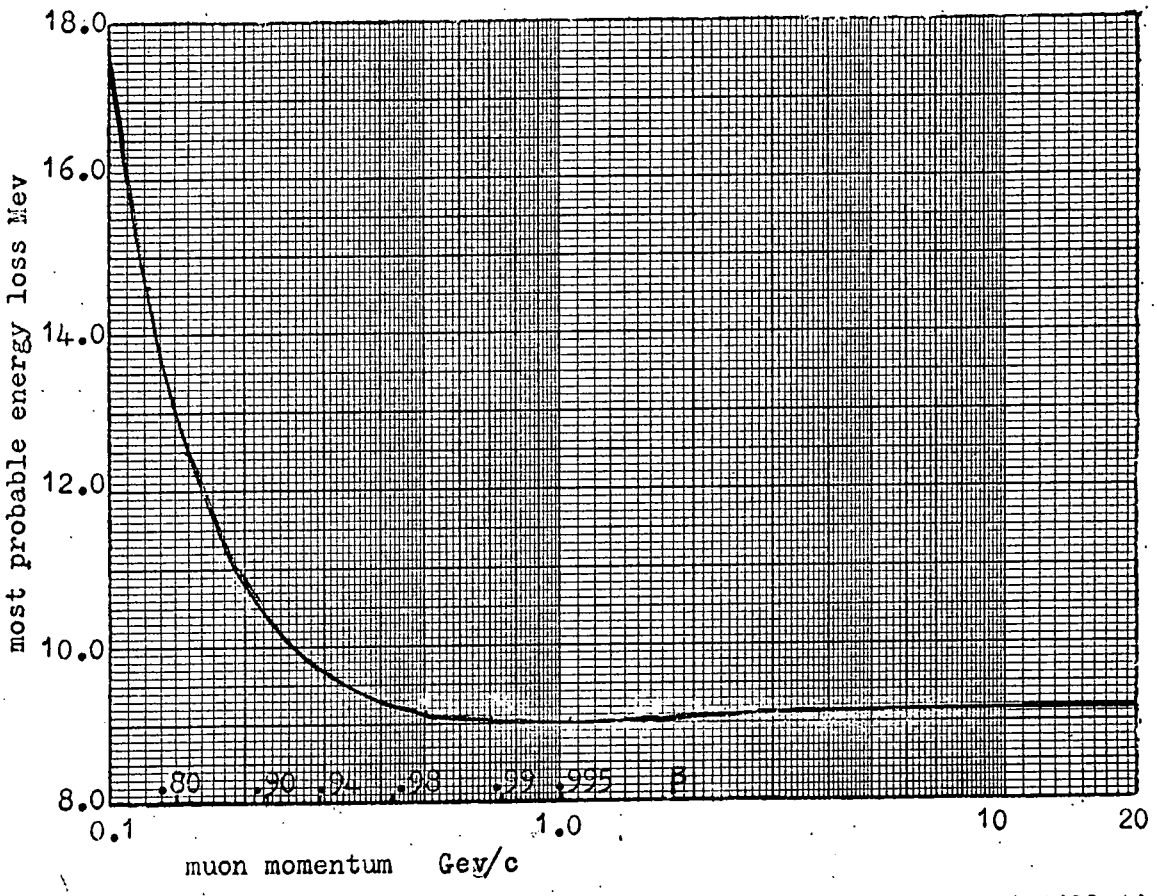

Figure 3.1 Most probable energy loss of a muon in the scintillation counter as a function of momentum. The corresponding values of β are also given.

loss for a thin absorber where the mean energy loss was small compared with the initial energy. Symon (1948) has worked out a complete solution of the probability of energy loss for thick and thin absorbers. Rossi (1952) plots Symon's result for a thin absorber as :

$$\frac{\Delta_o W}{F} \quad \text{against} \quad \frac{E - E_A}{\Delta_o}$$

where E and E_A are the most probable and actual energy loss respectively, WdE is the probability of energy loss in the range E to E+dE, $\Delta_o = Atb/\beta^2$ and is related to the resolution R% of the distribution, b and F are parameters given in graphical form by Rossi as a function of maximum transferable energy, E_m' and β. The Landau curves are shown in Figure 3.2 for different values of the parameter, λ. This parameter, related to the asymmetry of the distribution is also given graphically by Rossi as a function of E_m' and β. The relevant parameters are given in Figure 3.2.

For $E_m' > 50$ MeV, λ, b, and F approach an asymptotic limit and therefore the shape of the distribution is independant of the energy of an incident particle. For $E_m' < 50$ MeV the high energy tail of the distribution will become less extended and the resolution, i.e. the width at half height expressed as a percentage of the most probable energy loss will decrease. In this region the maximum transferable energy is given by:

$$E_m' = 2m_e c^2 \frac{\beta^2}{1-\beta^2} ,$$

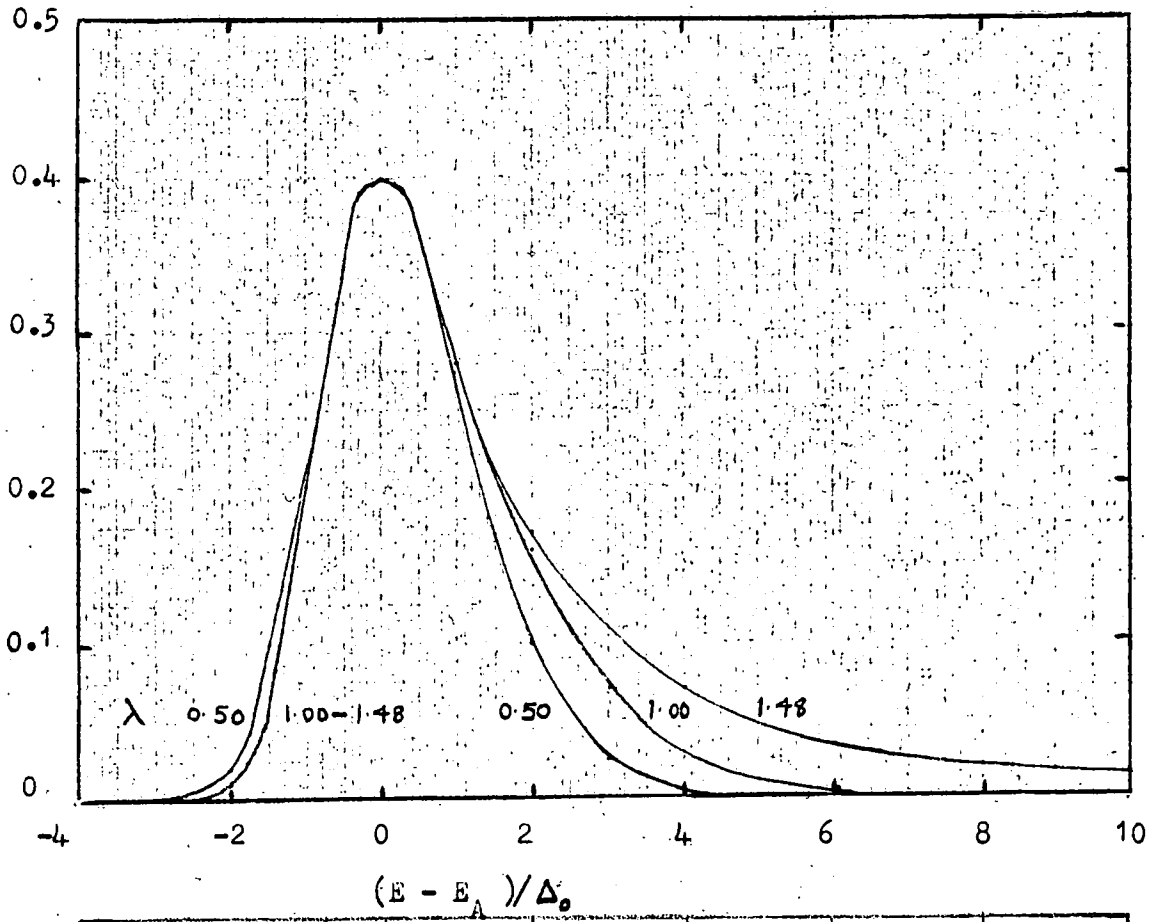

β	E'_m(MeV)	λ	f	b	Δ_o(MeV)	R%
0.4	.16	0.30	0.98	0.45	0.22	9.3
0.6	.49	0.50	0.95	0.75	0.37	13.0
0.8	1.7	1.00	0.85	1.30	0.63	13.0
0.99	4.9	1.48	0.66	1.48	0.72	17.5

Figure 3.2 Results of Symons' theory of the fluctuations in the collision loss. The various curves refer to different values of λ. The table gives the values of the parameters for the counter in the present experiment.

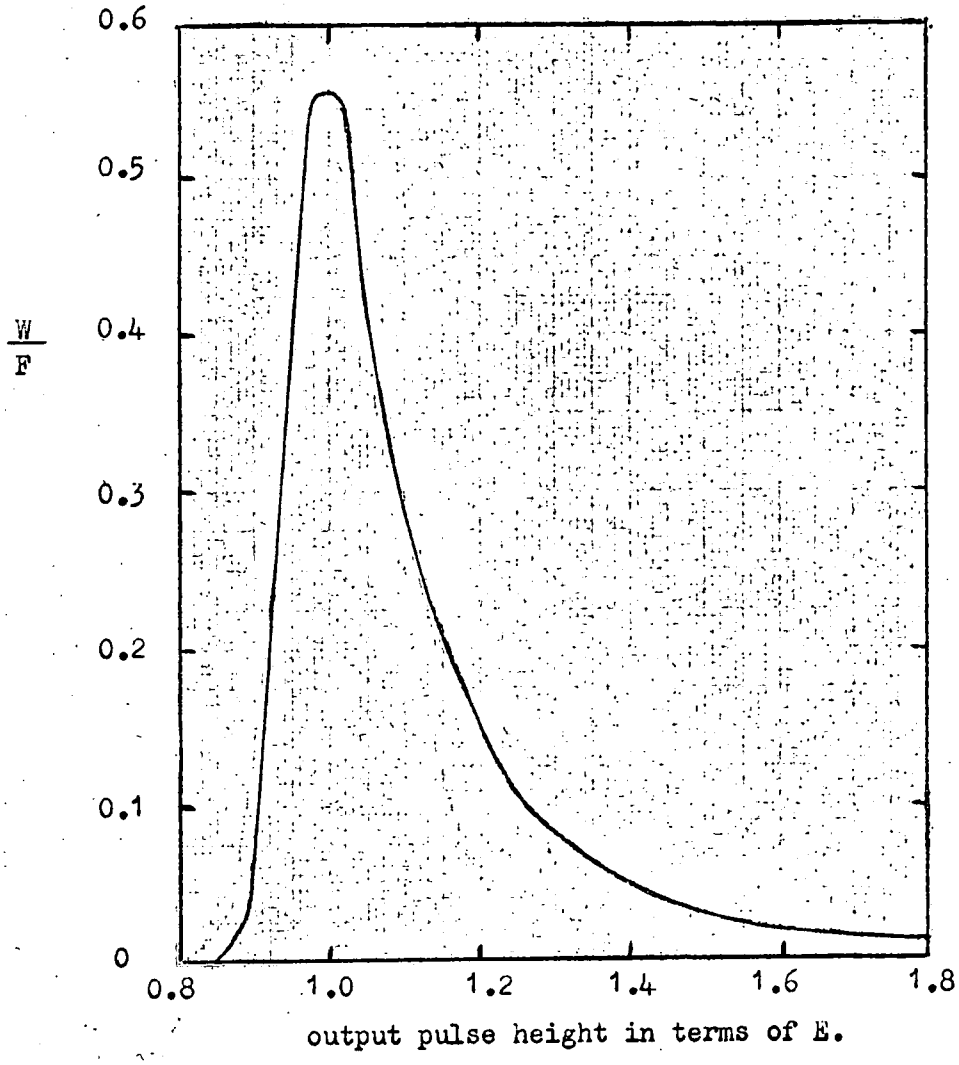

Figure 3.3 The Landau distribution for relativistic muons traversing the counter given in terms of E, the most probable pulse height.

where the mass of the incident particle is $>> m_e$. Hence the Landau curve is only dependant on β.

For relativistic muons traversing the counter E = 9.1 MeV and all other parameters have their asymptotic values, the resultant curve is given in Figure 3.3, with the actual energy loss given in terms of the most probable value.

Qualitatively thepeak of the distribution is due to losses by excitation and the long tail to knock-on electrons. For knock-on energies much less than the maximum transferable energy the Rutherford formula gives the probability of energy E to E + dE as

$$p(E)\,dE = \frac{2C\, m_e c^2 z^2}{\beta^2} \times \frac{dE}{E^2}$$

where ze is the charge on the incident particle.
This predicts that the Landau tail should fall as E^{-2}. If the most probable energy is taken as a zero point this is found to be the case for the curve $\lambda = 1.48$.

For an incident particle of charge ze when $z < 1.0$ the most probable energy loss decreases by a factor z^2 (z appears in the term A of Sternheimers formula, a term $\ln(At/\beta^2)$ appears inside the bracket but this is small compared with the other terms). In the Landau curve Δ_o contains the term A and hence the width of the distribution will also decrease by a factor z^2, the width as a percentage of the most probable value will be the same as that for

a muon. In the tail of the distribution, the probability of producing a knock-on electron of energy E to E + dE is also reduced by a factor z^2. Thus the shape of the Landau curve for $\frac{1}{3}e$ and $\frac{2}{3}e$ quarks is the same as that for muons with the same value of β. The Landau curve for relativistic particles ($\lambda = 1.48$) is used to predict the expected pulse height distributions for $\frac{1}{3}e$ and $\frac{2}{3}e$ relativistic quarks in the scintillation counter.

Many workers have obtained the expected $\frac{1}{3}e$ and $\frac{2}{3}e$ quark pulse height distributions by looking at muons with the photomultipliers masked such that only a fraction z^2 of the light incident on the photomultiplier reached the photocathode. This method also depends on the Landau curve for quarks being the same as that for muons.

3.2 Expected pulse height distributions for a single counter

As well as the fluctuations of the energy loss in the counter the observed distribution will include fluctuations due to the photomultiplier in the number of photo-electrons produced and the variation in the gain and due to the response of the counter to particle position and the variation in track length (angle of incident particle).

The fluctuations in the total number of photo-electrons produced in the photocathode is found to be Poisson so that the standard deviation $\sigma = \sqrt{N}$ where N is the mean number of photo-electrons emitted and therefore:

$$\left(\frac{\sigma}{N}\right)^2 = \frac{1}{N}$$

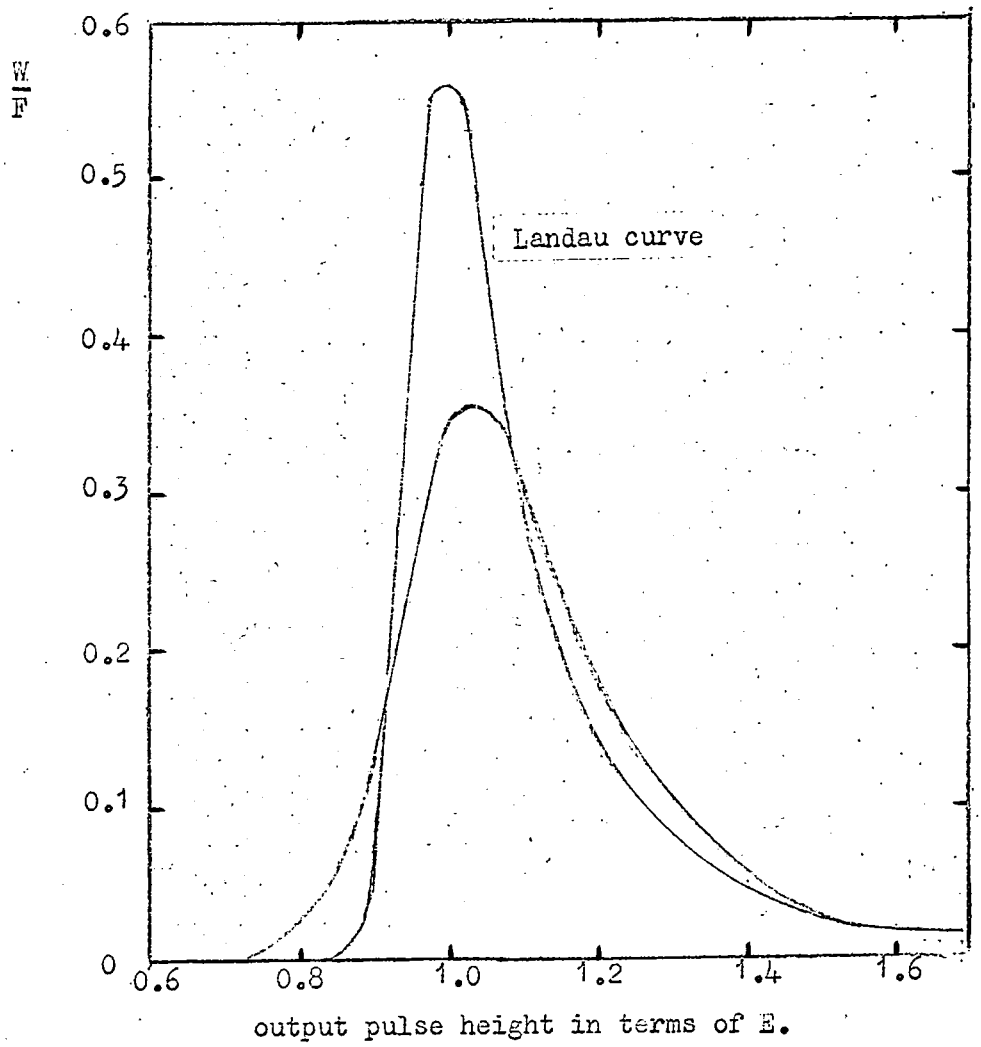

Figure 3.4 The Landau distribution and the expected output pulse height distribution for a relativistic muon traversing the counter in a G run.

For the fluctuation in the gain of the photomultiplier a comparable analysis was performed by Wilkinson (1950) who found that for large values of gain the fluctuations were only dependant on N and, in fact, were Poisson so that the total photomultiplier fluctuations are given by:

$$\left(\frac{\sigma}{\bar{v}}\right)^2_{P.M} = \frac{2}{N}$$

In Chapter 2 the value of N was calculated to be 220, thus for a $\frac{2}{3}$e quark $N_{\frac{2}{3}} = 96$ and for a $\frac{1}{3}$e quark $N_{\frac{1}{3}} = 24$, therefore:

$$\left(\frac{\sigma}{\bar{v}}\right)^2_{\frac{2}{3}} = \frac{2}{96}, \quad \left(\frac{\sigma}{\bar{v}}\right)_{\frac{2}{3}} = 0.144 \text{ and } \left(\frac{\sigma}{\bar{v}}\right)^2_{\frac{1}{3}} = \frac{2}{24}, \quad \left(\frac{\sigma}{\bar{v}}\right) = 0.289$$

Similarly for a charge e particle:

$$\left(\frac{\sigma}{\bar{v}}\right)^2 = \frac{2}{220}, \quad \left(\frac{\sigma}{\bar{v}}\right) = 0.095.$$

These fluctuations must be combined with the Landau distribution to give the expected distributions from the scintillation counter. This was done by dividing the Landau distribution into ten equal areas and then replacing the area by a Gaussian distribution of the same area and required value of σ, with the mean at the median point of the area. These Gaussian distributions were then added to give the resulting distribution. This in fact was only done for nine of the areas, the shape of the tail was left unchanged. This is a reasonable approximation since the tail is relatively flat and would not be altered by such fluctuations.

The resulting distribution for a charge e particle is shown in Figure 3.4. This in fact should correspond to a G run distribution

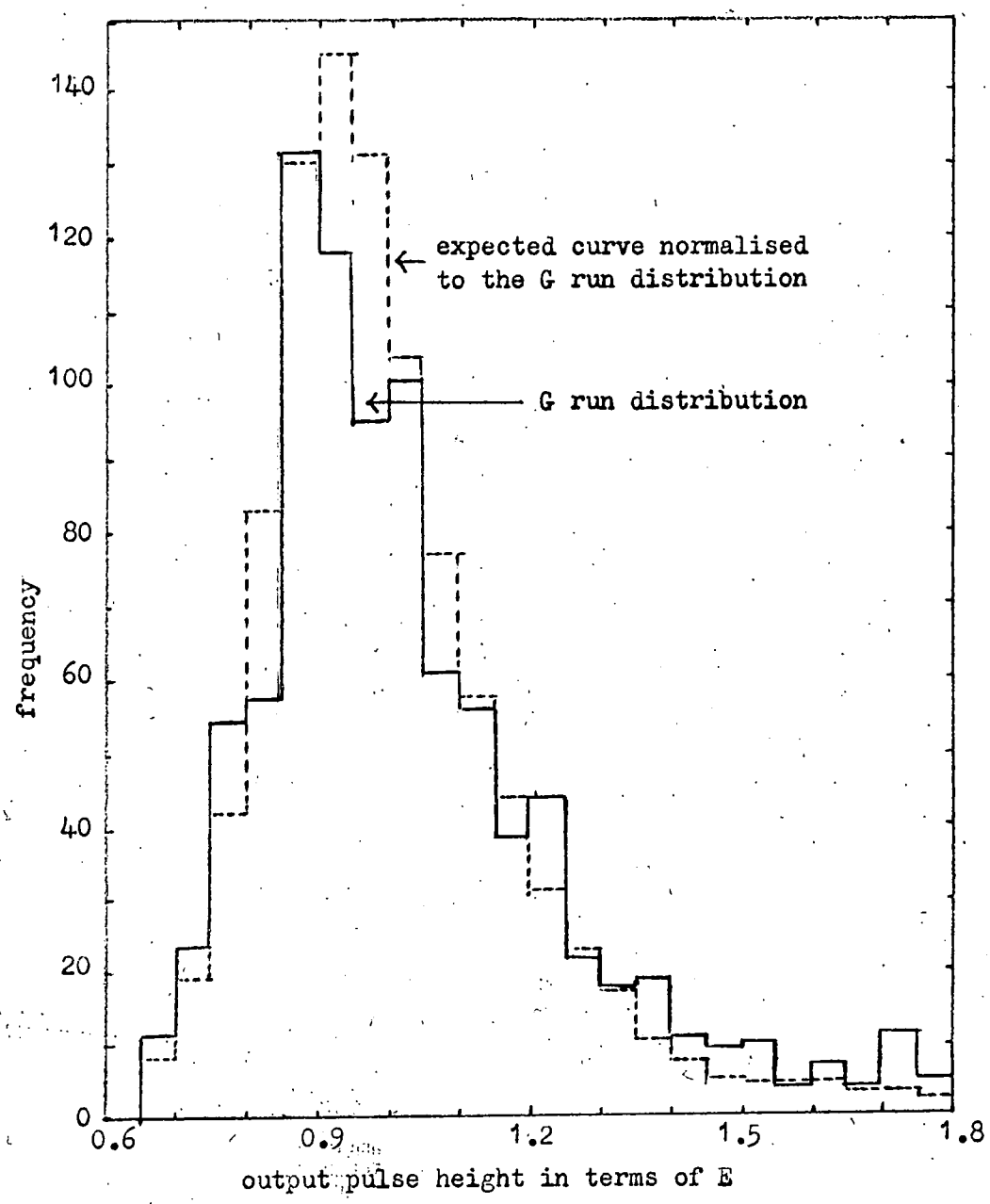

Figure 3.5 The output pulse height distribution for a G run (described in 2.3.5) compared with the expected distribution. The expected distribution is normalised to fit the G distribution over the range 0.66 to 2.0 of the most probable pulse height.

where there are comparatively no fluctuations in position in the counter and in the angle of the incident particle. The expected distribution was normalised to the G run distribution over the range 0.66 to 2.0 of the most probable pulse height and the result is shown in Figure 3.5. The reasonable agreement indicates the reliability of the method and thus the expected $\frac{1}{3}e$ and $\frac{2}{3}e$ quark distributions should lead to a good estimate of the acceptance of the telescope.

The fluctuations in position and angle of the incident particle are in fact the cause of the difference between the G and C run. The width of a C run is 40% and of a G run 25%. This can be regarded as an increase in $\sigma/\bar{v}$ of :

$$\frac{1}{2.3}\left\{(.40)^2 - (.25)^2\right\}^{\frac{1}{2}} = 0.14 ,$$

where 2.3 is the conversion factor of width at half height to σ for a Gaussian distribution. On the assumption that quarks have the same angular distribution as muons this can be added in quadrature to the above values of $\sigma/\bar{v}$. For these values the above procedure was followed to give the expected distributions for $\frac{1}{3}e$ and $\frac{2}{3}e$ quarks which are shown in Figures 3.6 and 3.7 respectively. From these distributions the percentage above and below values of pulse height in terms of E were calculated and the result is shown in Figure 3.8. On this basis the acceptance of $\frac{1}{3}e$ quarks within the range 0.05E to 0.30E is 96.5% and for $\frac{2}{3}e$ quarks within the range 0.30E to 0.85E is 92%.

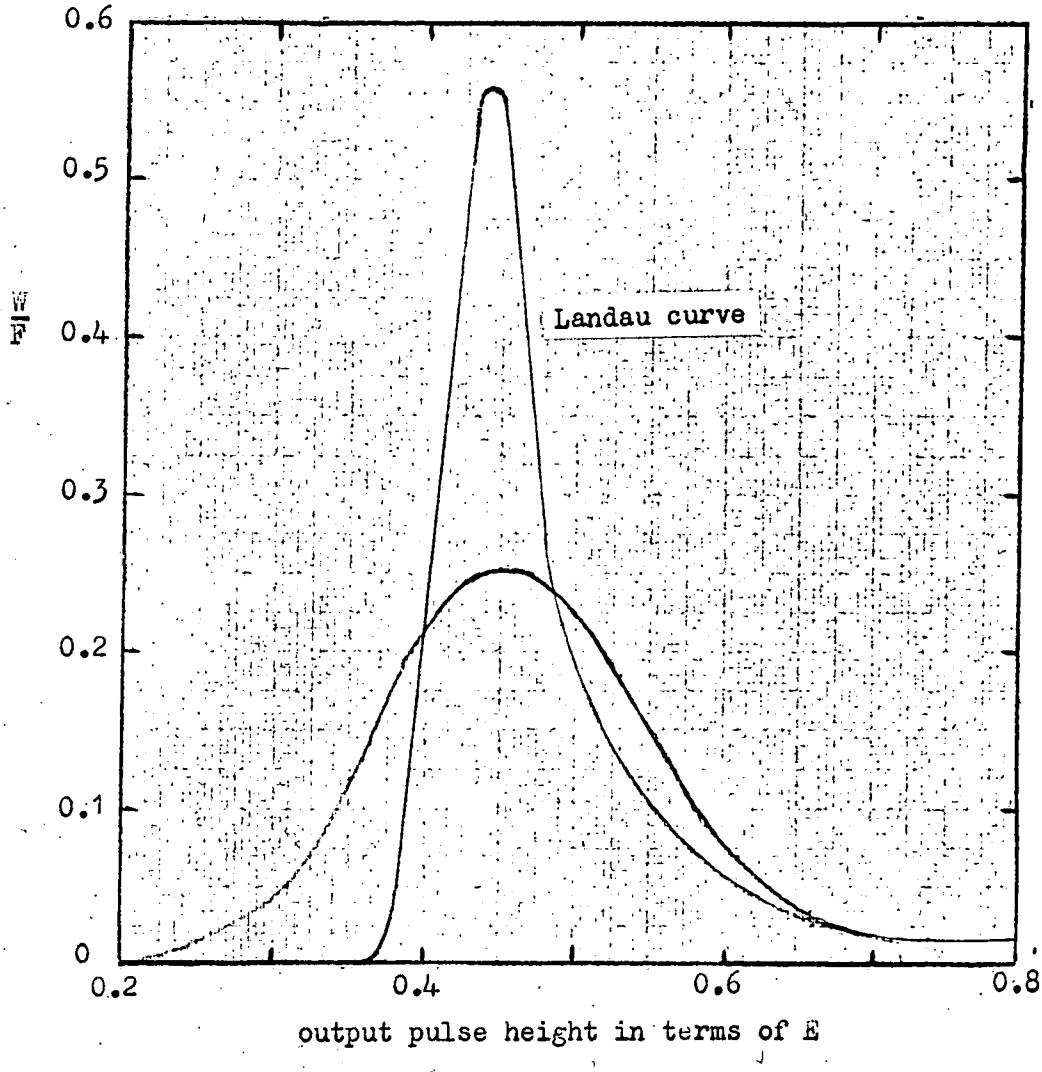

Figure 3.6. The Landau distribution and the expected output pulse height distribution for a relativistic $\frac{2}{3}$e quark accepted on the T or Q criteria.

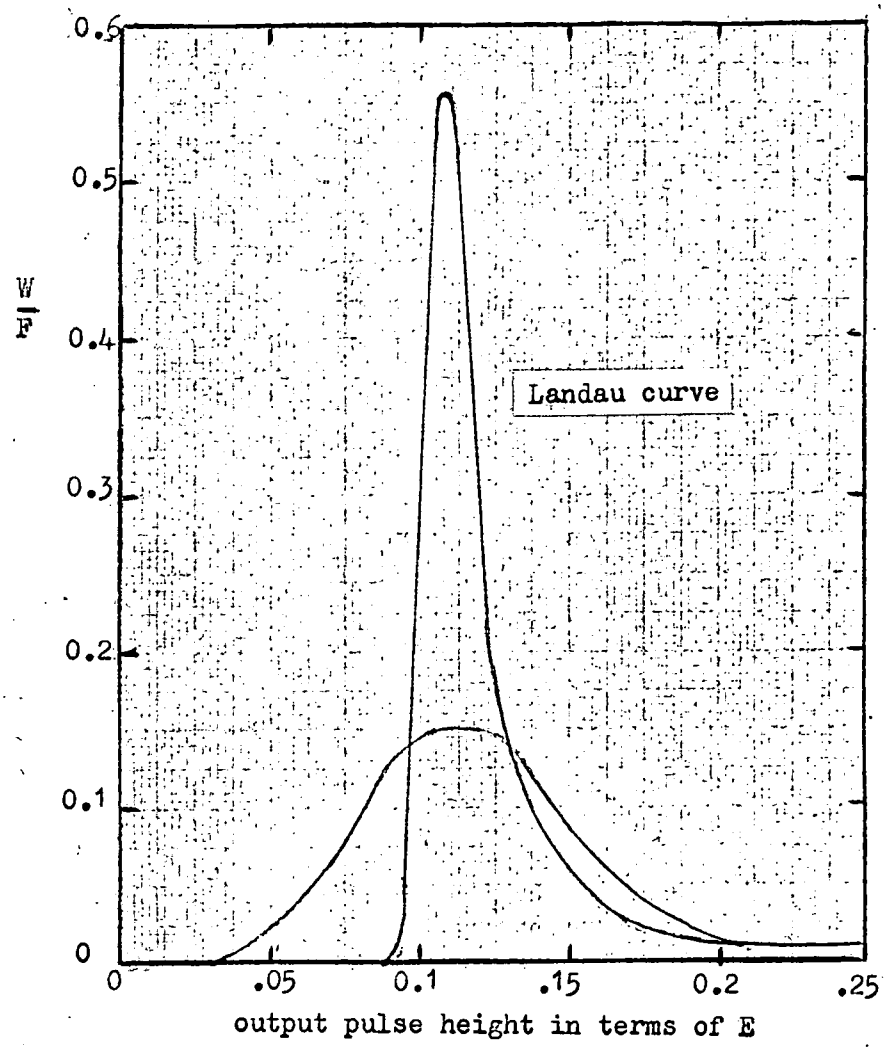

Figure 3.7 The Landau distribution and the expected output pulse height distribution for a relativistic $\frac{1}{3}e$ quark accepted in the Q criteria.

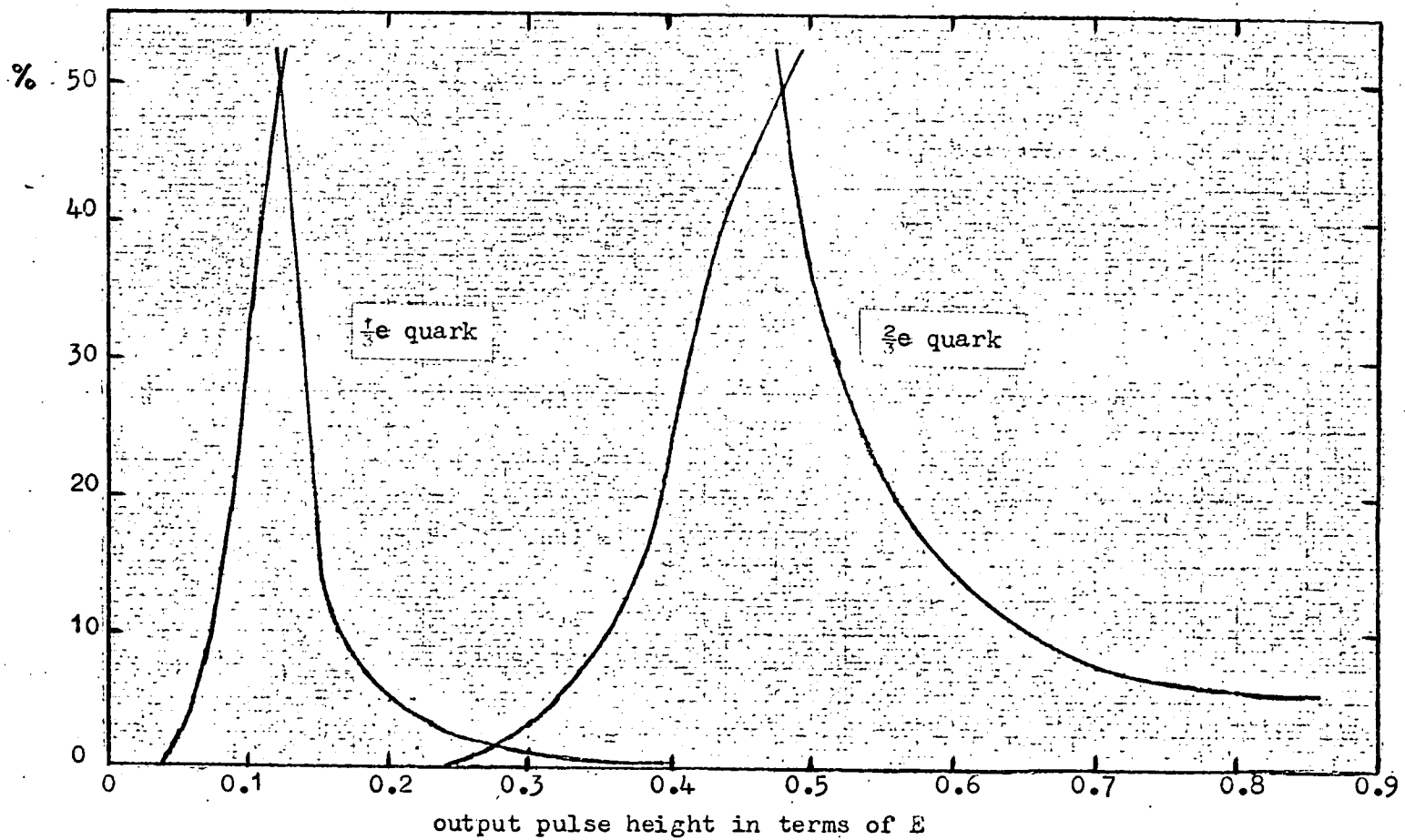

Figure 3.8 Percentage of the distribution for $\frac{1}{3}$e and $\frac{2}{3}$e relativistic quarks within upper and lower levels expressed in terms of output pulse height.

3.3 Expected distributions of $\bar{v}$ and $\frac{\alpha}{\bar{v}}$% for accepted quarks in the 6 counters

In the final analysis, events are plotted as a function of $\bar{v}$ and the acceptance is on the value of $\alpha/\bar{v}$%. For this reason the distributions of $\bar{v}$ and $\alpha/\bar{v}$ % were calculated from the expected distributions of $\frac{1}{3}e$ and $\frac{2}{3}e$ quarks.

For the $\frac{1}{3}e$ quark distributions the expected pulse height distribution between 0.05E and 0.30E was divided into 20 equal areas. The medians of these areas were then selected on a random basis and $\bar{v}$ and $\alpha/\bar{v}$% calculated 10^4 times. These values are plotted in Figures 3.9 and 3.10 respectively. Basically the $\frac{1}{3}e$ pulse height distribution for a single counter is Gaussian and has a resolution of 72.5%. The mean of six such Gaussian distributions would have a resolution of $72.5/\sqrt{6}\% = 29.5\%$, the resolution of the computed data is 31%, 90% of the events lie within a pulse height range of 0.091E to 0.138E. If the mean pulse height distribution is Gaussian 32% of the events would have $\alpha/\bar{v} > 0.31/2.3 = 13.4\%$ and in fact from the computed data 32% of the data have $\alpha/\bar{v} > 13.0\%$. The percentage of events with values of $\alpha/\bar{v}$ % greater than a certain value is plotted in Figure 3.11 as a function of $\alpha/\bar{v}$%, 90% of the events have $\alpha/\bar{v} < 16\%$.

For the $\frac{2}{3}e$ quark distributions a similar procedure of computation was followed. However, two distributions were used because of the independance of counter C:- the expected $\frac{2}{3}e$ distribution between

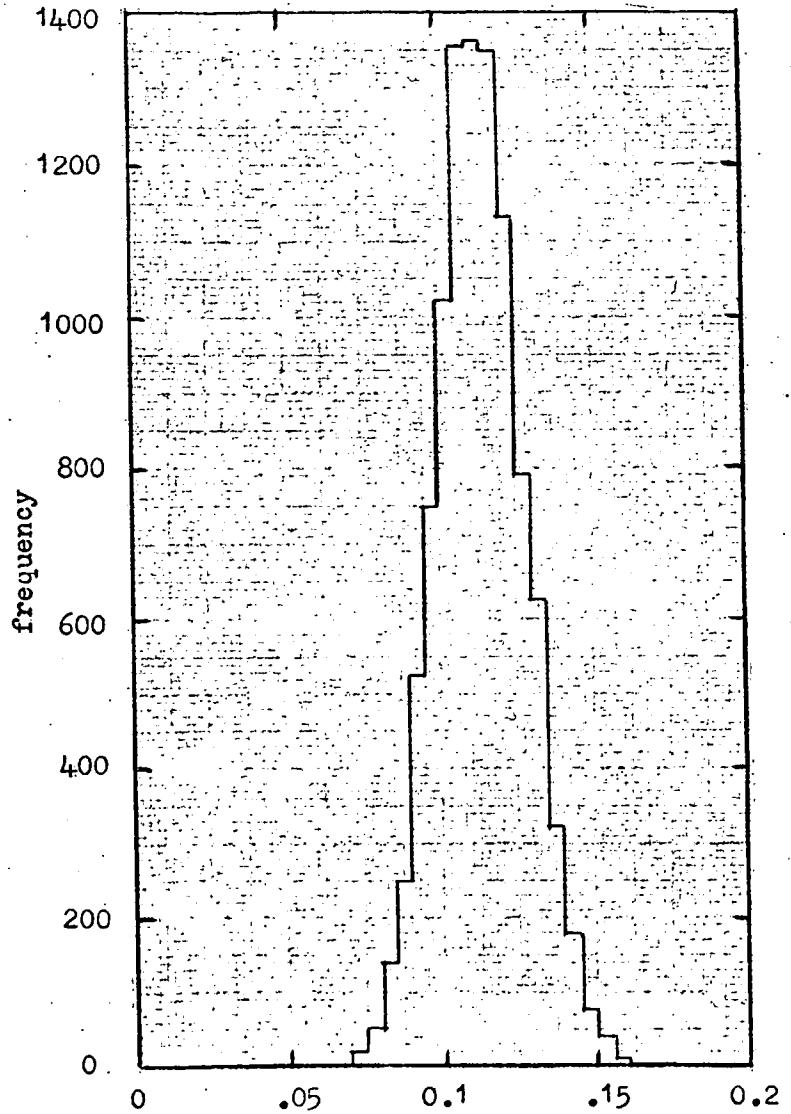

Figure 3.9 The expected distribution of the mean of the output pulse heights from counters A-F for relativistic $\frac{1}{3}e$ quarks traversing the telescope.

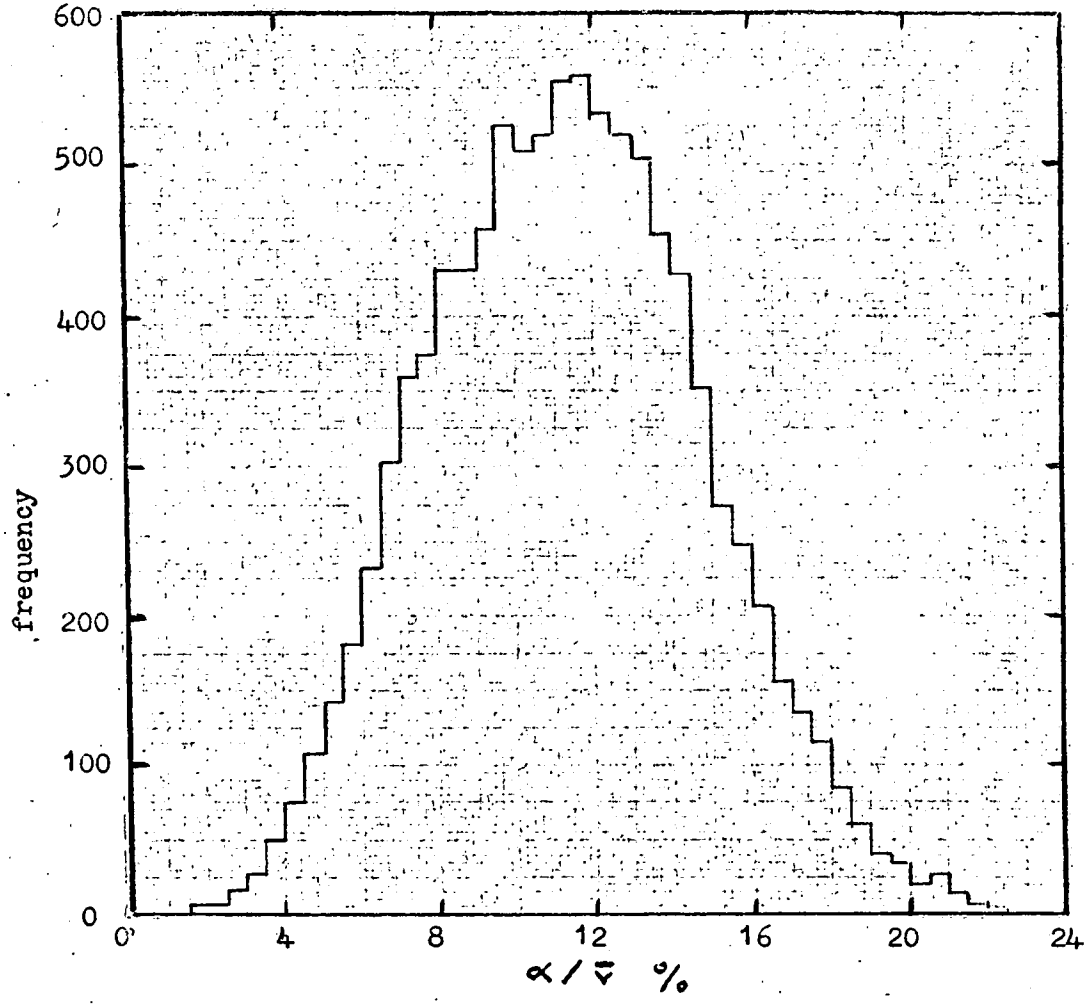

Figure 3.10 The expected distribution of $\alpha/\bar{v}$ % for relativistic $\frac{1}{3}e$ quarks traversing the telescope.

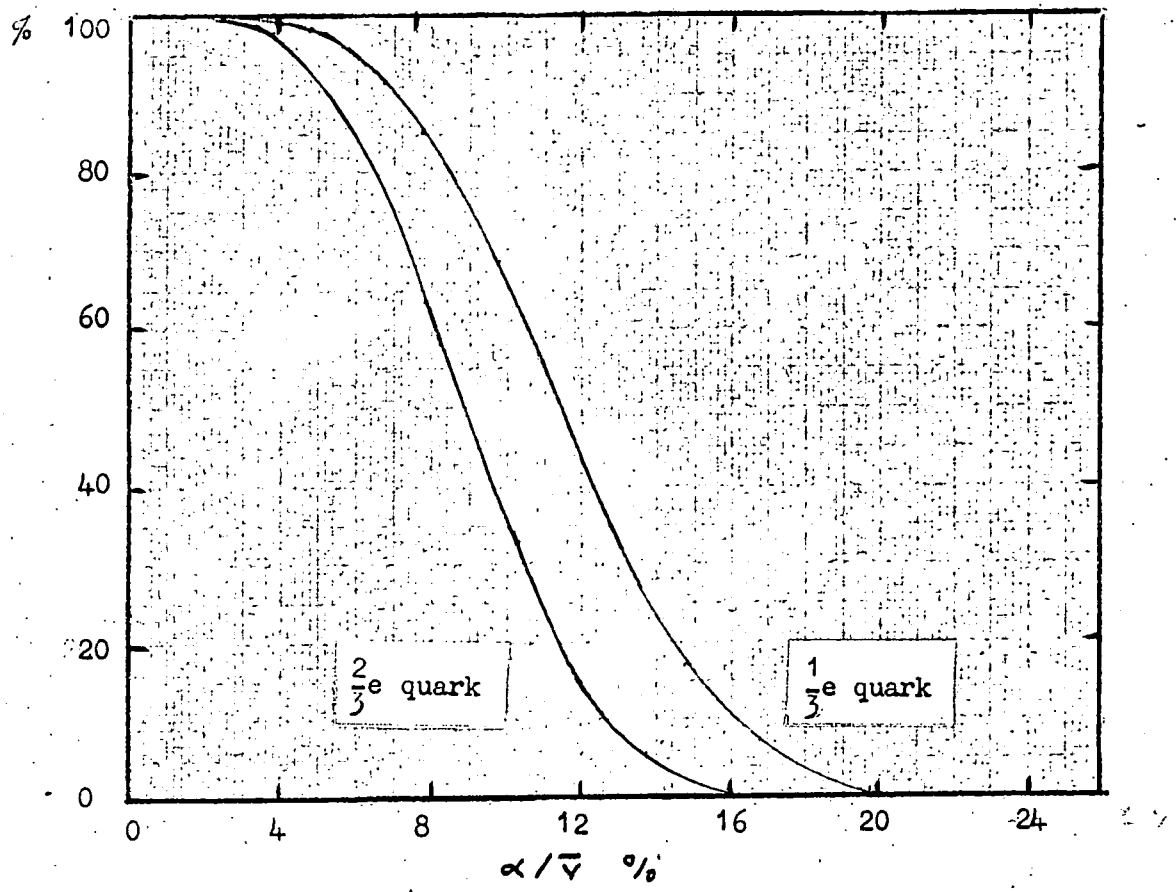

Figure 3.11 Cumulative percentage acceptance of relativistic $\frac{1}{3}e$ and $\frac{2}{3}e$ quarks as a function of $\alpha/\bar{v}$ %.

0.2E and 0.85E and the $\frac{2}{3}$e distribution $>$0.2E. Five values were randomly selected from the 0.2E - 0.85E distribution and one from the $>$ 0.2E distribution and $\bar{\nu}$ and $\propto/\bar{\nu}$ % calculated. This would give the expected distributions in the T selection, however only 3% of the distribution is $<$0.3E and therefore the distributions for the Q selection are not expected to be different. The distributions of $\bar{\nu}$ and $\propto/\bar{\nu}$ % are plotted in Figures 3.12 and 3.13 respectively. As the resolution of the $\frac{2}{3}$e distribution is 45% compared with that of the C distribution of muons of 40.0% the distribution of $\propto/\bar{\nu}$ % for muons with pulse height $<$ 2.0E should be the same as that for $\frac{2}{3}$e quarks in the experimental selection. A distribution of $\propto/\bar{\nu}$ % for such muons is also plotted in Figure 3.13 and is in reasonable agreement with the expected distribution. The percentage of events with values of $\propto/\bar{\nu}$ % greater than a certain value is plotted in Figure 3.11, 90% of the events have $\propto/\bar{\nu} \leqslant 12.5\%$.

3.4 Interactions of quarks in the telescope

Besides the acceptance of quarks depending on the pulse height distribution of a single particle relative to the selection, the possible interaction of quarks in the telescope will limit the acceptance. This is because the production of secondary particles will give pulse heights which will not be accepted by the selection.

Kasha et al. (1967b and c) and Lamb et al. (1966) have assumed an interaction length of 80 gm cm^{-2} for the quark and have

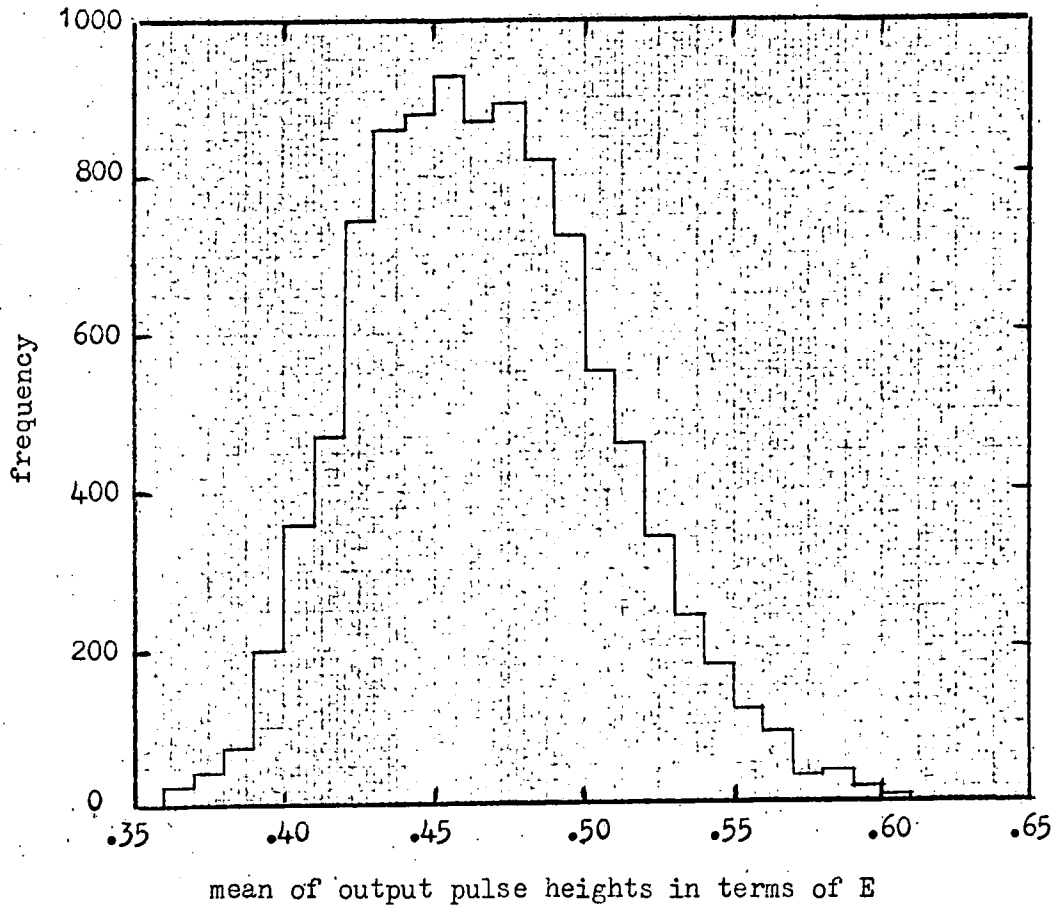

Figure 3.12 The expected distribution of the mean of the output pulse heights from counters A-F for $\frac{2}{3}e$ relativistic quarks traversing the telescope.

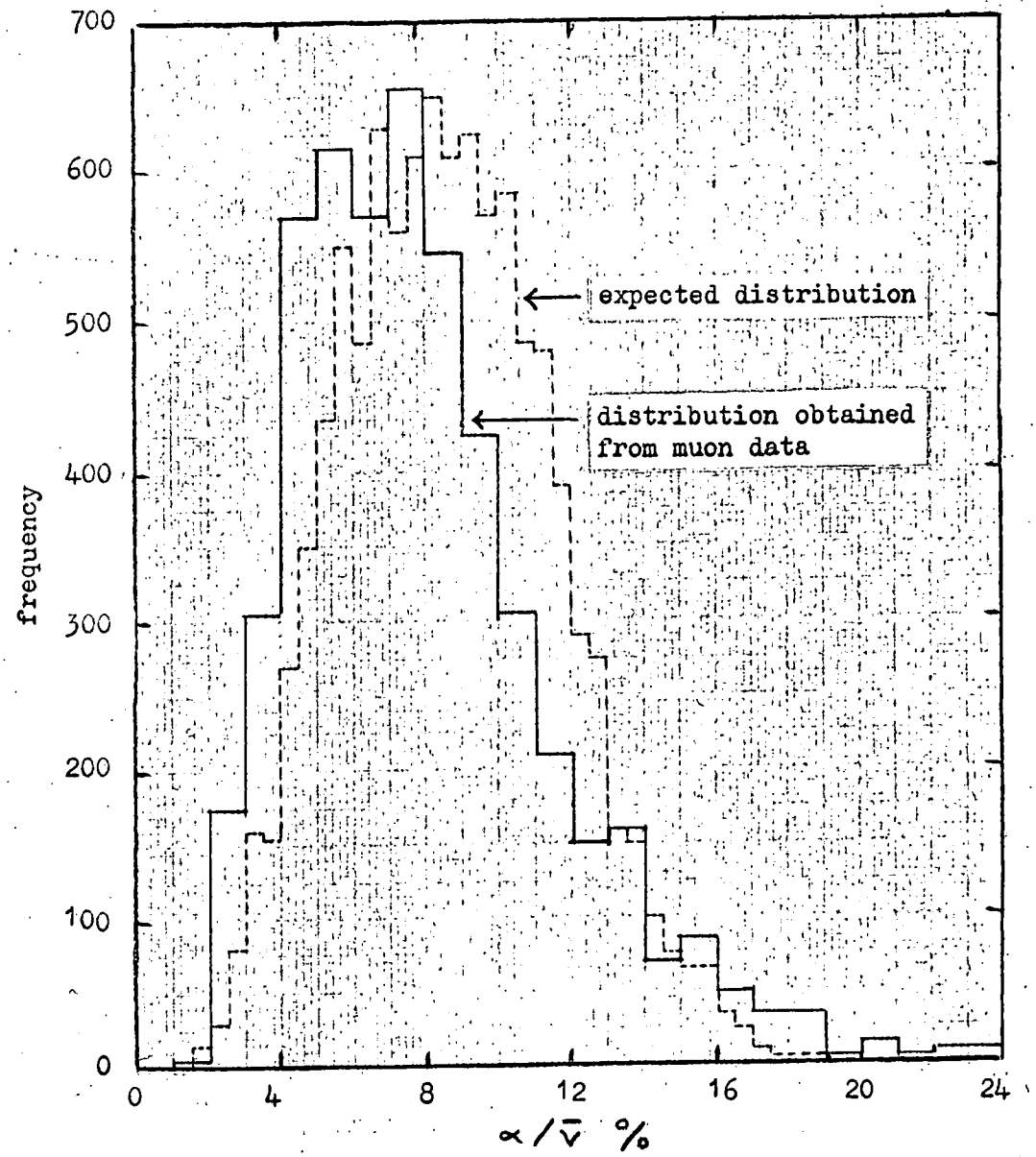

Figure 3.13 The expected distribution for $\propto/\bar{v}$ % for relativistic $\frac{2}{3}e$ quarks traversing the telescope compared with that for muons accepted in C runs with pulse heights in counters A-F <2.0E.

corrected their rates according to the expected interactions in their respective telescopes. For the present telescope with a depth of 60 gm cm^{-2}, the probability of interacting is 0.47. Thus $\sim 50\%$ of quarks passing through the stack will interact and thus will not be accepted.

However, because the interaction length is still a matter for conjecture and the majority of workers have quoted results without taking into account possible interactions, the final results of this experiment are also quoted without taking interactions into account.

3.5 Selection and percentage acceptances for quarks

The initial selection of quark candidates required a track in geometry in all counters in the front and side flash tube views and a value of $\alpha/\sqrt{\nu} < 20\%$. In the final analysis the tracks are accepted if the merit factor N/M lies within the 90% limit and the pulse height data if $\alpha/\sqrt{\nu}$ % also lies within the 90% limit, i.e. $\alpha/\sqrt{\nu} = 16.0\%$ for $\frac{1}{3}e$ quarks and $\alpha/\sqrt{\nu} = 12.5\%$ for $\frac{2}{3}e$ quarks. Thus the effective running time of the telescope for $\frac{1}{3}e$ and $\frac{2}{3}e$ quarks is reduced by a factor 0.81 by the analysis criteria.

CHAPTER 4

PRODUCTION OF QUARKS IN COSMIC RAYS

4.1 Introduction

The paramount importance of energy in revealing new phenomena in the interaction of elementary particles gives cosmic rays the advantage over accelerator physics since cosmic rays are available up to practically infinite energy. Thus, if quarks exist, they should be produced by cosmic rays of adequate energy in the atmosphere and the detection of such particles in the lower atmosphere should be feasible.

Estimates of the quark flux in cosmic rays at sea level depend on the following factors: the energy spectrum of primary protons, the interaction probability of the protons with the air nuclei, the cross-section or fraction of quarks produced in an interaction and the subsequent energy loss processes of quarks in their propagation through the atmosphere.

The intensity of the primary cosmic ray spectrum is now fairly well established as:

$$N(E_p)\, dE_p = 3.8 \times 10^8\, E_p^{-2.5}\, dE_p \ m^{-2}\ day^{-1}\ sterad^{-1}\ GeV^{-1}$$

where E_p is the energy of the primary nucleon in GeV. The total cross-section per nucleon is 30 mbarn at 30 GeV, equivalent to an interaction length $\sim$80 gm cm^{-2} in air.

The cross-section for the production of quarks will depend on the number of possible channels and the probability for each channel. The most probable reactions are:

$$p + N \rightarrow N + N + q + \bar{q}$$

and $$p + N \rightarrow N + q_1 + q_2 + q_3$$

where N represents the nucleon, q and $\bar{q}$ the quark and antiquark and q_1, q_2 and q_3 are the three constituent quarks of the proton. Above threshold energy, channels including pions and nucleon-antinucleon pairs are possible. For the mass of the quark much greater than that of the proton the first reaction will be the most probable and will have a lower threshold energy. By analogy with proton-antiproton production the cross-section can be approximated to:

$$\sigma = \pi(\hbar/M_q c)^2$$

where M_q is the mass of the quark, for M_q = 10 GeV, $\sigma = 10^{-29}$ cm^2.

The energy of the quarks will be moderated by their interactions with nucleons in the atmosphere and through ionisation loss. As there are three quarks in a proton, it might be expected that the quark interaction length in air is $\sim$240 gm cm^{-2}; however, the value 80 gm cm^{-2} is more generally used.

4.2 Production of quarks

Data on many aspects of high energy collisions is still quite inadequate, however the following simple picture gives a possible interpretation and is shown schematically in Figure 4.1.

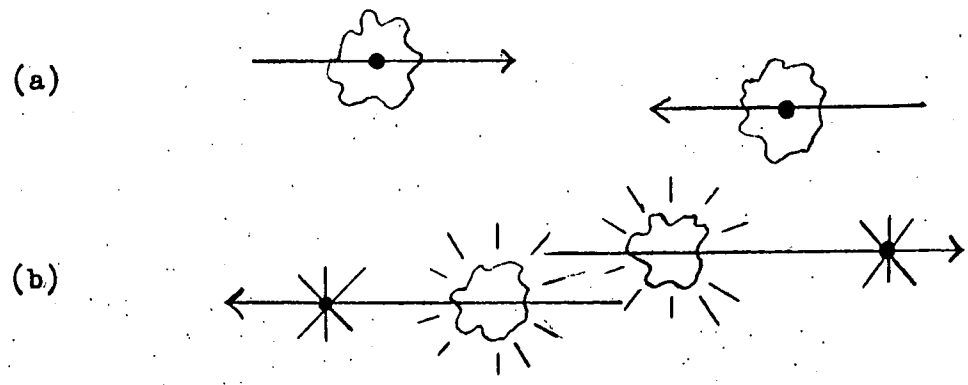

Figure 4.1 Schematic diagram of a nucleon - nucleon collision
(a) before collision
(b) after collision with bare nucleons and fireballs.

A collision between two nucleons can be regarded as a collision between the surrounding pion fields. As a result of the disturbance the nucleons proceed in their original direction in a 'bare' state and radiate mesons in the reconstruction of their field. The original meson fields have interacted and move with a lower velocity in the C.M. system. These 'fireballs' will radiate mesons and pairs including quark-antiquark pairs if they exist. The large number of energetic nuclear active particles found in air showers requires that if only 25% of created particles are non-pions, an important fraction would have to be nucleon-antinucleon pairs. Koba (1965) has presented a calculation in which a statistical equilibrium inside the fireball volume could lead to such a nucleon to pion ratio if one introduced real or imaginary quark states in the first stage of the fireball disintegration.

The cross-section for quarks in any particular production channel will rise immediately from the threshold energy as the phase space increases, the cross-section then reaches a maximum and then decreases as new channels are opened. However, if these new channels contain quarks the probability of quark production does not decrease, but would continue to increase slowly with energy.

Fermi (1950) formulated a statistical model for computing high energy collisons of protons with multiple production of particles. The model assumes a strong interaction between nucleons and mesons

and the probabilities of formation of various possible numbers of particles are determined by the statistical weights of the various possibilities. Fermi assumes that the nucleons produced in the interaction are classical and that the pions are relativistic and neglects the spin of the particles. This theory has been adopted to predict the production cross-section of quarks of various masses in the reaction:

$$p + N \rightarrow N + N + q + \bar{q} + (n-1)(N+\bar{N})$$

where quarks are considered classical and the nucleons relativistic.

The theory assumes that when two nucleons collide with large energy in the C.M. system, the energy will be dumped in a volume Ω. This would normally by a sphere of radius $\hbar/\mu c$ where μ is the pion mass, however due to the Lorentz contraction the volume becomes energy dependant according to the relationship:

$$\Omega = \Omega_o \frac{2Mc^2}{W} \qquad \text{where } \Omega_o = \frac{4}{3}\pi(\hbar/\mu c)^3,$$

W is the total energy of the colliding system and M is the nucleon mass. This volume is the only adjustable parameter in the theory and Fermi states that it is clearly arbitrary and so as suggested previously, the total quark production cross-section is taken to be:

$$\sigma \sim \pi(\hbar/M_q c)^2 .$$

The production cross-section for a quark of mass 2 GeV accompanied by (n-1) nucleon pairs (for n = 1 to 6) is shown in Figure 4.2.

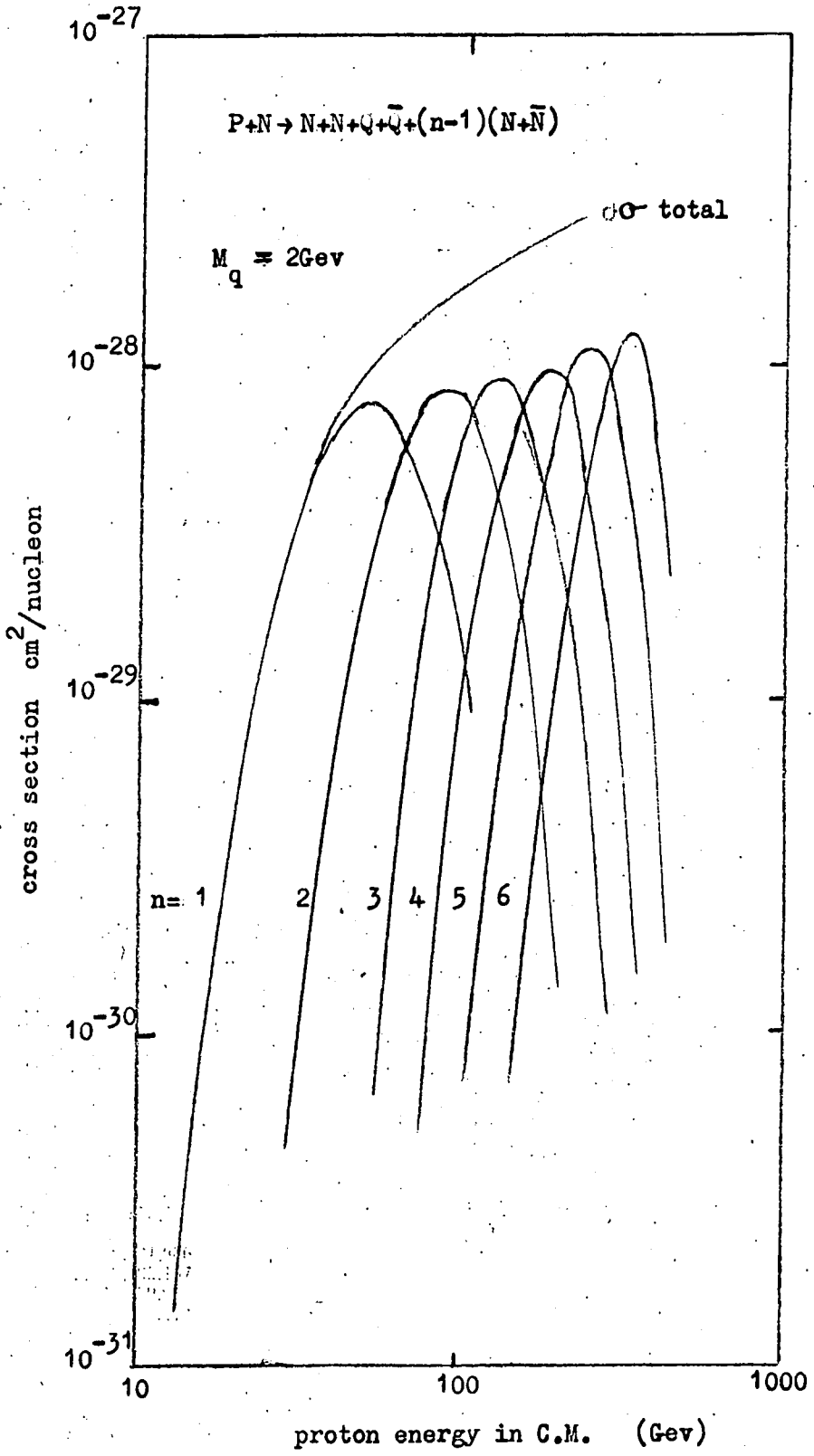

Figure 4.2 Cross section of quark pair production for quark mass of 2 Gev. σ total is the sum of the probabilities for (n-1) accompanying nucleon antinucleon pairs.

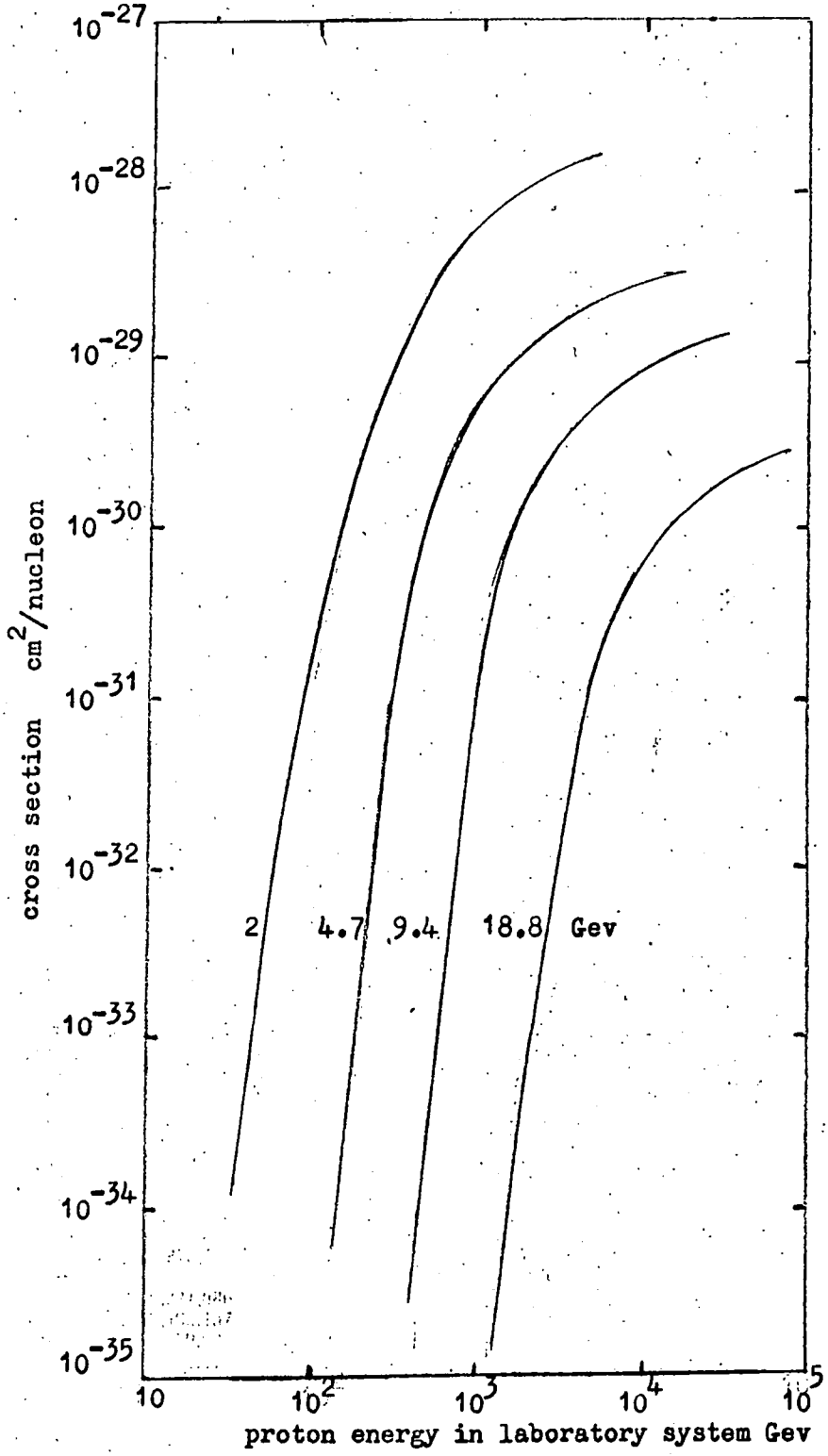

Figure 4.3 Total cross section of quark pairs for different quark mass.

together with the total cross-section. The total cross-section for quarks of different mass is given in Figure 4.3. The cross-sections were evaluated by Mr. T. Takahashi (private communication).

Numerous other models for quark production have been used by different authors with a wide range of values for the cross-section.

Adair and Price (1965), by analogy with proton pair production where the cross-section rises to a maximum at an energy $\sim$ four times the threshold energy use the following relationships:

$$\sigma_T = \sigma_o \left(E/3\, E_{TH} - \tfrac{1}{3}\right)^2 \text{ for } E_{TH} < E < 4E_{TH}$$

$$\text{and } \sigma_T = \sigma_o = \pi(\hbar/M_q c)^2 \text{ for } E > 4E_{TH}$$

where E_{TH} is the threshold energy and E the energy of the incident proton. Assuming the relationship:

$$E_{TH} = \left\{ 2(1 + M_q/M_p)^2 - 1 \right\} M_p c^2$$

where M_p is the mass of the proton, these relationships give reasonable agreement with the Fermi theory. In their presented results an asymptotic value of $\sigma_o = 10^{-30} cm^2$ is used. With the total proton-nucleon cross-section as 30 mb, this is equivalent to a rate of production of quarks of $2\sigma_o/30$ mb $\simeq 10^{-4}$ per proton interaction.

Chilton et al. (1966) have calculated the production cross-section of quark-antiquark pairs in proton-nucleon collisions using an peripheral model. On this model it is found that the cross-section is smoothly dependant on the mass of the quark, such that above the

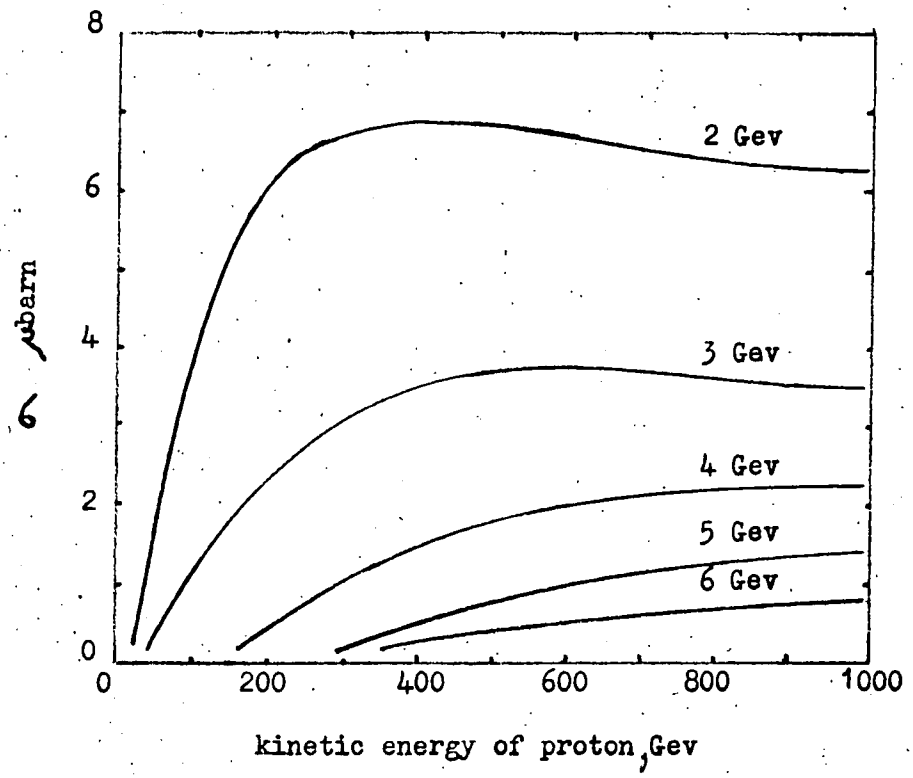

Figure 4.4 Quark production cross-section per nucleon as predicted by Chilton et al. (1966). The curves refer to quark masses as indicated.

threshold energy $\sigma \propto M_q^{-2}$. However, near threshold energies, where the model is not so reliable, an exponential dependance on M_q is obtained. For this reason, the authors suggest that experimental searches for quarks can only be reliably interpreted away from threshold energies. The results of Chilton et al. are shown in Figure 4.4.

Domokos and Fulton (1966) have used the Landau statistical model to calculate the cross-section. As with the Fermi model the reaction is assumed to take place in a volume L, where L is the mean free path of pions in the pion cloud. From this an effective reaction temperature T is obtained, where $T = 2\mu$ where μ is the mass of the pion. This particle gas is cold as far as quarks are concerned. This model gives a cross-section dependant on the quark mass as an exponential. This cross-section is compared with the other estimates as a function of quark mass in Figure 4.5.

Because of the steeply falling primary spectrum of cosmic rays the main production of quarks will take very close to the threshold energy and the statistical model is unlikely to be relevant at these energies as far as the total cross-section is concerned. Peters (1965) suggests that, since accelerator experiments have revealed that the emission of groups of hadrons of low energy cannot be satisfactorily described as the evaporation of an amorphous liquid, an intermediate state resembling a crystal many be a better analogy.

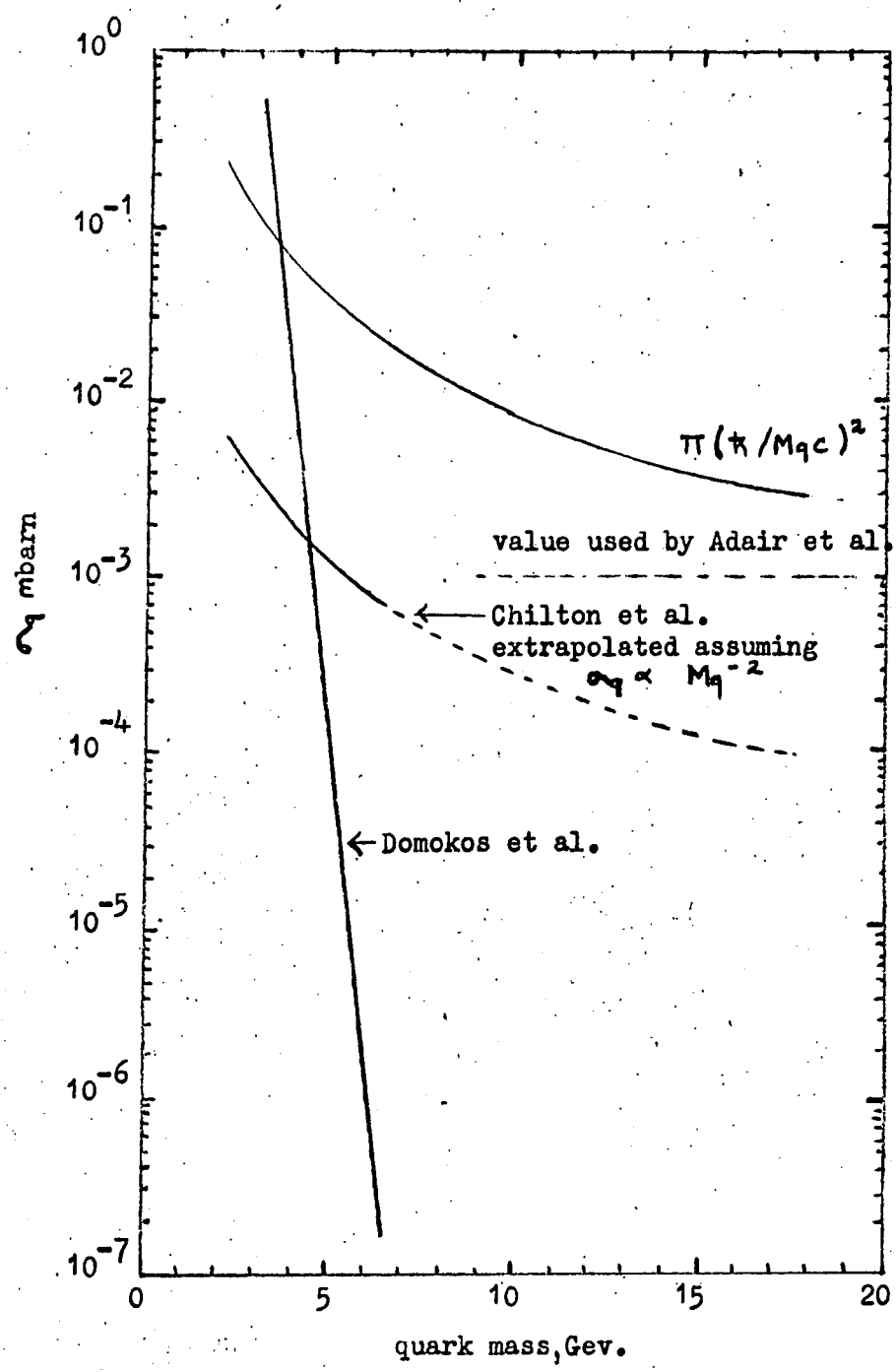

Figure 4.5 Quark production cross-section per nucleon as a function of quark mass as predicted by Chilton et al. (1966) and Domokos et al. (1966). The value used by Adair et al.(1965) and the curve $\pi(\hbar/M_qc)^2$ is also given.

Despite these uncertain theoretical predictions it is important that the search for quarks should be performed to give the best possible limit on the production cross-section.

Besides the production cross-section it is necessary to make assumptions concerning the angular and momentum dependance of quark production. Most models assume the production will be in the forward direction in the laboratory system. Since the incident flux is isotropic, small deviations from production in the forward direction will be irrelevant. Adair and Price assume that the momentum of the quark at threshold is half the momentum of the incident proton. Other workers, Sunjar et al. (1964) and Delise and Bowen (1965) assume that all quarks produced in the atmosphere are close to minimum ionisation loss at the energy at which they are produced.

4.3 Propagation through the atmosphere

Once produced, quarks will proceed through the atmosphere and lose energy by nuclear collisions with nuclei and ionisation loss. For high energies, nuclear collision energy loss is the most predominant. Cocconi (1965) suggests that if the interaction of quarks with nucleons is characterized by a four momentum transfer of ~ 1 GeV, they should lose only a few per cent of their energy in each collision and consequently behave more like muons than nucleons. If the inelasticity is taken to be $0.5\ M_p/M_q$, a quark of mass 10 GeV will lose only 5% of its energy in a collision.

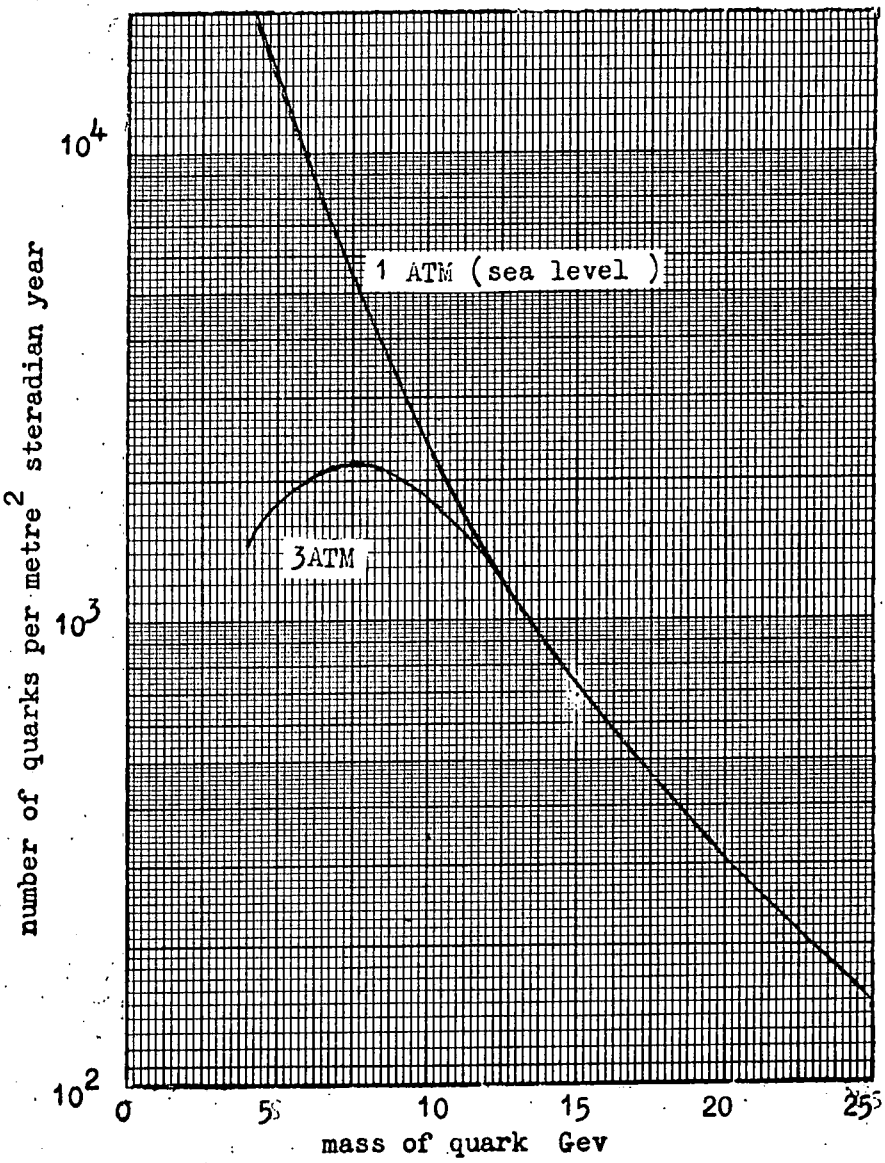

Figure 4.6 Intensity of quarks ($\beta > 0.7$) as a function of mass for a cross section of 10^{-30} cm.^{2} (Adair et al. 1966).

Adair and Price use a model of propagation on the basis that collisions can be described as a change in momentum transfer q, where $t = q^2 = p_x^2 - (E/c)^2$, and p_x is the momentum in the direction along the beam. The probability of a change q is proportional to $\exp(- |t|^{1/2}/q_o)$ where q_o is taken as 0.4 GeV. The model assumes that the nature of the interaction is the same as that described previously for a nucleon-nucleon interaction. Thus the energy of the interacting quark will be lost in two ways:

i) the formation of fireballs and,

ii) the radiation of mesons by the bare quark and nucleon.

Assuming a primary spectrum of $N(>E) = 1.4\ E^{-1.67}\ cm^{-2}\ sec^{-1}\ sterad^{-1}$ with E in GeV, incident protons are selected and assuming the cross-section previously described the produced quarks were followed through a series of random collisions for an interaction length of 80 gm cm^{-2} and an inelasticity as prescribed to obtain the momentum at sea-level. The history of each proton was also followed and the probability of producing a quark at the next collision evaluated etc. until the proton energy dropped below threshold for quark production. The intensity of quarks at sea-level as a function of mass is given in Figure 4.6 for $\beta > 0.7$. The expected rate of quarks for the present experiment estimated from the results of Adair and Price and Domokos and Fulton is given in Table 4.1.

Table 4.1 Expected rate of quarks in the present experiment

Mass of quark GeV	Rate hr^{-1}, according to Adair and Price	Rate hr^{-1}, according to Domokos and Fulton
5.0	8×10^{-1}	5×10^{-1}
6.0	5×10^{-1}	3×10^{-3}
7.0	4×10^{-1}	5×10^{-5}
9.0	2×10^{-1}	5×10^{-7}

Estimates by Sunjar et al. (1964) and Delise and Bowen (1965) give an expected rate of quarks of the same order as Adair et al. if the same production cross-section and attenuation is used.

4.4 Velocity distribution of quarks at sea-level

In the present experiment the rate of $\frac{1}{3}e$ quarks in the velocity range $0.4 < \beta < 1.0$ and $\frac{2}{3}e$ quarks in the velocity range $0.8 < \beta < 1.0$ is estimated and therefore the expected velocity distribution at sea-level is calculated in the following manner.

Ashton (1965) assumes that quarks are produced in the process:

$$p + N \rightarrow p + N + q + \bar{q}$$

and gives the threshold proton energy for production of quarks of mass M_q as:

$$\left\{ 2(1 + M_q/M_p)^2 - 1 \right\} M_p c^2.$$

In the region of threshold energy the quarks will have low kinetic energy in the C.M. system and the kinetic energy of the quarks in the

laboratory system, E_q is given by:

$$E_q = \left\{ \left[\tfrac{1}{2}(E_p/M_p c^2 + 1) \right]^{\frac{1}{2}} - 1 \right\} M_q c^2 \simeq \left(\frac{M_q c^2}{(2M_p c^2)^{\frac{1}{2}}} \right) E_p^{\frac{1}{2}}$$

The primary proton spectrum is taken as:

$$N(E_p)\, dE_p = K E_p^{-\gamma} dE_p \text{ per } m^2 \text{ day ster. GeV,}$$

where $\gamma = 2.5$ and $K = 3.8 \times 10^8$ and thus the integral quark production spectrum is given by:

$$N(>E_q) = \frac{2fK}{\gamma - 1} \left[\frac{M_q c^2}{(2M_p c^2)^{\frac{1}{2}}} \right]^{2(\gamma-1)} E_q^{-2(\gamma-1)}$$

where f is the fraction of p-N collisions that yield quarks.

This quark production spectrum with f = 1.0 is used with a Monte-Carlo calculation to give the velocity distribution at sea-level for a mean interaction length of 80 gm cm^{-2} and an inelasticity of $0.5M_p/M_q$. The production of quarks by the 2nd to 10th generation of protons is also considered. The proton spectrum for the n^{th} generation is:

$$N(E_p)\, dE_p = \frac{K}{(1-\eta)^n} \left(\frac{E_p}{(1-\eta)^n} \right)^{-\gamma} dE_p$$

the inelasticity η is taken as 0.5 (Brooke et al., 1965) and the mean interaction length 80 gm cm^{-2}. From this the equivalent spectrum for the n^{th} generation of quarks is calculated and the quarks again treated as above.

This procedure was followed for a quark of mass 5 and 10 GeV, considering the energy loss due to ionisation of the $\frac{2}{3}e$ quark and

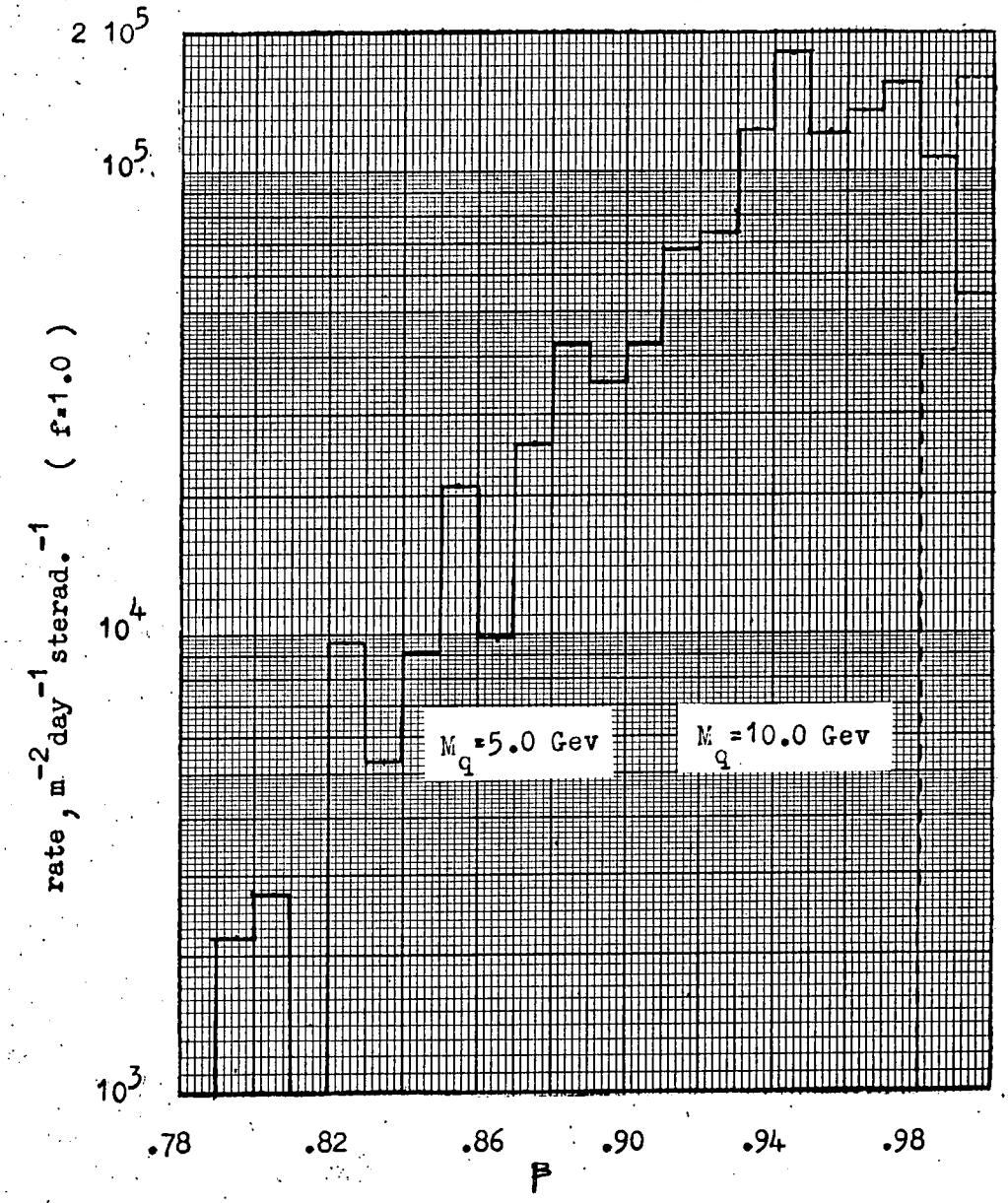

Figure 4.7 Velocity distribution of 2e/3 quarks of mass 5 & 10 Gev at sea level. Inelasticity of q-N collisions taken to be 0.5 Mp/Mq

the resulting velocity distribution is shown in Figure 4.7. The computer programme was compiled by G.N. Kelly (private communication). The result shows a rapid decrease in rate as β decreases. For $\frac{1}{3}$e quarks the decrease will be more steep. Thus the majority of quarks incident in the vertical direction at sea-level will have $\beta > 0.9$.

The rate of quarks of mass 5 GeV for $\beta > 0.8$ is 1.25×10^{6} m^{-2} day^{-1} $sterad^{-1}$, this is for f = 1.0. For a production cross-section of 1 μbam, $f = 3.3 \times 10^{-5}$ and thus the rate will be 42 m^{-2} day^{-1} $sterad^{-1}$. This is in good agreement with the rate given by Adair and Price at 41 m^{-2} day^{-1} $sterad^{-1}$. Similarly, for quarks of mass 10 GeV and a production cross-section of 1 μbam, the rate is 6.4 m^{-2} day^{-1} $sterad^{-1}$ compared with 6.6 m^{-2} day^{-1} sterad given by Adair and Price.

CHAPTER 5

SURVEY OF OTHER EXPERIMENTS

5.1 Introduction

If quarks exist as elementary particles they will be produced in the interaction of a proton with a nucleon:

$$p + N \rightarrow p + N + q + \bar{q} \; (+ n\pi)$$

and $$p + N \rightarrow N + q_1 + q_2 + q_3 \; (+ n\pi)$$

The interaction will produce either a quark and its anti-particle or the three constituent quarks of the proton as well as possible pions and maybe K mesons.

It should, therefore, be possible to detect stable quarks in machine experiments by scanning the secondary beam after the interaction of the proton beam with a target. Similarly primary protons in cosmic rays will interact in the atmosphere and, as well as the usual secondary particles detected, will produce quarks which can be detected assuming they are not absorbed by intervening matter.

If the quarks are absorbed by matter, the 'quarked' atoms will still display the peculiarity of quark charge and an individual atomic spectrum and thus form a basis for detection.

Production of quarks in cosmic rays will effect the production of the 'usual' secondary particles and a search for a discontinuity in the energy spectrum of such particles will lead to an indication

WORKERS	MOMENTUM OF PROTON BEAM Gev/c	DETECTOR	RANGE OF CHARGE & MASS	NUMBER OF TRACKS ANALYSED	UPPER LIMIT WITH 90% CONFIDENCE *
Morrison 1964	24.5	Hydrogen Bubble Chamber	-0.2 to -0.7	10^5	$\sigma_{0.7} < 10^{-33}$ cm^2 $\sigma_{0.2} < 4\times10^{-34}$ cm^2
Bingham et al. 1964	21.0	Heavy-liquid bubble chamber	-0.2 to -0.7	1.2×10^6	5×10^{-34} cm^2
Leipuner et al. 1964	28.0	Scintillation counters	$-\frac{1}{3}$	(i) $3\times10^7 \equiv 10^{10}$ π (ii) $2\ 10^9$	10^{-34} cm^2
Hagiopian et al. 1964	31.0	Hydrogen bubble chamber	+0.25 to +0.75	$\frac{1}{3}$; 6×10^5 $\frac{2}{3}$; 3×10^5	1 in 6×10^5 π 1 in 3×10^5 π
Blum et al. 1964	27.5	Hydrogen Bubble Chamber	-0.2 to -0.7	1.5×10^6	$\sigma < 10^{-35}$ cm^2
Franzine et al. 1965	30.0	time of flight and magnet for heavy mass detection	$-(\frac{2}{3})e$ 2.5 to 5.5 GeV	5×10^8	$\frac{\sigma_{quark}}{\sigma(\bar{p})} \leqslant 10^{-3}$
Dorfan et al. 1965	30.0	ditto	$-(\frac{2}{3})e$ 3.0 to 7.0 GeV	2×10^{10}	$\frac{d^2\sigma}{d\Omega dp} < 2.0\times10^{-36}$ cm^2 sterad^{-1} Gev^{-1}

* Where the limit is quoted as a total cross-section the mass of the quark is taken as 2Gev.

Table 5.1 Results of machine experiments.

of quark production.

5.2 The results of machine experiments

Machine experiments have been divided into a search for particles of sub-integral charge and for particles of mass > 3 GeV. In the former case, detection is by tracks of corresponding bubble density in a hydrogen bubble chamber and by pulses of corresponding height in the case of counters. Heavy particles are detected by a momentum measurement and time of flight technique.

The results of machine experiments are shown in Table 5.1.

Both Morrison (1964) and Bingham et al. (1964) made a study of old photographs of hydrogen bubble chamber tracks with the results as shown. However, as the experiment was not planned to study low density tracks, difficulty arose in distinguishing between apparent quark tracks and previous tracks ($1 < t < 2$ m sec). The efficiency of scanning $\frac{2}{3}$e quark tracks, ~ 12 bubbles cm^{-1} and $\frac{1}{3}$e quark tracks, ~ 3 bubbles cm^{-1} was unknown.

Leipuner et al. (1964) performed their counter experiment in two parts. The first part was based on the assumption that the quark would be weakly interacting. In the first part, absorber of thickness 1.6×10^3 gm cm^{-2} was placed between the target and the counters. The experiment detected 3×10^7 muons, equivalent to 10^{10} pions emitted from the target and no quarks were detected. The expected number based on weak interaction production is 5×10^2, therefore quarks are not produced in nucleon-nucleon interactions

with cross-section $> 10^{-34}$ cm^2 if their mass is $\leqslant$ 2 GeV. In the second part of the experiment the counter was placed in a negative pion beam and no quarks were detected in 2×10^9 pions giving the limit for quark production as: cross-section $< 10^{-34}$ cm^2 for a mass $\leqslant$ 2 GeV.

Hagiopian et al. (1964) performed an experiment designed for detecting positively charged particles in the range + 0.25e to + 0.75e in a hydrogen bubble chamber. To eliminate contamination due to earlier particles an electronic gate was devised such that if a particle entered the chamber in 10 to 1 m sec before its expansion the illumination was vetoed and no photograph was taken. However the upper limit obtained was only 1 in 3×10^5 pions for $\frac{2}{3}$e quarks and 1 in 6×10^5 pions for $\frac{1}{3}$e quarks.

In a similar experiment Blum et al. (1964) for each bubble chamber picture obtained a photograph of an oscilloscope trace giving the time relation between the light flash, the chamber pressure curve and the counter pulse for particles entering the chamber. They found that all low density tracks detected (19 in $\sim$ 154000) corresponded to a previous particle and vice versa so that the efficiency of detection of low density tracks is 100%.

The search for massive particles (mass $>$ 2 GeV) was motivated by the suggestion of Gursay et al. (1964) that triplets would have integral charge and heavy mass.

Franzini et al. (1965) using a system of magnets and scintillation and Cerenkov counters in a time of flight technique were sensitive for charge - $\geq (\frac{2}{3})e$ for the mass range 2.5 to 5.5 GeV. The upper limit for the observation of a heavy particle in the beam is 1 in 5×10^8 pions.

Dorfan et al. (1965) in a similar experiment puts the upper limit for $-\frac{2}{3}e$ quarks of mass 4.5 GeV as 1 in $2\ 10^{10}$ pions.

The negative result of these machine experiments suggests that if the quark exists in either integral or sub-integral charged form the mass is $\geq$ 4.0 GeV. This has lead workers to search for quarks in cosmic rays where incident protons are available with energy above that available in present machines.

5.3 The results of cosmic ray experiments

A series of experiments have been performed for the search of quarks in cosmic rays, the majority in the last two years, 1966 and 1967. A summary of the cosmic ray experiments and their results is given in Table 5.2.

All the experiments, excepting Kasha et al. (1967c), are basically a scintillation telescope where the quark is detected as a particle with non-integral charge $-\frac{1}{3}e$, $+\frac{2}{3}e$, $\pm\frac{4}{3}e$, having energy loss $\frac{1}{9}$, $\frac{4}{9}$ and $\frac{16}{9}$ that of a charge e particle traversing the counter. Because the selection is on energy loss in the counter, and in the $-\frac{1}{3}e$ and $+\frac{2}{3}e$ cases the upper selection is $< E$, events accompanied by another particle will be rejected. Kasha et al. (1967a and b) and

Table 5.2 Results of Previous Cosmic Ray Experiments

WORKERS	DETECTOR	T	D	Q	ACCEPTANCE cm^2 ster sec	RATE cm^{-2} ster sec^{-1}
Sunjar et al. 1964	7 plastic scintillation counters	37*	1000 sea-level	$\frac{1}{3}$	-	$< 4.3\times10^{-8}$
Delise et al. 1965	6 liquid scintillation counters	48	760 (mountain)	$\frac{1}{3}$	9.4×10^{8}	$\leqslant 8.7\times10^{-9}$ +
				$\frac{2}{3}$	9.4×10^{8}	$\leqslant 1.8\times10^{-8}$ +
Massam et al. 1965	6 plastic scintillation counters	32.5*	1000	$\frac{2}{3}$	-	$< 5 \times 10^{-8}$ +
Buhler-Broglin et al.1966	ditto with addition of 2 spark chambers	30.5*	ditto	$\frac{1}{3}$	3.5×10^{9}	$< 1.5\times10^{-9}$ +
				$\frac{2}{3}$	3.5×10^{9}	$< 1.4\times10^{-9}$ +
Buhler-Broglin et al.1967	ditto. 790gm cm^{-2} of iron above telescope	ditto	ditto	$\frac{4}{3}$	-	$< 1.6 \pm 0.8\ 10^{-7}$ +
Lamb et al. 1966	layer of proportional counters 6 scintillation counters	60	1000	$\frac{4}{3}$	2.5×10^{10}	$< 1.2\times10^{-9}$ +
				$\frac{2}{3}$	2.5×10^{10}	$< 4.2\times10^{-9}$ +
Kasha et al.( ) 1966	6 scintillation counters	50	1000	$\frac{1}{3}$	5.9×10^{9}	$2.6^{+2.1}_{-1.3}\times10^{-9}$
				$\frac{2}{3}$	2.1×10^{9}	$2.1^{+1.8}_{-1.5}\times10^{-9}$
Kasha et al.(a) 1967	7 scintillation counters	50	1000	$\frac{2}{3}$	4.3×10^{9}	$< 2.0\times10^{-9}$ +
Kasha et al.(b) 1967	hodoscope of 48 scintillation counters	50	1000	$\frac{2}{3}$	3.25×10^{10}	$< 2.7\times10^{-10}$ +
Kasha et al.(c) 1967	scintillation counters spark chamber momentum spectrometer	-	4000	selection on mass	$\leqslant 7.8\times10^{7}$	$< 2.8\times10^{-8}$ + for 5 Gev $.5 < \beta < .75$
Gomez et al. June 1967	6 trays of scintillation counters 2 spark chambers	-	1000	$\frac{1}{3}$	1.8×10^{10}	$< 1.7\times10^{-10}$ +
				$\frac{2}{3}$	1.8×10^{10}	$< 3.4\times10^{-10}$ +
Barton 1967	6 scintillation counters	102*	60mwe underground	$\frac{2}{3}$	2.95×10^{10}	$< 3.9\times10^{-10}$

T = Thickness of telescope gm cm^{-2}, D is depth in atmosphere gm cm^{-2}, Q is charge acceptance.

* estimated by present author

+ quote with 90% confidence limits.

Lamb et al. (1966) have taken into account the possible interaction of the quark in the telescope and its subsequent rejection assuming an interaction length of 80 gm cm^{-2}. The rates given in Table 5.2 for these authors include this effect.

All authors except Buhler-Broglin et al. (1966) and (1967) and Gomez et al. (1967) had no visual detector to supplement their analysis. Thus the elimination of background showers simulating quarks in these cases is dependant on a strict analysis of the data relying upon the expected pulse height distributions. These distributions for quarks have been obtained by masking the photomultipliers in each counter such that the fraction of light collected is equivalent to that obtained by the energy loss of a sub-integral charge particle. This assumes that the widths of the distributions is entirely dependant on the number of photons collected by the photomultipliers and that the observed Landau energy loss distribution is the same shape for e, $\frac{2}{3}$e and $\frac{1}{3}$e particles.

The main workers in this field have been the Kasha group at Brookhaven and the Massam and Buhler-Broglin group at CERN being an extension from previous workers on machines. The work of these two groups is presented first in more detail and then interesting points in the work of other authors is compared.

Kasha et al. (1966) have used a telescope of six scintillation counters with an acceptance of 650 cm^2 steradian. In (1967a), an extra counter was included to give an acceptance of

600 cm^2 steradian. The positive result of the first experiment for $\frac{1}{3}e$ and $\frac{2}{3}e$ quarks was reduced to an upper limit for $\frac{2}{3}e$ quarks by the second. In neither experiment was there any device to reject weak photon-electron showers simulating quarks. In (1967b) a hodoscope of 48 scintillation counters arranged in 8 trays was used. The 6 counters in a layer were positioned orthoganally, layer by layer. The output of the 6 counters were added for analysis, however for selection a set of counters had to define a straight line thus eliminating much of the background. The acceptance of this array is 1.0 m^2 sterad and the result effectively lowered the limit for $\frac{2}{3}e$ quarks.

Kasha et al. in these three experiments have assumed that there would be a strong and well defined correlation between the pulse heights from the scintillation counters in their stack and that background events such as weak showers would have little correlation since their pulse heights would be distributed at random throughout the acceptance region. They define the quantity:

$$C = \sum_j (h_j - h_{av})^2/(D_j h_j/h_q)^2$$

where h_j is the normalised pulse height in counter j, h_{av} is the weighted average of pulse heights for all the counters, h_q is the pulse height for a fractionally charged particle and D_j is the standard deviation of the pulse heights of such a fractionally charged particle in counter j. Events with $C < 4.0$ were selected comprising 45% of all possible quarks.

In the same notation the acceptance for the present experiment would be:

$$\sum_j (h_j - h_{av})^2 / h_{av}^2 < 1.2 \quad (\sigma/\bar{v} < 20\%)$$

The essential difference is the factor $\frac{D_j}{h_q}$ and is 0.20 for $\frac{2}{3}$e quarks and 0.32 for $\frac{1}{3}$e quarks. If this factor is included to make the acceptance similar to that of Kasha et al., the limits would be:

$$C < 30 \text{ for } \tfrac{2}{3}e \text{ quarks}$$

$$C < 12 \text{ for } \tfrac{1}{3}e \text{ quarks}$$

Thus the present selection is much wider than that of Kasha et al. An important parameter when the pulse height distribution cannot be defined precisely.

The Kasha group have proceeded (1967c) to build a momentum spectrometer at 15° to the horizontal ($\equiv 4000$ gm cm^{-2}) comprising of scintillation counters, spark chambers and bending magnet. It is expected that at such depths the majority of quarks will be non-relativistic. The particles are identified by their momentum, charge, and time of flight through the apparatus. Preliminary investigations give a limit of 2.8×10^{-8} cm^{-2} sterad^{-1} sec^{-1} at 90% confidence for particles with mass > 5 GeV and $0.50 < \beta < 0.75$.

The Massam and Buhler-Broglin group have published three papers. The first, Massam et al. (1965) is a search for $\frac{2}{3}$e quarks using a telescope of six scintillation counters. The analysis was based

on the pulse heights from the six counters alone. In a search for $\frac{1}{3}e$ and $\frac{2}{3}e$ quarks, Buhler-Broglin et al. (1966), two spark chambers, each with four 8 mm gaps were incorporated in the initial telescope. They were filled with a 3:7 helium-neon mixture and operated at zero clearing field when their sensitive time was 60 μsec. The estimated gap efficiency for $\frac{1}{3}e$ quarks was 60%. If a particle was incident in the 100 μsec before an accepted event, its existence was recorded. This eradicated possible events where previous particles could simulate quark tracks.

All events were rejected on either pulse height data or on an inadequate track in the spark chambers with the result as shown in the Table 5.2. The validity of this experiment as with the present experiment, depends largely upon the value of 60% given as the gap efficiency for $\frac{1}{3}e$ quarks. In the case of flash tubes the sensitive time was 100 μsec and this as explained in Chapter 2 is equivalent to an efficiency of 60% after a delay of 5 μsec. This is comparable with the data on the spark chambers.

The third paper Buhler-Broglin et al. (1967) is concerned with the search for quarks of charge $\frac{4}{3}e$. This is regarded as a combination of two $\frac{2}{3}e$ quarks. The combination is expected to have a lower mass than a single quark and hence be more readily produced in proton-nucleon interactions.

The experimental set-up is the same as the previous paper with the main difference that it was covered with 80 cm of iron

(mean thickness for cosmic ray muons $\sim$ 790 gm cm^{-2}). This reduced the cosmic ray flux by 30%. Because of the long tail of the energy loss distribution, the rate of singly charged particles will restrict the detectable upper limit of $\frac{4}{3}$ e quarks. The iron also means that any quarks detected would be leptonic in character. The limit was taken up to the expected background with the result as shown in Table 5.2.

Sunjar et al. (1964) operated a telescope of seven cylindrical scintillation counters with an anticoincidence counter entirely surrounding the telescope at half height in a search for $\frac{1}{3}$e quarks. During the running time of 1 month ($\equiv$ 3.3 x 10^5 muons), 1 event within the selection criteria was detected. This event had pulses in two counters with height twice that expected and the probability of this being due to a single quark is given as 4 x 10^{-4}. Accordingly, the rate of quarks is given as $<$ 1 in 10^5 muons, this is equivalent to a rate of $<$ 4.3 x 10^{-8} cm^{-2} sterad^{-1} sec^{-1}.

The experiment of Delise and Bowen (1965) in a search for $\frac{1}{3}$e and $\frac{2}{3}$e quarks is significant because it was performed at mountain altitude at an atmospheric pressure of 760 gm cm^{-2}. The thickness of the telescope is quoted at 48 gm cm^{-2} although no allowance is made for possible nuclear interaction in the final rates. Because of the absence of a visual detector, certain events could not be rejected so that the result is nominally positive as in the paper of Kasha et al. (1966). The quoted upper limit in an order above

that for experiments performed at sea-level.

The telescope of Lamb et al. (1966) consisted of six scintillation counters and a single layer of proportional counters and was used in a search for $\frac{1}{3}e$ and $\frac{2}{3}e$ quarks. For the analysis of the scintillation counter pulses a similar function to that used by Kasha et al. is defined:

$$C = \sum_j (h_j - h_{av})^2/(S_j\, h_{av})^2$$

where S_j is the percentage half width at half height of the pulse height distribution ($\frac{1}{3}e$, $\frac{2}{3}e$, or e) for counter j. For a Gaussian distribution

$$S_j = 1.15\, \frac{D_j}{h_q} \times 100\%$$

A further selection incorporates the proportional counters where

$$D = C + \left(\frac{h_p - h_{av}}{S_p\, h_{av}}\right)^2$$

and S_p is equivalent to S_j for the proportional counter. Events are selected for $C < 6$ and then $D < 9$.

As well as reducing the accepted background data by the increase from six-fold to seven-fold coincidence, the proportional counter has the advantage of being more sensitive to gamma radiation than the scintillation counter and therefore the background, especially in the $\frac{1}{3}e$ region, will be further reduced. The selection gave one event in the $\frac{1}{3}e$ region and ten events in the $\frac{2}{3}e$ region (the latter being mainly in the beginning of the muon distribution). The rates are given in Figure 5.2 and include the probability of a quark interacting in the 60 gm cm^{-2} of the telescope and the 20 gm cm^{-2}

of the roof immediately above.

The telescope of Gomez et al. (1967) was used in a search for $\frac{1}{3}e$ and $\frac{2}{3}e$ quarks. The stack comprised of twelve scintillation counters arranged in six layers and two four-gap spark chambers. A system was included to indicate the passage of a previous particle in the sensitive time of the spark chambers. The spark chambers were assumed to be 100% efficient for both $\frac{2}{3}e$ and $\frac{1}{3}e$ quarks. Preliminary measurements suggested that the efficiency was above 90%. The minimum definition of a track was two sparks in one chamber and three in the other chamber in line (i.e. a track efficiency of 62.5%). Tracks were not accepted if "extra particle" lights occurred in the chamber, this is equivalent to rejecting particles that were preceded by another within 10 μ sec or followed by one within 1 μ sec. With this assumption the upper limits with 90% confidence are given as 1.7×10^{-10} and 3.4×10^{-10} cm^{-2} $sterad^{-1}$ sec^{-1} for $\frac{1}{3}e$ and $\frac{2}{3}e$ quarks respectively.

Finally, the experiment of Barton (1967) was performed at a depth of 60 metres water equivalent below sea level with a stack comprising of six liquid scintillation counters. The stack was originally designed to measure the rate of muons penetrating to that depth, the gain of the photomultipliers was increased to make the telescope sensitive to particles of $\frac{2}{3}e$ charge. This experiment like that of Buhler-Broglin et al. (1967) is based on the possibility that quarks may be weakly interacting. The rate

of $\frac{2}{3}e$ quarks is quoted as not greater than 3.9×10^{-10} cm^{-2} $ster^{-1}$ sec^{-1}.

These experiments lead to a flux of quarks at sea-level of $< 1.7 \times 10^{-10}$ cm^{-2} $ster^{-1}$ sec^{-1} for charge $\frac{1}{3}e$ and $< 2.7 \times 10^{-10}$ cm^{-2} $ster^{-1}$ sec^{-1} for charge $\frac{2}{3}e$ both quoted with 90% confidence. Experiments at mountain altitude have only given limits of $\lesssim 10^{-8}$ with 90% confidence for $\frac{1}{3}e$ and $\frac{2}{3}e$ quarks.

5.4 The search for quarks by indirect methods

A search has been made for negative quarks which have been produced in the atmosphere, thermalised and then absorbed into the nucleus of some atom. This has the initial advantage that although the flux of quarks in cosmic rays is $< 10^{-9}$ cm^{-2} $sterad^{-1}$ sec^{-1} the collection time for quarks will be the life of the earth $\sim 5\ 10^{9}$ years. If the rate of cosmic rays is assumed constant over this time the total flux would be 1.6×10^{8} cm^{-2} $sterad^{-1}$. This would lead to a concentration of quarks of $\sim 10^{-18}$ per atom assuming all quarks are evenly absorbed in the first 1000 gm of the earth's surface.

Nir (1967) has worked out a merit factor, M for the concentration of quarks in various materials based on the following factors:

1 The depth intensity of quarks in cosmic rays.

2 The length of the irradiation time of the sample.

3 The enrichment in the collection of the sample.

4 The dilution of the quark material by other material.

Typical values of M are 10 for sea water, 3×10^5 for aerosols in the troposphere, 3×10^9 for aerosols in the stratosphere and 10^8 for meteorites.

McDowell and Hasted (1967) consider the case of negative quarks absorbed into the oxygen nucleus in the oceans. Capture will cause dissociation of the water molecule and the quarked oxygen will eventually leave the ocean and be carried to a height of 50 km by the vertical component of the atmospheric electric field. The authors suggest that collection of air in 10^4 gm of charcoal at this height and subsequent analysis by mass-spectrometric methods should give for a negative result an upper limit of 10^{-12} cm^{-2} sec^{-1} for the quark flux.

In the treatment of samples it is important to ensure that the chemical procedures in processing the sample do not in fact remove the object of the search. For this reason previous Millikan oil drop experiments and the experiment of Hillas and Cranshaw (1959) are insensitive to quarks.

Chupka et al. (1967) have exploited this technique for the search of negative quarks in the air at ground level, sea water and iron meteorites. Samples in a gaseous form were passed through a strong electric field and negatively charged atoms would be collected at the anode. The collection plate was then placed in a positive field and the negative atoms accelerated onto the first dynode of an electron mutliplier. The number of output pulses was

recorded as a function of time. For the sample of iron meteorites positive and negative particles were also observed in a mass spectrometer, in this case all masses observed could be identified with known atoms and molecules but the limits for quark concentration were not taken very low. The results of the counting experiment are shown in Table 5.3.

The result for iron meteorities is not a reduction on the upper level of the quark flux given by direct measurement but the results for air and sea water appear to give a much lower level. However, McDowell and Hasted have pointed out that owing to the atmospheric electric field no quarks will be expected in the air at ground level. (Nir did not take this into account when calculating the merit factors). Also the authors admit idiosyncrasies in the results of the air sampling data. In the case of the sea water results the most important factor is the irradiation time of the sample. Nir assumes that the quark will be preferentially absorbed by the heavier elements such as aluminium and iron and gives a time of 10^3 years so that the concentration for quarks would be $\sim 10^{-26}$ per atom. If the assumption of McDowell and Hasted is correct the concentration will be even less than this.

This method therefore, although basically simple in concept introduces many unknown factors into the determination of the rate of quarks without giving an increase in the sensitivity of detection except possibly for samples from the stratosphere.

A different approach to captured quarks in matter was adopted

MEDIUM	N	NUMBER OF COUNTS	CONCENTRATION PER NUCLEON	MASS OF QUARK
iron meteorites	10^{19}	10^{4}	10^{-17}	
air 25°C	$3\ 10^{33}$	10^{2}	10^{-33}	
air 200°C	$3\ 10^{33}$	10^{5}	10^{-30}	10 Gev*
dust 200°C	10^{32}	10^{6}	$3\ 10^{-27}$	
water 25°C	$7\ 10^{26}$	10^{2}	$5\ 10^{-27}$	
water 200°C	$7\ 10^{26}$	5×10^{4}	$3\ 10^{-24}$	50 Gev**

* calculated assuming irradiation time of 10 days

** calculated assuming irradiation time of 10^{9} years

N is the number of molecules sampled

Table 5.3 Results of the experiment of Chupka et al. (1966)

by Sinanoglu et al. (1966). Their search for negative $\frac{1}{3}e$ quarks was directed to the 'quarked' atoms of carbon, nitrogen and oxygen in the sun. These atoms should exhibit distinct electronic spectra in the ultra-violet region. Lines were predicted and a search made in the solar spectrum. Although certain lines were found to be correlated for the carbon and nitrogen atoms, the overall result was negative, and the upper limit for the concentration per nucleon of 'quarked' atoms was less than 10^{-4}.

In cosmic rays, an indirect method was adopted by Ashton and Coats (1967). The aim was to search for a discontinuity in the energy spectrum of neutrons at sea level. If the fraction of nucleon collisions above threshold in which a nucleon dissociates into quarks if f, then the fraction of nucleons reaching sea level is $(1-f)^5$ for 5 nuclear collisions in the atmosphere. Thus above threshold (equated to sea level energy) the spectrum should exhibit a downward displacement. For a quark mass of 10 GeV, the discontinuity at sea level is expected at 90 GeV. For $f = 0.1$ the displacement would be $\sim 50\%$. The results of the experiment would nominally substantiate these figures which would, of course, produce a notable flux of quarks at sea level. The sources of this discrepancy in the experiment could lie in the assumption of the incident proton spectrum having a constant exponent and the estimation of the neutron energy by measuring the size of the burst produced by the nuclear interaction of the particle in iron placed

immediately above a scintillation counter. This experiment is to continue with a larger acceptance and a more refined technique for the detection and energy estimation of neutrons.

5.5 Summary

The machine experiments have put a lower limit of the mass of the quark as 4 GeV for quarks of charge: $-\frac{2}{3}e$, $-\frac{1}{3}e$, $\frac{1}{3}e$, $\frac{2}{3}e$ and e. The results of cosmic ray experiments to date give the upper limit of the rate with 90% confidence as:

$< 1.7 \times 10^{-10}$ cm^{-2} sterad^{-1} sec^{-1} for $\frac{1}{3}e$ quarks

and $< 2.7 \times 10^{-10}$ cm^{-2} sterad^{-1} sec^{-1} for $\frac{2}{3}e$ quarks.

Indirect experiments have been unable to reduce these values.

CHAPTER 6

RESULTS OF THE TELESCOPE EXPERIMENT

6.1 Selection criteria and effective running time

The selection criteria, counting rates and running time for all runs is shown in Table 2.1. The experiment was performed in two parts. The first, called the T series, was a search for relativistic $\frac{2}{3}e$ quarks, the selection would also permit non-relativistic $\frac{1}{3}e$ and $\frac{2}{3}e$ quarks over a certain range of velocities to be accepted. The second, called the Q series, was a search for relativistic $\frac{1}{3}e$ quarks in the lower selection and relativistic $\frac{2}{3}e$ quarks in the upper selection, again non-relativistic $\frac{1}{3}e$ and $\frac{2}{3}e$ quarks would be accepted over certain velocity ranges.

To select particles of sub-integral charge on their energy loss in a counter it would be sufficient to discriminate against particles of incident charge. In practise, however, it is also necessary to employ a discriminator below the energy loss range of the sub-integral particle to eliminate low energy background events.

In the T series, the required condition for acceptance was a 5-fold coincidence of pulses from the counters A B D E F in the range 0.20E to 0.85E. In the first three runs the lower discriminator was set at 0.05E, but due to weak electron-photon showers incident on the sides of the telescope, the rate of events was intolerably high and so the level was increased to 0.20E for the remainder of the run.

Run	T1-70	Q UPPER		Q LOWER	
		1-49	50-97	1-49	50-97
Comments (P.P.I. = previous particle indicator)	No P.P.I.	No P.P.I.	P.P.I. included in selection	No P.P.I.	P.P.I. included in selection
Selection on counters A	.20E - .85E	.30E - .85E		.05E - .30E	
B	.20E - .85E	.30E - .85E		.05E - .30E	
C	independant	.30E - independant		.05E - .30E	
D	.20E - .85E	.30E - .85E		.05E - .30E	
E	.20E - .85E	.30E - .85E		.05E - .30E	
F	.20E - .85E	.30E - .85E		.05E - .30E	
Single counter rates - min^{-1}	$>$ .20E $1.3 \pm .1 \times 10^4$ $>$ .85E $0.9 \pm .1 \times 10^4$	$>$ .30E $1.0 \pm .1 \times 10^4$		$>$ .05E $1.0 \pm .1 \times 10^5$	
Anticoincidence counter rates - min^{-1}	$>$ .20E $4.5 \pm 0.5 \times 10^4$				
Coincidence rates - min^{-1}	5 fold $>$ .20E 1700 ± 100	6 fold $>$ .30E 1600 ± 100		6 fold $>$ .05E 1700 ± 100	
Trigger rate - $hour^{-1}$	2.3	0.5	1.0	1.2	1.6
Total running time - hrs	1225	720	591	758	888
Effective running time - hours	$\frac{2}{3}$e quark, $\beta \neq 1$ 1002	$\frac{2}{3}$e quark $\beta \leq 1$ 610	$\frac{2}{3}$e quark $\beta \leq 1$ 506	$\frac{1}{3}$e quark $\beta \leq 1$ 669	$\frac{1}{3}$e quark $\beta \leq 1$ 776
Number of quark candidates on initial selection	13	1	1	6	7
Expected number of previous particle tracks in candidates	2.3 ± 0.8	$.09 \pm .03$	$.09 \pm .03$	2.7 ± 0.9	4.3 ± 1.5
Number indicated by PPI.			0		3

Table 6.1 Selection criteria and counting rates for all runs

In this selection as in the selection of $\frac{2}{3}e$ quarks in the ψ series, there will be a considerable number of muons from the section $< 0.85E$ of the muon pulse height distribution. To distinguish between quark candidates and muons in the final analysis the upper limit of $\bar{v}$ for quark candidates is taken as $0.65E$. From the expected $\bar{v}$ distribution of relativistic $\frac{2}{3}e$ quarks $> 99\%$ will have $\bar{v} < 0.65E$. If the lower portion of the muon distribution is assumed to be Gaussian, $\sigma = \frac{0.40}{2.3} = 0.174$, and therefore $0.65E$ lies at two standard deviations from the most probable pulse height. The fraction below $0.65E$ is thus 2.3×10^{-2} and for a six-fold coincidence the fraction will be 1.5×10^{-10}. The six-fold rate of muons is ~ 30 sec^{-1} and hence in 1000 hours with $\sim 10^{8}$ muons, the number with $\bar{v} < 0.65E$ will be $\sim 1.5 \times 10^{-2}$. This level of $0.65E$ puts a lower limit of $\beta = 0.8$ on the acceptance of non-relativistic $\frac{2}{3}e$ quarks and correspondingly of $\beta = 0.4$ on $\frac{1}{3}e$ quarks.

In the Q series the lower acceptance for relativistic $\frac{1}{3}e$ quarks was a six-fold coincidence of pulse heights in the range $0.05E$ to $0.30E$ and the upper acceptance for relativistic $\frac{2}{3}e$ quarks and non-relativistic $\frac{1}{3}e$ quarks was a five-fold coincidence A B D E F of pulse heights in the range $0.30E$ to $0.85E$ in coincidence with a pulse of height $> 0.30E$ from counter C.

Slight fluctuations in the discriminator settings can be expected. For every run, therefore, the pulse heights in terms of E for all events were plotted for each counter. This gave an

experimental value of the acceptance range for each counter.

From the expected $\frac{1}{3}e$ quark and $\frac{2}{3}e$ quark pulse height distributions for a single counter the fraction of incident quarks accepted in such a pulse height range can be calculated. These values for the six counters can be multiplied together to give the total fraction of relativistic quarks accepted. For the acceptance of non-relativistic quarks, the most probable energy loss given by Sternheimer is proportional to β^{-2} (Chapter 3), thus the pulse height distribution for relativistic $\frac{2}{3}e$ quarks is also that for $\frac{1}{3}e$ quarks with $\beta = 0.5$, and the fraction accepted will be the same. For the acceptance within this range of β the actual discriminator value was multiplied by β^2 and the fraction found from the relativistic distributions. As mentioned in Chapter 3 the Landau curve for non-relativistic particles has a shorter high energy tail and hence this method will give a slight under-estimate of the actual fraction.

As stated above the limit in the T series is $\beta = 0.8$ for $\frac{2}{3}e$ quarks and $\beta = 0.4$ for $\frac{1}{3}e$ quarks. In the ζ series the resolving time (10n sec) of the coincidence system increases the lower level for $\frac{1}{3}e$ quarks to $\beta = 0.5$.

6.2 Procedure in analysis

For all events the cathode ray oscilloscope (C.R.O.) film and the front flash-tube film was scanned. The six pulse heights on the C.R.O. were measured and the data was then computed to give the

output pulse height from each counter in terms of E and the mean $\overline{v}$, the standard error on the mean α, and $\alpha/\overline{v}$% were calculated. If the front flash tube view had a track (i.e. three flashes in different trays in a straight line) the side flash tube film for that event was scanned to see if the track was reproduced.

The data was divided into events with $\alpha/\overline{v} \leqslant 20\%$ and $\alpha/\overline{v} > 20\%$ and into events with a track in both flash tube views and events with no correlation (n/c) in the flash tube views. Quark candidates were initially accepted for $\alpha/\overline{v} \leqslant 20\%$, $\overline{v} < 0.65E$, and a track in both flash tube views. Similar events with $\overline{v} > 0.65E$ will be mainly muons although some electron-photon showers with the necessary conditions satisfied will be included. Events with $\alpha/\overline{v} > 20\%$ with or without a track will be mainly electron-photon showers although a few muons will be included.

The quark candidates accepted can be one of three possibilities:

1) Genuine quarks such that they fulfill the expected characteristics; i.e. for relativistic $\frac{2}{3}e$ quarks, a most probable $\alpha/\overline{v} \doteq 8.0\%$ and 90% of such quarks with $\alpha/\overline{v} \leqslant 12.5\%$, a mean pulse height such that 90% lie within the range 0.40E to 0.55E, and a flash tube track efficiency of 80% with a low number of background flashes; and for relativistic $\frac{1}{3}e$ quarks, a most probable $\alpha/\overline{v} = 11.5\%$ and 90% of such quarks with $\alpha/\overline{v} \leqslant 16\%$, a mean pulse height such that 90% lie within the range 0.09E to 0.14E, and a flash tube track efficiency of 60% also with a low number of background flashes.

2) A sample of electron-photon showers which would normally be n/c data and would have a random pulse height distribution in the accepted range with the corresponding values of $\alpha/\bar{v}$ %. The track in this case would be expected to be very low in efficiency with considerable background.

3) Pulse heights from an electron-photon shower with the characters described in 2) with a track due to a previous muon (as discussed in Chapter 2 the expected rate of these tracks is ~ 1 in 140). A good track would be observed but the background would be associated with the actual triggered event.

To distinguish between these types of track in the flash tubes the merit factor N/M is used, with N and M as defined in 2.4.2. In that section it was shown that 90% of muons have N/M > 2.0 in both flash tube views. The layer efficiency of the flash tubes for quarks relative to muons is 1.0 and 0.75 for $\frac{2}{3}$e and $\frac{1}{3}$e quarks respectively, therefore 90% of $\frac{2}{3}$e quarks have N/M $>$ 2.0 and 90% of $\frac{1}{3}$e quarks have N/M $>$ 1.5.

The expected distributions of N/M for events of type 2) and 3) are difficult to estimate (8 events of type 3) have been measured and the N/M values are plotted in Figure 2.17) however the following qualitative picture will show the extent to which the criteria can be usefully applied. Events of type 2) and 3) both contain the flash tube data associated with n/c events which in both cases is essentially background. Frequency distributions of

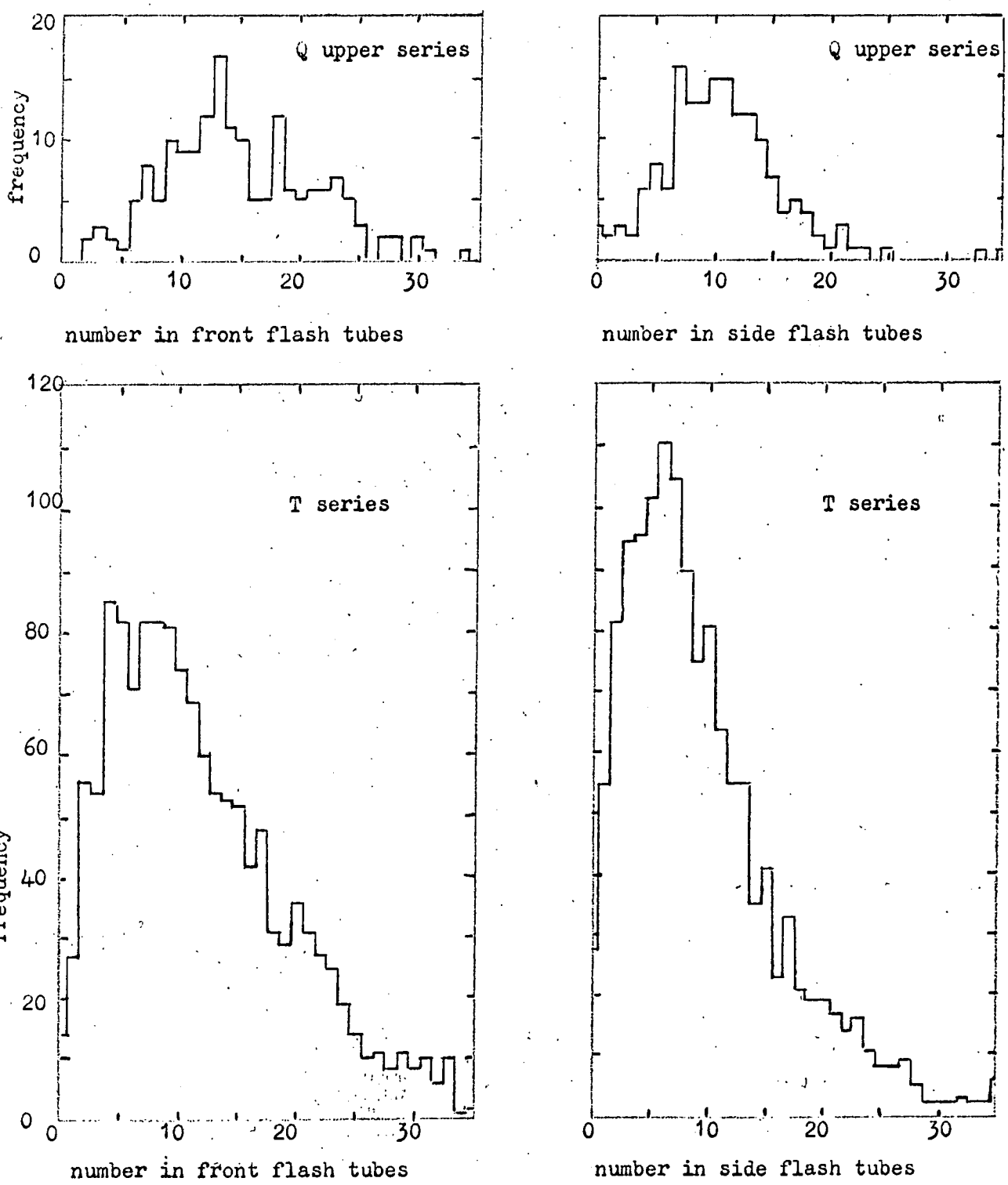

Figure 6.1 Frequency distribution of the number of flashes in the front and side flash tube views for n/c events in the T and Q upper series.

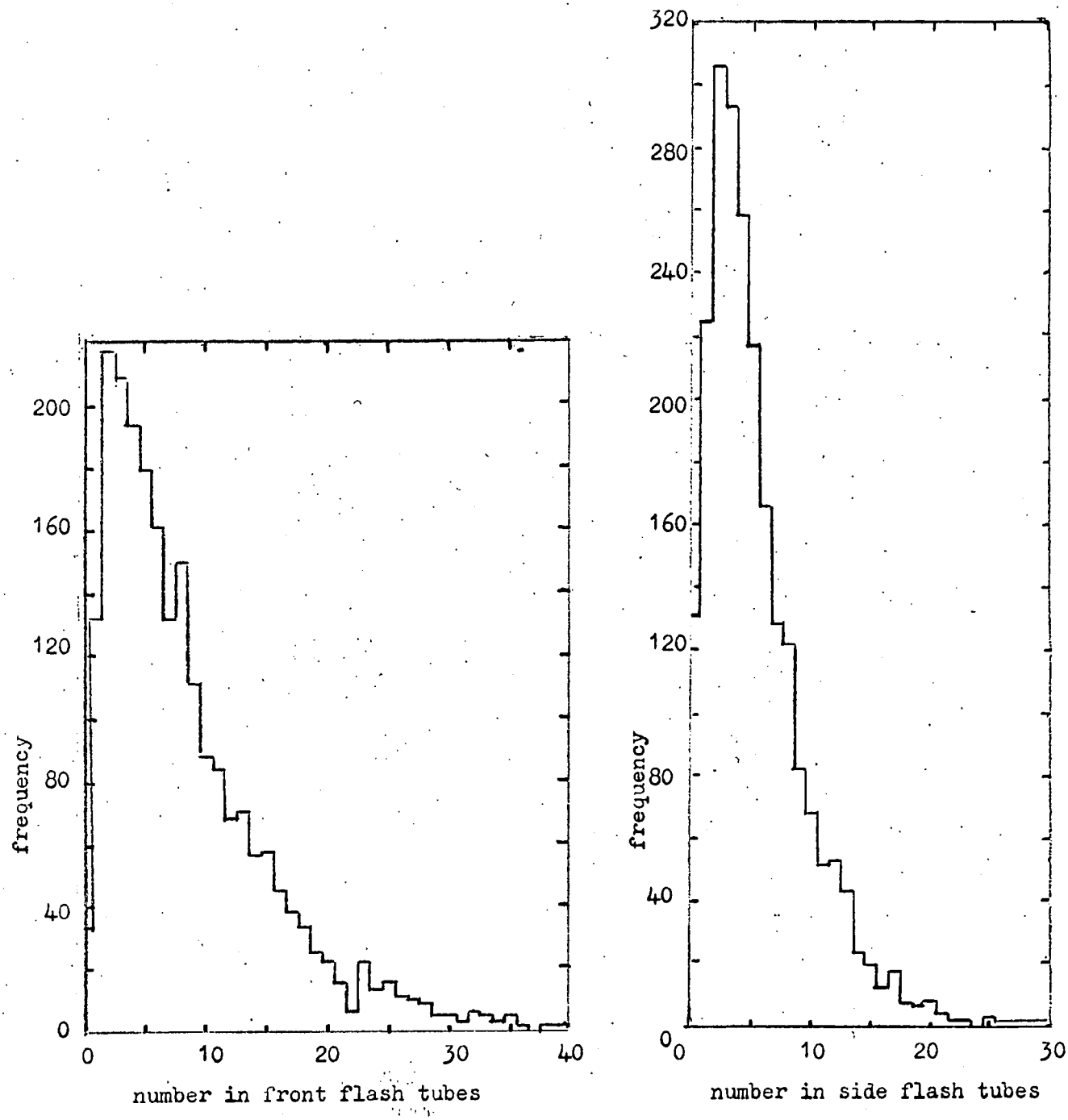

Figure 6.1 Frequency distribution of the number of flashes in the front and side flash tube views for n/c events in the Q lower series.

the number of flashes in the front and side views for n/c events in the T, ½ upper and ½ lower selections are shown in Figure 6.1. Thus in the T and ½ upper selections ~ 50% of events will have $M > 10$ so that even for a track efficiency of 100%, 50% of events will have $N/M < 2.0$ and so a comparison with events of type 1) is possible. In the ½ lower selection, the most probable number of flashes in a n/c event is 2 in both views which is the most probable background for a muon. Hence although events of type 2) will have low N/M, events of type 3) are likely to have similar values of N/M as a genuine quark candidate and the usefulness of the merit factor is limited.

In the final analysis of quark candidates, events are accepted if the values of $\alpha/\bar{v}$ % and N/M lie within the 90% limits. For relativistic $\frac{2}{3}e$ quarks this is equivalent to $\alpha/\bar{v} < 12.5\%$ and $N/M > 2.0$ and the relativistic $\frac{1}{3}e$ quarks $\alpha/\bar{v} < 16.0\%$ and $N/M > 1.5$.

6.3 The T series analysis of events

The T series consisted of 70 runs over a period of 13 weeks. With a useful running time of 1255 hours, the effective running time for relativistic $\frac{2}{3}e$ quarks is 1002 hours and the effective running time for non-relativistic $\frac{1}{3}e$ and $\frac{2}{3}e$ quarks as a function of β is shown in Figure 6.2.

The total number of events was 2851 and the breakdown of these events is given in Table 6.2. The initial analysis gives 13 quark candidates and their values of $\bar{v}$, $\alpha/\bar{v}$ %, and N/M values are given

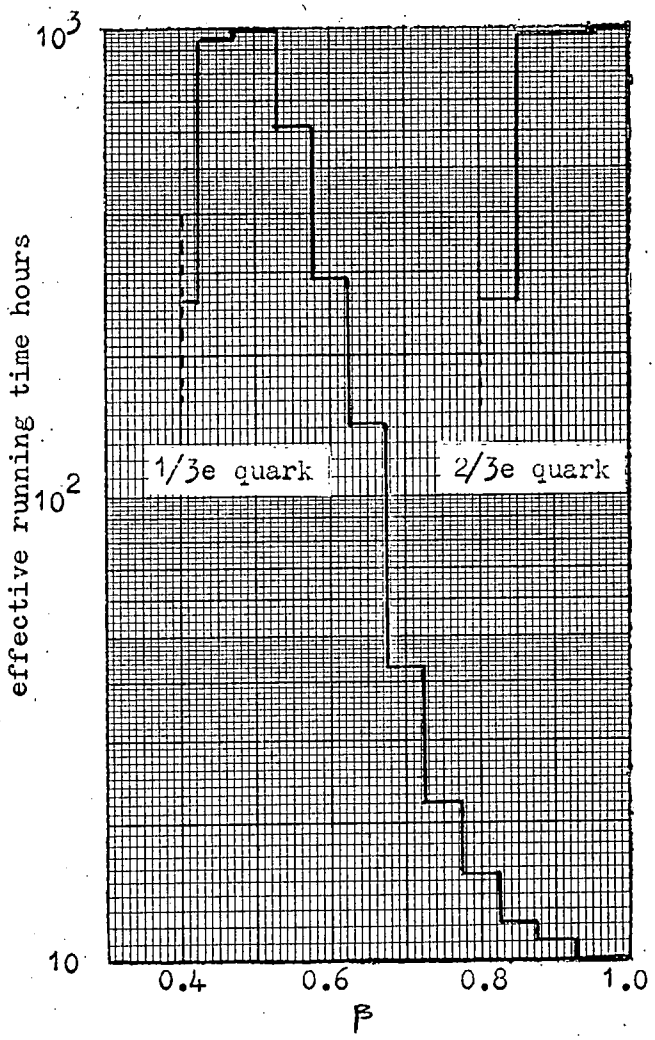

Figure 6.2 Effective running time for 1/3 e & 2/3e quarks as a function of β for the T series. Cut off is due to selection of $\bar{v}<0.65E$.

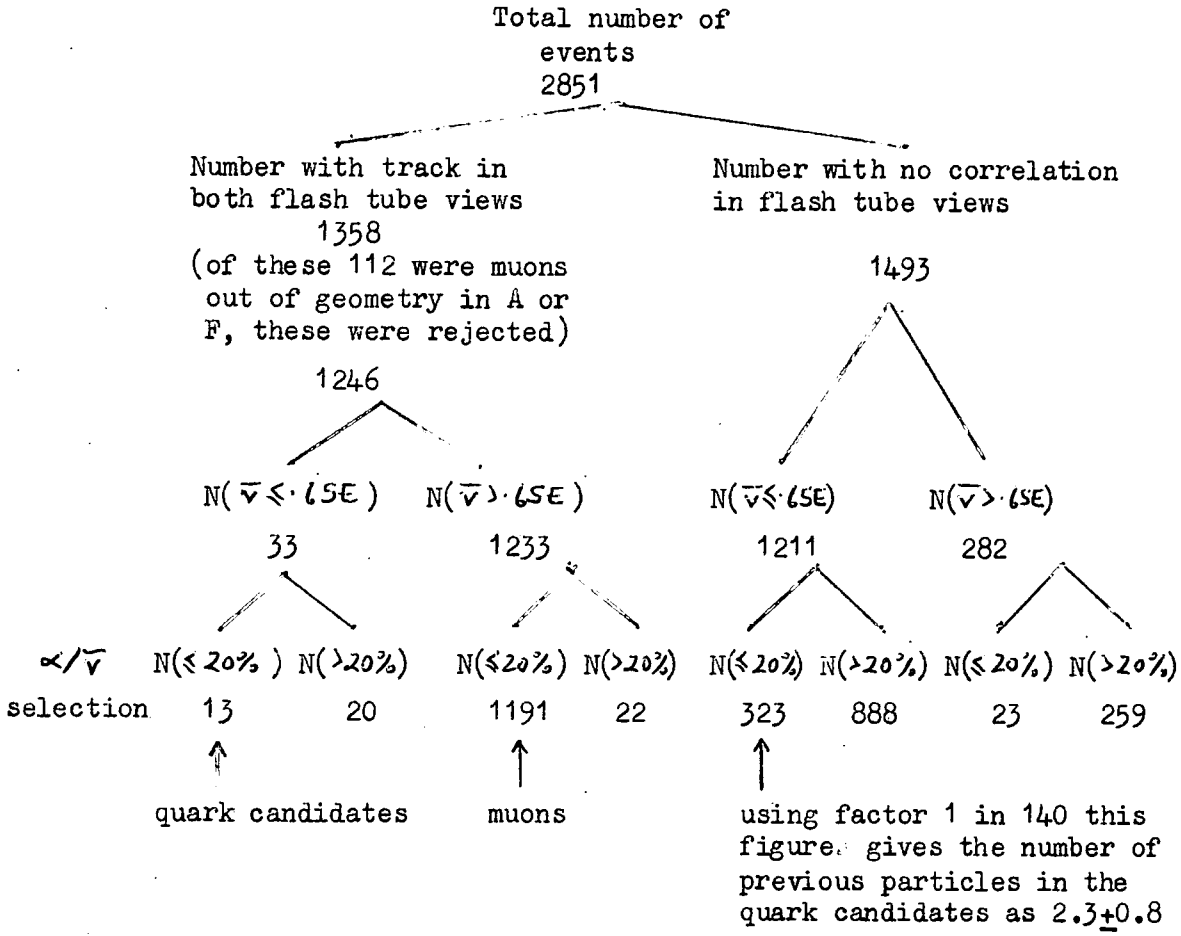

Table 6.2 Breakdown of events in the T series

Run Number	$\bar{\nu}$	$\alpha/\bar{\nu}$ %	N_{front}	M_{front}	$\frac{N}{M}_{front}$	N_{side}	M_{side}	$\frac{N}{M}_{side}$
T16	0.34E	19.7^{i}_{ii}	11 12	14 14	0.79 0.85	3 5	7 7	0.43 0.72
T19	0.51E	15.9	3	5	0.60	3	9	0.33
T48	0.27E	16.7	10	16	0.63	4	10	0.40
T49	0.56E	19.0	5	17	0.30	8	10	0.80
T51	0.61E	18.6	8	8	1.00	7	3	2.33
T52i	0.49E	14.5	10	20	0.50	4	11	0.37
T52ii	0.33E	18.1	8	30	0.27	4	11	0.37
T53	0.63E	16.8	6	24	0.25	6	14	0.43
T55	0.22E	12.5	9	17	0.53	5	16	0.31
T56	0.49E	19.7	4	8	0.50	6	5	1.20
T61i	0.43E	13.1	7	12	0.58	7	7	1.00
T61ii	0.34E	9.8	8	26	0.31	12	11	1.09
T61iii	0.52E	10.3	9	22	0.41	3	4	0.75

Table 6.3 Values of scintillation counter and flash tube data for the 13 quark candidates in the T series

in Table 6.3. The flash tube diagrams for the quark candidates are shown in Figures 6.13 to 6.19 at the end of the Chapter. In the 13 candidates, 2.3 ± 0.8 previous particle tracks are expected.

A frequency distribution of $\overline{v}$ for the 13 candidates and the 1191 muons is given in Figure 6.3, this emphasises the sharp decrease of the lower part of the muon distribution although it will include a few electron-photon shower events. The range of $\overline{v}$ for the quark candidates is virtually over the whole range of possible values and extends to lower values than those of the expected $\frac{2}{3}e$ quark mean pulse height distribution. From this distribution the fraction with $\overline{v} < 0.40E$ is 3.5×10^{-2} and hence the five candidates below this level must be regarded as non-relativistic $\frac{2}{3}e$ quarks. Also shown in Figure 6.3 is the frequency distribution of $\overline{v}$ for n/c events with $\alpha/\overline{v} \leqslant 20\%$. If these candidates are not genuine quarks but events of type 2) and 3) the pulse height data should follow the same distributions as n/c events with $\alpha/\overline{v} \leqslant 20\%$. A comparison of the distributions in Figure 6.3 shows that the quark candidates are a reasonable sample of the electron-photon shower data. For a further comparison of the two sets of data a scatter plot of the mean pulse height $\overline{v}$ against $\alpha/\overline{v}$ % for the quark candidates and n/c data with $\alpha/\overline{v} \leqslant 20\%$ is shown in Figure 6.4. This shows that the frequency of quark candidates increases with the frequency of n/c data, whereas 90% of $\frac{2}{3}e$ quarks should have $\alpha/\overline{v} < 12.5\%$. A final comparison is shown in Figure 6.5 where a frequency distribution of $\alpha/\overline{v}$ % for

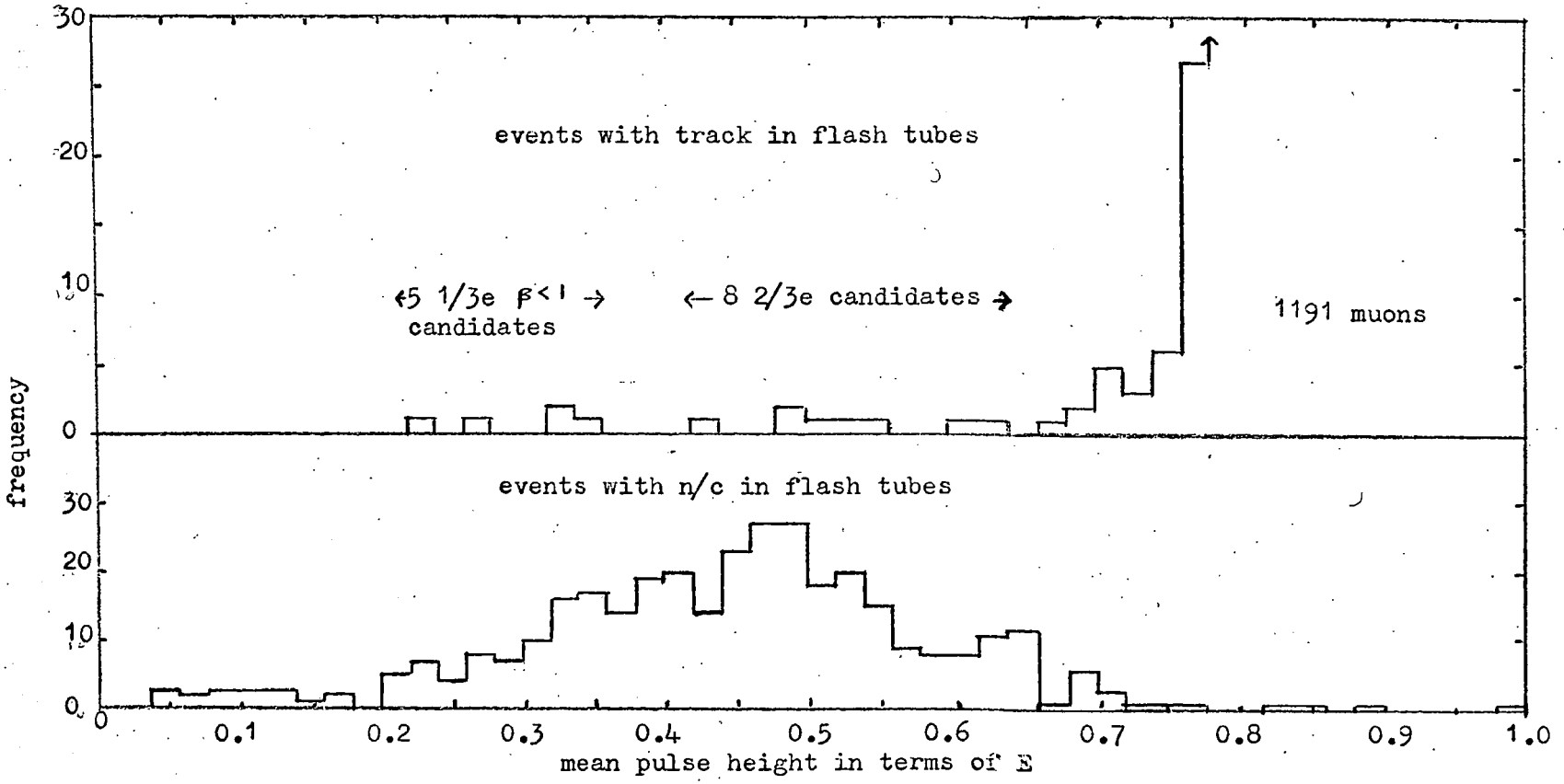

Figure 6.3 Frequency distribution of mean pulse height for events with $\frac{\alpha}{\nu} < 20\%$ for the T series.

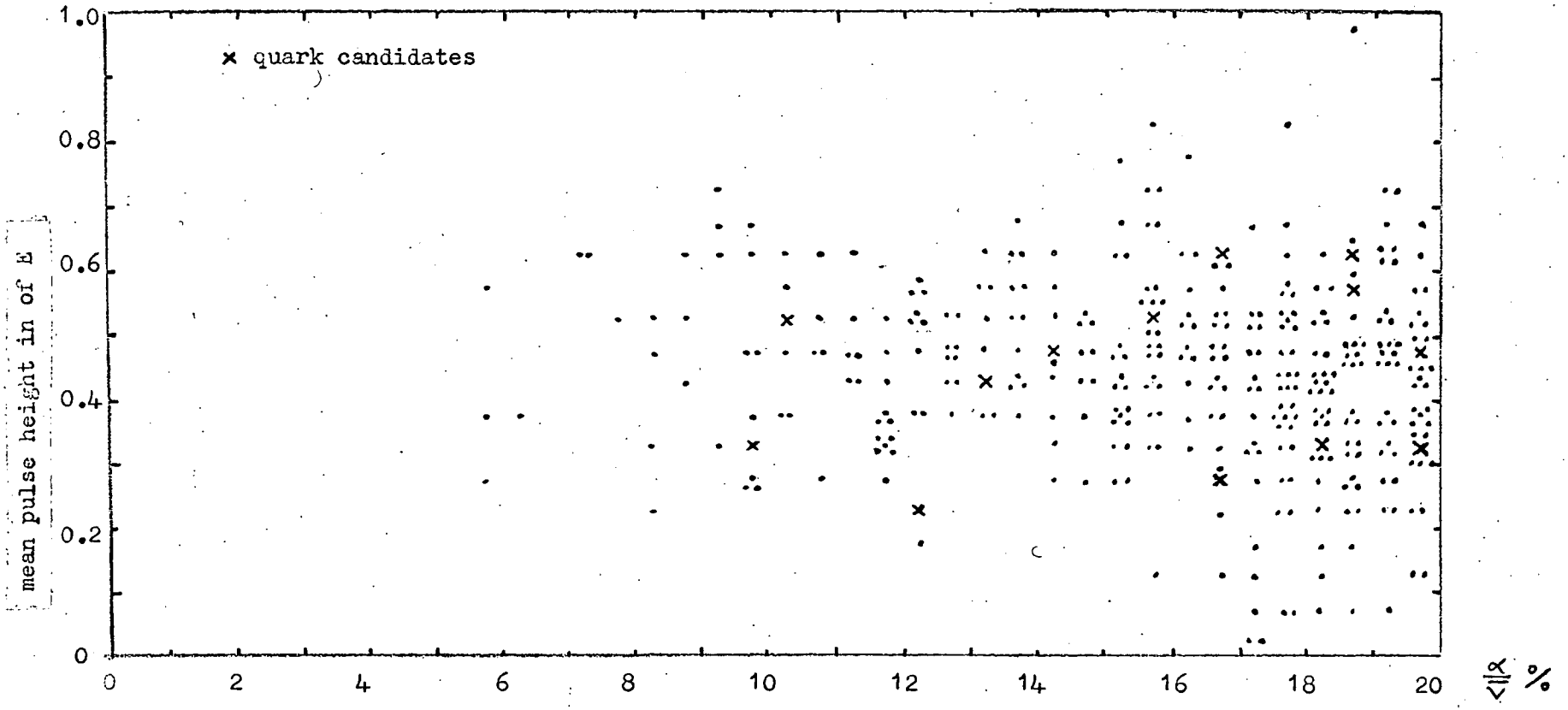

Figure 6.4 Scatter plot of $\bar{v}$ against $\propto/\bar{v}$ for n/c data and the quark candidates in the T series.

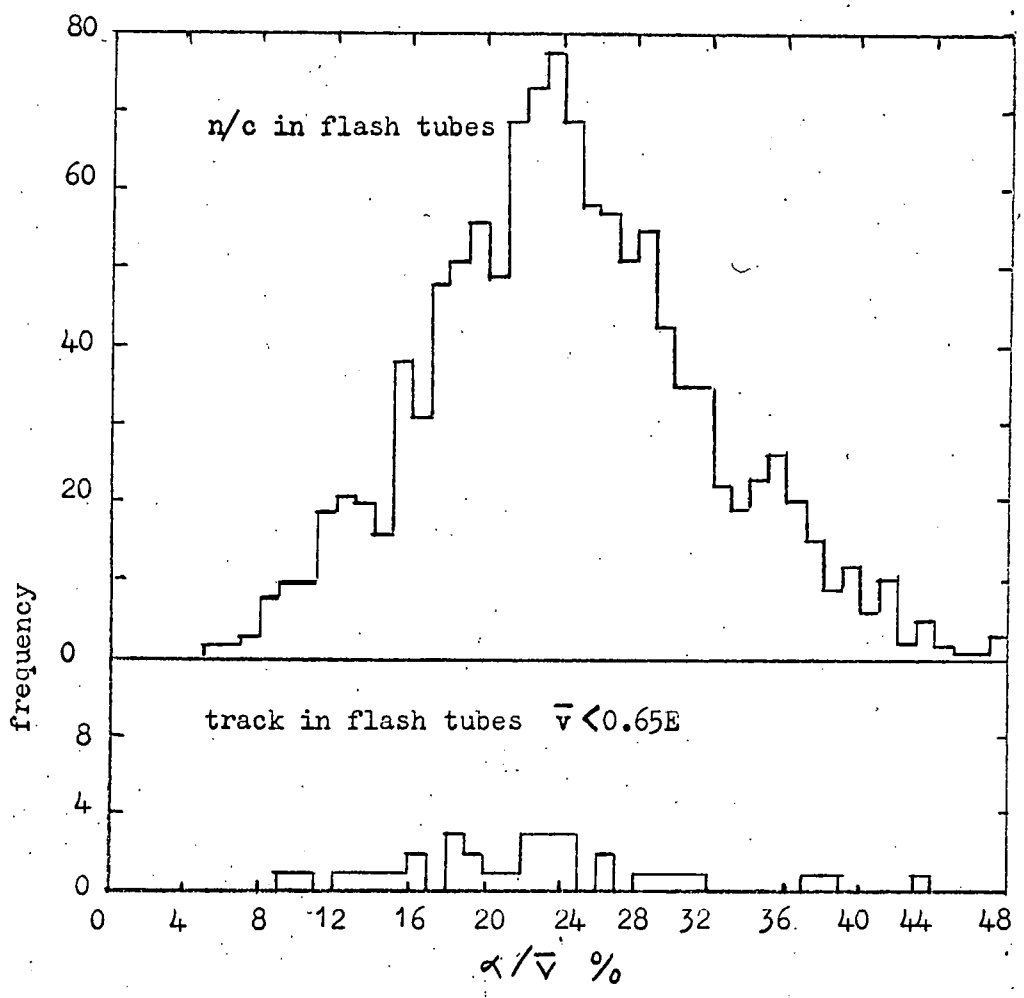

Figure 6.5 Frequency distribution of $\alpha/\bar{v}$% for n/c data and events with track in flash tubes with $\bar{v} < 0.65E$. in the T series.

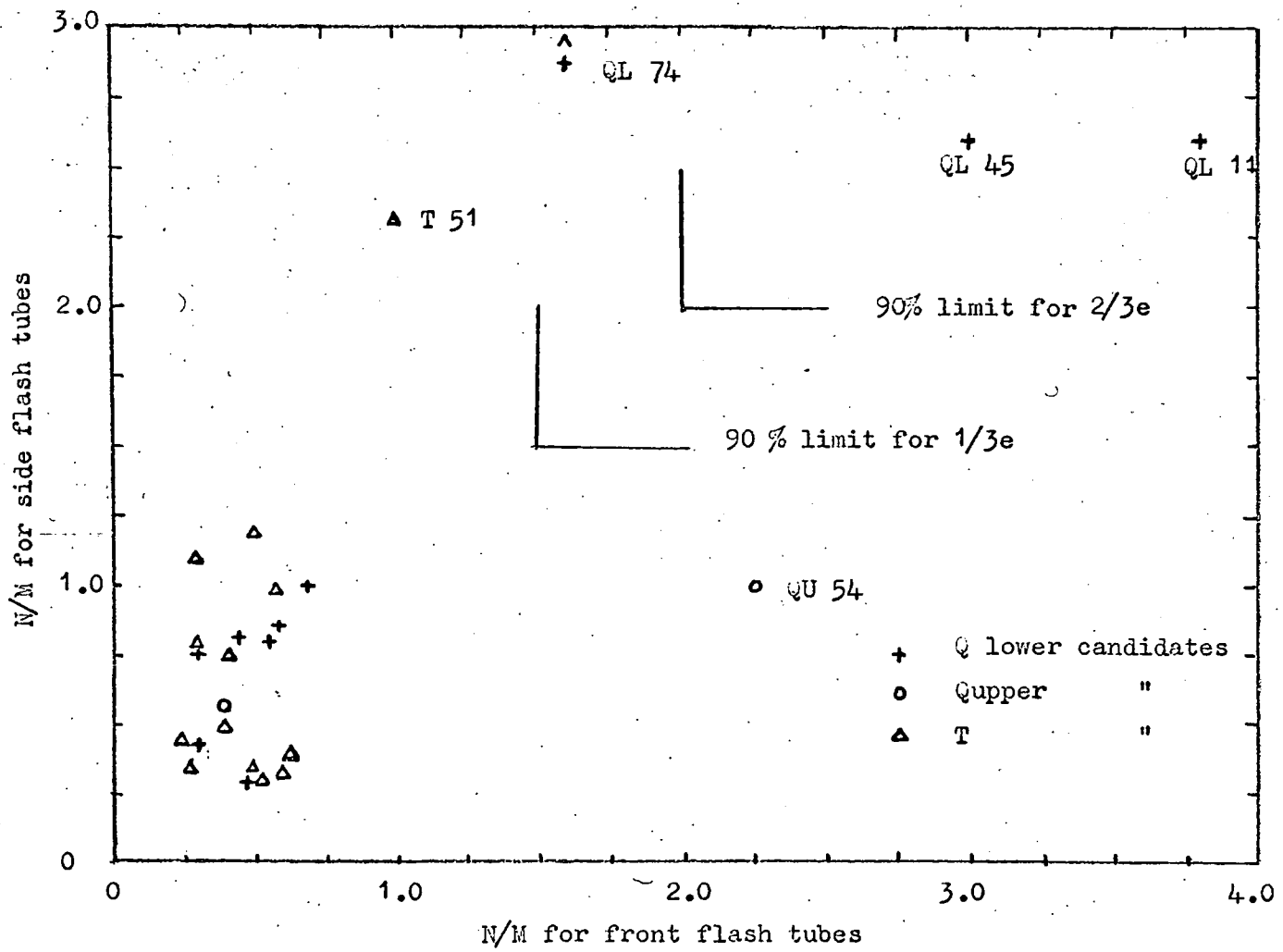

Figure 6.6 Scatter plot of N/M values for all quark candidates. Only events with N/M>1.5 are identified.

all n/c events in the T series (excluding the first three runs where the lower discriminator was at 0.05E) is compared with that for events with a track in both flash tube views.

A quantitative comparison of these distributions is difficult because of the low number of quark candidates, however such events display a typical representation of the electron-photon shower pulse height characteristics. If, indeed, the pulse height information is a sample of such showers, the flash tube data should be of all type 2) and 3) where low values of N/M compared with the 90% limit for $\frac{2}{3}$e quarks (i.e. N/M > 2.0) are expected. A plot of N/M for the front and side views of the 13 quark candidates in the T series is shown in Figure 6.6. One event has N/M > 2.0 and in the side view only, this is T51 with $\alpha/\bar{v}$ = 18.6%.

Three candidates are within the 90% limit of $\alpha/\bar{v}$ %, they are T55, T61(ii) and T61(iii), none have the required N/M values.

6.4 The Q upper series, analysis of events

The Q upper series consisted of 89 runs over a period of 20 weeks. The useful running time was 1311 hours and with the correlation for acceptance the effective running time for relativistic $\frac{2}{3}$e quarks was 1116 hours. As with the previous selection the lower limit of β for $\frac{2}{3}$e quarks was 0.8, but as explained earlier the lower limit for $\frac{1}{3}$e quarks is 0.5. The effective running time for $\frac{1}{3}$e and $\frac{2}{3}$e quarks over these ranges of β is shown in Figure 6.7.

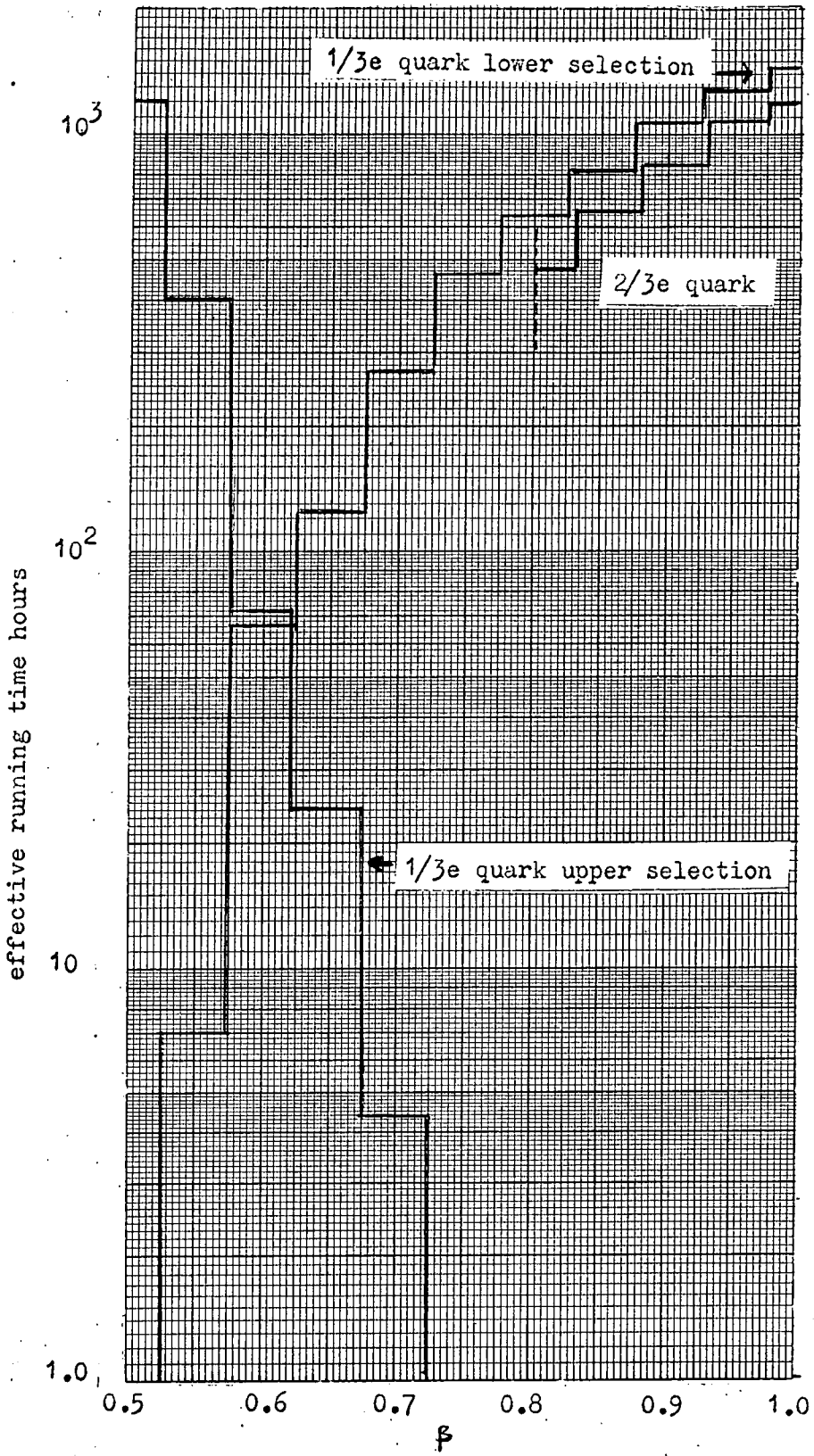

Figure 6.7 Effective running time for 1/3e & 2/3e quarks as a function of β for the Q series. Cut off is due to selection of $\bar{v}<0.65E$.

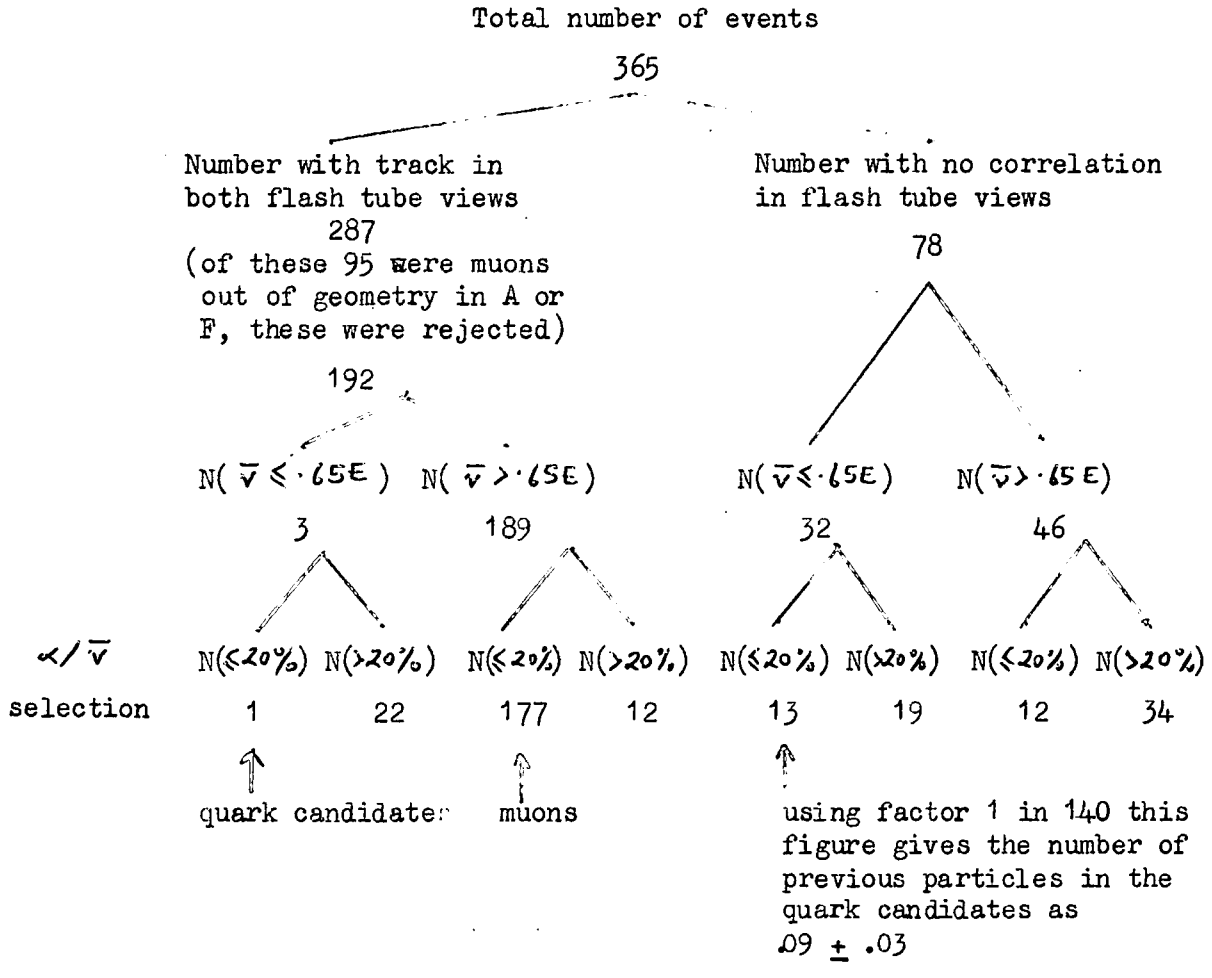

Table 6.4 Breakdown of events in the ψ upper selection for runs 41-49 where the previous particle indicator was not incorporated.

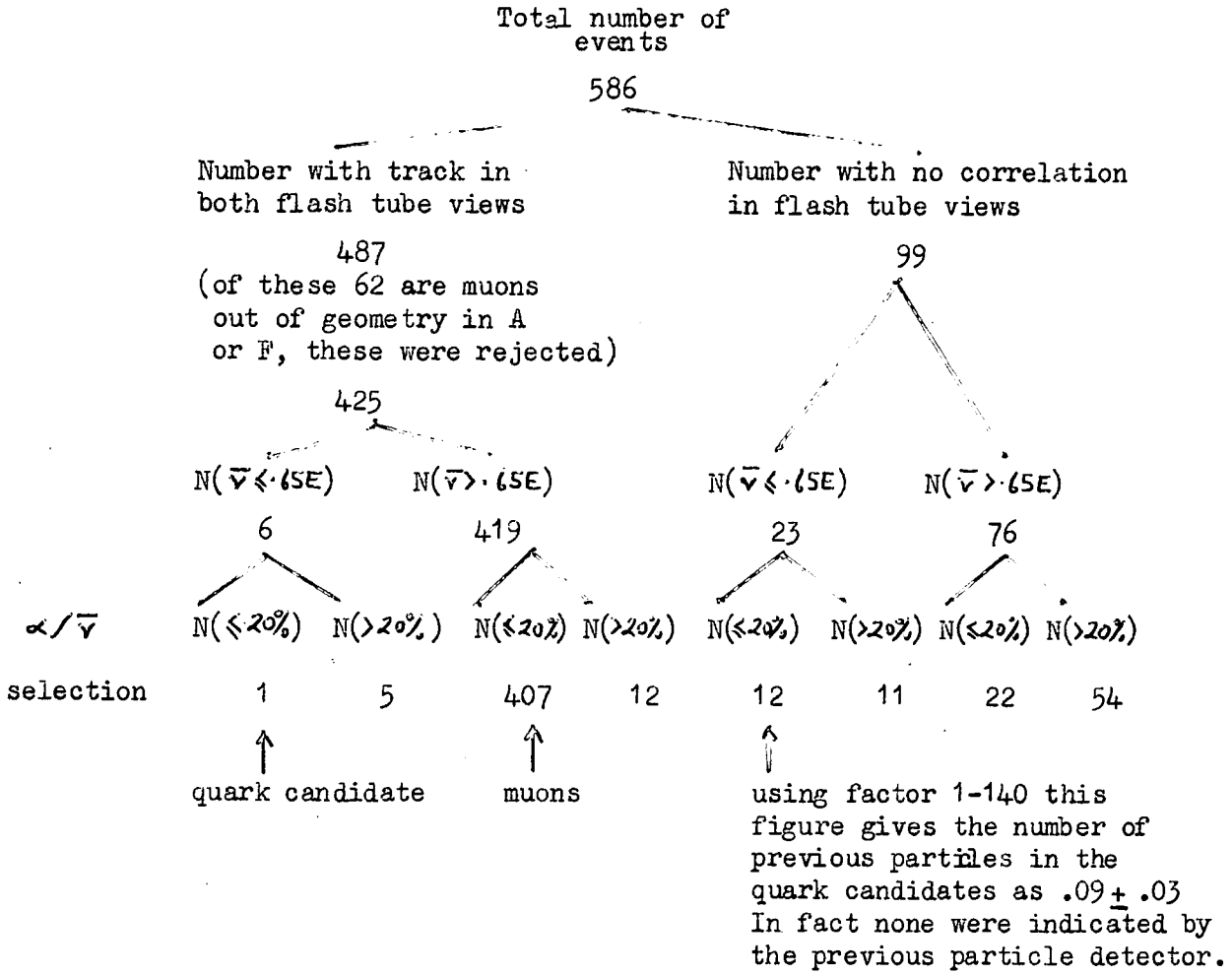

Table 6.5 Breakdown of events in the Q upper selection for runs Q50-97 where the previous particle indicator was incorporated.

Run Number	$\bar{v}$	$\alpha/\bar{v}$ %	N_{front}	M_{front}	$\frac{N}{M}_{front}$	N_{side}	M_{side}	$\frac{N}{M}_{side}$
QU18	0.46E	12.5	14	37	0.38	8	14	0.57
QU54	0.63E	18.9	9	4	2.25	8	8	1.00
QL11	0.13E	19.9	19	5	3.80	13	5	2.60
QL13	0.11E	18.1	5	16	0.31	6	8	0.75
QL14	0.06E	18.9	8	17	0.47	3	9	0.33
QL26	0.16E	11.7	4	7	0.57	5	6	0.84
QL38	0.18E	13.1	12	18	0.67	6	6	1.00
QL45	0.11E	15.0	9	3	3.00	13	5	2.60
QL66	0.16E	17.2	9	24	0.38	4	5	0.80
QL74	0.14E	18.0	8	5	1.60	3	0	∞
QL84	0.17E	13.0	8	29	0.28	9	20	0.45
QL88	0.14E	18.2	10	22	0.46	9	11	0.82

Table 6.6 Values of scintillation counter and flash tube data for the 2 quark candidates in the Q upper selection and the 10 quark candidates in the Q lower selection

The breakdown of the events is in two parts because of the inclusion of the previous particle indicator at Q50, the breakdowns of Q1-49 and Q50-97 are shown in Tables 6.4 and 6.5 respectively. The initial analysis give two quark candidates one in each half and the expected number of previous particle tracks is .09 $\pm$ .03 in each half. In the runs Q50-97 no previous particle was indicated. The values of $\bar{\nu}$, $\propto/\bar{\nu}$ % and N/M for the candidates are given in Table 6.6 and the flash tube diagrams in Figure 6.20. The low number of candidates compared with 13 in the T series is because of the tighter selection. This emphasises the electron-photon shower nature of the candidates in the T series.

The results are treated in the same manner as those for the T series. A frequency distribution of $\bar{\nu}$ for the two candidates and the 584 muons is given in Figure 6.8 together with a frequency distribution of $\bar{\nu}$ for the 59 n/c events with $\propto/\bar{\nu} \leqslant 20\%$. A scatter plot of $\bar{\nu}$ against $\propto/\bar{\nu}$ % for the two quark candidates and the n/c data with $\propto/\bar{\nu} \leqslant 20\%$ is shown in Figure 6.9. The frequency distribution for all events in the Q upper series is shown in Figure 6.10.

Again the quark candidates exhibit the pulse height characteristics more general of electron-photon showers than the expected behaviour for $\frac{2}{3}$e quarks.

The N/M values of the two quark candidates are plotted in Figure 6.6. One event has N/M >2.0, but only in the front view, this is QU54 with $\propto/\bar{\nu} = 18.9\%$. One candidate is within the 90%

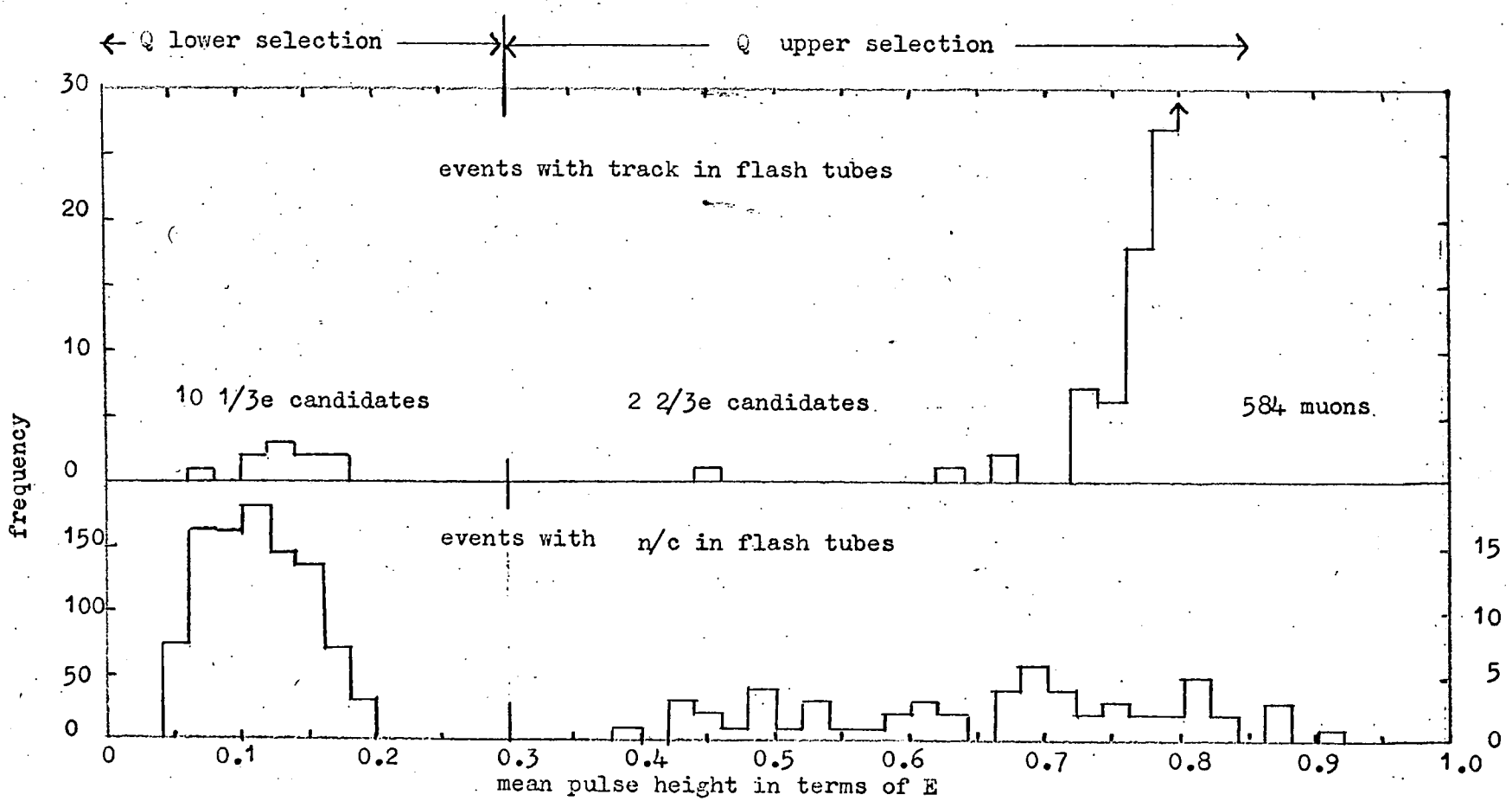

Figure 6.8 Frequency distribution of mean pulse height for events with $\frac{\sigma}{\mu}$<20% for the Q series.

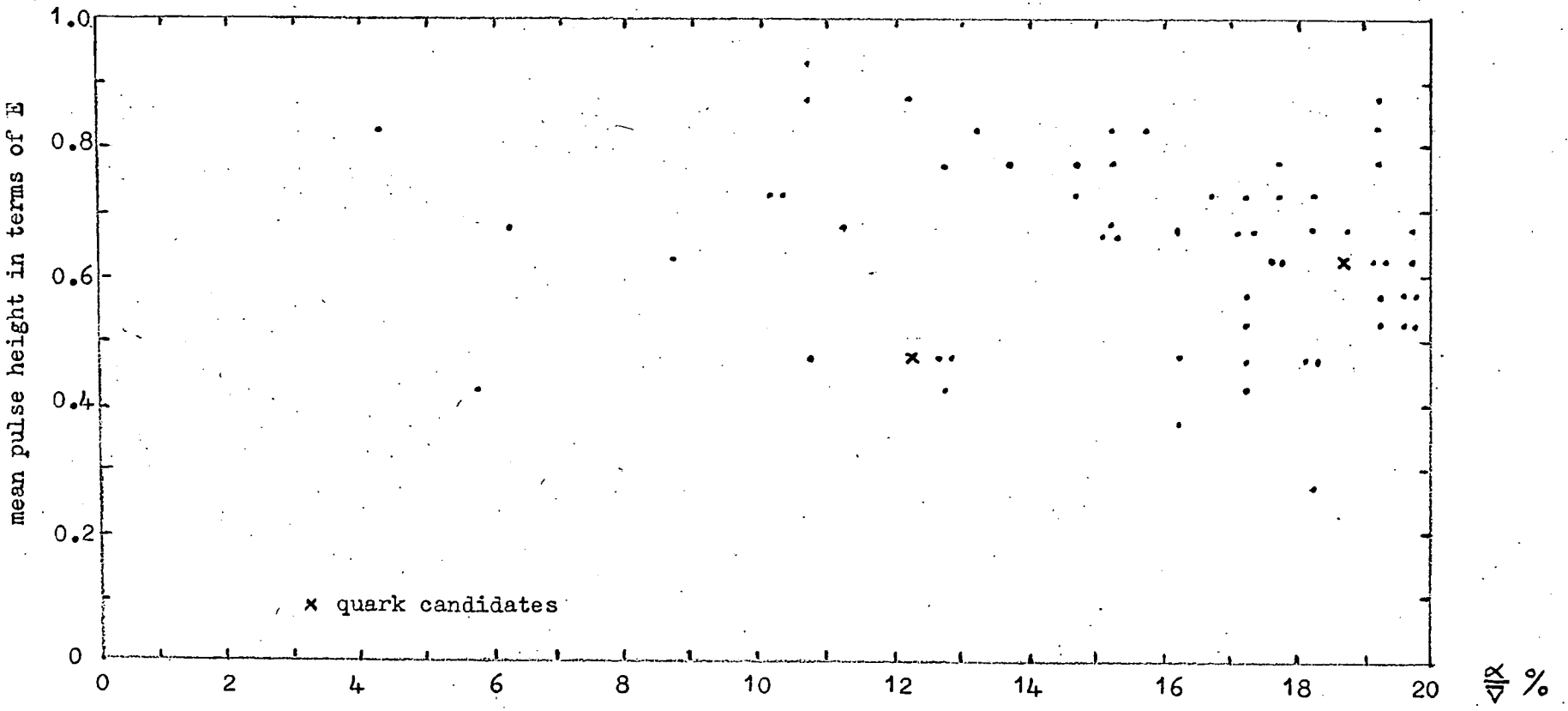

Figure 6.9 Scatter plot of $\bar{v}$ against $\alpha/\bar{v}$ for n/c events and the quark candidates in the Q upper series.

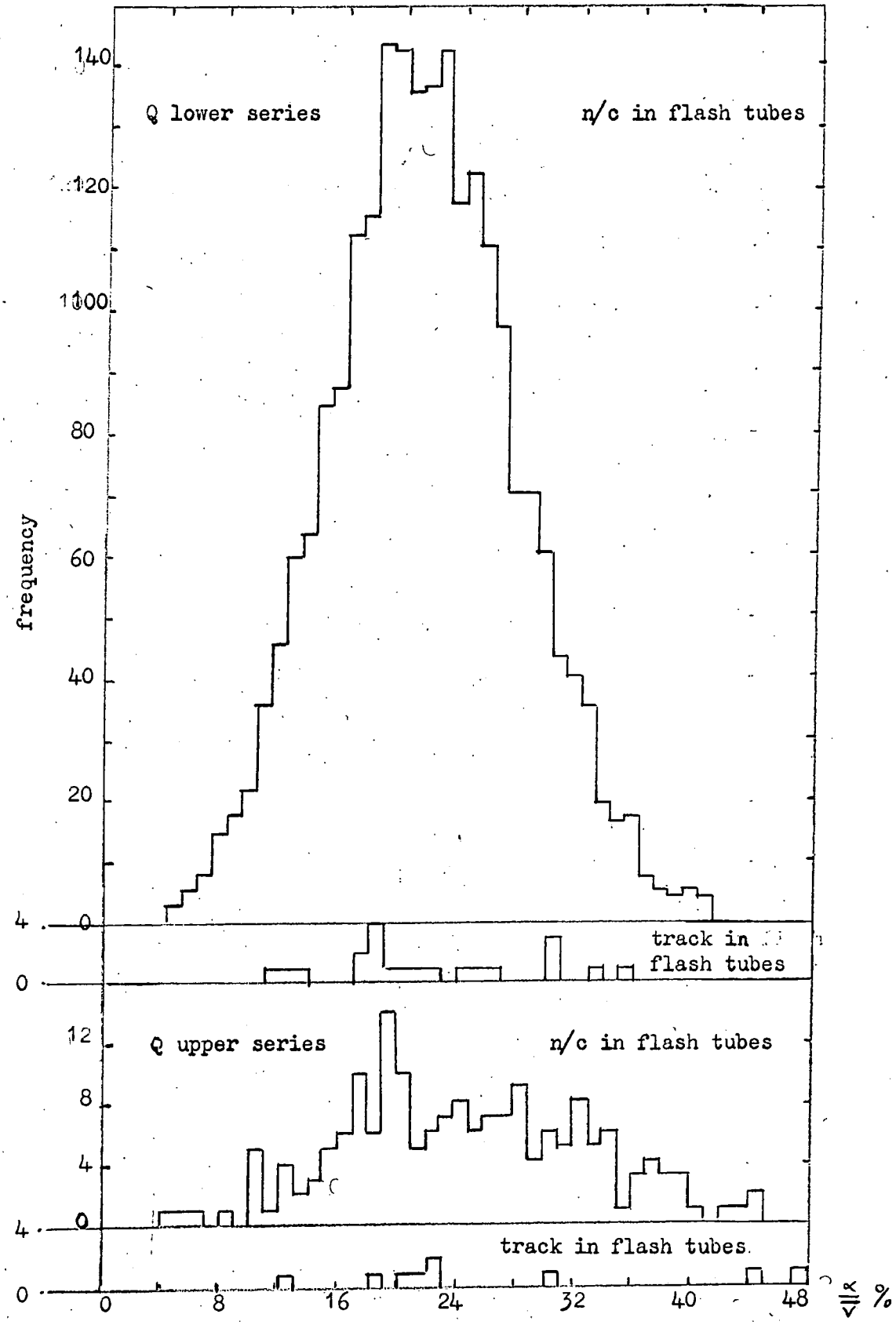

Figure 6.10 Frequency distribution of $\alpha/\bar{v}$ % for n/c data and events with track in flash tubes with $\bar{v}<0.65E$ for the Q series.

limit of $\propto/\bar{v}$ %, this is QU18, but it has not the required N/M values.

6.5 The Q lower series, analysis of events

Three important points to note in the Q lower selection are:

1) Because of the increased width of the expected pulse height distribution in a single counter the 90% limit of $\propto/\bar{v}$ % is increased to 16%. This means that a greater fraction of n/c events are capable of simulating quarks.

2) The large number (2273) of n/c events accepted not only gives a further increase in events simulating quarks but also an increase in the number of previous particle tracks which can appear as quark candidates.

3) The low number of flashes in the front and side views in the n/c data which leads to values of N/M for previous particle tracks which are similar to those expected for quark candidates.

The last two arguments refer only to the runs Q1-49 where in previous particle indicator was not incorporated in the selection system.

The Q lower series consisted of 95 runs over a period of 20 weeks. The useful running time was 1646 hours and after correctionn for acceptance the effective running time for relativistic $\frac{1}{3}e$ quarks was 1445 hours. The effective running time for non-relativistic $\frac{1}{3}e$ quarks as a function of β is given in Figure 6.7.

The breakdown of events is again done in two parts and shown in Tables 6.7 and 6.8 for QL1-49 and QL50-97 respectively. In

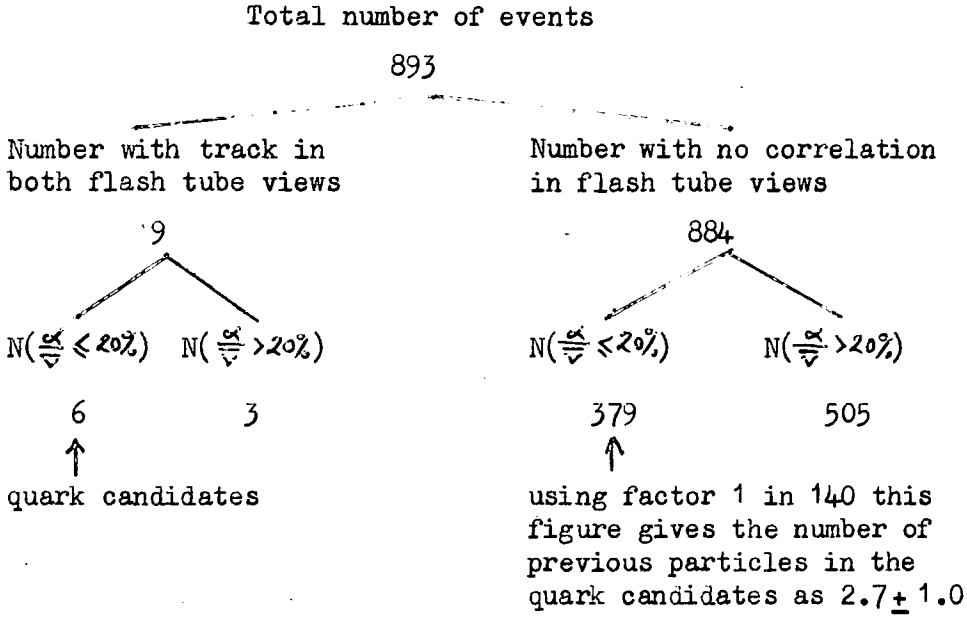

Table 6.7 Breakdown of events in the Q lower selection for runs Q1-49 where the previous particle indicator was not incorporated.

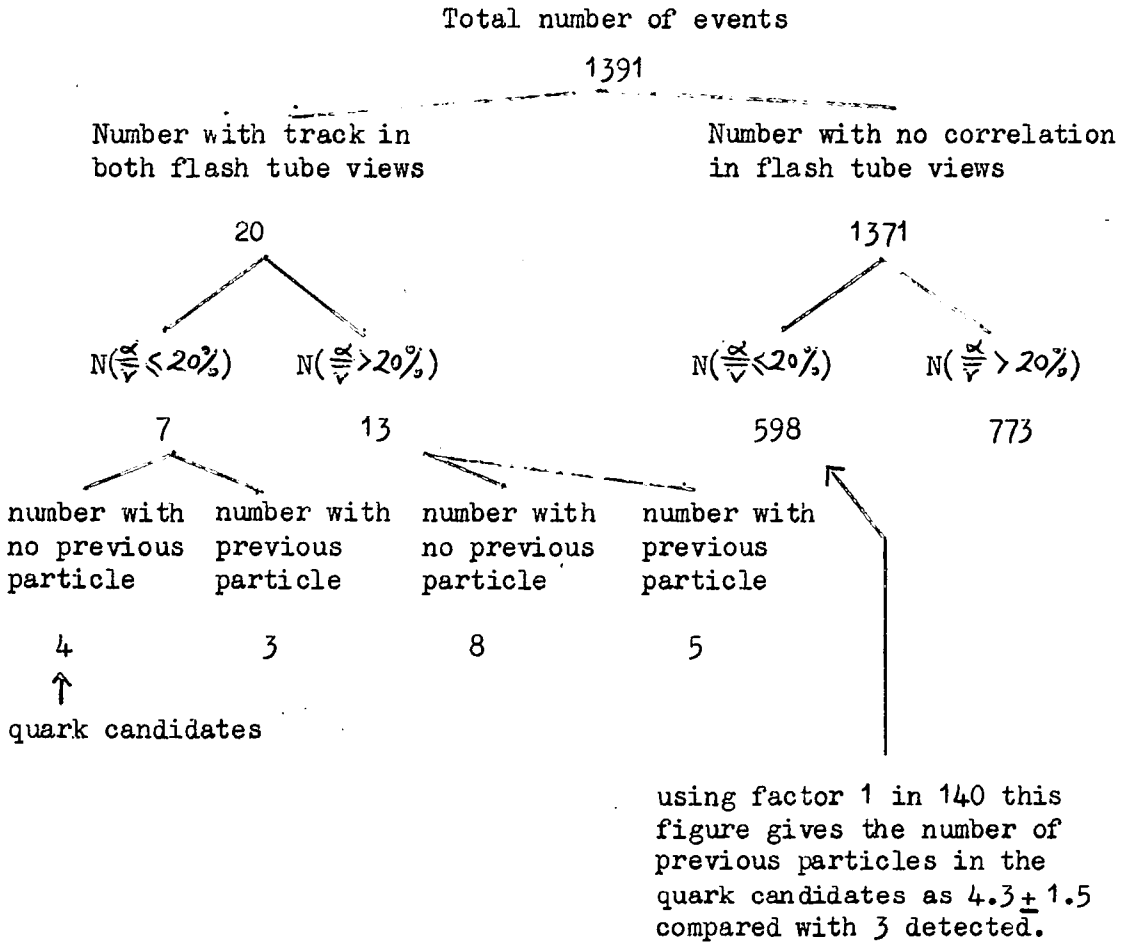

Table 6.8 Breakdown of events in the Q lower selection for runs Q50-97 where the previous particle indicator was incorporated.

QL1-49 the initial analysis gives 6 quark candidates and the expected number of previous particle tracks among these 6 is 2.7 ± 0.9. In QL50-97 the initial analysis gives 7 quark candidates where 4.3 ± 1.5 previous particle tracks are expected. In fact 3 events occurred where a previous particle was indicated and so these were rejected to leave 4 quarks candidates in QL50-97, leaving 10 candidates in the whole series. The values of $\bar{\nu}$, $\alpha/\bar{\nu}$ % and N/M for the 10 quark candidates are given in Table 6.6 and the flash tube diagrams are given in Figures 6.21 to 6.25.

The frequency distribution of $\bar{\nu}$ for the 10 quark candidates is shown in Figure 6.8 together with the frequency distribution of $\bar{\nu}$ for the n/c data with $\alpha/\bar{\nu} \leqslant 20\%$. The scatter plot of $\bar{\nu}$ against $\alpha/\bar{\nu}$ % for all the data with $\alpha/\bar{\nu} \leqslant 20\%$ is shown in Figure 6.11. The frequency distribution over all values of $\alpha/\bar{\nu}$ % for the quark candidates and the n/c data is shown in Figure 6.10. Here again the quark candidates fit the overall distributions of the n/c data.

The values of N/M for the 10 candidates are plotted in Figure 6.6. Three candidates are within the 90% level of N/M. They are events QL11, 45 and 74 with values of $\alpha/\bar{\nu}$ of 19.9% 15.0% and 18.0% respectively. Of these events Q11 and Q45 could be due to previous particle tracks and electron-photon shower pulse heights. Four events are within the 90% level of $\alpha/\bar{\nu}$ %. They are events QL, 26, 38, 45, and 84. The event QL45 is included in both selections.

Since in QL1-49, 2.7 ± 0.9 previous particle tracks will occur in the quark candidates and as explained earlier these tracks have

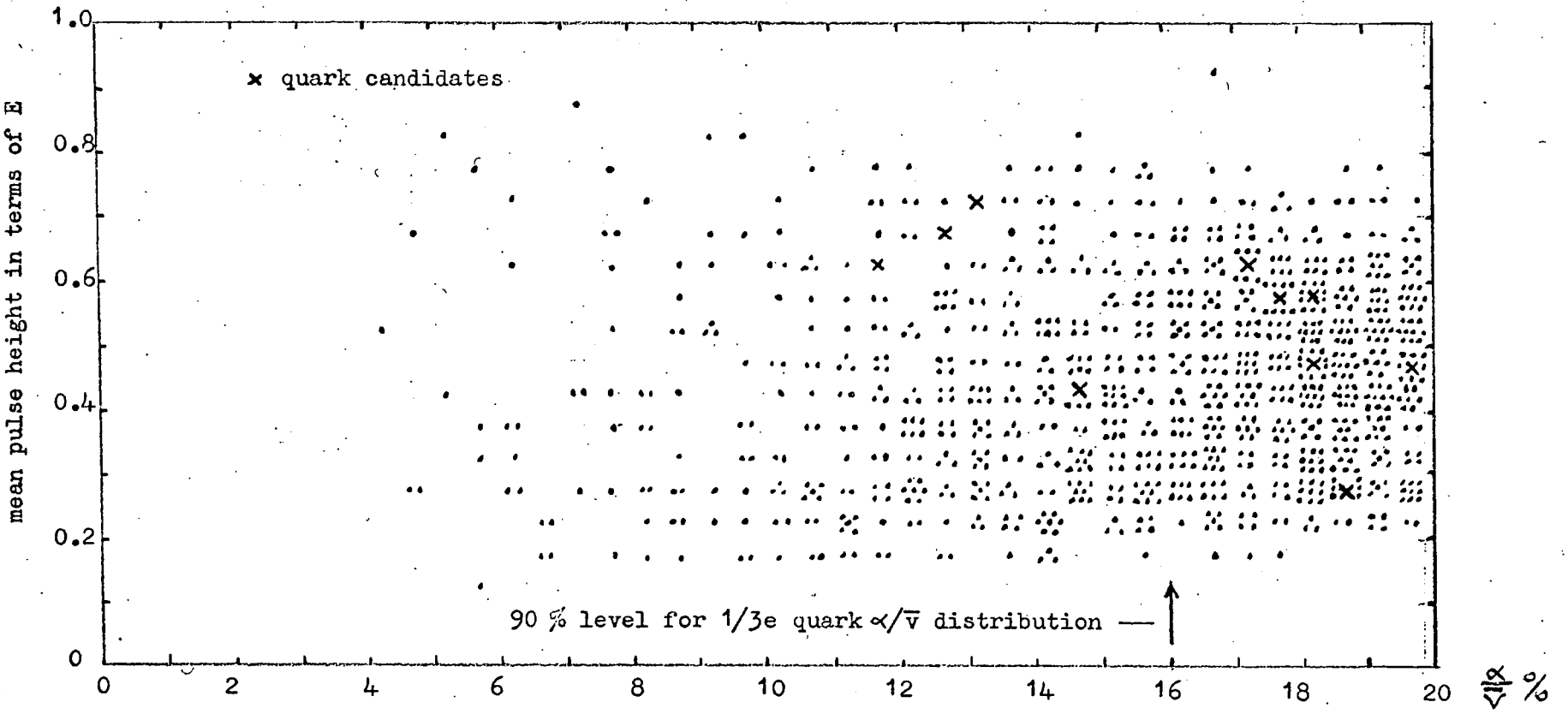

Figure 6.11 Scatter plot of $\bar{v}$ against $\propto/\bar{v}$ for n/c events and the quark candidates in the Q lower serie

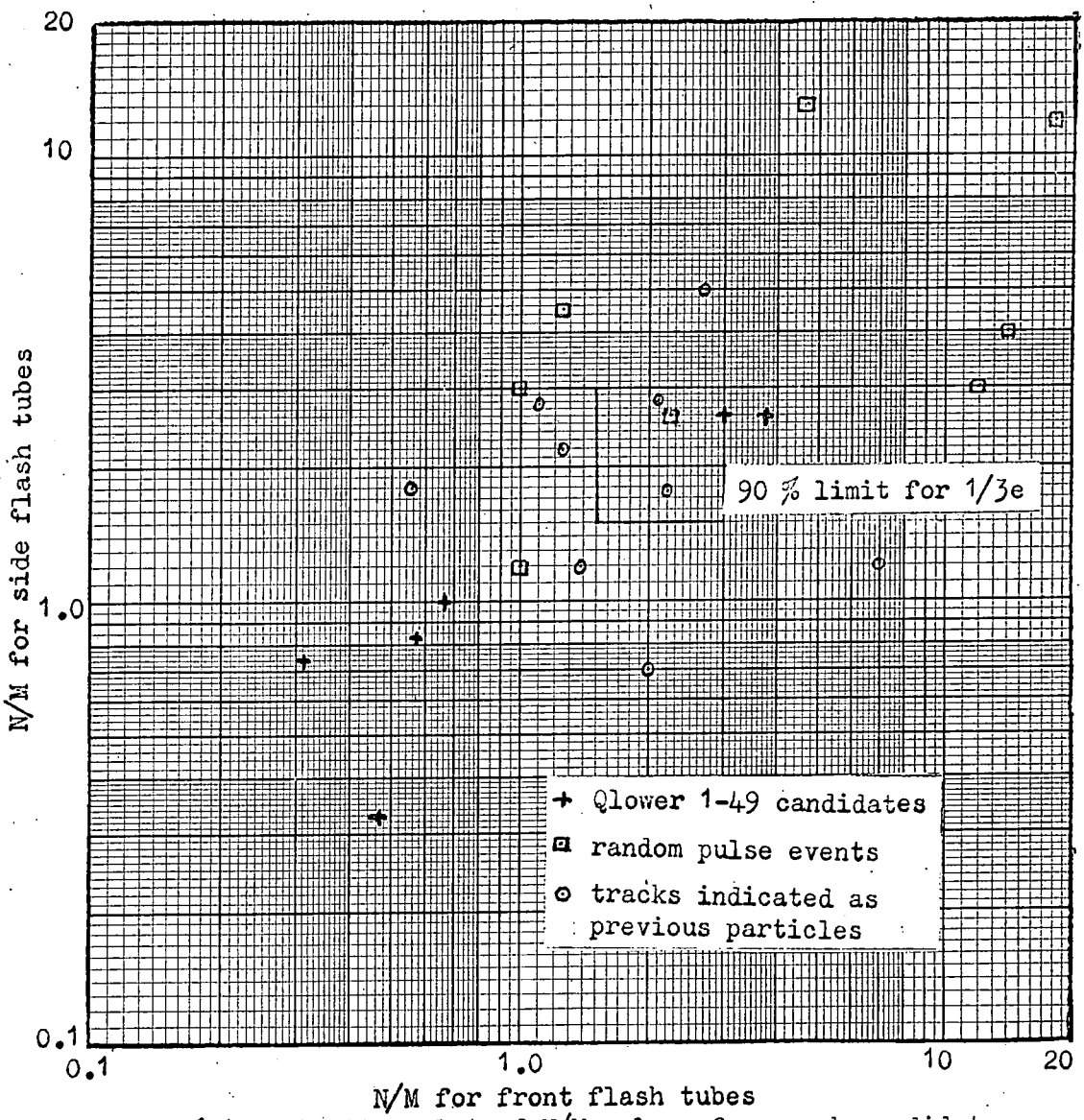

Figure 6.12 Scatter plot of N/M values for quark candidates in Q lower 1-49 compared with random pulse and previous particle detector events.

a higher probability of large N/M values the track in event QL45 could be due to a previous particle. Therefore it is important that the previous particle track events in QL1-49 should be identified and rejected from the quark candidates. This is done in the following way.

The N/M values for the 6 quark candidates from QL1-49 are compared with those of the 8 track events from the random pulsing run and the 8 events in which a previous particle had been indicated from QL50-97 and shown in a scatter plot in Figure 6.12. All the previous particle events lie outside the square for N/M = 1.0 and form a distinct group. The 6 quark candidates are divided into 2 distinct groups, a group of 4 with values of $N/M \leqslant 1.0$ and the group of 2 with values similar to the previous particle group. Now the number of previous particle tracks in QL1-49 is 2.7 ± 0.9, that is at least 2 previous particle tracks. Thus the group of 2 quark candidates, QL11 and 45, must have previous particle tracks and hence must be rejected from the quark candidates.

This leaves only one event in the QL series with N/M values within the 90% limit, this is event QL74 and as mentioned earlier is rejected on its $\alpha/\bar{\nu}$ % value.

6.6 Upper limit on the rate of quarks

From the 25 quark candidates initially accepted on the basic track and $\alpha/\bar{\nu} \leqslant 20\%$ criteria, none are accepted on the 90% limits of $\alpha/\bar{\nu}$ % and N/M. Of these events ~5 can be explained as electron-photon showers with a previous particle track. The remainder must

be regarded as electron-photon showers where the components of the shower have been sufficient to define a line of flashes which is taken as a single particle track. The comparison of the candidates with the n/c data which is typical of low energy electron-photon showers indicates that this is the case.

For no quark detected the upper limit of the rate with 90% confidence is equivalent to 2.3 detected. For an acceptance of 90% in values of $\alpha/\bar{\nu}$% and N/M the effective running time is reduced by 0.81.

For relativistic $\frac{2}{3}$e quarks the effective running time is 1002 hours and 1116 hours for the T and $\bar{T}$ upper series respectively. For the final acceptance this becomes 812 hours and 900 hours respectively. These times are added to give the rate of relativistic $\frac{2}{3}$e quarks with 90% confidence as:

$$< 8.0 \times 10^{-11} \text{ cm}^{-2} \text{ sterad}^{-1} \text{ sec}^{-1}$$

For relativistic $\frac{1}{3}$e quarks the effective running time is 1445 hours, for the final acceptance this becomes 1175 hours. The rate of relativistic $\frac{1}{3}$e quarks with 90% confidence is:

$$< 1.2 \times 10^{-10} \text{ cm}^{-2} \text{ sterad}^{-1} \text{ sec}^{-1}$$

For non-relativistic $\frac{1}{3}$e and $\frac{2}{3}$e quarks, the effective running time as a function of β from both series was added for all possible values of β. The upper limit for $\frac{1}{3}$e and $\frac{2}{3}$e quarks as a function of β is obtained and shown in Figure 6.13.

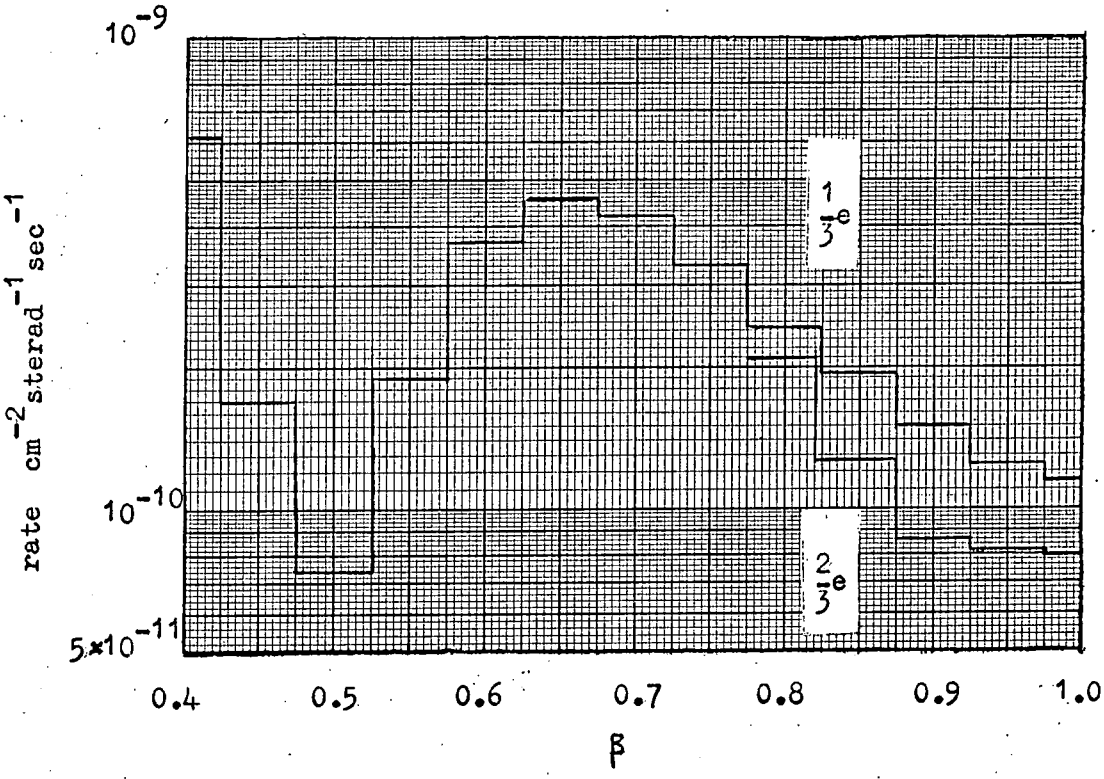

Figure 6.13 The upper limit for the rate of $\frac{1}{3}e$ & $\frac{2}{3}e$ quarks with 90% confidence as a function of β.

6.7 Two extraneous events

Throughout the scanning and analysis all events were carefully scrutinised for possible quarks which were outside the selection criteria on flash tube or pulse height data. Two such events occurred, one in T7 and the other in QL64.

The pulse height information and flash tube diagram for the T7 event is shown in Figure 6.19. This event is interesting because the side flash tube view shows the track out of geometry in counter A, which is why it was rejected. However, although the output pulse height from counter A is small (0.20E) compared with other counters ($\bar{v}_{B-F}$ = 0.45E), it is still considerable. This suggests that the pulse heights may be associated with an electron-photon shower and the track that of a previous particle. The large number of background in the flash tube views would suggest this too. The event would also be rejected on its N/M values.

For the QL64 event the pulse height and flash tube data is given in Table 6.8.

Table 6.8 Values of pulse height and flash tube data for event QL64

V_A = 0.15E
V_B = 0.30E
V_C = 0.11E
V_D = 0.14E
V_E = 0.04E
V_F = 0.18E

$\bar{v}$ = 0.15E $\quad \alpha/\bar{v}$ = 22.5%

$N/M_{FRONT} = \frac{17}{9} = 1.9$

$N/M_{SIDE} = \frac{12}{2} = 6.0$

This event occurred when the previous particle indicator was included and in this event no previous particle was indicated.

However it is possible that particle could traverse the telescope in the time ($\sim 1\,\mu$sec) between the last pulse displayed on the C.R.O. and the application of the pulse on the flash tubes. At a rate of muons through the telescope of 30 sec^{-1}, the number of frames for such an event is 3.3×10^{4}, for runs 4L50-92 the number of events was 1391 and hence the probability of such an event is $\sim 10^{-1}$.

The high value of $\alpha/\bar{\nu}$ % is due to the pulses from counters B and E. If the $\frac{1}{3}$e quark pulse height distribution for one counter is assumed Gaussian such that $\sigma = 0.035E$, the pulse from B lies at 5.4 σ and that from E at 2 σ from the most probable pulse height 0.11E. The probability of a pulse height at 2σ is 0.02 and at 5.4 σ is $< 10^{-7}$ and hence the probability of the track being due to a previous particle in the 1 μsec is much greater than the pulse heights being in a $\frac{1}{3}$e quark pulse height distribution.

The nine background flashes in the front flash tube view are all in trays F_a and F_b with counter B between them. Thus the large pulse in counter B could be associated with these flashes which could be due to some weak electron-photon shower accompanying the quark. However this is the limitation of all telescope experiments in that such events have to be rejected.

6.8 Conclusion

With no events of either $\frac{1}{3}$e or $\frac{2}{3}$e quarks in the β ranges studied, the 90% confidence limit for the existence of quarks in

cosmic rays at sea-level is:

for a relativistic $\frac{1}{3}e$ quark $< 1.2 \times 10^{-10} cm^{-2} ster^{-1} sec^{-1}$.

for a relativistic $\frac{2}{3}e$ quark $< 8.0 \times 10^{-11} cm^{-2} ster^{-1} sec^{-1}$.

for a $\frac{1}{3}e$ quark, $0.4 < \beta < 1.0$ $< 6.2 \times 10^{-10} cm^{-2} ster^{-1} sec^{-1}$.

for a $\frac{2}{3}e$ quark, $0.8 < \beta < 1.0$ $< 2.2 \times 10^{-10} cm^{-2} ster^{-1} sec^{-1}$.

These rates do not include the possibility of the quark interacting in the stack, in common with other workers. They represent the lowest limit to date for the flux of quarks in cosmic rays at sea-level.

Diagram of relevant data on initial quark candidates. Pulse heights from each counter are given together with $\bar{v}$ and $\alpha/\bar{v}$ %. The flash tube views are shown diagrammatically with the accepted track. The merit factor for each track N/M (where N is the number of flash tubes in the track and M is the number of background) are given for both views.

The candidates in the T selection are shown in Figures 6.13 to 6.19. The final diagram in Figure 6.19 is the extraneous T7 event discussed in section 6.7.

The candidates in the ψ upper selection are shown in Figure 6.20.

The candidates in the ψ lower selection are shown in Figures 6.21 to 6.25.

* indicates that the previous particle indicator was included in the system and for the particular events shown no previous particle had been indicated.

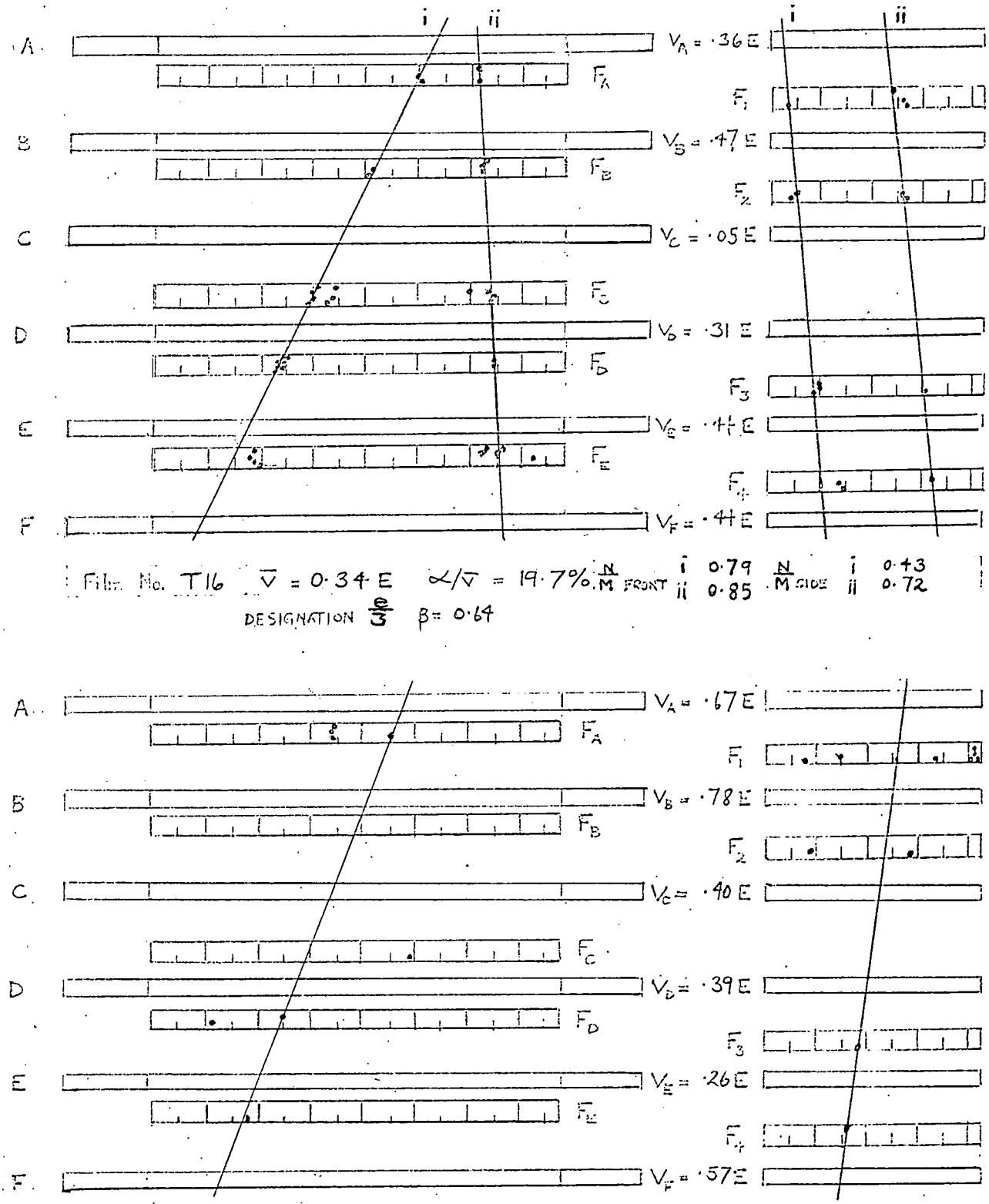

Figure 6.13. Flash tube diagrams and pulse height data for quark candidates T16 and T19.

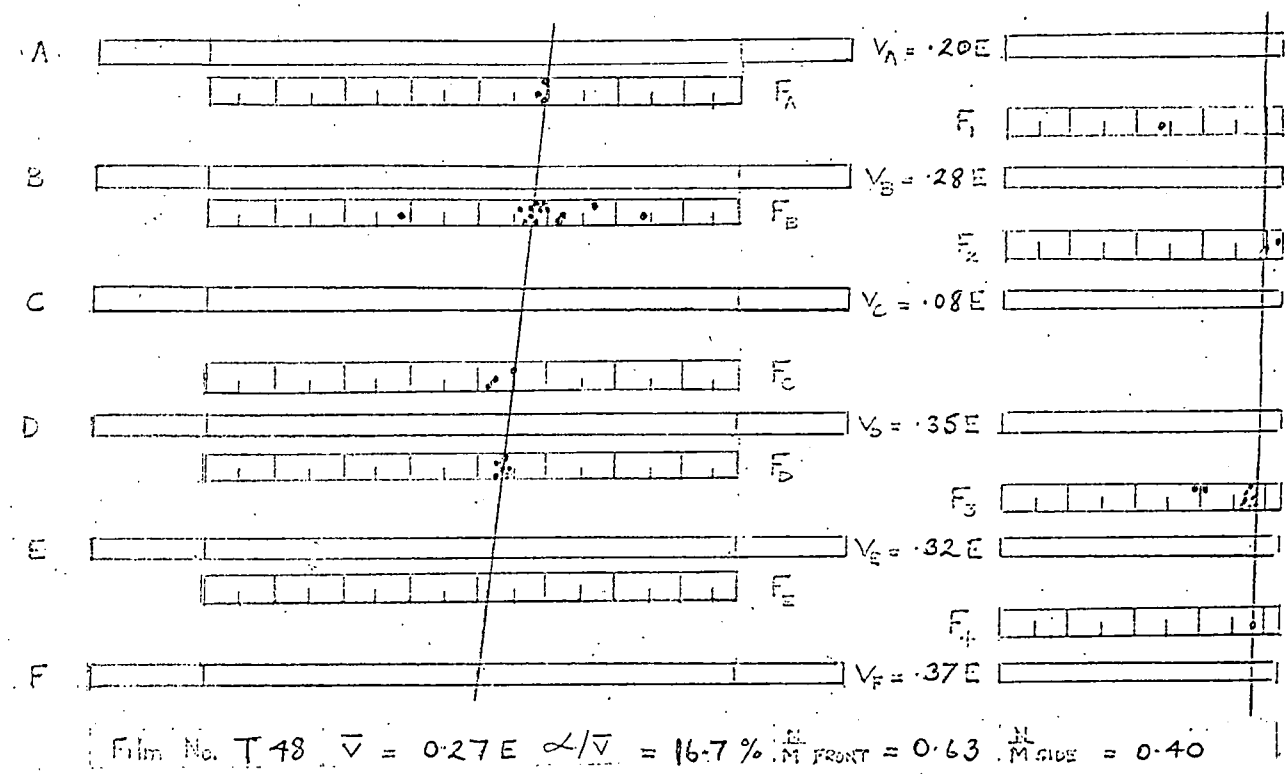

Film No. T48 $\bar{v}$ = 0·27 E $\alpha/\bar{v}$ = 16·7 % $\frac{N}{M}$ FRONT = 0·63 $\frac{N}{M}$ SIDE = 0·40

DESIGNATION $\frac{e}{3}$ β = 0·71

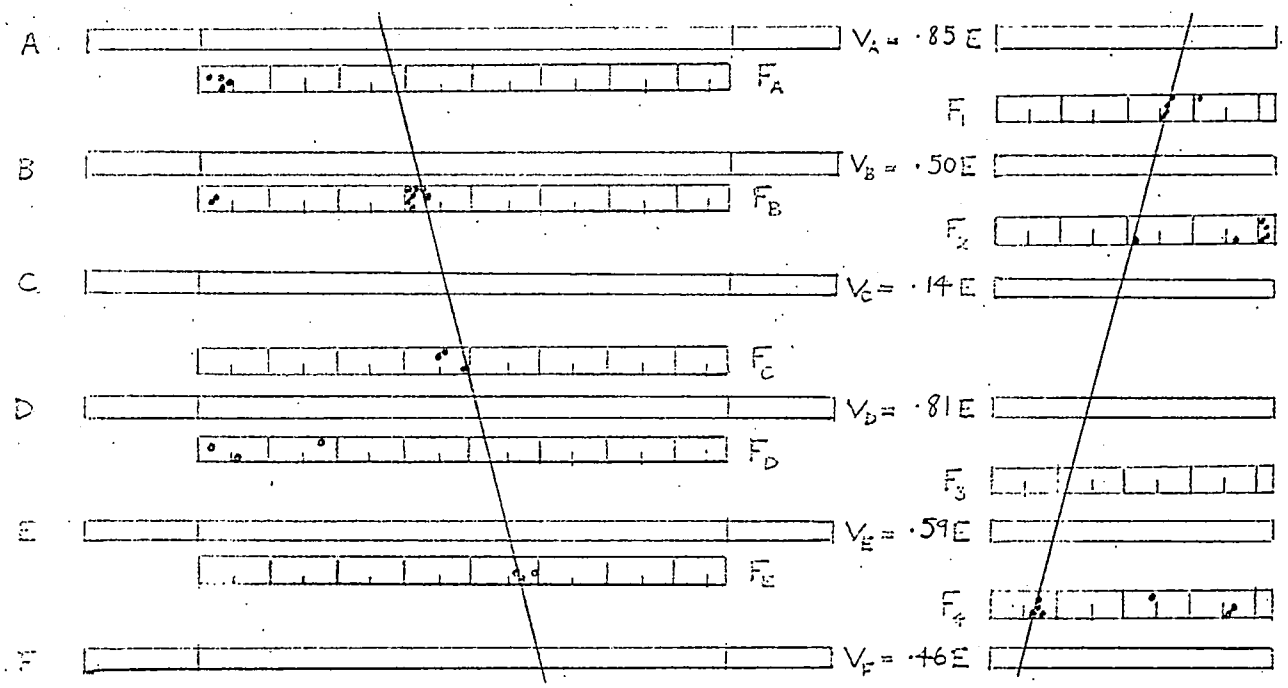

Film No. T49 $\bar{v}$ = 0·56 E $\alpha/\bar{v}$ = 19·0 % $\frac{N}{M}$ FRONT = 0·30 $\frac{N}{M}$ SIDE = 0·80

DESIGNATION $\frac{2e}{3}$

Figure 6.14 Flash tube diagrams and pulse height data for quark candidates T48 and T49.

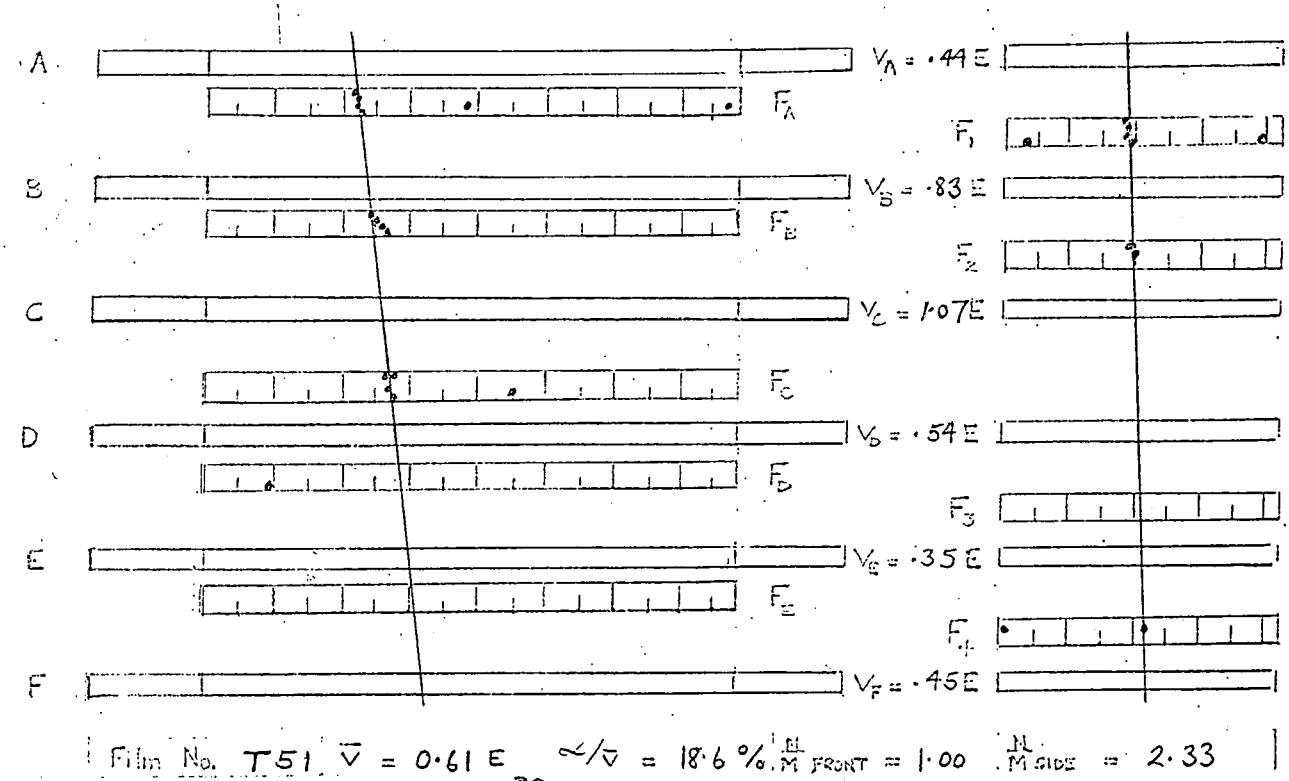

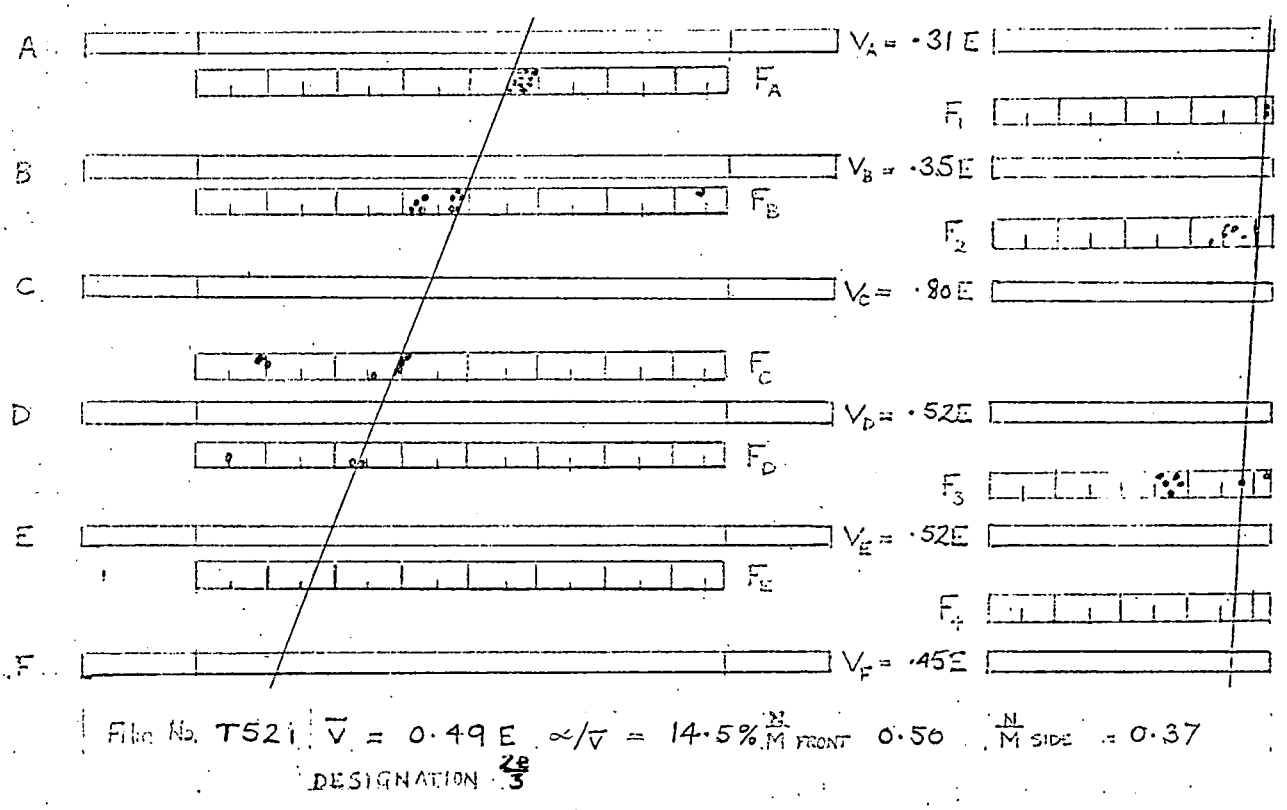

Figure 6.15 Flash tube diagram and pulse height data for quark candidates T51 and T52i.

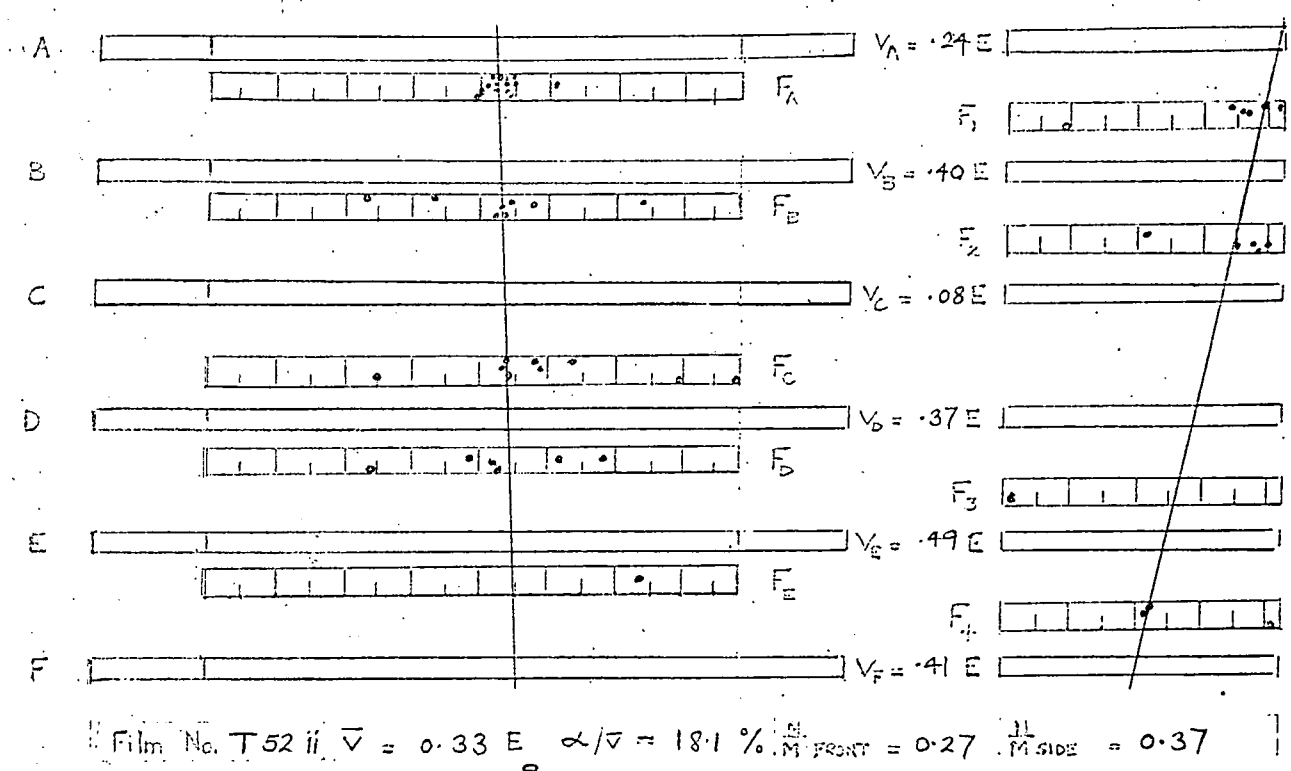

Film No. T52 ii $\bar{V}$ = 0·33 E $\alpha/\bar{v}$ = 18·1 % $\frac{N}{M}$ FRONT = 0·27 $\frac{N}{M}$ SIDE = 0·37

DESIGNATION $\frac{e}{3}$ β = 0·64

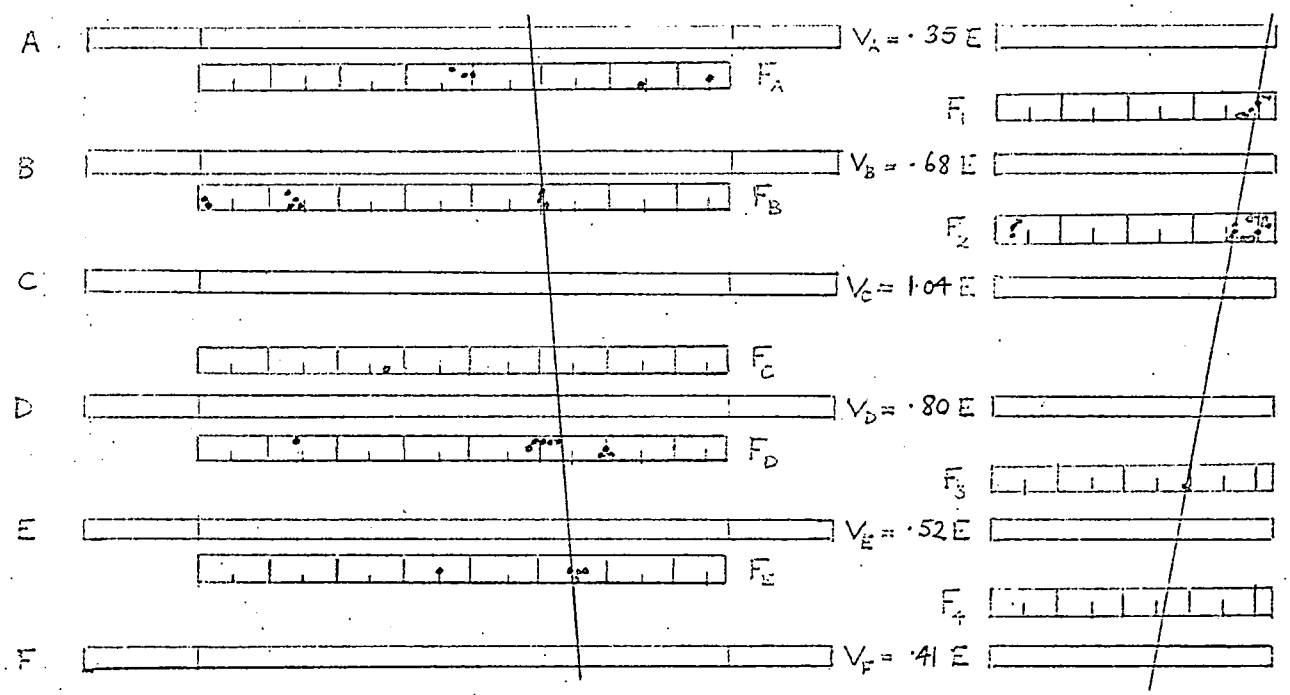

Film No. T53 $\bar{V}$ = 0·63 E $\alpha/\bar{v}$ = 16·8 % $\frac{N}{M}$ FRONT = 0·25 $\frac{N}{M}$ SIDE = 0·43

DESIGNATION $\frac{2e}{3}$

Figure 6.16 Flash tube diagrams and pulse height data for quark candidates T52ii and T53.

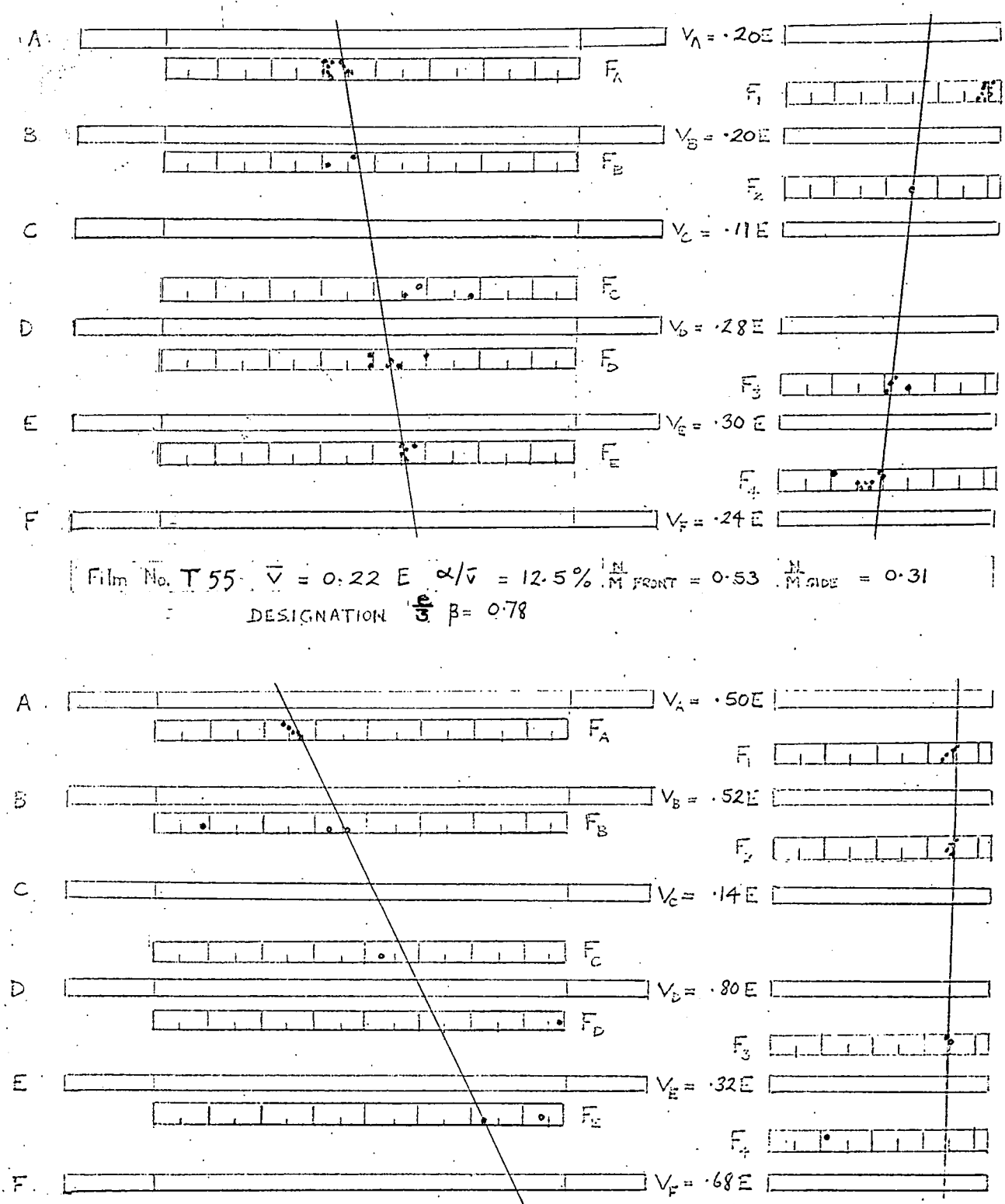

Figure 6.17 Flash tube diagrams and pulse height data for quark candidates T55 and T56.

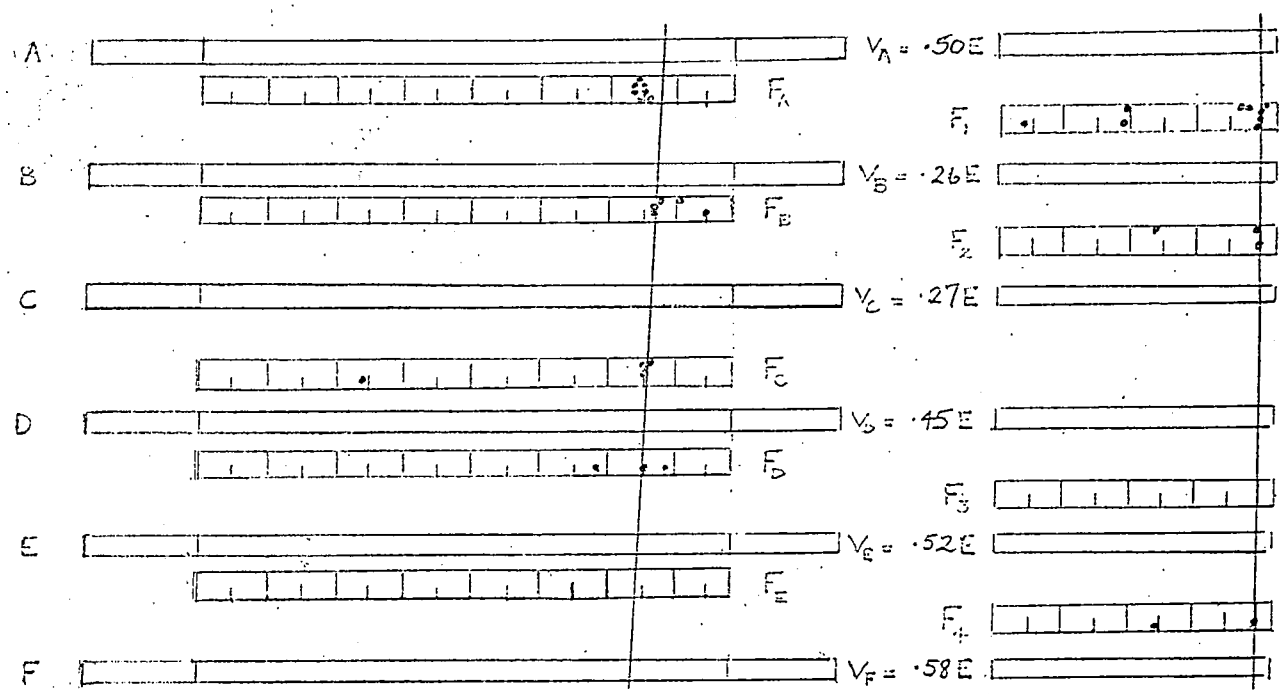

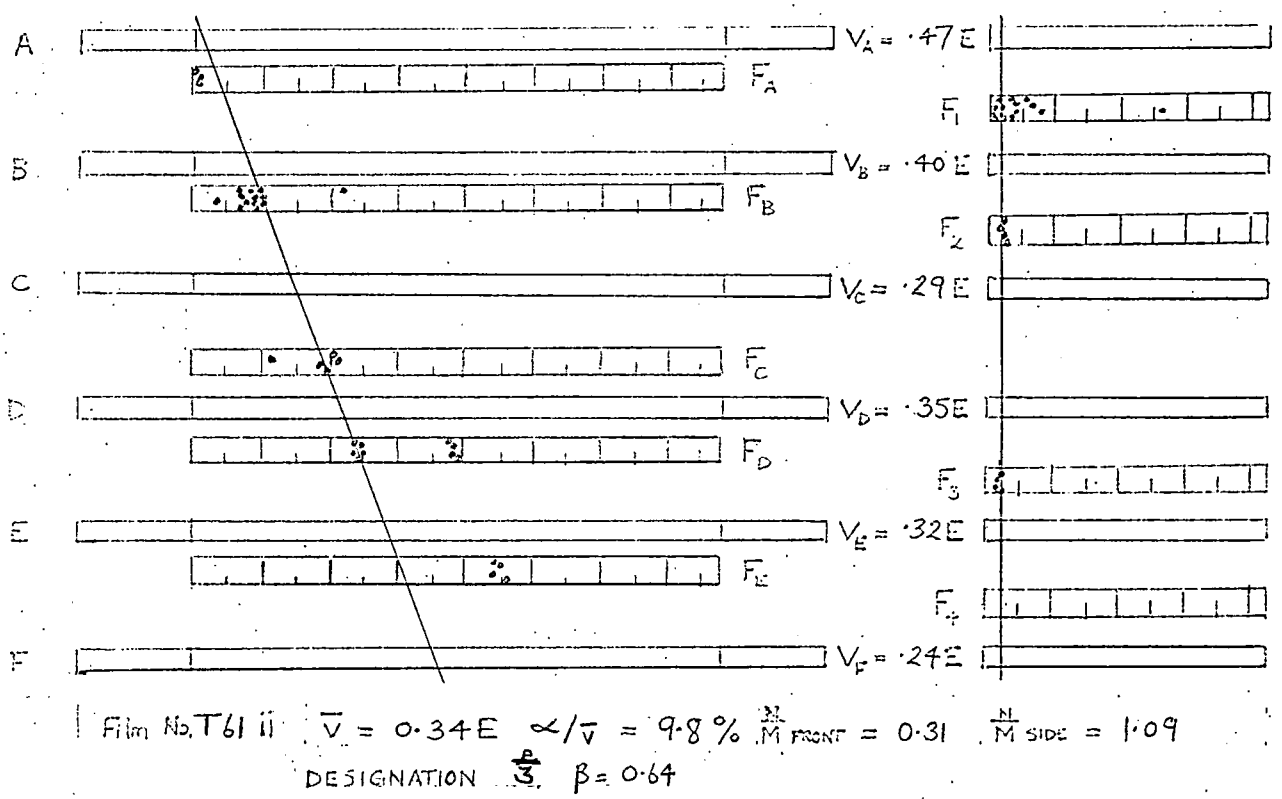

Figure 6.18 Flash tube diagrams and pulse height data for quark candidates T61i and T61ii.

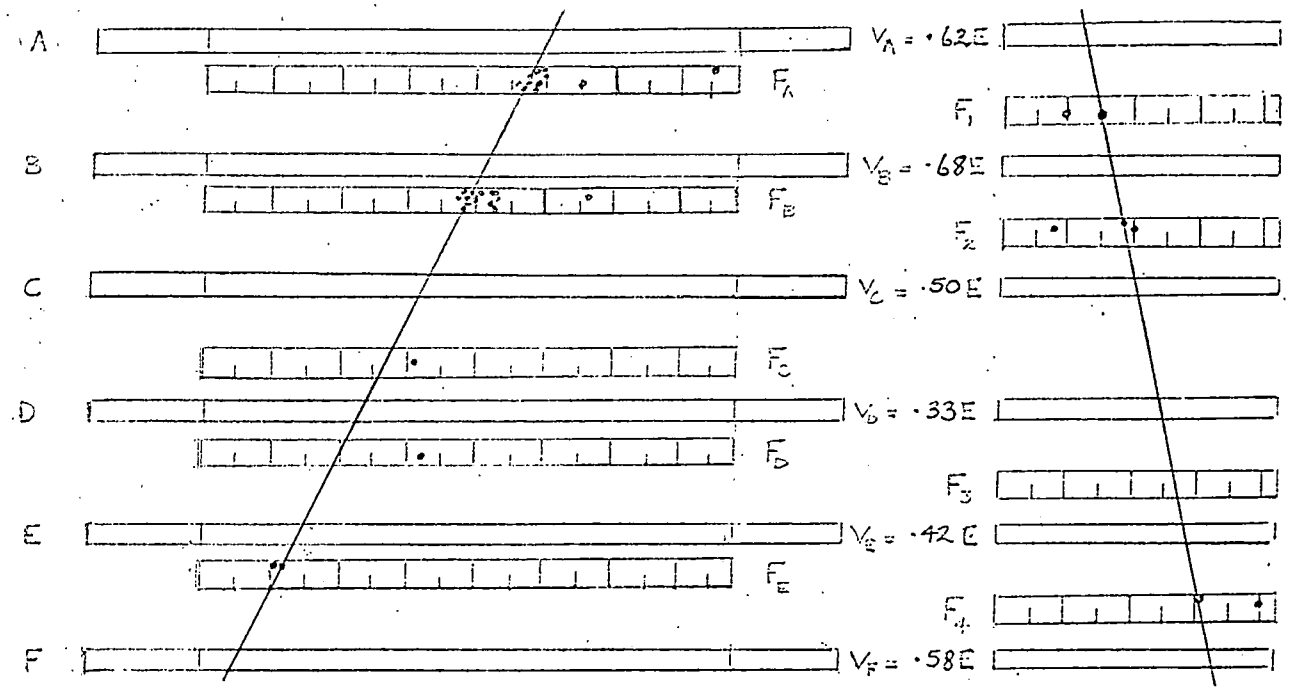

Film No. T61 iii $\bar{V}$ = 0·52 E $\alpha/\bar{v}$ = 10·3 % $\frac{11}{M}$ FRONT = 0·41 $\frac{11}{M}$ SIDE = 0·75

DESIGNATION $\frac{2e}{3}$

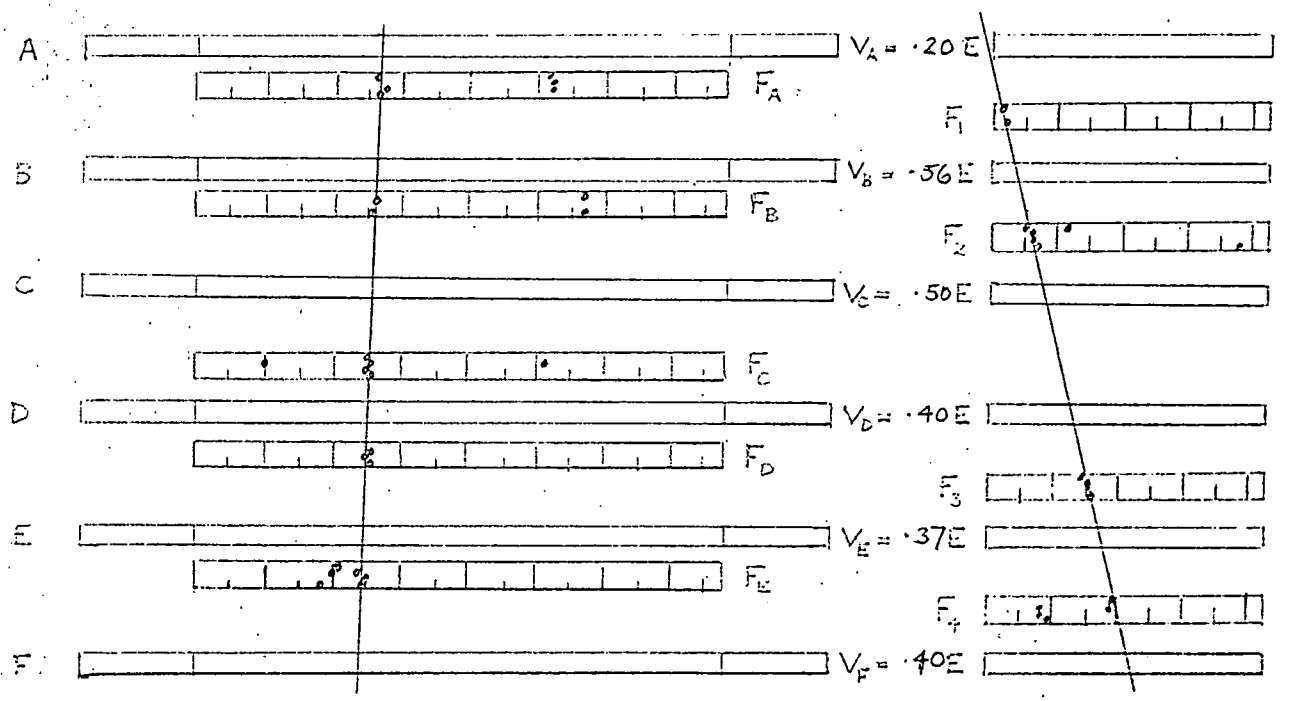

Film No. T7 $\bar{V}$ = 0·40E $\alpha/\bar{v}$ = 12·1 % $\frac{33}{M}$ FRONT = 1·50 $\frac{11}{M}$ SIDE = 1·66

Figure 6.19 Flash tube diagrams and pulse height data for quark candidate T61iii and the extraneous event T7.

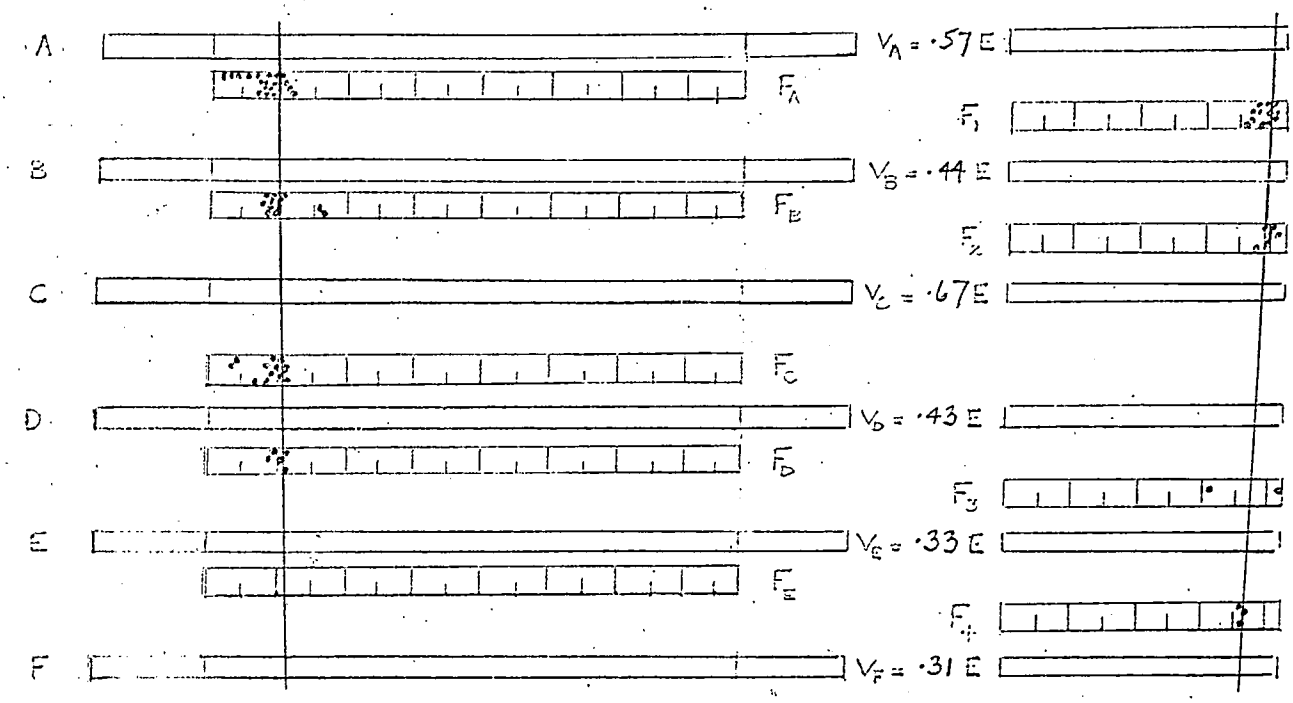

Film No. QU 18 $\bar{V} = 0.46\,E$ $\alpha/\bar{V} = 12.5\,\%$ $\frac{N}{M}_{FRONT} = 0.38$ $\frac{N}{M}_{SIDE} = 0.57$

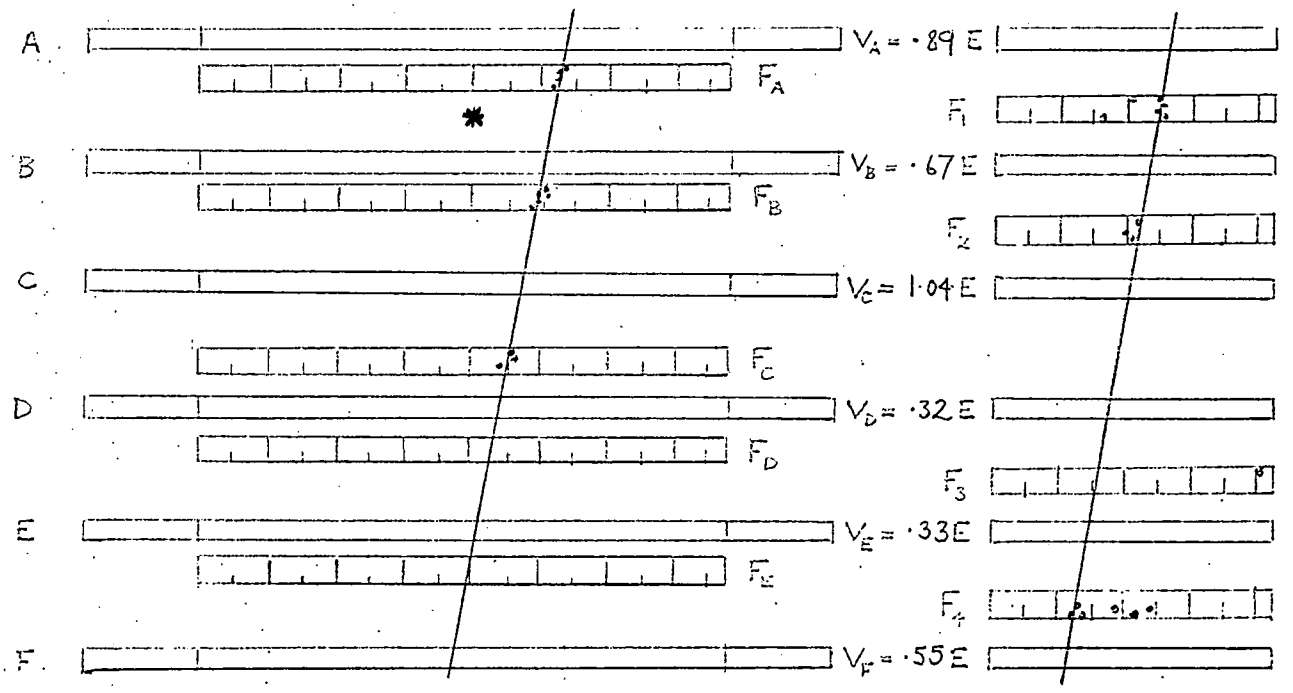

Film No. QU 54 $\bar{V} = 0.63\,E$ $\alpha/\bar{V} = 18.9\,\%$ $\frac{N}{M}_{FRONT} = 2.25$ $\frac{N}{M}_{SIDE} = 1.00$

Figure 6.20 Flash tube diagrams and pulse height data for quark candidates QU18 and QU54.

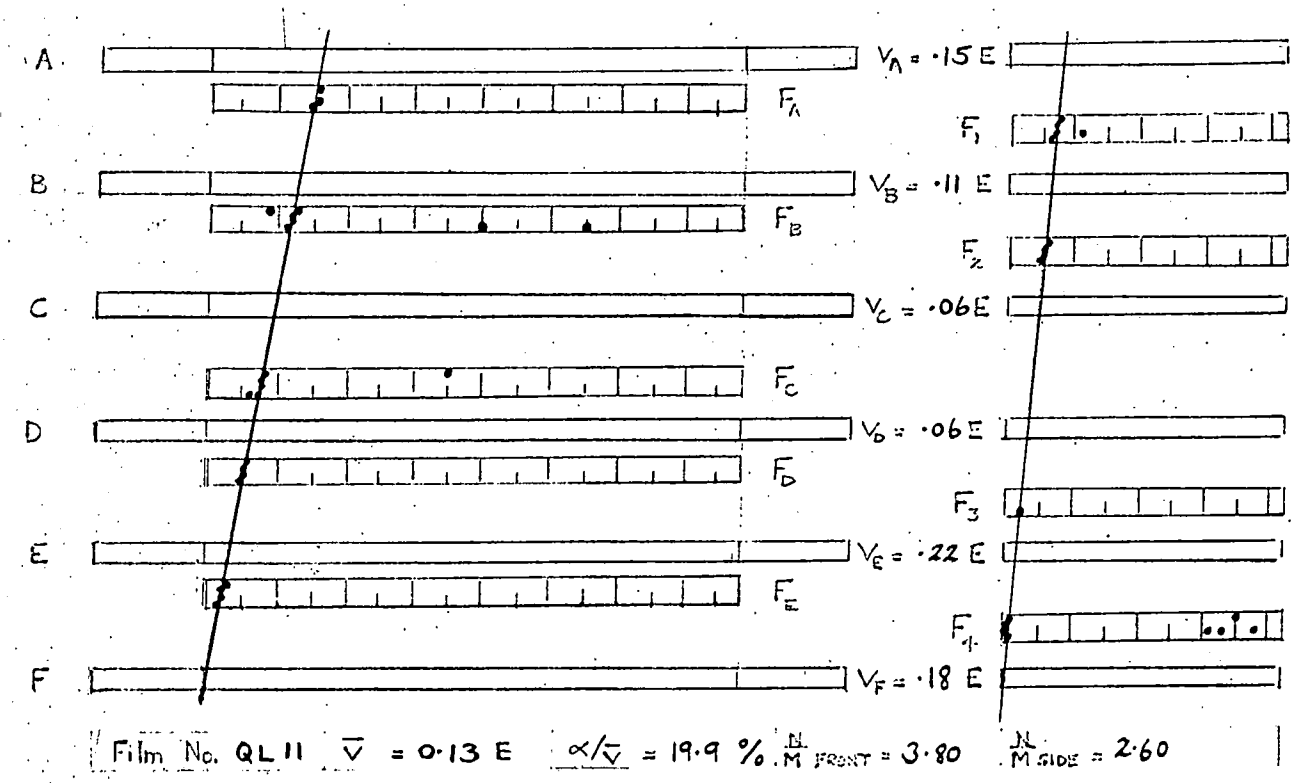

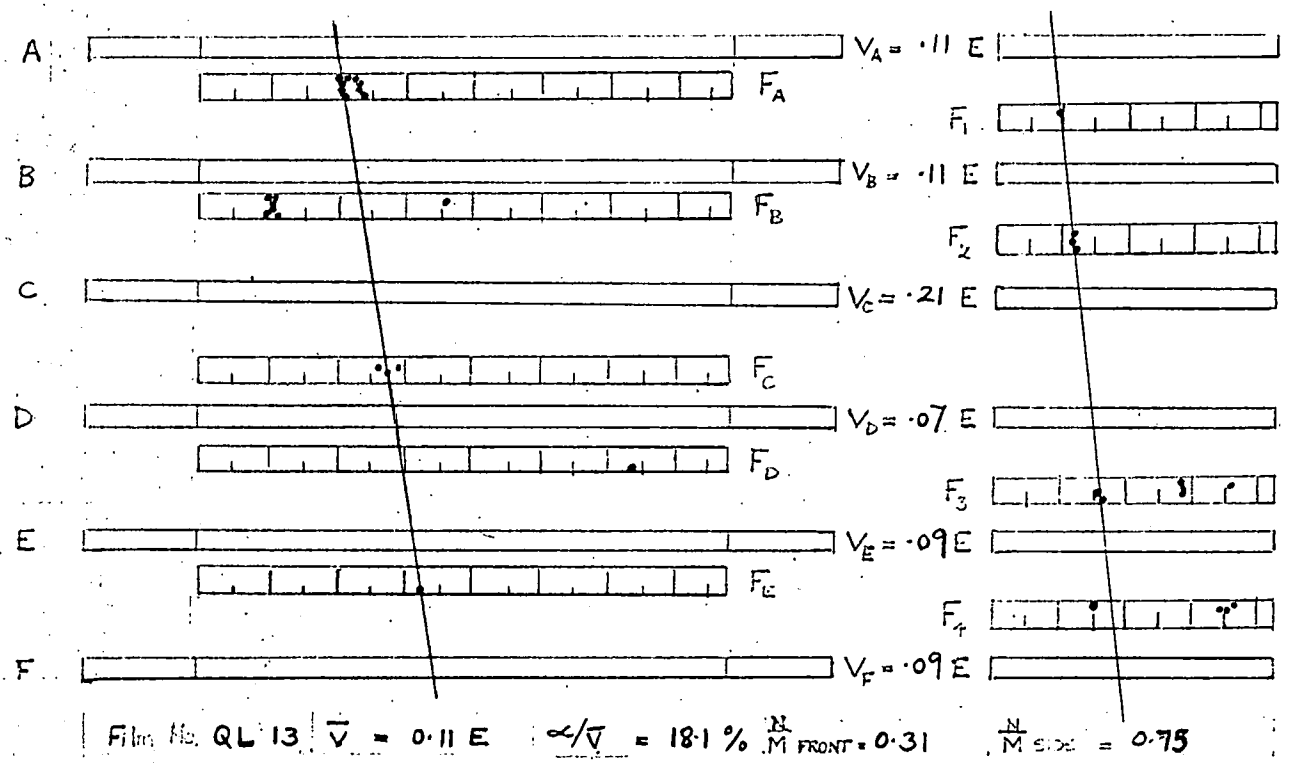

Figure 6.21 Flash tube diagrams and pulse height data for quark candidates QL11 and QL13.

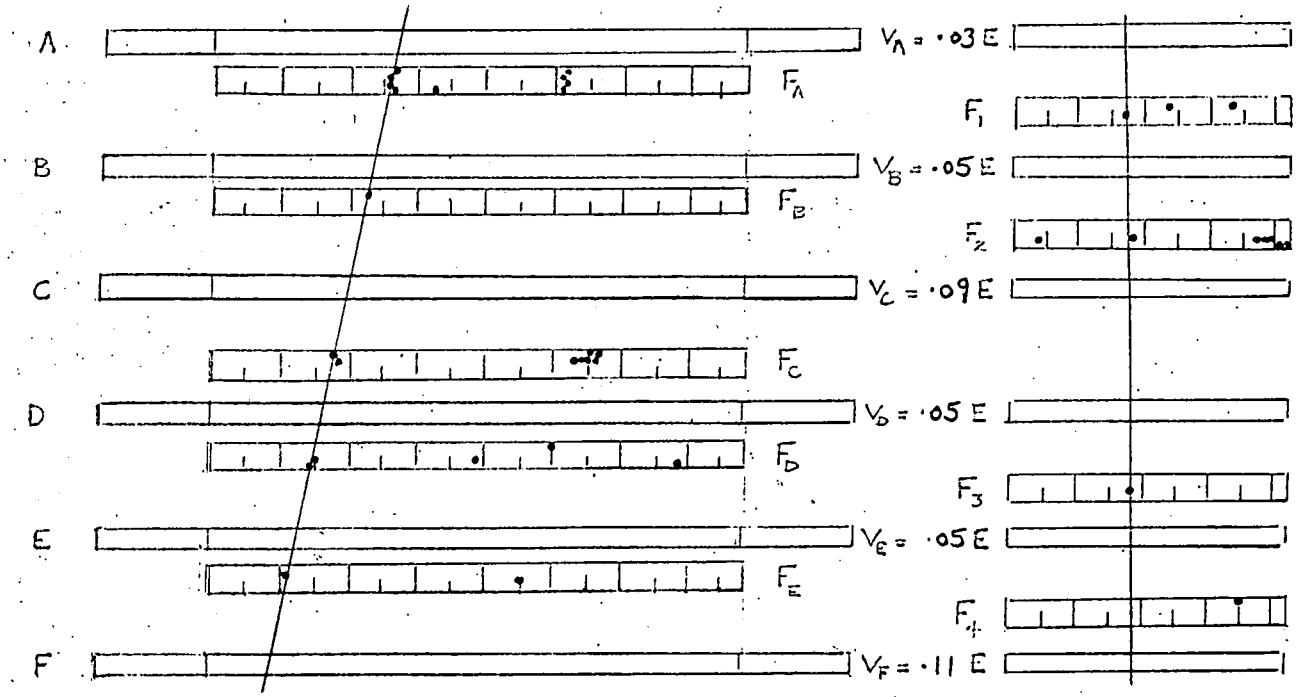

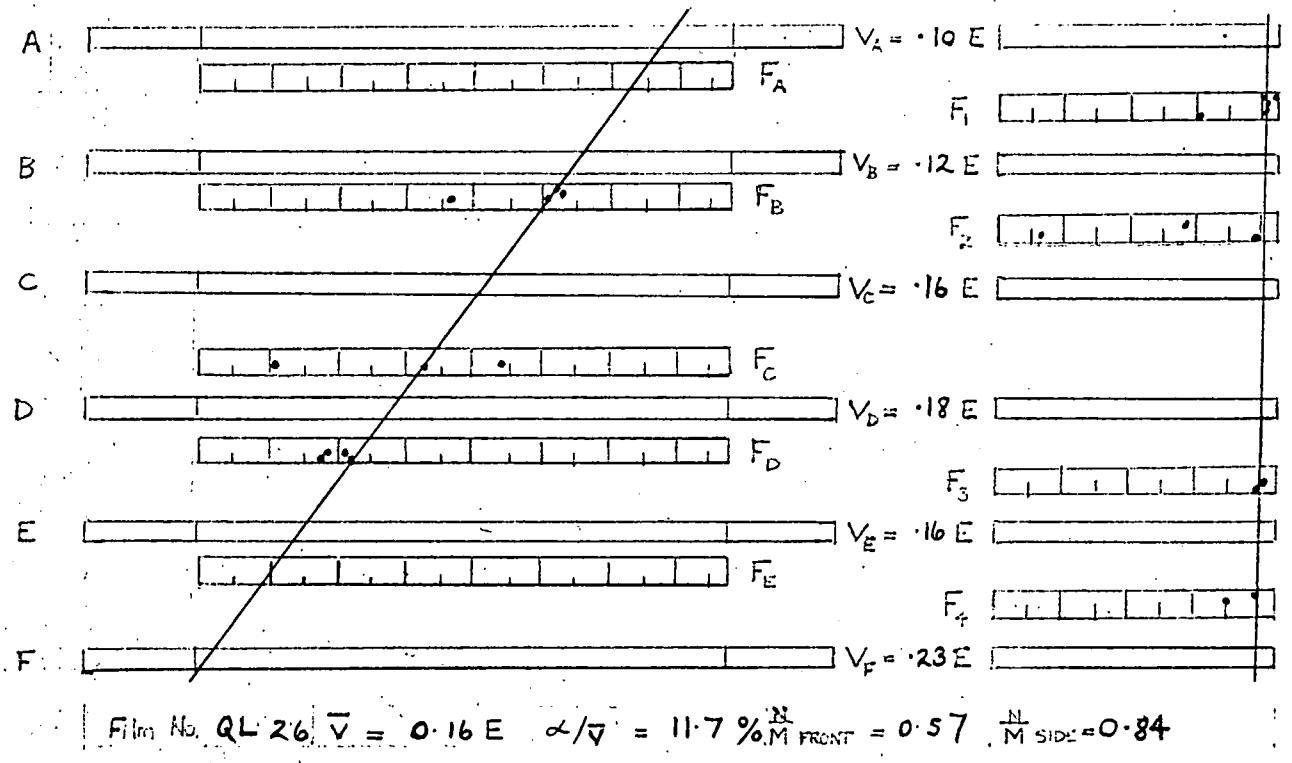

Figure 6.22 Flash tube diagrams and pulse height data for quark candidates QL14 and QL26.

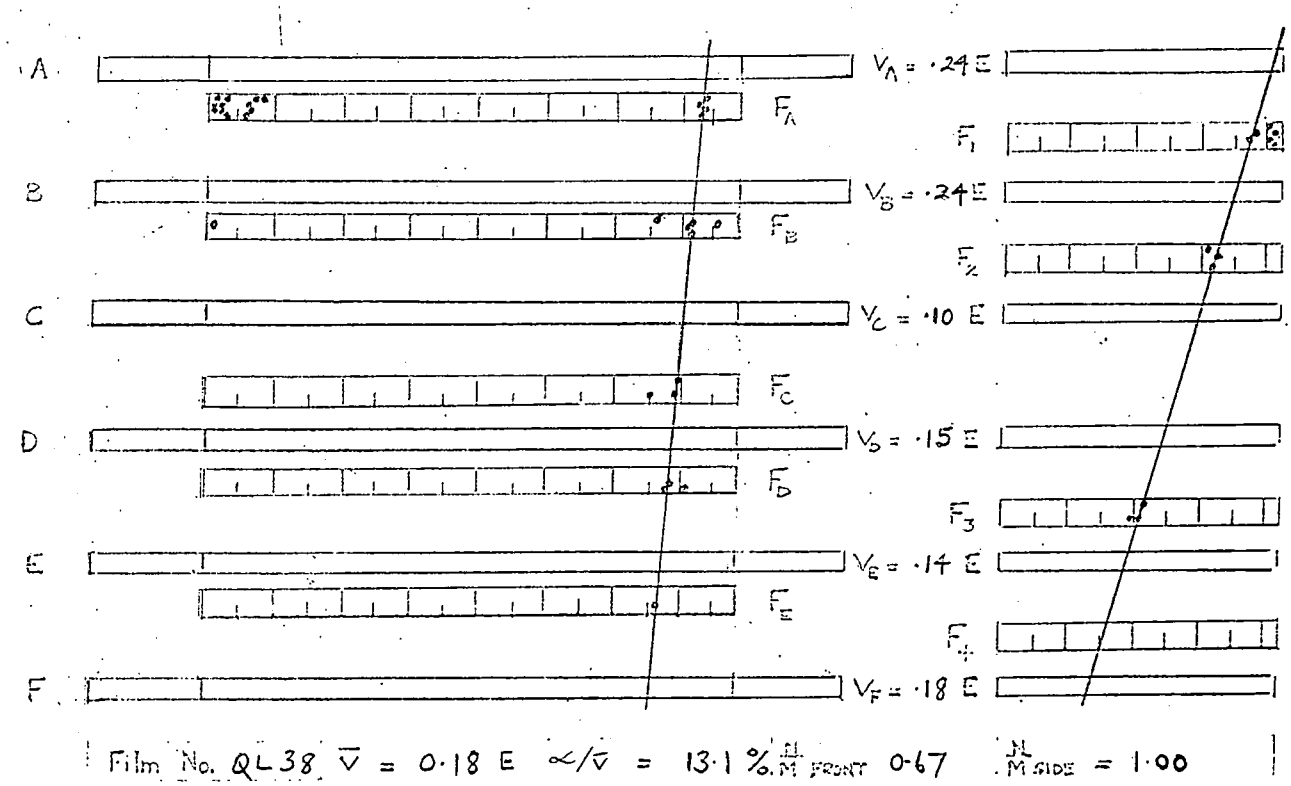

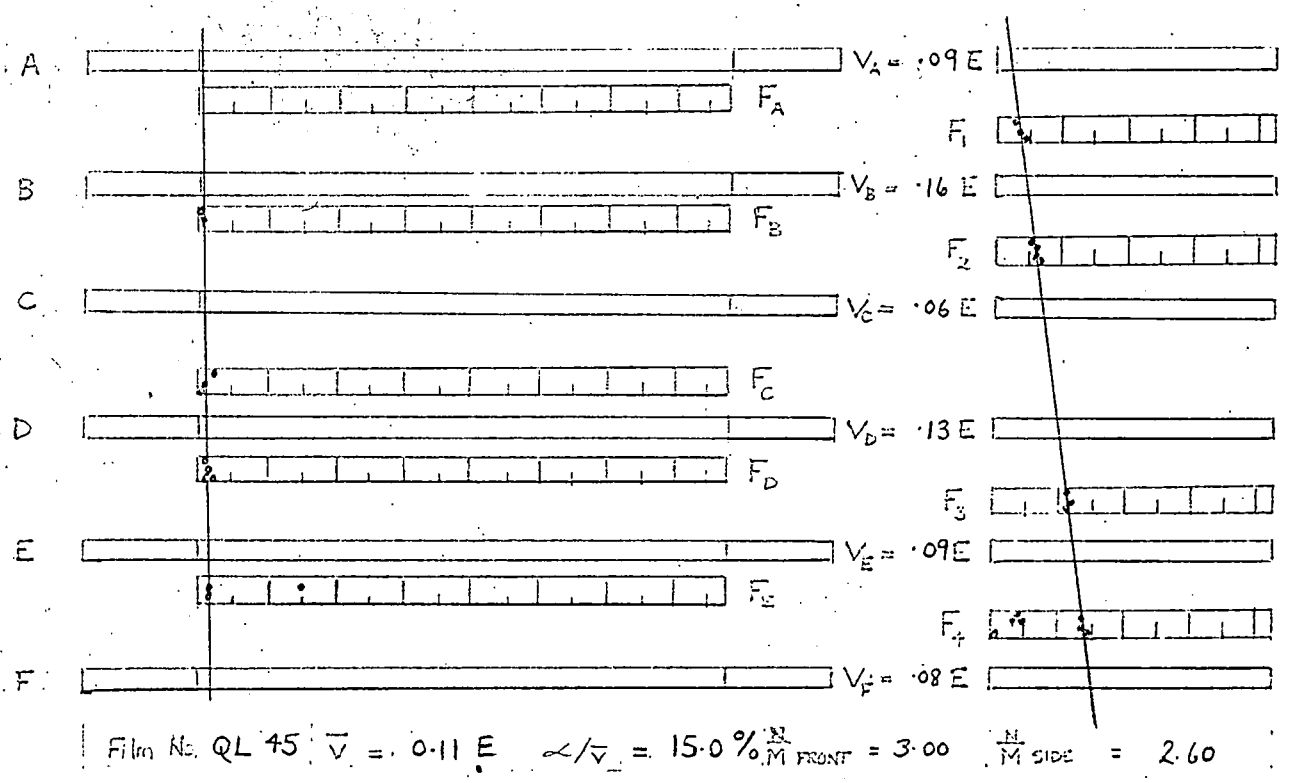

Figure 6.23 Flash tube diagrams and pulse height data for quark candidates QL38 and QL45.

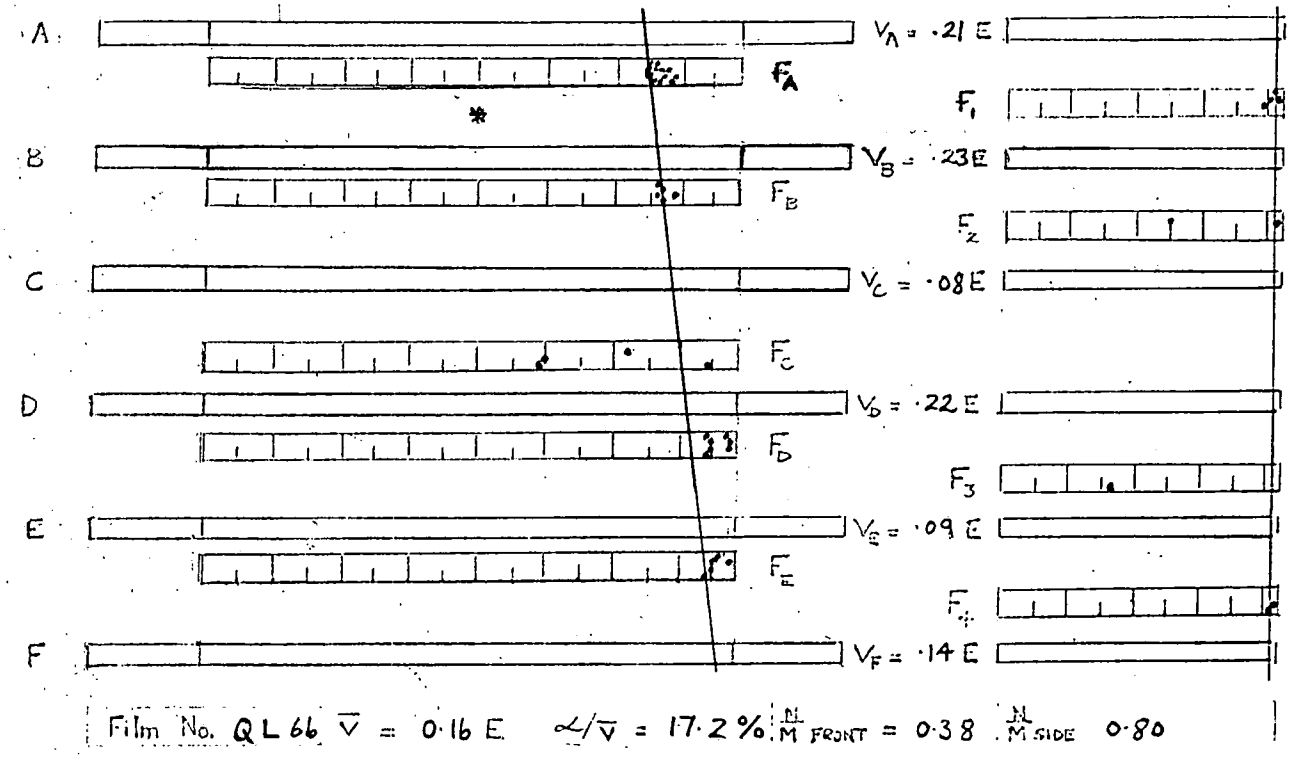

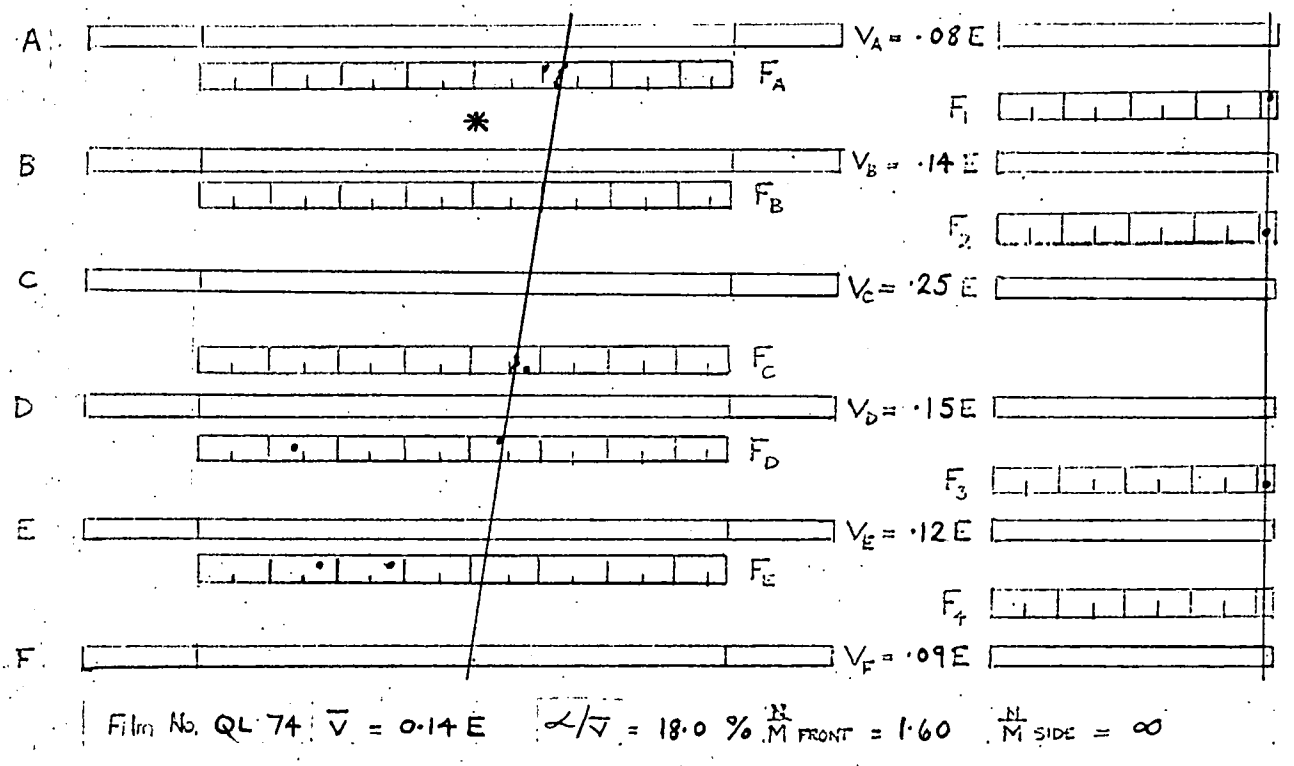

Figure 6.24 Flash tube diagrams and pulse height data for quark candidates QL66 and QL74.

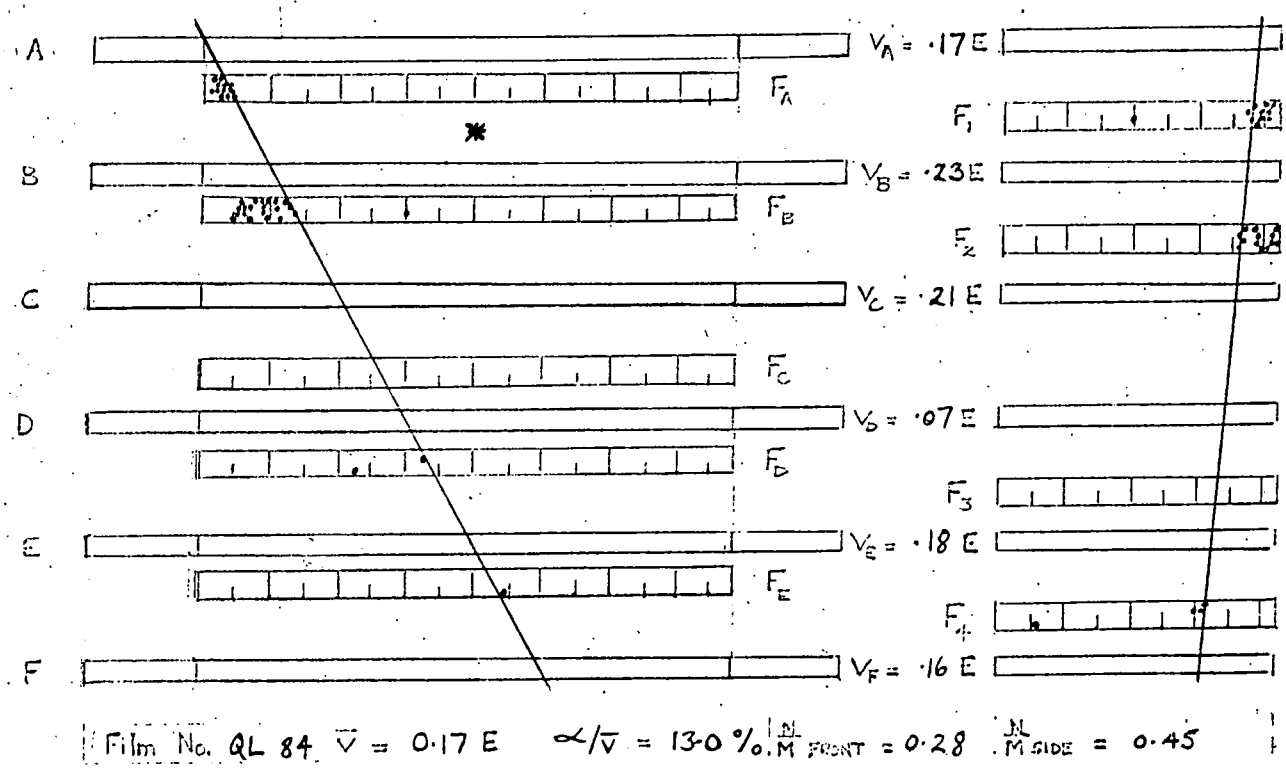

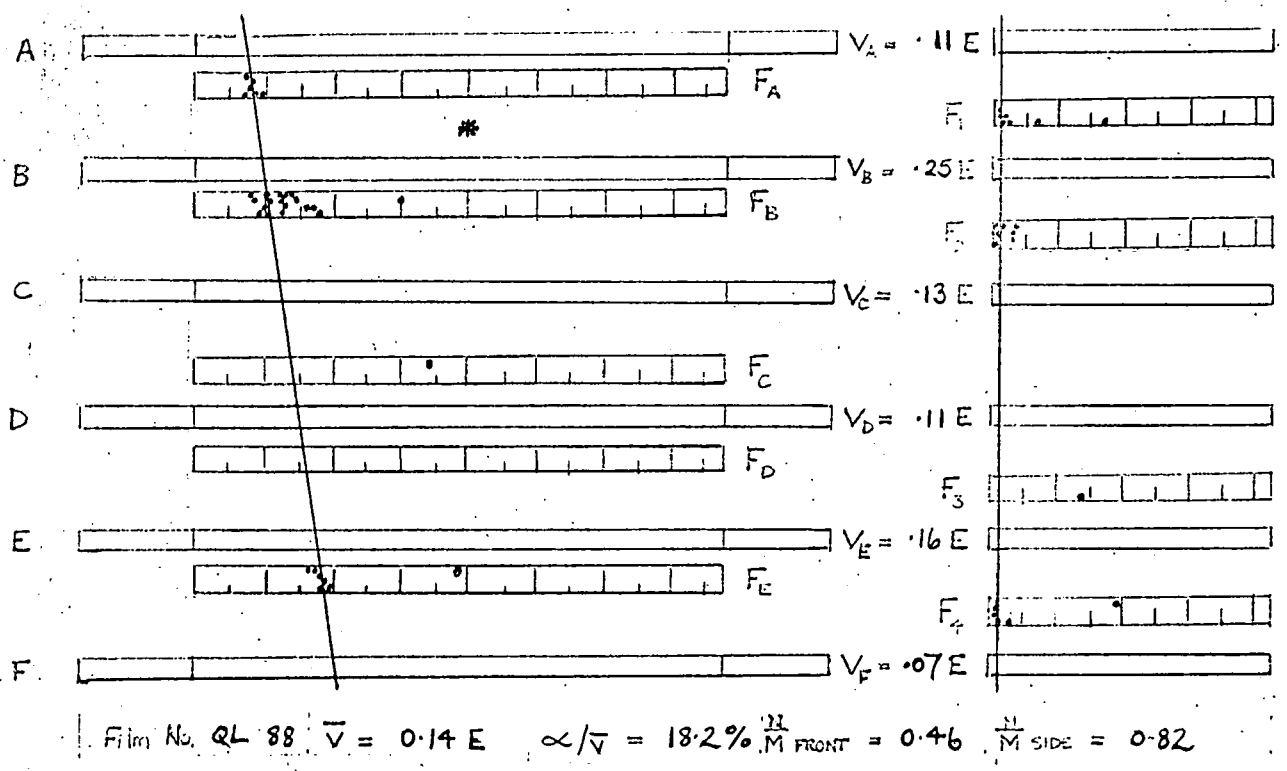

Figure 6.25. Flash tube diagrams and pulse height data for quark candidates QL84 and QL88.

CHAPTER 7

SUMMARY

7.1 Limits on the production cross-section for quarks

For a limit on the production cross-section for quarks the expected rate for a fixed production cross-section has to be compared with the upper limit of the quark rate obtained in the telescope experiment.

Because of the rapid decrease in rate with decreasing β the expected rates given by Adair and Price for $\beta > 0.7$ can be compared with the obtained rates for relativistic quarks. Adair and Price have used an asymptotic cross-section of $1.0\,\mu$ barn. Hence the ratio of the experimental rate of quarks to the expected rate for a given quark mass gives the value $\sigma_q / 1.0\,\mu$ barn, where σ_q is the upper limit of the cross-section for the given quark mass. This was obtained for a range of quark mass 5 to 20 GeV and the result is shown in Figure 7.1 together with the theoretical predictions of the cross-section.

Interpretation of these results depends on the particular model giving the theoretical production cross-section. On the model of Chilton et al. the upper limit of the quark mass is ~ 20 GeV and on the model of Domokos and Fulton the upper limit is ~ 6 GeV.

7.2 Future experiments

The results of the telescope experiment represent the best value of the upper limit of the quark production cross-section and

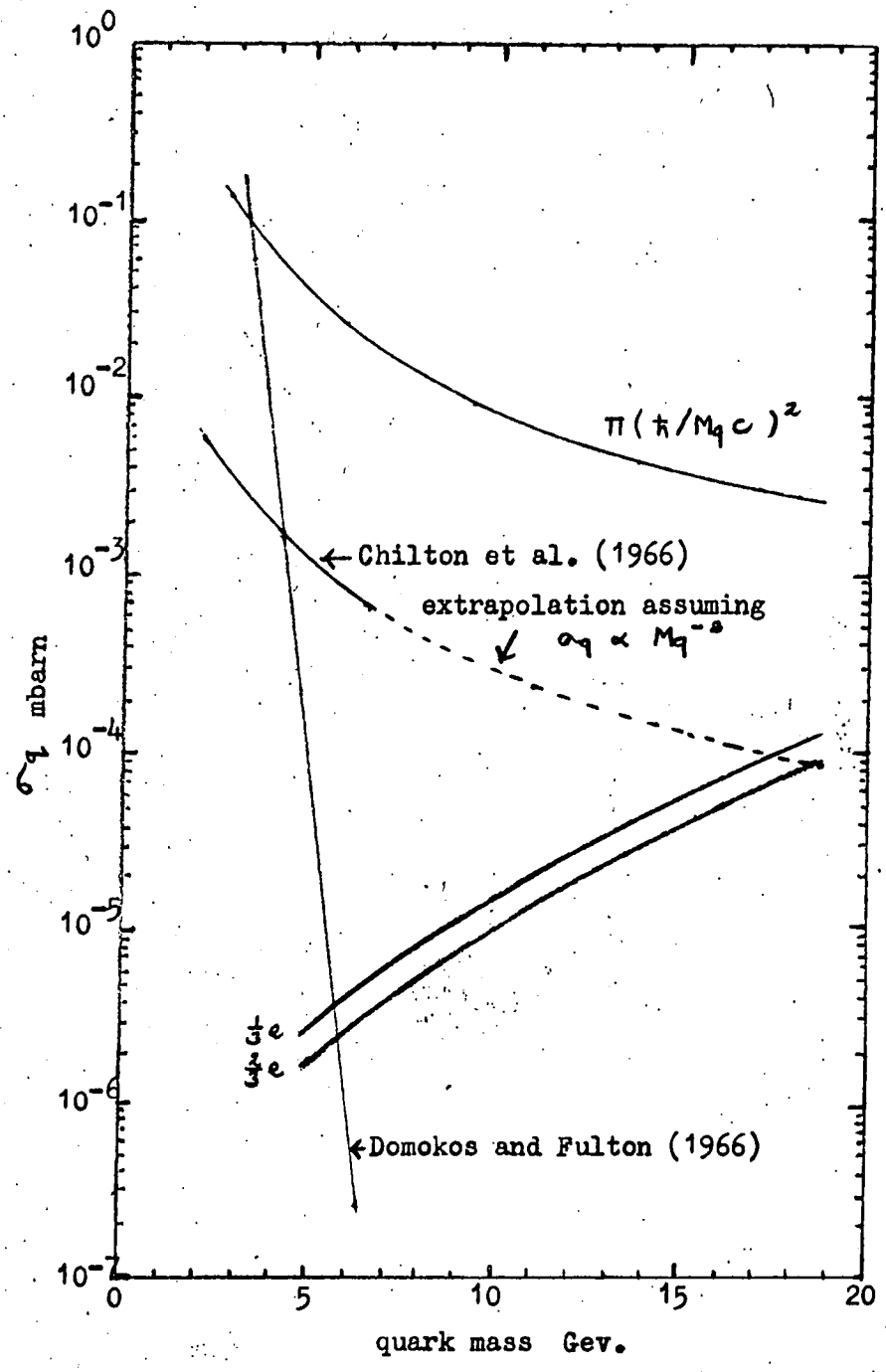

Figure 7.1 Upper limit on the quark production cross-section against quark mass. Theoretical predictions are also shown.

the rate of quarks in cosmic rays at sea-level to date. With no quarks yet detected the design of future experiments will be determined by two main factors:

1) the theoretical estimates of the production cross-section and

2) the actual nature of the quark (i.e. integral or non-integral charge).

If the production cross-section shows the rapid exponential decrease with mass as predicted by Domokos and Fulton, detection in cosmic rays will prove difficult unless telescopes of acceptance $\sim 10^3$ m^2 sterad. are used.

On the actual nature of the quark, models have been postulated to fit quarks with integral charge although these have not the simplicity nor all the successes of the quark model with non-integral charge. However, searches have been continued in cosmic rays (Kasha et al. (1967c)) by measuring the momentum and time of flight of incident particles. Another method has been proposed by Ashton (1965). In this the range of incident particles with $\beta < 0.75$ would be measured. These would be selected by a water Cerenkov counter and their subsequent range in a stack of scintillation counters, neon flash tube trays and iron would be measured. Since the range of quarks will be increased by a factor $\sim M_q/M_p$ on that of protons they can be identified if they lie within certain β and range limits. This experiment is at present in preparation at Durham University.

Acknowledgements

The author wishes to thank Professor G.D. Rochester for the provision of the facilities for this work, and for his interest and support.

He is grateful to his supervisor, Dr. F. Ashton, for his willing guidance and invaluable help throughout the work. The author would also like to thank Professor A.W. Wolfendale for his interest in the work, and for his freely given advice.

Members of the Cosmic Ray Research Group are thanked for helpful discussion and especially Mr. G.N. Kelly and Mr. T. Takahashi are thanked for their friendly assistance.

The technical staff of the Physics Department, in particular Mr. W. Leslie, Mr. K. Tindale, Mr. J. Webster and Miss P. Wallace are thanked for their willing help.

The author is grateful to Mrs. P. Wilson for her patient work in typing this thesis.

Finally the Research Corporation of New York is thanked for the provision of a Research Studentship and the Science Research Council and the National Institute for Research into Nuclear Science (Rutherford Laboratories) are thanked for providing much of the equipment.

REFERENCES

P.I.C.C.R. : Proceedings of the International Conference on Cosmic Rays.

Adair, R.K. and Price, N.J., (1966), Phys. Rev., 142, 844.

Ashton, F., (1965), P.I.C.C.R., London, 2, 1108.

Ashton, F., Coats, R.B., Holyoak, B., Simpson, D.A., and Thompson, M.G., (1965a), Nuc. Instrum. and Methods, 37, 181.

Ashton, F. and Coats, R.B., (1965b), P.I.C.C.R., London, 2, 959.

Ashton, F. and Coats, R.B., (1967), Journal of Physics A (General), To be published.

Barnaby, C.F. and Barton, J.C., (1960), Proc. Phys. Soc., 76, 745.

Barton, J.C., (1967), Proc. Phys. Soc., 90, 87.

Bingham, H.H., Dickinson, M., Diebold, R., Koch, W., Leith, D.W.G., Nikolic, M., Ronne, B., Husch, R., Musset, P., and Veillet, J.J., (1964), Physics Letters, 9, 201.

Birks, J.B., (1951), Proc. Phys. Soc., A64, 874.

Blum, W., Brandt, S., Cocconi, V.T., Czyzewski, O., Danysz, J., Jobes, M., Kellner, G., Miller, D., Morrison, P.R.O., Neale, W., and Rushbrooke, J.G., (1964), Phys. Rev. Letters, 13, 353a.

Brini, D., Peli, L., Rimondo, O., and Veronesi, P., (1955), Il Nuovo Cimento, Series X, 2, 1048.

Brooke, G., Hayman, P.J., Kamiya, Y., and Wolfendale, A.W., (1964), Proc. Phys. Soc., 83, 853.

Buhler-Broglin, A., Fortunato, G., Massam, T., Muller, Th., and Zichichi, A., (1966), Il.Nuovo Cimento, Series X, 45, 520.

Buhler-Broglin, A., Fortunato, G., Massam, T., and Zichichi, A., (1967), Il Nuovo Cimento, Series X, 49, 209.

Burnham, J.U., Rogers, I.W., Thompson, M.G., and Wolfendale, A.W., (1963), J. Sci. Instrum., 40, 296.

Charpak, G., Massonnet, L., and Favier, J., (1965), Progress in Nuclear Techniques and Instrumentation, Volume 1, edited by F.J.M. Farley, published by the North-Holland Publishing Co.

Chilton, F., Horn, D., and Jabbur, R.J., (1966), Physics Letters, 22, 91.

Chupka, W.A., Schiffer, J.P., and Stevens, C.M., (1966), Phys. Rev. Letters, 17, 60.

Cocconi, G., (1965), P.I.C.C.R., London, 2, 616.

Currie, W.M., Azuma, R.E., and Lewis, G.M., (1961), Nuc. Instrum. and Methods, 13, 215.

De-Lise, D.A. and Bowen, T., (1965), Phys. Rev. 140, 2B, 458.

Domokos, G. and Fulton, T., (1966), Physics Letters, 20, 546.

Dorfan, D.E., Eades, J., Lederman, L.M., Lee, W., and Ting, C.N., (1965), Phys. Rev. Letters, 14, 999.

Fermi, E., (1950), Prog. of Theoretical Phys., 5, 570.

Franzini, P., Leontic, B., Rahm, D., Samios, N., and Schwartz, M., (1965), Phys. Rev. Letters, 14, 196.

Frohlick, A., (1967), Nature, 215, 1362.

Fukui, S., and Miyamoto, S., (1959), Il Nuovo Cimento, 11, 113.

Gell-Mann, M., (1964), Phys. Letters, 8, 214.

Gomez, R., Kobrak, H., Moline, A., Mullins, J., Orth, C., Van Putten, J., and Zweig, G., (1967), Phys. Rev. Letters, 18, 1022.

Gursey, F., Lee, T.D., and Nauenburg, M., (1964), Phys. Rev., 135B, 467.

Hagiopian, V., Selove, W., Ehrlich, R., Leboy, E., Lanza, R., Rahm, D., and Webster, M., (1964), Phys. Rev. Letters, 13, 280.

Hillas, A.M. and Cranshaw, T.E., (1959), Nature, 184, 893.

Kasha, H., Leipuner, L.B., and Adair, R.K., (1966), Phys. Rev., 150, 1140.

Kasha, H., Leipuner, L.B., Wangler, T.P., Alspector, J., and Adair, R.K., (1967a), Phys. Rev., 154, 1263.

Kasha, H., Larsen, R.C., Leipuner, L.B., and Adair, R.K., (1967b), P.I.C.C.R., Calgary, To be published.

Kasha, H., Hawkins, C.B.J., and Stefanski, R.J., (1967c), P.I.C.C.R., Calgary, To be published.

Kerns, Q.A., Kirsten, F.A., and Cox, G.C., (1959), Review Sci. Instrum., 30, 34.

Koba, Z., (1965), P.I.C.C.R., London, 2, 893.

Landau, L., (1944), J. Phys. U.S.S.R., 8, 201.

Lamb, R.C., Lundy, R.A., Novey, T.B., and Yovanovitch, D.D., (1966), Phys. Rev. Letters, 17, 1068.

Lattes, C.M.G., Muirhead, H., Occhialini, G.P.S., and Powell, C.F., (1947), Nature, 159, 694.

Leipuner, L.B., Chu, W.T., Larsen, R.C., and Adair, R.K., (1964), Phys. Rev. Letters, 12, 423.

Lloyd, J.L., (1960), Proc. Phys. Soc., 75, 387.

Massam, T., Muller, Th., and Zichichi, A., (1965), Il Nuovo Cimento, 40, 589.

McDowell, M.R.C., and Hasted, J.B., (1967), Nature, 214, 235.

Morrison, D.R.O., (1964), Physics Letters, 9, 199.

Nagano, M., and Shibata, S., (1965), Journal of the Physical Society of Japan, 20, 685.

Nir, A., (1967), Phys. Rev. Letters, 19, 336.

Peters, B., (1965), P.I.C.C.R., London, 2, 922.

Rossi, B., (1952), High Energy Physics (page 34), published by Prentice Hall.

Schiff, L.I., (1966), Phys. Rev. Letters, 17, 714.

Sinanoglu, O., Skutnik, B., and Tousey, R., (1966), Phys. Rev. Letters, 17, 785.

Sternheimer, R.M., (1952), Phys. Rev., 88, 851.

Sternheimer, R.M., (1953), Phys. Rev., 91, 256.

Sternheimer, R.M., (1956), Phys. Rev., 103, 511.

Sunyar, A.W., Suhwarzschild, A.Z., and Connors, P.I., (1964), Phys. Rev., 136B, 1157.

Symon, K.R., (1948), Ph.D. Thesis, Harvard University.

Wilkinson, P.H., (1950), Ionisation chambers and counters (pages 144-145), Cambridge Monograph.

Yukawa, H., (1935), Proc. Phys. Math. Soc., Japan, 17, 48.

Zweig, G., (1964), CERN Reports 8182/TH 401 and 8419/TH 412.

Plate A.1

The glass plate spark chamber showing the stranded wire electrode.

SCALE 4:1

Plate A.2

View of an event in the chamber showing the top view (looking through the wire electrode) and the side view.

SCALE 4 : 1

Plate A.5

Top view of an event in two chambers, one vertically above the other.

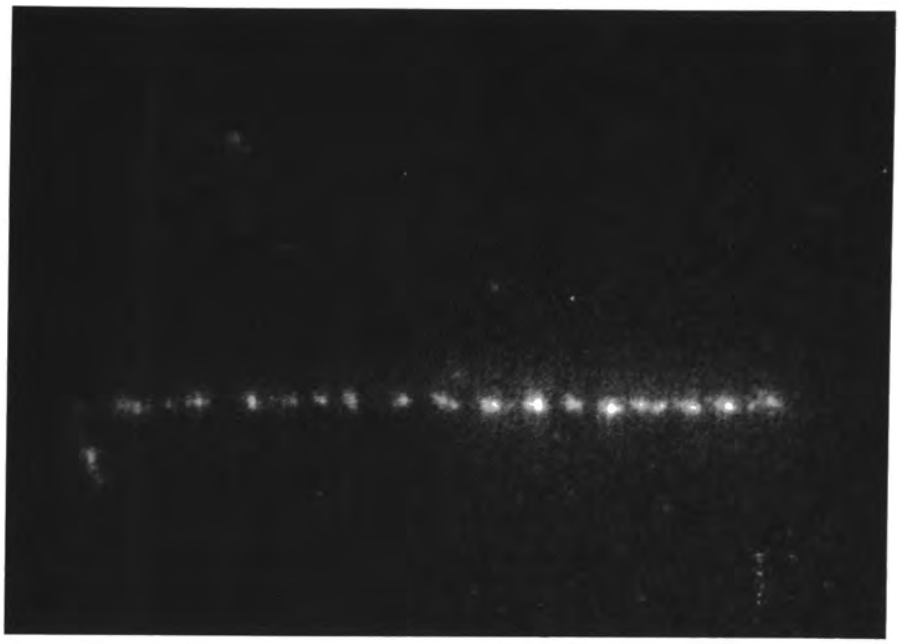

Plate A.4 SCALE 3:1.

Top view of an event passing through the chamber approximately in the plane of the wire electrode.

APPENDIX A

A PARALLEL GLASS PLATE SPARK CHAMBER

A.1 Introduction

Prior to the quark experiment the characteristics of a parallel glass plate spark chamber were investigated. These were designed to study the lateral structure of bursts produced by the interaction of relativistic muons and nucleons in an absorber, such as in the experiment of Ashton and Coats (1965). Other applications such as the study of the multiple core structure of extensive air showers are also possible.

Spark chambers have been extensively employed by accelerator workers (e.g. Charpak et al., 1965) during the past few years but the technique has not been widely used in cosmic ray experiments. The main reason for this is that such experiments require large area ($> 1.0\ m^2$) chambers in which complex events with many particles traversing the chamber simultaneously are accurately recorded. However, Nagano and Shibata (1965) have shown that chambers in which the electrodes are covered with a layer of insulating material are capable of recording $\sim 10^3$ particles in a square metre. The reason for this is that, whereas in a chamber with bare metal electrodes the fluctuations in the development of avalanches leads to a low multiple track efficiency, with a high resistance between the electrodes the field is maintained for sufficient time for multiple discharges to develop efficiently.

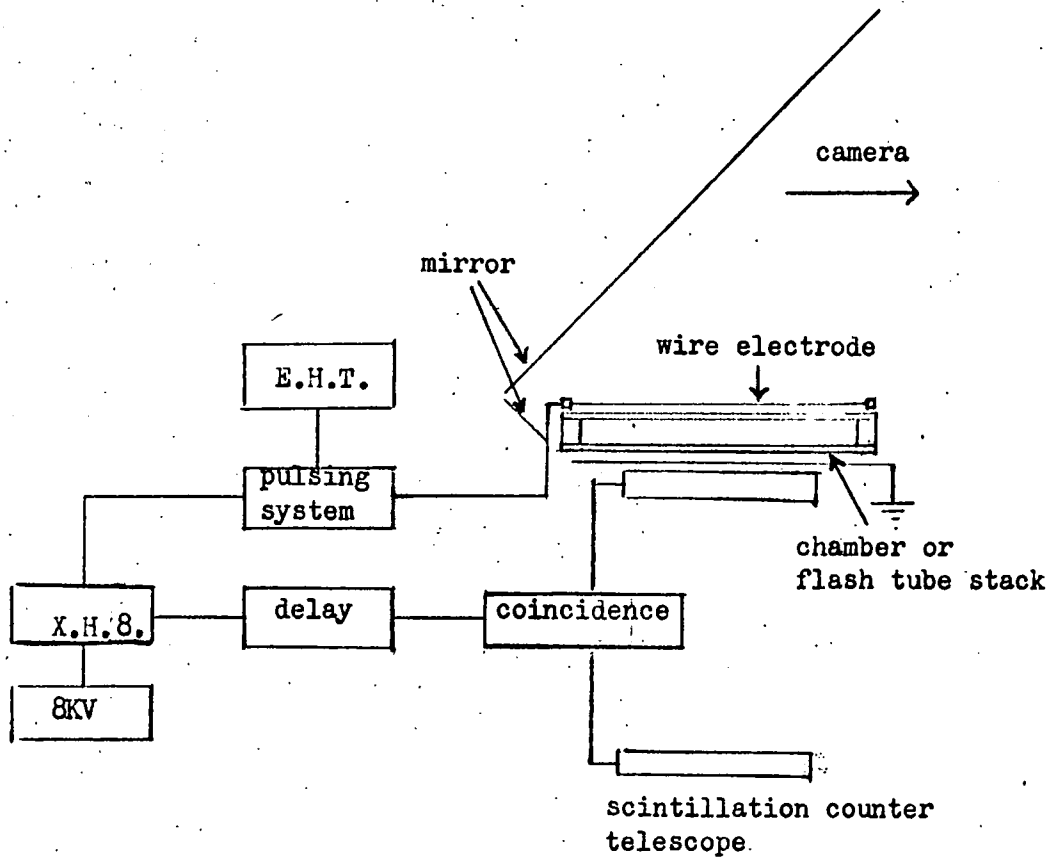

Figure A1(a) Block diagram of triggering system used in the investigation of spark chambers and localised discharge in flash tubes.

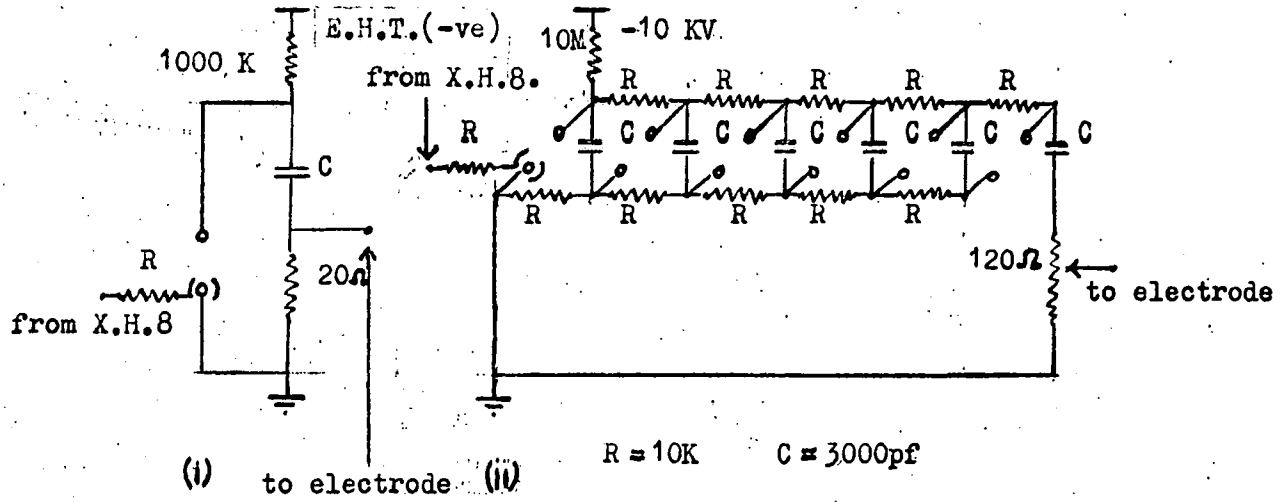

Figure A1(b) Diagrams of the two types of pulsing system used to supply the high voltage pulse to the wire electrode,
(i) single variable spark gap,
(ii) Marx impulse generator.

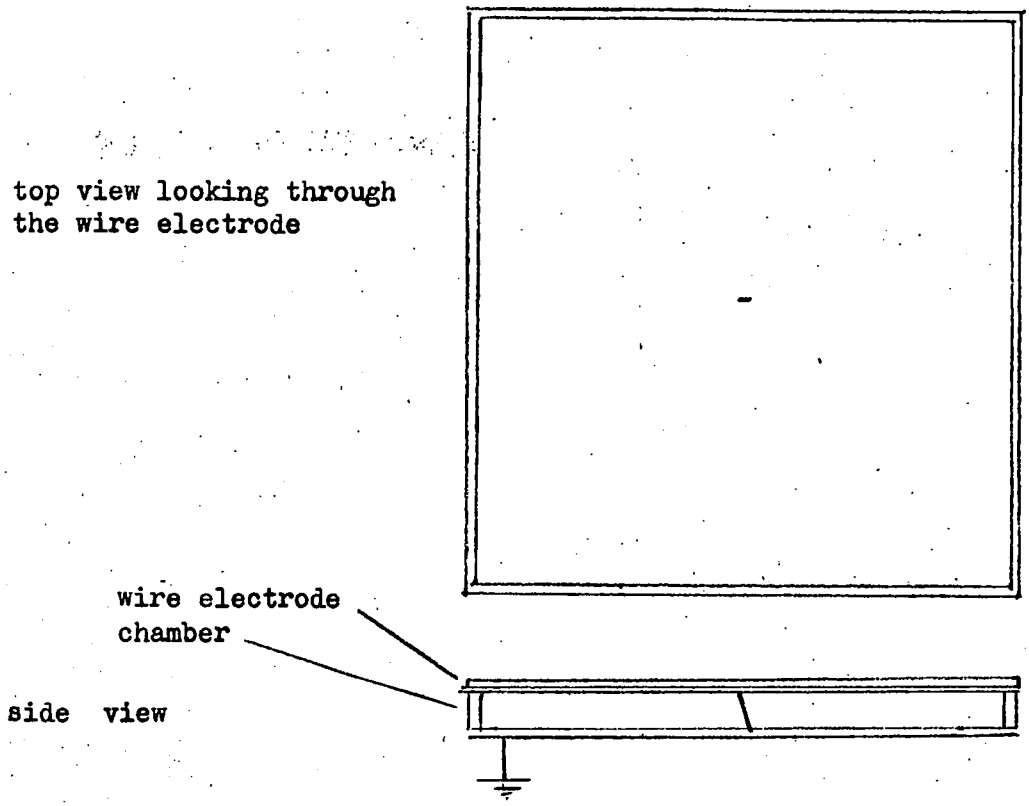

Figure A.2 Diagram showing the top and side views of the glass plate spark chamber. A typical track is shown.

A.2 Construction and operation of the spark chambers

The chamber under investigation is shown in plate A.1. It is a completely enclosed box (30 x 30 x 2 cm^3) containing neon gas (98% pure). The two large areas are glass plates of thickness 3 mms and the sides are perspex fixed to the glass with araldite epoxy resin. For filling, the chamber was placed in a steel enclosure and both were evacuated to 10^{-4} mm of mercury pressure. They were then filled simultaneously with neon to atmospheric pressure then the enclosure was opened and the chamber sealed off. Throughout this operation the pressure difference across the glass plates was less than a few cm of mercury, thus avoiding the danger of cracking. The chambers were able to withstand the normal changes in atmospheric pressure.

The upper electrode consists of a framework on which is strung tinned copper wire (diameter 0,34 mm) in parallel spacings of 2mm. The advantage of this type of electrode is that tracks can be viewed through it and if several chambers with similar electrodes are mounted in a vertical stack, the trajectory of a particle can be followed through the chambers. This procedure was used to compare the angle of the spark with the inclined angle of incident particles. On occasions during the investigation of the chamber a tin plate electrode and a glass electrode with a conducting layer of tin oxide were used with no change in performance.

The characteristics of the chamber were studied by selecting cosmic ray muons with a scintillation counter telescope. The

geometrial arrangement of the chamber and the telescope and the block diagram of the pulsing system is shown in Figure A.1. Two types of pulsing system were used and these are also shown in Figure A.1. The first type was a single spark gap with a variable gap distance, the pulse height was varied by varying the supply voltage and the gap distance. The second was a Marx impulse generator with 6 spark gaps. In this case the supply voltage was fixed at - 10 Kv and the pulse height was varied by tapping off the 120 Ω at different positions. In both cases the decay time constant was 60 n sec and the performance of the chamber was the same for the same pulse height from each system.

A.3 Characteristics of the chamber

The chamber was viewed through the electrode (top view) and in the plane of the electrode (side view). The two views are shown in Figure A.2 and a typical spark in the chamber in both views is shown in Plate A.2. In many cases a glow surrounds the spark at the glass plates due to space charge effects. This could possibly be improved by having a conducting layer on the inside of the glass (not in electrical contact with the electrodes) so that space charge effects could be dispersed. For high fields and pulse lengths >1 μsec the glow spread and seperate discharges occured throughout the chamber due to the ultra-violet radiation emitted by the initial discharge causing secondary avalanches. At the voltages operated normally in the investigation this did not occur.

However, the width of the discharge varied from 1 to 2 mm in diameter, although this appeared to be unrelated to the field applied.

The visual efficiency of the chamber was measured by eye, counting the percentage of visible tracks in the total number of coincident triggers. This was done for different applied fields and delay time between the coincident pulse and application of field. The results are shown in Figure A.3. The sensitive time of the chamber is given as:

$$\int_0^\infty \eta\,(T_D)\, dT_D$$

where $\eta(T_D)$ is the efficiency at a time delay of T_D. For pulse heights > 14 kV where the efficiency reaches anasymptotic limit, the sensitive time is 46 μsec. This is not a long time for Cosmic Ray experiments where the background is small and can be overcome by an electronic device such as that described in Chapter 2.

Many workers since Fukui and Miyamoto (1959) have noted that for small inclined angles of incident particles the spark appears to follow the path of the particle. This is because in a spark chamber the ionisation extends initially along the path of the incident particle and the spark is the result of several electron avalanches. For a pulse of rise time $\sim$10 n sec, these avalanches interact and cause a resultant field along the path of the particle such that the spark tends to follow this path.

This effect was studied with the present counter by viewing two chambers, one vertically above the other as explained previously.

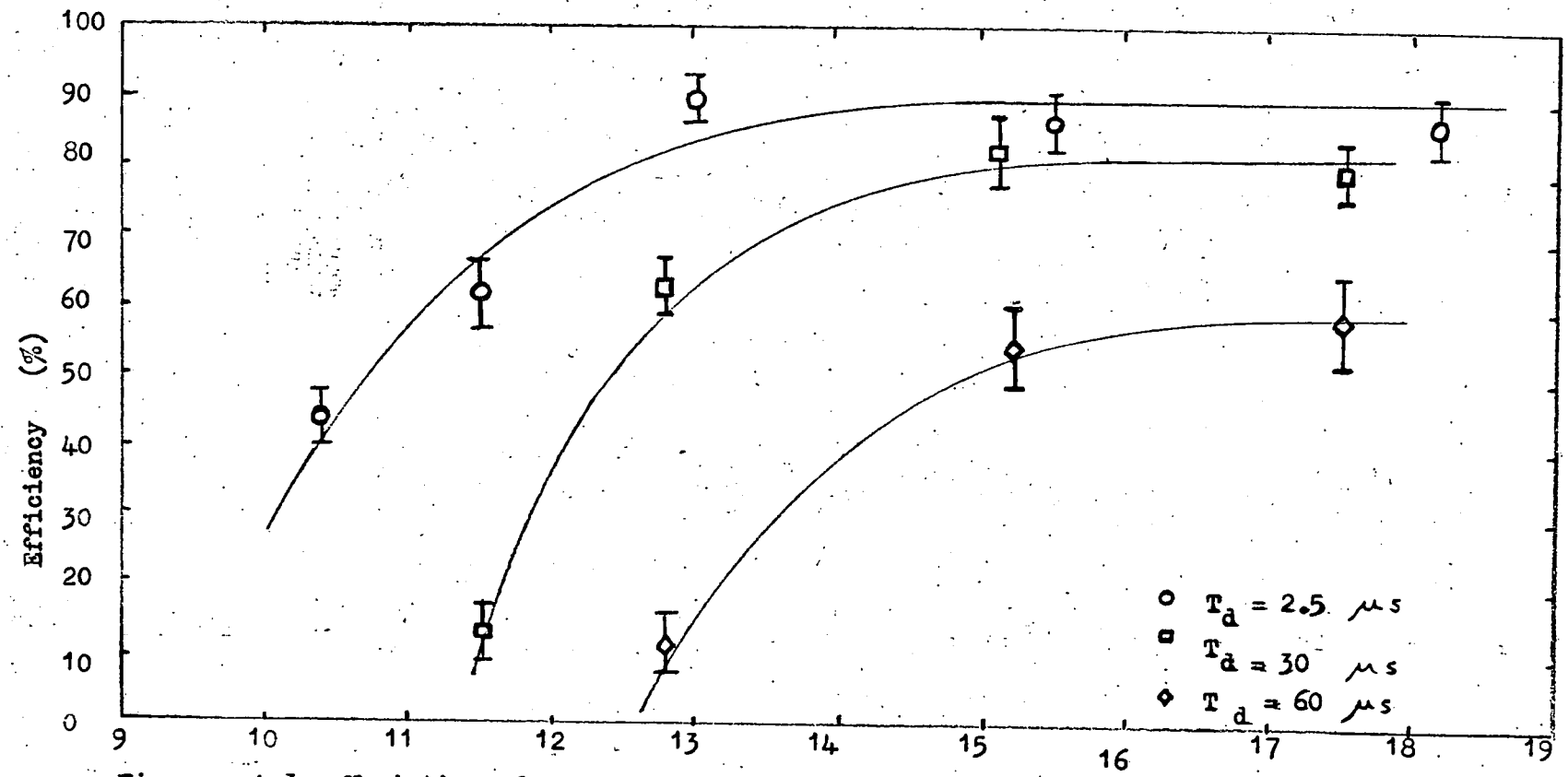

Figure A.3 Variation of efficiency with pulse height for different time delays T_d

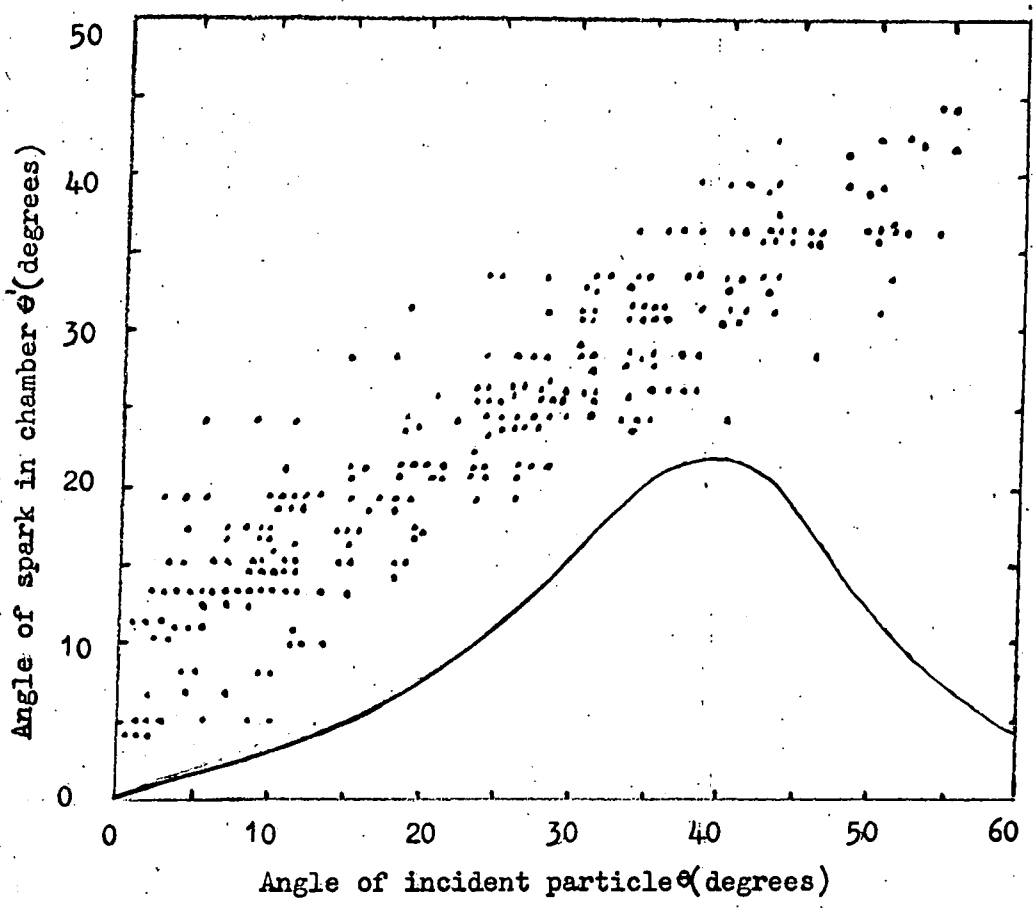

Figure A.4 Plot of angle of spark against angle of incident particle traversing the chamber. Each point represents a single observation. The line gives the results of Burnham et al. (1963) for a chamber in which both electrodes were metal.

A photograph of one event is shown in plate A.3. The displacement of the two sparks gave the angle of the incident particle, $\hat{\theta}$ and the projected length of the spark gave its inclined angle, $\hat{\theta}'$ the results are shown in Figure A.4. The displacement of the results from the $\theta' = 0$ point is due to the fluctuations in the size and shape of the spark. This could be improved as explained earlier. The fluctuations in angle occur because of the initial variation in ionisation density and the later variation in the spacing and development of avalanches. It is suggested that at higher gas pressures these fluctuations would decrease.

The results are compared with the best line for the results of Burnham et al. (1963) for a 1 cm chamber with bare metal electrodes. For these results also, $\tan\theta'/\tan\theta < 1.0$, but the authors point out that the ratio increased for decreasing rise time of the applied pulse. Frohlick (1967) using a similar chamber to Burnham et al. found the maximum inclined angle of track $\sim 30^{\circ}$ compared with 20° for Burnham et al. The present results show an improvement upon these values. However, at angles $> 50^{\circ}$, the discharge broke into 2 or more separate sparks in the vertical plane of the incident particle. An example of this effect for an incident particle passing almost parallel to the electrodes is shown in Plate A.4.

A.4 Conclusions

From these initial investigations the chamber appears to be a useful device in the study of complex events due to Cosmic Rays.

Further development is necessary if an accurate estimate of the incident angle of a particle is required. This would take the form of investigations using a pulse with a shorter rise time, higher pressure of gas and possibly the effect of the addition of alcohol.

SCALE 3·1

Plate B.1

View of an event in the double layer of flash tubes operated for localised discharge showing the top view (looking through the wire electrode) and the side view. The light in the edge flash tubes is daylight transmitted along the tube.

APPENDIX B

LOCALISED DISCHARGE IN NEON FLASH TUBES

A small array of unpainted neon flash tubes was made as shown in Figure B.1. The tubes had internal diameter 1.5 cm and 1 mm wall thickness. The tubes were investigated for localised discharge using the experimental arrangement as described in Appendix A. Again the wire electrode was used so that the top view and side view of the discharge could be photographed.

In the normal operation of flash tubes with applied pulses of several μsec the discharge spreads along the whole length of the tube. This is due to the emission of photons by the initially excited electrons which then start secondary photon-electron cascades throughout the gas. When a pulse of $\sim$100nsec is applied the flash tube behaves like a normal spark chamber and the discharge is localised around the initial trajectory of the ionising particle.

However, unlike the parallel plate spark chamber with constant geometry and constant field, the stack of flash tubes introduces a varying geometry and the glass of the tube creates a distorted field within. Thus it was found that the size of the discharges showed great variation for a fixed applied field. The size varied from 1 mm in diameter to 5 mm and sometimes a greater elongation, generally in the direction of the length of the tube.

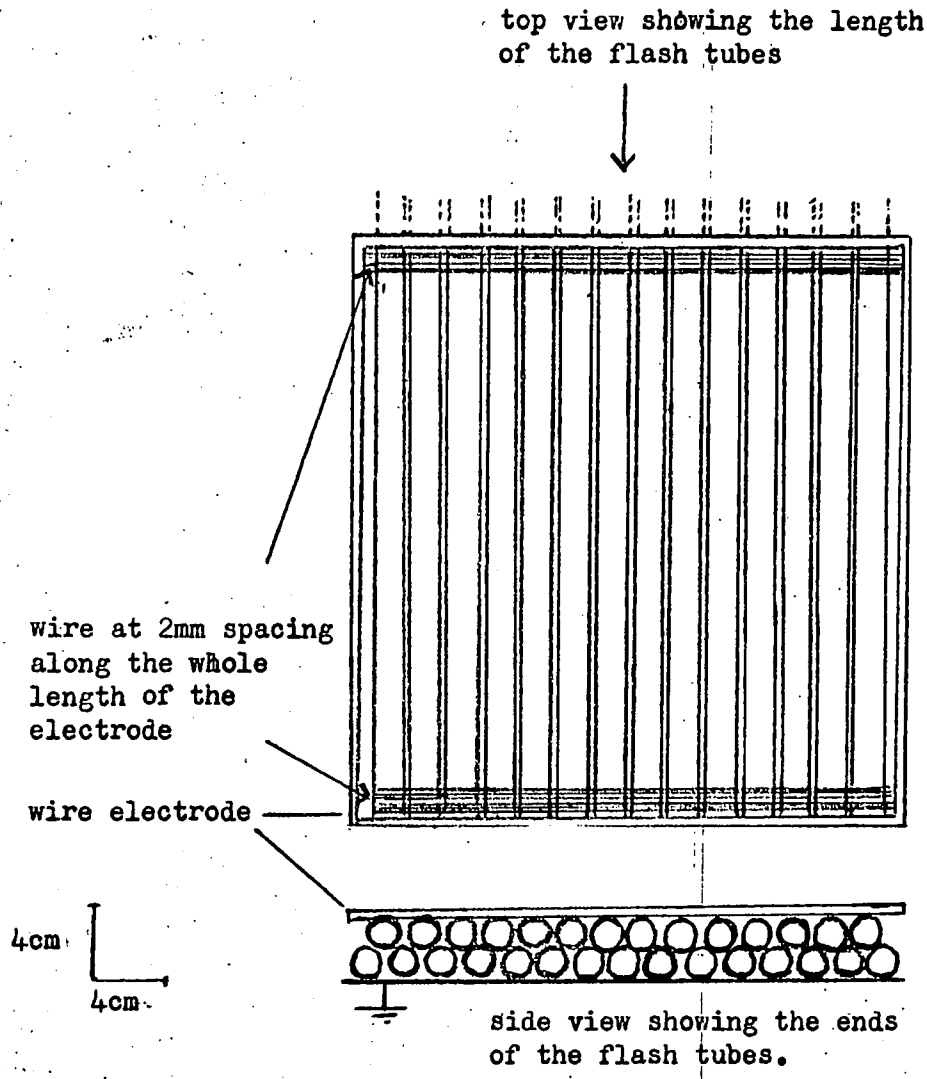

Figure B.1 Diagram showing the top and side views of the flash tube stack in the localised discharge investigation.

Photography is also made difficult from the perpendicular direction (top view) because of reflection and scattering of light in the walls of the neighbouring tubes. The photograph of an event showing the discharge in the top and side views is shown in Plate B.1, and although the side view shows a clear track the top view shows some distortion. The light in the edge flash tubes is daylight transmitted along the tube.

Visual efficiency measurements were made as a function of applied voltage for a time delay of 2.5 μsec for a single and a double layer and the results are shown in Figure B.2. The efficiency of the double layer approximately represents the internal efficiency of the flash tube for localised discharge. The single layer shows a decrease of 75% from the double layer because of the spacing of the tubes in the single layer cover only 75% of the total area. The decrease from $\sim$ 95% for the normal operation of flash tubes may be due to the short time of applied field leading to a weak discharge which is not visible.

For a fixed field of 12 kv/cm the efficiency of the single and double layers was investigated as a function of time delay between the incident particle and the application of the pulse. The result is shown in Figure B.2. compared with the previous result for a glass plate spark chamber and the internal efficiency of flash tubes under normal pulsing conditions. Lloyd's theoretical curve for afq = 12 is shown together with 0.75 afq and 0.50 afq.

With further development in the control of the applied field

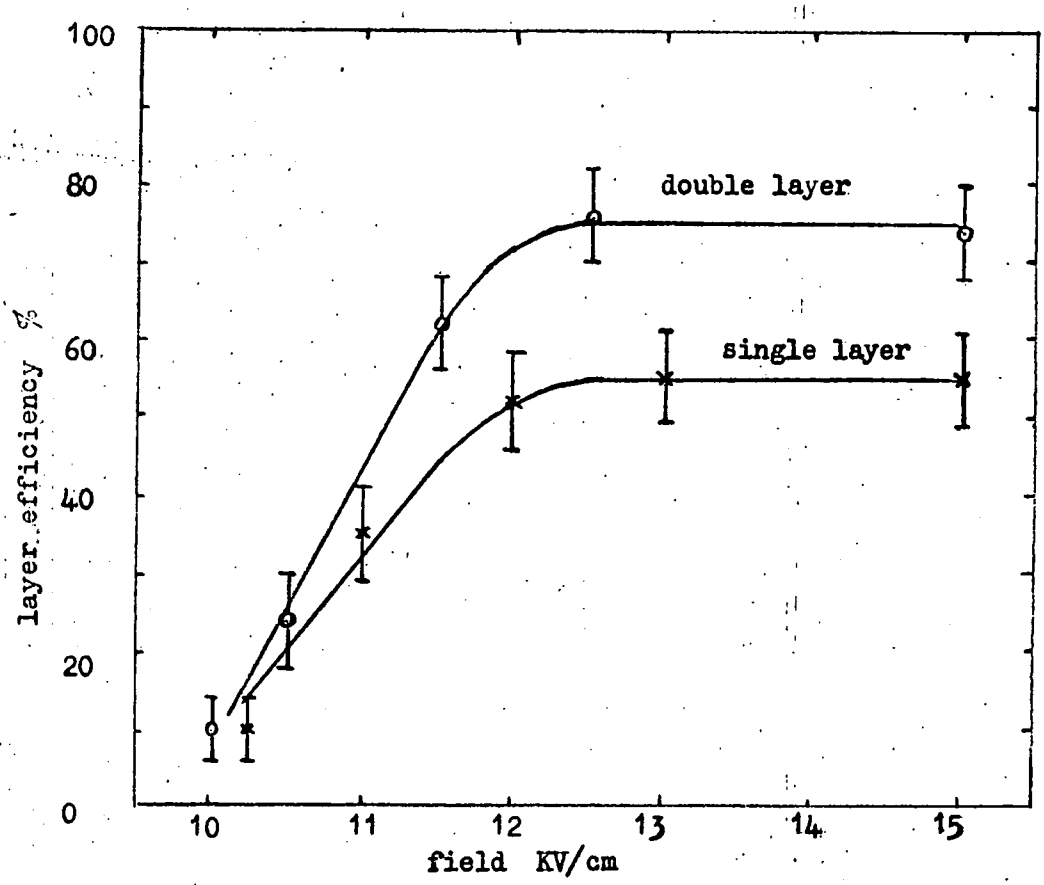

Figure B.2 Variation of efficiency of flash tubes operated in the localised discharge regime for a time delay of 2.5 μsec.

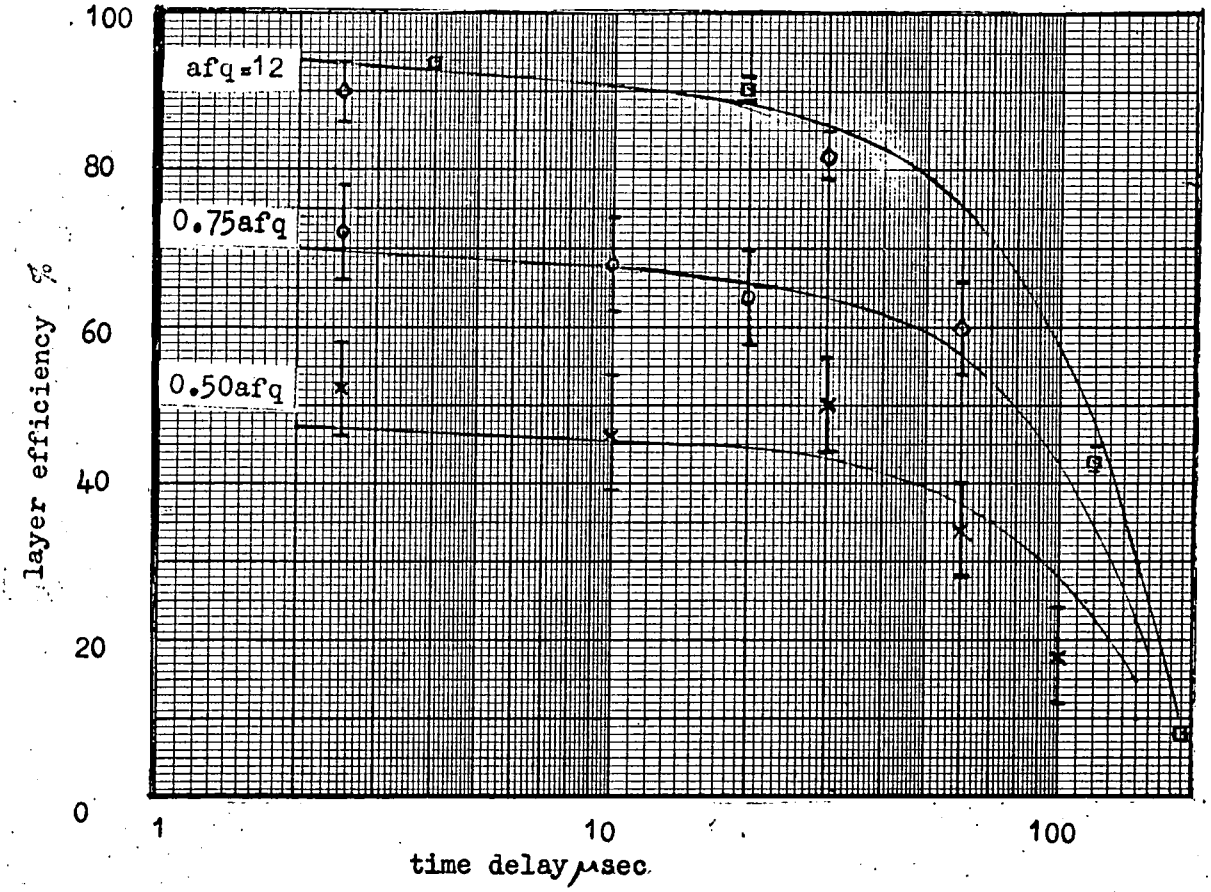

Figure B.3 Variation of efficiency with time delay for
× single layer of flash tubes (localised discharge regime)
o double layer of flash tubes (localised discharge regime)
◇ glass plate spark chamber
□ flash tubes under normal operation.

The theoretical curve of Lloyd (1960) for afq=12 is shown together with fractional decreases of 0.75 and 0.50.

and on the nature of the flash tube, this technique could be used as a cheap and convenient method of building up large areas of visual detector for cosmic ray experiments.

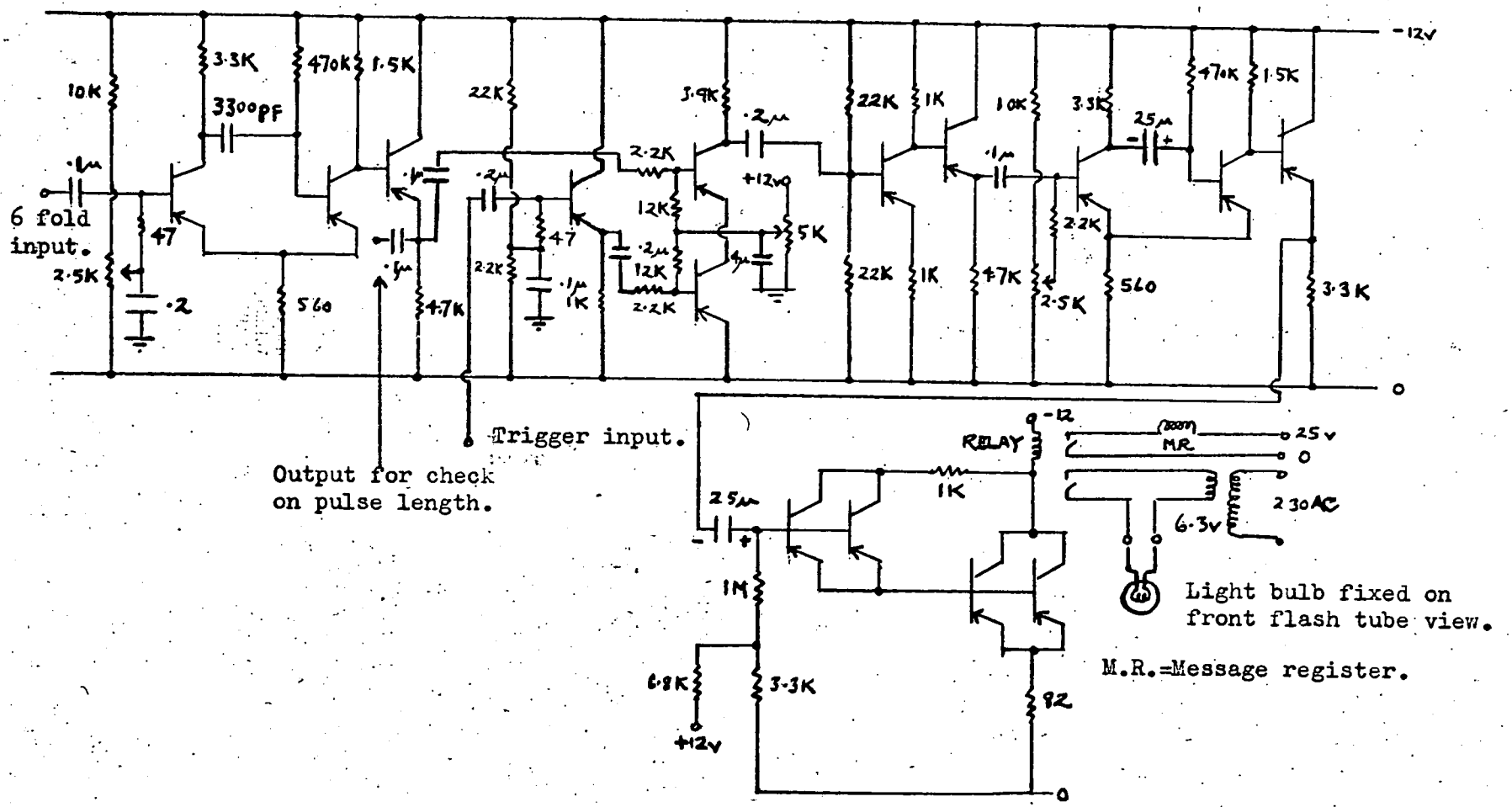

Appendix C Ciruit of previous particle indicator. The 6fold input is delayed by 200nsec. so that normally accepted events did not register a coincidence.

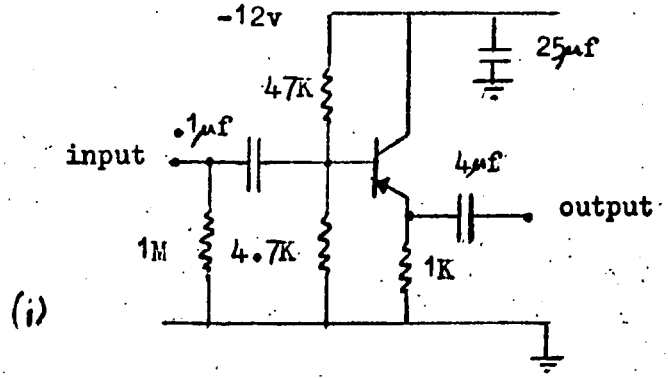

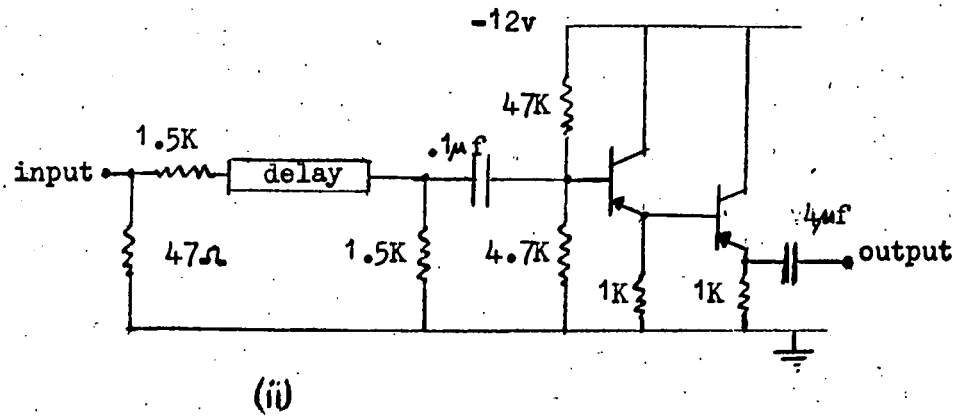

Appendix C The two types of emitter follower used in the telescope electronics,

(i) feeds the output from the photomultipliers into the 50Ω system;

(ii) feeds the output from the delay line (characteristic impedance = 1.5K) into the 50Ω system.